# RESPONSE EVALUATION OF FREESTANDING SYSTEMS SUBJECTED TO SEISMIC LOADING

*By*

**ANUPAM SARASWAT**

**ENGG01201004010**

**BHABHA ATOMIC RESEARCH CENTRE**

***A thesis to be submitted to***

***Board of Studies in Engineering Sciences***

***In partial fulfillment of requirements***

***for the Degree of***

**DOCTOR OF PHILOSOPHY**

***of***

**HOMI BHABHA NATIONAL INSTITUTE**

**March, 2018**

# Homi Bhabha National Institute[1]

## Recommendations of the Viva Voce Committee

As members of the Viva Voce Committee, we certify that we have read the dissertation prepared by Mr. Anupam Saraswat entitled "Response Evaluation of Freestanding Systems subjected to Seismic Loading" and recommend that it may be accepted as fulfilling the thesis requirement for the award of Degree of Doctor of Philosophy.

| | |
|---|---|
| Chairman – Prof. B.K. Dutta | **Date:10/11/2017** |
| Guide / Convener – Prof. G.R Reddy | **Date:10/11/2017** |
| Examiner – Prof. R.S. Jangid | **Date:10/11/2017** |
| Member 1- Prof. J. Chattopadhyay | **Date:10/11/2017** |
| Member 2- Prof. T.A. Dwarkanath | **Date:10/11/2017** |

Final approval and acceptance of this thesis is contingent upon the candidate's submission of the final copies of the thesis to HBNI.

I/We hereby certify that I/we have read this thesis prepared under my/our direction and recommend that it may be accepted as fulfilling the thesis requirement.

**Date: 10/11/2017**

**Place: Mumbai**

**(Prof. G.R. Reddy)**
**Guide**

[1] This page is to be included only for final submission after successful completion of viva voce.

# STATEMENT BY AUTHOR

This dissertation has been submitted in partial fulfillment of requirements for an advanced degree at Homi Bhabha National Institute (HBNI) and is deposited in the Library to be made available to borrowers under rules of the HBNI.

Brief quotations from this dissertation are allowable without special permission, provided that accurate acknowledgement of source is made. Requests for permission for extended quotation from or reproduction of this manuscript in whole or in part may be granted by the Competent Authority of HBNI when in his or her judgment the proposed use of the material is in the interests of scholarship. In all other instances, however, permission must be obtained from the author.

Anupam Saraswat

# DECLARATION

I, hereby declare that the investigation presented in the thesis has been carried out by me. The work is original and has not been submitted earlier as a whole or in part for a degree / diploma at this or any other Institution / University.

Anupam Saraswat

## List of Publications arising from the thesis

### Journal

1. "Seismic stability of a standalone glove box structure", A. Saraswat, G.R. Reddy, S. Ghosh, A.K. Ghosh, Arun Kumar, Nuclear Engineering and Design, Volume 276, September 2014, Pages 178-190, ISSN 0029-5493
2. "Seismic stability of interconnected glove boxes", A. Saraswat, G.R. Reddy, S. Ghosh, A.K. Ghosh, Arun Kumar, Nuclear Engineering and Design 293 (2015) 357–370
3. "Effects of base excitation frequency on the stability of a freestanding rigid block", A. Saraswat, G.R. Reddy, S. Ghosh, A.K. Ghosh, Acta Mechanica 226/11(2015), DOI 10.1007/s00707-015-1484-2
4. "Seismic stability of two interconnected steel structures freely standing on the floor", A. Saraswat, G. R. Reddy,C. Umashankar, Y. M. Parulekar & A. K. Ghosh, Bulletin of Earthquake Engineering(Official Publication of the European Association for Earthquake Engineering), 2016, DOI 10.1007/s10518-016-9936-1

### Conferences

1. Seismic Analysis of a Free-standing Glove Box Structure, A.Saraswat et.al, SMiRT21 Conference(2011), New Delhi
2. Development of automation and remotisation systems for fabrication of MOX fuel for AHWR; Anupam Saraswat et.al.,2nd International Workshop on ADS and Thorium Utilization at BARC, December 11-14, 2011
3. Design of fuel fabrication plant of FRFCF for reload requirement of prototype fast breeder reactor, K. M. Danny, Anupam Saraswat , S.Chakraborty, P.S. Somayajulu, Arun Kumar , Characterization and Quality Control of Nuclear Fuels(CQCNf) 2012, Hyderabad, India

Anupam Saraswat

**Dedicated to the almighty and my loving family**

ACKNOWLEDGEMENTS

I take this opportunity to acknowledge the support and guidance of all the people who were involved in this research work. Due to the limitation of space, I would be able to mention only a few of them, however, support of anyone left out is highly acknowledged.

Firstly, I sincerely thank my guide **Dr G.R. Reddy** for his constant support and guidance throughout this work. This is because of his consistent motivation and encouragement I could be able to successfully accomplish the research work. I thank **Dr A.K. Ghosh** for his guidance and regular support during this period. Moreover, I thank my earlier division head **Mr Arun Kumar** and superior **Mr P.S. Somayajulu** for allowing me to pursue this research and providing constant support throughout this research. Constant guidance and support of **Professor S. Ghosh** of IIT Bombay is highly appreciated.

This thesis comprised of a lot of experimental studies performed on the shake table facilities. I thank the facility providers, especially Mechanical Metallurgy Division of BARC for providing the shake table required for experimental studies. A special thanks to **Dr J. Chakraborty**, **Dr R.N. Singh**, **Dr C. Gupta** and their team in providing technical and logistic support for the testing. The constant help of **Mr P.N. Dubey** in carrying out experiments is highly acknowledged.

A significant portion of this research was based on the available experimental data on glove boxes. I am thankful to **Dr Y.M. Parulekar** and **Mr C. Umashankar** for providing useful information and their valuable feedback on experimental data obtained from Central power research institute (CPRI).

Critical review and guidance of Doctoral Committee members (**Dr B.K.Dutta, Dr J.Chattopadhyay, Dr V.K. Suri, Dr R. Balasubramanium and Dr T.A. Dwarkanath**) is highly acknowledged. Moral support and guidance of Mr. Vivek Bhasin is highly appreciated.

I am also thankful to my friend and colleague **Mr Tarvinder Singh** for giving me hands-on training in finite element software ABAQUS. A special thanks to **Mr R.K. Singh** for helping in numerical coding and providing constant technical and moral support throughout this period.

Regular help and logistics support provided by my colleagues **Mr S. Chakraborty, Mr. Anil Bhandekar, Mr. Kamlesh Pandit and Mr. K.M. Danny** is also acknowledged.

Constant moral support and encouragement of all my family members especially mother, father, wife and brother is highly appreciated. Without their love and affection, it would not be possible to complete this work. The presence of my wonderful kids had made this arduous research process enjoying.

March, 2018

Anupam Saraswat

# TABLE OF CONTENTS

# ABSTRACT

A free standing structure/body is a common appearance in many of the industries and household. Due to various reasons, they are not fixed to the base which gives rise to an important question - What will happen to the body, in case of an earthquake? This research emanated from this basic question and attempted to ascertain stability of a free standing body subjected to seismic excitations. Surveying past the existing literature on the subject, it was observed that seismic stability of free standing bodies of simple shapes like parallelepiped, cylinder etc. has been explored by the various researchers with the underlying assumption of a rigid body. However, not much of work was available without the above mentioned assumption, i.e. for a flexible body. This research was carried out with the objective to study effects of various system parameters like geometrical characteristics of the body, base excitation characteristics and interfacial contact properties on the dynamics of a flexible vis-à-vis rigid body. Analytical formulation was carried out to determine conditions for initiation termination, and sustenance of the possible motions like rocking, sliding and rocking cum sliding from the rest state. Closed form analytical solution was obtained with some basic assumptions, for the limited cases of pure rocking and pure sliding mode of motion. A more generic numerical formulation of the problem was carried out in two dimensions and a solution was obtained using a developed FORTRAN code. Extensive experimental studies were carried out on the geometrically similar rigid and flexible test specimens. Experimental and numerical studies highlighted some novel findings. A new parameter known as base excitation frequency was observed to govern motion initiation of a body from the rest state in addition to the other three known parameters of aspect ratio, coefficient of friction and amplitude of base excitation. Three dimensional motion initiation criteria diagram was developed for the rigid test specimen

using frequency as an independent parameter. Flexible specimens were observed to be susceptible to a particular range of base excitation frequencies corresponding to free rocking frequencies of the specimens. Studies revealed that for the base excitation frequencies matching the specimen's free rocking frequency an uplift occurred at base excitation amplitudes lower than the statically required minimum value. This highlighted a new phenomenon of ***frequency induced uplift/rocking*** in a flexible body. Motion initiation criteria diagram was developed for the flexible specimen considering the effect of frequency induced rocking. Compared to the available diagram for a rigid body, an increase in the rocking and slide/rock region was observed. A clear distinction in the dynamic behavior of geometrically similar rigid and flexible body was highlighted. Overturning curves indicating two possible modes of overturning for both the rigid and flexible specimens were developed by varying frequency and amplitude of base excitations.

A three dimensional model of a glove box structure, extensively used in the nuclear facilities across the world, was analyzed using nonlinear finite element analysis tools. Three possible configurations were examined for the seismic stability. Recommendations for the safe operation, in case of an earthquake, and guidelines to determine requirement of fixing a glove box with the base have been discussed.

# LIST OF FIGURES

# LIST OF TABLES

# ABBREVIATIONS

AR- Aspect Ratio

AF- Amplification Factor

PBA- Peak Base Excitation

PGA- Peak Ground Acceleration

HDPE- High Density Poly Ethylene

TS- Test Specimen

FE- Finite Element

FEA- Finite Element Analysis

NM-No Motion

GB- Glove Box

2D- Two-Dimensional

3D- Three-Dimensional

FFT- Fast Fourier Transform

PRV- Pressure Regulating Valve

# SYMBOLS

g- Acceleration due to gravity (m/s$^2$)

μ - coefficient of friction

α- critical angle (Radians)

R- Diagonal length (m)

t- Sectional thickness (m)

p- Frequency parameter (Hz)

ω – Cyclic frequency (Hz)

$\omega_r$- Free rocking frequency (Hz)

$\omega_n$- Natural frequency (Hz)

E- Modulus of elasticity (Pa)

ρ- Density (Kg/m$^3$)

$\ddot{X}_g$ – Horizontal base acceleration (m/s$^2$)

$\ddot{Y}_g$- Vertical base acceleration (m/s$^2$)

$F_F$ - Frictional resistance (N)

$F_N$- Normal resistance (N)

X(t)- Sliding displacement (m)

$\dot{X}$(t)- Sliding velocity (m/sec)

$\ddot{X}(t)$- Sliding acceleration (m/sec$^2$)

I- mass moment of inertia about an edge (Kg.m$^2$)

$\theta$(t) - angular rotation from the base (Radians)

$\dot{\theta}$(t) - angular velocity about the base (Radians/sec)

$\ddot{\theta}$(t) - angular acceleration about the base (Radians/sec$^2$)

B- Width of a body (m)

H- Height of a body (m)

$A_g$ - non-dimensional peak amplitude

# CHAPTER 1 INTRODUCTION

## 1.1 General Overview

In many applications, some critical systems are not anchored to the base. The common examples are laboratory equipment, medical equipment in hospitals, vending machines, common household goods etc. In the case of an earthquake, there is a historical evidence that these free-standing systems pose a serious threat to human lives and valuables. The seriousness of damages caused by excessive sliding and overturning of free-standing systems motivated many regulatory agencies to frame guidelines for seismic hazard mitigation. For example, Federal Emergency Management Agency (FEMA) of United States has framed a practical guide known as FEMA E74 [1], to help general public from seismic hazards arising due to free standing nonstructural components (NSCs). When unrestrained, inertial forces may cause them to slide, rock, strike other objects or overturn during an earthquake. File cabinets, emergency generators, free-standing bookshelves, office equipment, and items stored on shelves or racks can all be damaged as they move and impact other items, fall, overturn or become disconnected from attached components. As the objective is a higher level of earthquake protection, it is important to understand the realistic behavior of free-standing NSCs. The failures of these components during an earthquake may result in injuries or fatalities, cause costly property damage; and force the closure of residential, medical and manufacturing facilities, businesses, and government offices until appropriate repairs are completed. These components can be broadly divided into four main categories viz. mechanical, electrical, storage racks and monuments. The first step to improving their performance is to observe and understand their behavior under real earthquakes. The following paragraph discusses the behavior and failures of some free-standing nonstructural components under real earthquakes.

In the 1994 Northridge Earthquake and the 2010 Christchurch New Zealand Earthquake, damage to free-standing industrial storage racks has been reported. Damage has ranged from dislodged contents from the racks to partial collapse of racking systems as shown in Fig.1-1 below.

**Figure 1-1** ***Failure of free-standing racks and office furniture in the 1994 Northridge Earthquake (FEMA 74, 1994).***

Nonstructural components, such as mechanical and electrical equipment and distribution systems and architectural components, account for 75-85% of the original construction costs of a typical commercial building. For example, a high-tech fabricating facility may have contents that are worth many times the value of the building and built-in components of the building. The nonstructural property losses can be much larger if they occur at library and museum facilities whose function is to store and maintain valuable contents. For example, as a result of the 1989 Loma Prieta Earthquake, two libraries in San Francisco each suffered over a million dollars in damage to building contents. Many of the artworks were toppled and damaged during the earthquake.

In addition to life safety and property loss considerations, there is an additional possibility that equipment damage will make it difficult or impossible to carry out the functions that were normally accomplished in a facility.  Similarly, mechanical components like compressed gas cylinders and fire extinguishers are anchored to carts for mobility and carts kept free-standing. In the case of a seismic excitation, they are vulnerable to damage. Unanchored cylinders may slide, overturn, and roll; connected piping may be damaged. Contents may be flammable or hazardous which makes leaking more dangerous. During magnitude-6.7, Northbridge earthquake in 1974 many of the free-standing gas cylinders were overturned due to inertial forces generated by seismic motions as shown in Fig.1-2.

Moreover, there are electrical and communications equipment like tall, narrow floor-mounted electrical items in sheet metal cabinets such as electrical control panels, motor control centers, switchgear etc. In the case of earthquake excitation, there is a possibility of overturning or sliding due to the absence of anchorage or inadequate anchorage, loss of function due to the failure of internal components caused by inertial forces. In addition to that, damaged electrical equipment may cause electrical hazards and fire hazards.

In the Mexico earthquake during 1985, many free-standing electrical equipment were toppled due to inertial forces as shown in Fig.1-3. Similarly, unanchored control panels of a power plant had been damaged due to excessive sliding and overturning during Haiti earthquake as shown in Fig.1-4. All these failures indicate behavior of free-standing components. It can be observed that failure of any free-standing component is mainly governed by the rigid body sliding and rotational motion arising due to inertial forces. If this rigid body motion is arrested with adequate anchoring, then seismic performance can be enhanced.

**Figure 1-2 Unanchored tanks inside fenced enclosure overturned in the 1994 magnitude-6.7 Northridge Earthquake (Photo courtesy of OSHPD, FEMA E-74)**

**Figure 1-3 Overturned equipment in the 1985 magnitude-8 Mexico Earthquake, note absence of anchorage of equipment base to the floor (Photo courtesy of Degenkolb Engineers, FEMA E-74).**

**Figure 1-4 Damage to unanchored electrical cabinets at a power plant in Port-au-Prince in the 2010 magnitude-7 Haiti Earthquake (Photos courtesy of Eduardo Fierro, BFP Engineers, FEMA E74).**

In a nuclear industry, some critical equipment like glove boxes as shown in Fig.1-5 are not anchored to the base. When excited by a base excitation, these equipment may respond in rigid body modes like sliding, rocking, lift-off or in flexural deformations. Stability and integrity of glove boxes are of prime concern. Any breach of integrity or stability due to seismic excitations may have serious safety consequences. [2]

The research carried out as a part of this thesis emanated from a fundamental question - Does a free-standing glove box is seismically safe for earthquake excitations? Hence all the studies carried out focuses on the generic evaluation of seismic performance of free-standing systems like glove boxes. Initial studies present experimental and numerical studies on simple test models representing rigid and flexible components. Finally, extensive studies carried out to determine the seismic stability of actual free-standing glove boxes are presented.

**Figure 1-5 Glove boxes freely standing in a radiological laboratory**

## 1.2 Problem Statement and Scope of Work

Excited by a base excitation, a free-standing body, resting on a rigid floor may undergo various possible rigid body modes of motion like sliding, rocking, rotation, a combination of sliding-rocking-rotation and even complete lift off from the base. In addition to that, a component with a finite stiffness can also exhibit flexible modes of motion.

Important parameters which affect stability of a free-standing body can be given as below:

i. Base motion characteristics like harmonic, pulse and seismic or random excitations.
ii. Geometric properties of the structure like, mass distribution, inertia and aspect ratio.
iii. Contact interface properties in tangential and normal direction.

Consider an arbitrary two-dimensional body, resting freely on a rigid floor, and subjected to base excitations in horizontal ($\ddot{X}_g$) and vertical ($\ddot{Y}_g$) directions, as shown in Fig.1-6. Parameters required to represent any three-dimensional rigid component in two dimensions are location of center of gravity (c.g.) and position of rocking edges with respect to the center of gravity. In present case distance of c.g. is given by $R_1$ ($B_1$, H) from the left rocking edge ($O_L$) and by $R_2$ ($B_2$, H) from the right rocking edge ($O_R$). Critical angles of rotation about left and right edges are given by $\alpha_1$ and $\alpha_2$ respectively. Critical angle about any edge of a rocking body is the maximum uplift angle above which a body becomes unstable and overturn by the inertial moment arising due to self-weight. Asymmetric body shown in Fig.1-6 can be simplified for numerical calculations by assuming uniform mass distribution around C.G. This reduces the number of parameters required for defining position and shape of the body at any instant of time. In a simplistic case of a rectangular symmetric body, $R_1=R_2$, $B=B_1=B_2$ and $\alpha=\alpha_1=\alpha_2$. This rectangular block representation of a rigid body in two dimensions is widely referred in the literature.

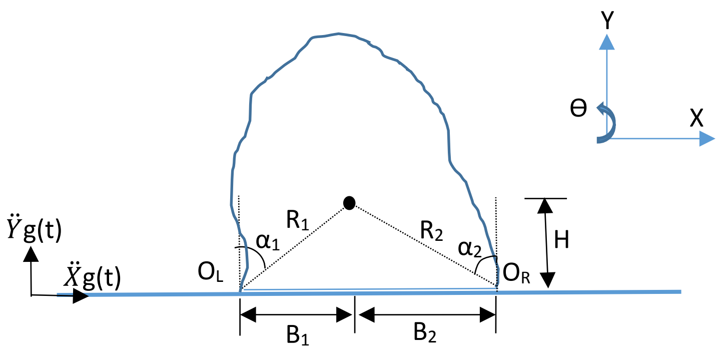


**Figure 1-6 A free-standing body in two dimensions subjected to base excitations**

Hence, with the assumption of a symmetrical rectangular rigid body as shown in Fig. 1.7, equations of motion for possible modes of rigid body motions can be derived. Different possible modes of motion are sliding, rocking, uplift, rotation (in three dimensions) and any combination of the above. For a simple sliding motion, equations of motion can be framed by taking equilibrium of all the forces acting on the body. Derived equations of motion (Eqns.1.1 & 1.2) are nonlinear due to the presence of friction at contact points.

$$M\ \ddot{X}\ (t) + Sgn\ (\dot{X}(t))\ F_F\ (t) + M\ \ddot{X}_g(t) = 0 \qquad 1.1$$

$$F_F\ (t) = \mu\ M\ (g \pm \ddot{Y}_g(t)) \qquad 1.2$$

Here, M- mass of the block, $F_F$ (t) - frictional resistance at the interfaces and X(t)- sliding displacement of the block. Similarly, Equations of motion for rocking motion can be obtained by taking equilibrium of moments about either center of gravity or pivoting edge. Balancing moments around a pivoting edge, we can write:

$$I\ \ddot{\theta} = M\ \ddot{X}g\ (t).\ R\ Cos\ (\alpha-\theta) - F_N\ (t).\ Sin\ (\alpha-\theta) \qquad 1.3$$

$$F_N\ (t) = M\ (g \pm \ddot{Y}_g\ (t)) \qquad 1.4$$

Here, I- mass moment of inertia about an edge, $F_N$ (t) - time dependent normal reaction force, θ (t) - angular rotation from the base. Moment equilibrium equations (Eqn.1.3) can be written about both the pivoting edges. Derived equations will be similar in form, with a difference of sign of vertical force component. Hence, derived equations are discontinuous which can be suitably integrated by using a scalar parameter whose sign depends on the rotation of the block. Moreover, every change of direction involves an impact with the base, which adds nonlinearity in otherwise discontinuous equations of motion.

The mathematical formulation in two dimensions should consider three possible rigid body motions a body can undergo. A meticulous investigation of various boundary conditions like motion initiation, transition between different modes and motion termination is required for obtaining time-varying solution. An analytical solution is possible only for very limited cases like small rotation without impact or pure sliding motion with linear friction law. To find exact position of the body during motion, it is required to numerically integrate governing equations of motion and consistently check for transition conditions from one mode of motion to the other.

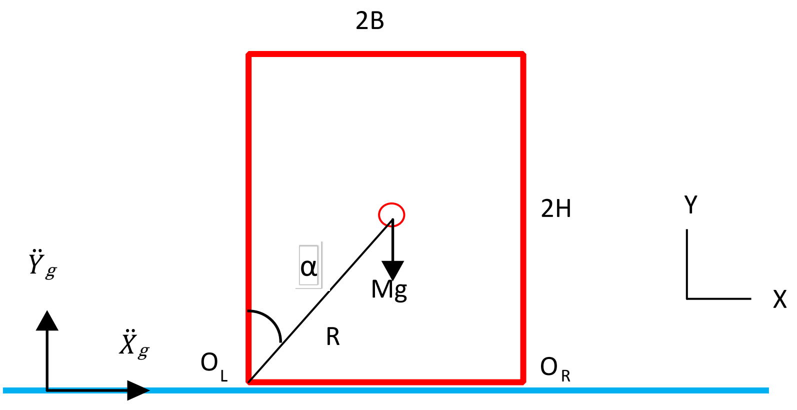


**Figure 1-7 A Symmetrical rectangular rigid body in two dimensions**

Consider a simple cantilever model, as shown in Fig.1-8, where mass of a body is lumped at the center of gravity. Two beam elements are connected together for representing effective height and width of the block. In case of a rigid body, beams are considered as very stiff and body may slide or rock rigidly as shown in the Fig.1-8. Removing the rigid body assumption, introduces additional degree of freedom, due to elastic bending of the beam (shown by dotted blue line). This adds one more dimension to the existing nonlinear problem. It is important to note that equations of motion developed with a rigid body assumption, neither consider elastic effects arising due to stiffness nor vibrational damping due to material characteristics.

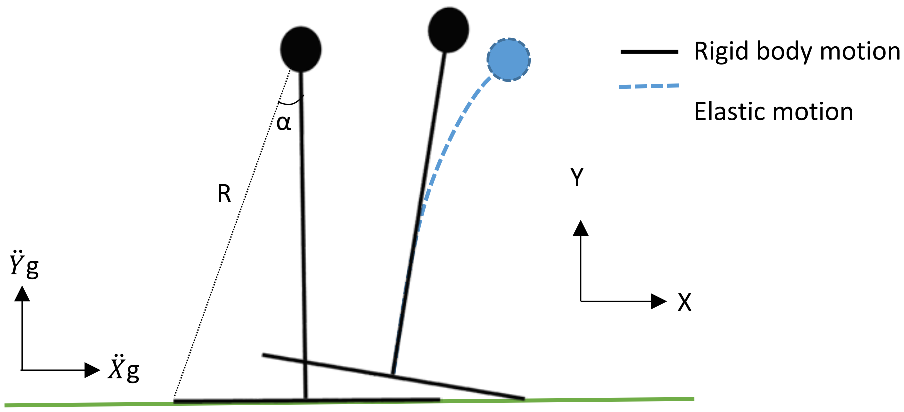


**Figure 1-8 Simple beam model showing possible rigid body and flexible planar motions of a body subjected to base excitations**

In Fig.1-8, base accelerations in X and Y directions are given by $\ddot{X}_g$ and $\ddot{Y}_g$ respectively. Equations of motion to be framed in a fixed Cartesian Coordinate system considering dynamic equilibrium of all the forces acting on the body.

Dynamic behavior of free-standing flexible bodies is geometrically nonlinear due to large displacements/rotations and low strains. Study of its behavior requires investigation of various parameters affecting stability and integrity.

The scope of work includes finding solution of the dynamic problem and identifying variables affecting seismic stability of free-standing rigid and flexible bodies. Further, develop a generic methodology to ascertain requirement of anchoring of nonstructural components. This research shall clearly bring out advantages and disadvantages of anchoring over not anchoring of a component.

This research is undertaken with a mandate of providing an answer to the persisting question "Whether a Glove box shall be anchored to the floor or not?"

With this objective in mind, experimental and numerical studies are planned to evolve a simple and robust methodology which can assist future nuclear facility designers to take an informed and correct decision about anchoring/non-anchoring of glove boxes.

## 1.3 Organization of Work

The thesis is divided into seven chapters. Chapter 1 (present chapter) is the introduction chapter which gives brief outline of the work. The problem being studied is discussed. It briefly highlights scope of the research.

Chapter 2 gives background of the problem being studied. It presents relevant literature available on the topic. Reported work on dynamics of flexible and rigid freestanding structure is presented. Surveying past research, the pertinent aspects of each work is recognized and placed in context. Although a major portion of literature is presented in this chapter, still some of the literature having direct relevance with the chapters is presented there. Hence some overlap between them is inevitable. Gap areas are highlighted and objectives of research are underlined.

Chapter 3 explores fundamental dynamics of a free-standing rigid body. A three-dimensional rigid test model was fabricated and tested on a shake table. A rigid parallelepiped model was deliberately selected to utilise and compare data readily available in the literature. An Analytical formulation for the symmetric model in two dimensions is presented. Moreover, experimental findings of shake table testing are highlighted and compared with the numerical calculations.

Chapter-4 presents dynamics of a free-standing flexible body. A flexible test model was fabricated using plates and beam sections. Effects of finite stiffness on dynamic behaviour of a non-structural component are presented. Moreover, experimental and numerical results highlighting significance of natural rocking frequency of a flexible structure in initiation of rocking motion are presented. A comparison between experimental and numerical results of geometrically similar rigid and flexible test models is drawn. Important differences in fundamental dynamic behaviour of geometrically similar (same aspect ratios) rigid and flexible bodies are highlighted.

After analysing behaviour of rigid and flexible test models in Chapters 3 and 4, Chapter-5 investigates dynamics of a glove box, used as a containment structure in nuclear facilities. Seismic stability of this component under design basis and beyond design basis earthquakes is studied. It is a flexible structure, which is critical component of a nuclear facility. Similarities in fundamental dynamic behaviour of flexible test models analysed in Chapter-4 and flexible glove box structure are highlighted. Effects of free rocking frequencies in motion initiation are studied. It also presents a generalised methodology to evaluate requirement of anchoring of a glove box to the floor. This can act as a guideline for existing and future facilities, which can help the decision makers to take informed decision to prevent components failures and damage during earthquakes.

Chapter-6 further extends work done in Chapter-5 to present generalized methodology for assessment of seismic stability of multiple interconnected glove boxes. Methods developed in Chapter-5 are extended to a more generic case of series of interconnected glove boxes. Two configurations are considered. In the first configuration, both the boxes are connected by a flexible link (material transfer tunnel) which can constrain relative motion between the boxes to a very limited extent. While in the second configuration, relative movement between the boxes is completely arrested using rigid links. Chapter-6 investigates case of the first configuration while Chapter-7 discusses the details of second possible configuration. It also compares seismic stability of both the configurations

Chapter 8 highlights important results and final conclusions drawn from the study carried out as a part of this research program. Significant contributions to the scientific community are highlighted. Finally, it gives the direction for the possible future work in the field of dynamics of free-standing components and discusses limitations of the present work.

# CHAPTER 2 LITERATURE SURVEY

## 2.1 Outline

Seismic stability of free-standing bodies with limited permissible uplift has been attracting the interest of researchers for more than a century now. Studies carried out in the field of structural dynamics were driven by the basic assumption that foundation can undergo limited uplift. This resulted in the evolution of analytical models which can very well handle the rocking motion of a structure but doesn't allow any sliding. However, there were few systematic studies which consider effects of all possible modes of motion (rocking and sliding) in the developed analytical model. Many of the studies considered the body to be rigid, while few of them relaxes rigid body assumption in deriving equations of motion. Therefore, for a clear understanding, this chapter is divided into two main sections. Section 2.2 ensembles literature available on the dynamics of a freestanding rigid body subjected to base excitations. It is further divided into three parts; first part present works carried out considering pure rocking motion, while the second and third part present works carried out considering the pure sliding motion and combination of both respectively. Section 2.3 ensembles literature available on the dynamics of a flexible body subjected to base excitations. This section is also divided into two parts. The first part gives literature available on the pure rocking behavior of flexible bodies, while second part gives literature available on the combination of rocking and sliding behavior of flexible bodies. Further, Section 2.4 presents shake table test data generated as a part of extensive testing carried out by a team of engineers from BARC and CPRI. Finally, Section2.5 highlights the gap areas existing in the present literature and the direction for the present research work.

## 2.2 Dynamics of Freestanding Rigid Bodies

A large part of research available on the subject stems from the basic premise that a freestanding body can be assumed as a rigid body. Motivated by the overturning stability of a structure, significant amount of research was carried out by engineers working in the domain of structural dynamics and earthquake engineering. Some of the early investigations in the field started with the observations on the uplift, rocking, or overturning, of a variety of slender structures such as equipment, retaining walls, liquid storage tanks, and rigid building structures following strong earthquakes. The need to understand and predict these failures, along with a craving to estimate levels of ground motions by examining overturning of slender structures, had motivated a number of studies on the rocking response of rigid blocks [3] [4] [5] [6] .

### 2.2.1 Rocking Mode of Motion

A free-standing structure can be modeled as a rigid body allowed to uplift or rock on the rigid foundation. This was a predominant assumption with which a lot of researchers had carried out research work. However, there were studies which had incorporated effects of foundation flexibility on overall dynamics of a freestanding structure. These studies were more relevant for the civil structure which stands on the soil. Hence soil-structure interaction modeling became important. The simplest and most widely used analytical model of a rocking structure was a rectangular, uniform, rigid mass resting on a rigid base and pivoting about its corners 0 or 0' as shown in the Fig.2-1. On changing direction of rocking from one edge to the other (impact), energy is lost. The first systematic study of the dynamic response of a rigid yet slender block supported on a base undergoing horizontal acceleration was presented by Housner [7]. He examined the free and forced vibration responses to rectangular and half-sine pulse base accelerations. It was assumed that the limiting friction force is large enough to ensure that no sliding will occur between the block and supporting foundation. Using an energy approach, he presented an approximate analysis of the dynamics of a rigid block subjected to a white-noise excitation, uncovering a scale effect that explained why the larger (larger *R in* Fig. 2-1) of two geometrically similar blocks (same aspect ratio) could survive the excitation while the smaller block topples. Housner also pointed out that the overturning potential of a pulse is characterized not merely by its acceleration amplitude but by the product of its acceleration amplitude and duration. This work was limited only to the study of rocking behavior of a rigid block. No consideration of sliding motion or combination of both was given while deriving governing equations of motion.

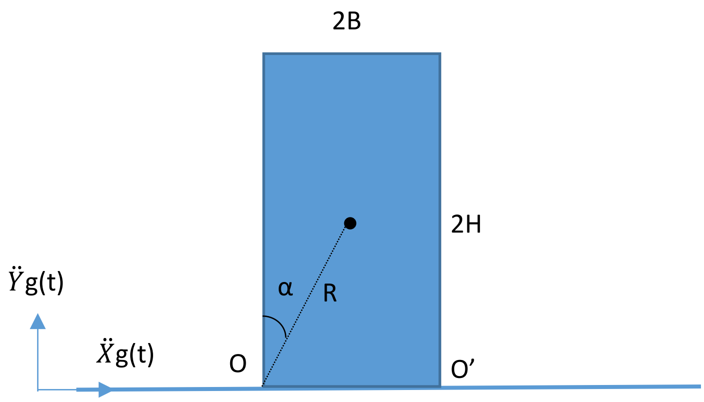


**Figure 2-1 A simple rectangular rigid block model**

Motivated by the need to investigate the response of solid concrete blocks used as radiation shields in particle accelerator laboratories, Aslam et al. [8], conducted shake table and analytical studies on the rocking and overturning of rectangular blocks of various sizes, R, and aspect ratios. It was concluded that, in general, the rocking response of blocks subjected to earthquake motion was in line with the conclusions derived from single pulse excitations. However, when artificially generated motions were used, the response showed high sensitivity to the coefficient of restitution, base geometry and characteristics of the input motion.

Yim et.al [9], numerically investigated the rocking response of a rigid block. They investigated the effect of geometric properties of the block (slenderness and size) and variation of ground motion on the rocking response and observed no systematic trend. Hence, it was concluded that probabilistic estimation of rocking behavior was more reliable and accurate than deterministic studies. It was observed that the probability of a block exceeding a certain response level, or of overturning, increases with increase in ground motion intensity, decrease in aspect ratio and decrease in size.

Ishiyama [10], investigated rigid body motions of a free-standing body subjected to base excitations. He introduced significance of tangent coefficient of restitution to estimate the magnitude of the tangent impulse at the instant of impact. The numerical investigation was carried out to determine criteria for the overturning of rigid bodies. He observed that the motions after impact from translation jump are greatly influenced by the normal and tangent restitution coefficients. The Importance of two factors: horizontal acceleration and the velocity of the floor were highlighted in determining overturning stability.

Lipscombe [11] experimentally and analytically investigated the free rocking of a prismatic block supported on a rigid stationary base. It was reported that the free-rocking response of short blocks depends critically on bouncing after each impact. Out-of-plane effects were significant and hence can't be ignored for short blocks. However, they found that the response of slender blocks was easier to predict.

Makris and Roussos [12], examined in depth the transient rocking response of a rigid block subjected to trigonometric pulses and near-source ground motions. They showed that under a half-sine pulse, a block overturns during its free-vibration regime and not at the instant the pulse expires. The coherent component of some near-source acceleration records was examined. It was concluded that the toppling of smaller blocks was more sensitive to peak ground acceleration, while the toppling of larger blocks was more sensitive to incremental ground velocity. Furthermore, the high-frequency fluctuations that override a long duration pulse will topple a small block, while a large block will topple because of the long duration pulse itself.

Zhang and Makris [13]studied the effect of cycloidal pulses on the overturning potential of a rigid block. The dynamic interface forces that develop during rocking motion were derived, and it was shown that the level of the friction coefficient needed to sustain rocking motion during the entire duration of the pulse is an increasing function of the acceleration level of the pulse. They established that under cycloidal pulses, a free-standing block can overturn with two distinct modes: (1) by exhibiting one or more impacts; and (2) without exhibiting any impact. The existence of the second mode resulted in a safe region that was located on the acceleration-frequency plane over the minimum overturning acceleration spectrum. This safe region contained acceleration amplitudes with magnitudes larger than the minimum overturning acceleration (which corresponds to mode 1) and was unable to overturn the block. It was found that the shape of this region depends on the coefficient of restitution and is sensitive to the nonlinear nature of the problem. The transition from mode 1 to mode 2 is sudden and results in a finite jump in the minimum overturning acceleration spectrum. They concluded that the sensitive nonlinear nature of the problem, in association with the presence of the safe region that embraces the minimum overturning acceleration spectrum, complicates further the task of estimating the peak ground acceleration by only examining the geometry of freestanding objects that either overturned or survived a ground shaking.

Makris and Konstantinidis [14], investigated systematically the fundamental differences in a fixed base SDOF oscillator system and rocking base SDOF oscillator system. The idea was to evaluate the effectiveness of response spectrum method for the structures allowed to uplift. The study concluded that a rocking structure cannot be replaced by an equivalent SDOF oscillator and that the simple design approach presented in Priestley et al. [15] and adopted in FEMA

356 [16] was flawed. This conclusion motivated the proposal to use the rocking spectra as an additional measure of earthquake intensity. Together with the response spectra, rocking spectra can provide a more lucid picture of the kinematic characteristics of ground motions and their implications on the response of rigid, yet slender, structures. It was also concluded that exact rocking spectra (plots of max angle (ϕ) versus the frequency parameter (*p*) and max angular velocity ($\dot{\emptyset}$) versus (p) emerge as distinct intensity measures of a ground motion.

Prieto et al. [17] presented a Dirac-delta interaction as an impact mechanism alternative to the classical method of using the coefficient of restitution to account for energy lost during the impact of a rocking block. The agreement with the classical system was excellent for slender block and for small rotations and good agreement was found with the experimental data. The approach was attractive in that it appears amenable to a more generalized formulation for the case of a multi-block assembly in rocking motion.

Prieto & Lourenco [18], introduced a formulation for the rocking motion of a rigid block. The traditional piecewise equations were replaced by a single ordinary differential equation. In addition, damping effects were introduced by means of impulsive forces instead of using the coefficient of restitution as done earlier.

Chen et.al [19] explored the feasibility of utilizing a rocking mechanism as an effective means of seismic isolation. Authors have performed experiments on a scaled down model and subsequently numerical simulations to demonstrate the effectiveness of rocking mechanism for seismic isolation of viaduct pier structures. It was also shown that stronger the earthquake intensity the more pronounced the control efficiency.

Pena et.al [20]performed extensive shake table tests to study the rocking response of granite stones with different geometrical characteristics. Various tests were performed like free vibration, harmonic, and random base excitations. They compared generated experimental data with the numerical results available in the literature. They highlighted effects of three-dimensional motions during two directional testing (horizontal and vertical) for a nearly square base parallelepiped blocks. Hence concluded that it is important to consider three- dimensional effects even for two-directional excitations for square base structures.

Zhang et.al [21]proposed multiple impact model with coulomb friction that allows one to correctly determine rocking behavior of a rigid block. They used free rocking experiments to fit the impact law parameters. Several existing experimental records were utilized to benchmark the proposed impact model.

Egidio et.al. [22]analyzed the rocking response of a three-dimensional parallelepiped block. Main objectives were: experimental characterization of the overturning of a rigid block in the shape of a parallelepiped and with a square base and validation of the results obtained by the model developed by Zulli et.al [23]through a campaign of experimental tests. The experiments with a rigid wooden block had shown that the angular region of 3D rocking motion, where the overturning amplitude was smaller than the one of a 2D rocking motion, decreases for higher periods of the excitation. The experimental results confirmed that, for near-square based bodies, a three-dimensional model provides more accurate results than the classical bi-dimensional models.

Dimitrakopoulos and Paraskeva [24]investigated seismic fragility of single degree of freedom rocking structures within a probabilistic framework. They focused on slender rigid structures that exhibit negative stiffness during rocking. The analysis considered ground motions with near-fault characteristics, either solely coherent pulses or synthetic ground motions that include, in addition, a stochastic high-frequency component. They proposed normalized fragility curves that estimate the overturning tendency, as well as the peak response rotation of a rocking structure. The study advocated the use of dimensionless–orientation less Intensity

Measures (IM's), a normalized description almost indifferent to the amplitude and the predominant frequency of the excitation or the size and the slenderness of the rocking structure. Importantly, they highlighted a critical peak ground acceleration, below and above which, peak rocking response scales differently.

### 2.2.2 Sliding Mode of Motion

Sliding is a possible mode of motion of a freestanding structure provided that some conditions are fulfilled. Under favorable values of coefficient of friction and amplitude of base excitation, sliding initiation may take place. In a way, sliding may be a favorable response since it doesn't involve risk of overturning. Nevertheless, large displacements may hamper integrity of the structure itself and even endanger stability and integrity of a nearby structure. Hence there is always a need to constrain sliding displacements within allowable limits.

The sliding of a freestanding object is governed by the frictional resistance of the contact interface between the object and the base on which it rests. The French physicists Amonton [25] and Coulomb [26] were the first to note that dry friction is a manifestation of the roughness along the contact between bodies. Amonton observed that the force of friction is directly proportional to the weight of the object and that friction is independent of the surface area in contact. Coulomb added that the friction force of an object in motion is independent of the velocity

The sliding response of a rigid mass on a moving base had been examined by investigators within the context of earthquake engineering for the purpose of estimating sliding displacements of nonstructural components and equipment such as the ones that are of interest in this study. The solution for the response of a rigid block subjected to a rectangular pulse base acceleration provided by Newmark in 1965 had generated interest [27]. Using an ensemble of 75 earthquake records, Choi and Tung [28]obtained numerical solutions for the maximum sliding displacement of a rigid body subjected to those ground motions and to floor motions of a 5-story building. After an averaging procedure, the peak sliding responses were compared to the responses estimated by Newmark's formula [27]for a rectangular pulse. The authors concluded that Newmark's formula can be used with a reasonable accuracy.

Garcia and Soong [29]investigated the vulnerability of a sliding rigid body to a suite of synthetic earthquake motions generated on the basis of current seismic codes. Sliding displacements and absolute accelerations above a defined value were considered as failure modes. A collection of fragility curves (curves that give the conditional probability of failure: the probability that some quantity, e.g., sliding displacement of a piece of equipment, will exceed a certain threshold, given the intensity of the excitation) were generated using Monte-Carlo simulations for different friction coefficients with peak base acceleration being the random variable. In a companion paper, Garcia and Soong [30]investigated the response of a restrained rigid body with restrain breakage and excessive absolute accelerations being the failure modes. Fragility curves were again generated using Monte-Carlo simulation.

Hutchinson and Chaudhuri [31]conducted shake table and field experiments on different bench-shelf configurations and small equipment and contents mounted on benches and shelves. They observed a significant amplification in acceleration between the benches or shelves and the floors, ranging from 1.4 up to 4.3 for different boundary conditions. It was concluded that unless the amplification effect is taken into account, estimated sliding displacements of small equipment mounted on shelves and benches above floor level will, in general, be un-conservative.

Taniguchi and Miwa [32] proposed a simple procedure for estimating absolute maximum slip displacement of a freestanding rigid body placed on the ground or floor of linear/nonlinear multistory building during an earthquake. They used displacement induced by the horizontal sinusoidal acceleration to approximate the absolute maximum slip displacement. The effect of vertical acceleration was considered to reduce the friction force.

### 2.2.3 Combination of Sliding and Rocking Mode of Motion

Under suitable values of system parameters like coefficient of friction and amplitude of base excitation, a free-standing structure, in a plane, can undergo combination of sliding and rocking motion.

Ishiyama [10]investigated response of a freestanding rigid block in a plane and subjected to one-dimensional base excitation. He investigated motions of a rigid body in response to earthquake excitations, using the computer simulation program which classified the types of motion into six (rest, slide, rotation, slide rotation, translation jump and rotation jump). Several types of simulations were conducted to study the characteristics of motions and overturning of bodies. Criteria for the overturning of bodies were proposed after experiments and simulations of frequency sweep tests. He concluded that it is possible to estimate the lower limits of the maximum horizontal acceleration and velocity of the input excitations from the overturning of bodies.

Shenton and Jones [33] [34]presented general two-dimensional formulation for the response of free-standing rigid bodies to base excitation. The behavior was described in terms of five possible modes of response viz. sliding, rocking, slide-rocking, and free flight. A model governing impact from a rock, slide-rock or free flight mode was derived from first principles using classical impact theory. This model assumed a point impact and non-zero coefficient of friction. A generalized formulation for the planar rigid body dynamics was presented. In a companion paper, approximate closed-form solution for a single-mode, steady-state slide-rock response resulting from a harmonic ground acceleration was presented. The approximate solution was developed using the method of slowly varying parameters and was valid for a rectangular block undergoing small angles of rotation at the frequency of base excitation. Impacts with the foundation were assumed to be perfectly plastic and frictional impulses were included. Periodic solutions were found to exist in general only for relatively high amplitudes of ground acceleration and frictionless than the inverse aspect ratio of the block. The rock component of the response was sensitive to changes in aspect ratio and friction and insensitive to changes in ground acceleration. The slide component of response was approximately equal to the amplitude of ground displacement and found to be insensitive to changes in friction and aspect ratio. The accuracy of the approximate solution was shown to depend heavily on the magnitude of impulse applied during impact.

Early researchers had a feeling that initiation of combined rocking and sliding motion from rest state was not possible. Only after analytical formulation presented by Shenton and Jones [35], possibility of initiation of combination of sliding and rocking motion from the rest was shown.

Their work resulted in evolution of motion initiation criteria diagrams [35] as shown in Fig.2-2. This diagram pictorially represented initiation of any planar mode of motion from the rest state. Boundaries of various possible planar modes of motion were shown in the diagram. Abscissa of the figure is represented by a non-dimensional amplitude parameter-$A_g$, given as $\ddot{X}_g(t)$= $A_g$.f(t). Where, f (t) is the time-varying component of base acceleration. On the other side, ordinate of the graph is given by a non-dimensional term $\mu_s$, representing coefficient of friction. The results demonstrated that it was incorrect to assume that a rock mode will govern, if static friction coefficient ($\mu_s$) is simply greater than the inverse aspect ratio of the block *(B/H* <$\mu_s$). Here, B and H was width and height of the block respectively. A slide-rock mode governs for friction greater than the inverse aspect ratio, but less than that given by Eqn.2.1.

$$\left|\frac{f_x}{f_y}\right| = \left|\frac{3\gamma+4A+\gamma^2 A}{1+4\gamma^2+3\gamma A}\right| \leq \mu_s \qquad 2.1$$

Here $f_x$ and $f_y$ were horizontal and normal reactions at the base respectively. $\Upsilon$ and $A_g$ are inverse of aspect ratio and amplitude of base motion respectively. Value of friction required to sustain a rock mode increases with the magnitude of base acceleration. These results suggested that analyses of pure-rocking response, in which the available static friction was just greater than the width-to-height ratio of the body, was most likely in error (i.e., could not be physically realized). The criteria derived demonstrated a more natural transition from pure sliding to pure rocking when viewed in the $\mu_s$ versus $A_g$ parameter space, than found in the traditional criteria for initiation.

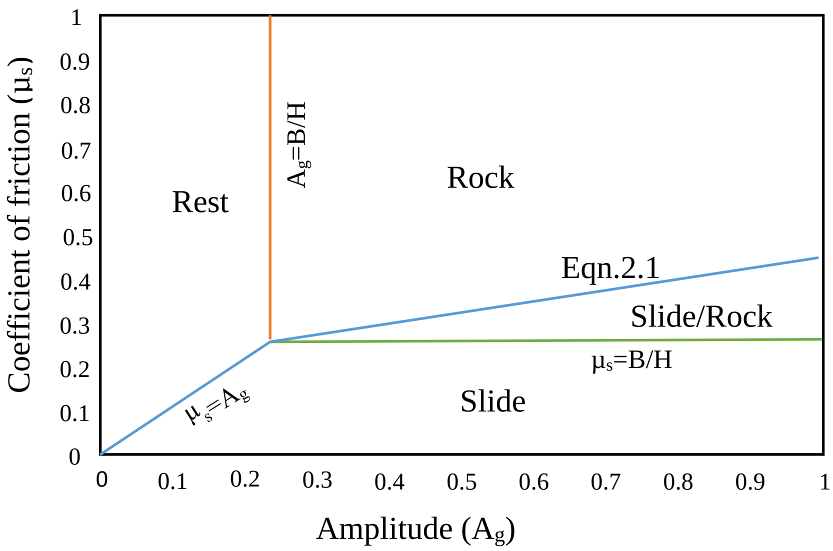


**Figure 2-2 Motion initiation criteria diagram for a block of aspect ratio of four**

Further working on diagrams proposed by Shenton and jones, Shao and Tung [36], carried out extensive numerical calculations to develop motion initiation criteria diagrams for various possible values of aspect ratios. Using an ensemble of 75 real earthquakes records, they plotted graphs showing mean plus standard deviation of the sliding distance relative to the base. Graphs showing the probability of overturning during rocking mode of motion were developed.

Andreaus and Casini [37] and Jeong et.al [38]investigated influence of nonlinearities associated with impact and sliding upon the rocking behavior of a rigid block, subjected to two-dimensional horizontal and vertical excitation. Highly nonlinear nature of the problem was mathematically revealed using a series of Poincare maps and bifurcation diagrams.

Taniguchi [39] investigated non-linear seismic responses of free-standing rectangular rigid bodies on horizontally and vertically accelerating rigid foundations. The responses were classified into two initial responses namely pure sliding and rocking and four subsequent responses including combination of sliding and rocking motions. The equations of motion governing the lift-off, slip and lift-off–slip interaction motions and boundary conditions corresponding to commencement and termination of the motions were derived. Numerical calculations using two recorded accelerograms were carried out to examine effects of earthquake properties on the response. Intensities and the value of friction coefficients were varied. In addition, to highlight the effects of vertical ground motion on the responses, the intensity of vertical ground motion was also varied. It was concluded that the body on a low-grip foundation may avoid overturning, even though subjected to high-intensity base excitations, while it should be allowed to have large slip displacement. In contrast, the body on a high-grip foundation may be overturned. Sufficient friction can be used to judge the grip condition during the entire motion. The long-period earthquake may raise the risk of large slip displacement and overturning of the body, since it may possess prolonged favorable horizontal accelerations for a slip and lift-off. The lift-off–slip interaction motion may occur in limited conditions and may reduce the slip displacement. The vertical accelerations helped to begin the lift-off–slip interaction motion by sufficiently reducing the friction. Since vertical accelerations add irregularities to responses of the body, it cannot be ignored when evaluating the responses of the body. In addition, to simulate actual motions of the body, governing equations of motion derived from a view of non-linear discontinuous systems were necessary.

Egidio and Contento [40], analyzed influence of the base isolation on the behavior of rigid blocks representing works of art. In order to better understand the behavior of a real base isolated art object, it had been modelled as non-symmetric rigid body, where the centre of gravity was not equally distant from the two base corners. The rigid body was sat upon a base which was connected to a linear viscoelastic device representing a passive control system. Security stops had been introduced to prevent the breaking of the isolation devices for very high displacements of the oscillating base. Both rocking and sliding motions had been considered in the model. Exact nonlinear equations of motion were written for the different phases of motion: full-contact, sliding, rocking, slide-rocking; transition phase conditions were also derived. Two different kinds of collapse condition were considered: the fall from the oscillating base of the rigid block, and the overturning of the body. To evaluate the performance of the base isolation, the results had been compared with those obtained for the non-isolated rigid block for two types of external excitations: impulsive and seismic excitations. They also generated motion initiation criteria diagrams for the base isolated free-standing structures.

Extensive experimental and numerical investigation to study seismic behavior of freestanding laboratory equipment was carried out by Konstantinidis and Makris [41] [42]. In the earlier paper [41], authors presented experimental and analytical studies on the seismic vulnerability of freestanding laboratory equipment located on various floor levels of a research laboratory building located at the University of California, Berkeley, campus—herein referred to as the UC Science Building. The equipment of interest included low-temperature refrigerators, freezers, incubators, and other heavy equipment. The study investigated the response of equipment to moderately strong motions (50 and 10% probability of being exceeded in 50 years) which resulted in Peak Ground Displacements (PGD) or Peak Floor Displacements (PFD) that could be accommodated by the shake table at the Pacific Earthquake Engineering Research (PEER) Center, University of California, Berkeley. Shake table tests showed that there was no incidence of overturning due to excessive uplift. Uplift rotations ranged from very low, for two of the three specimens, to moderate, for the third, never exceeding 50% of the stockiness, α (the angle between a vertical line and the line that passes through the pivoting point and the center of mass of the equipment). For motions in this hazard level, the equipment tested exhibited excessive sliding displacements, reaching up to 60 cm. The results of the tests were used to develop a dimensionless Engineering Demand Parameter (EDP) (a parameter that quantifies the response of the equipment), as a function of the Intensity Measure (IM) (a parameter of the excitation that corresponds to a certain seismic hazard level). Ready-to-use fragility curves, which give the probability that the EDP will exceed a specific limit c, were generated.

In the companion paper [42], they investigated the seismic response of freestanding equipment when subjected to strong earthquake motions (2% probability of being exceeded in 50 years). A two-step approach was followed because the displacement limitations of the shake table do not permit full-scale experiments. First, shake table tests were conducted on quarter-scale wooden block models of the equipment. The results were used to validate the commercially available dynamic simulation software Working Model 2D. Working Model was then used to compute the response of the full-scale freestanding equipment when subjected to strong, 2% in 50 years hazard motions. The response was dominated by sliding, with sliding displacements reaching up to 70 cm. A physically motivated dimensionless intensity measure and the associated engineering demand parameter were identified with the help of dimensional analysis, and the results of the numerical simulations were then used to obtain a relationship between the two that leads to ready-to-use fragility curves.

In an effort to understand effect of asymmetric mass distribution of a freestanding structure on its seismic stability, Wittich and Hutchinson [43]carried out an extensive shake table testing.

They presented dynamic tests on single, stiff unattached model structures. The centre of mass of the structure was systematically translated vertically and horizontally to investigate the effects of geometric eccentricities on the bodies seismic response. The primary modes of rocking, sliding, and twisting as well as interactive modes were recorded for the duration of numerous earthquake motions. The magnitude and direction of response were experimentally correlated with the geometric variations in the various models. These tests indicated that even for symmetric structures with uniaxial shaking, multiple modes, and three-dimensional responses were probable. Furthermore, certain asymmetric geometries exhibited both increased rocking (and overturning) as well as increased sliding when compared with their symmetric counterparts. A final aspect of this study compared the free rocking response of symmetric and asymmetric structures to classical, two-dimensional rocking analysis. While the theoretical values for the coefficient of restitution yielded a significant overestimation in the simulation (up to ≈90%), reduced coefficients greatly improved the performance of the model.

It is important to observe that none of the studies mentioned above, highlighted effects of base excitation frequencies on the motion initiation (sliding, rocking and a combination of two) of a rigid body.

## 2.3 Dynamics of Freestanding Flexible Bodies

Structural engineers working in the field of earthquake engineering had generated interest in examining seismic response of relatively flexible structures. This interest was generated mainly from the premise that some of the civil structures may be allowed to undergo limited uplift when subjected to earthquake motion. If the soil-structure interaction is ignored, then a civil structure standing on a rigid ground and allowed to uplift can be assumed as a freestanding body with limited rocking motion. This basic presumption led to formulation of analytical models for civil structure, which were analogous to that of a free-standing body with pure rocking motion without sliding. This section is divided into two parts. First part presents research work carried out on the dynamics of flexible bodies considering only rocking motion whereas second part focuses on research work carried out for studying combined effect of all possible mode of motion.

### 2.3.1 Rocking Mode of Motion

Motivated by the need to investigate seismic stability of a flexible structure, with a limited foundation uplift, researchers had investigated rocking dynamics of a flexible structure. These studies were mainly focused on to study the dynamic behavior of structures allowed to uplift and assess effect of uplift on structural deformations and quantify the base isolation effect provided by rocking motion.

The initial investigation that dealt with the uplift of the foundation in flexible system was experimental research conducted by Muto et al. [44], on the dynamical response of a lumped mass structure which in its fixed-base condition behaves as a single-degree-of-freedom system. Later, Meek [45], considered the same structural model and, from the analysis of the dynamical behavior in small displacements, concluded that uplifting leads to a favorable reduction in the maximum transverse deformation of the structure. Meek also conducted other studies on braced-core multistory buildings and found that tipping greatly reduces the base shear and moment, making a more economical design possible.

Yim and Chopra [9] considered the typical structural lumped mass model that, in its fixed base condition, has a single degree of freedom, and pointed out the influence of earthquake intensity, geometric parameters, soil flexibility and p-δ effects on the response of uplifting structures. They observed that, apart from very stiff structures, the uplift has the effect of reducing the structural deformations and forces. Later Yim and Chopra [46], developed simplified procedures to consider the beneficial effects of foundation-mat uplift in computing the earthquake response of structures which behave essentially as single-degree-of-freedom systems in their fixed-base condition.

Initial analytical analysis of the dynamic behavior of a simplified model of a multistory building, supported by an elastic foundation and allowed to uplift, was done by Psycharis [47] [48].The building was modeled as an n-degree-of-freedom shear-type frame while the foundation was represented by a viscously damped two-spring model which permitted uplift. The study showed that the dynamic behavior of structures allowed to uplift may be very different from the response of fixed base ones. From the analysis of the applications performed, Psycharis concluded that the uplift often decreases the structural response. He also observed that this is not a general result because the dynamical behavior of structures is strongly affected either by the structural parameters or by the nature of the excitation. Later, Psycharis [49] conducted a parametric study to evaluate the effect of base-uplift on the maximum response of a single degree of freedom structure on elastic soil for harmonic excitation and small displacements.

Till that time, all the studies on the effect of foundation uplift on the dynamical behavior of flexible systems had been conducted under the hypothesis of small displacements and therefore without considering the eventual overturning of the system. Oliveto et.al. [50] removed limitation of small displacements and presented analytical formulation considering overturning of the structure. The study had been conducted with reference to the model already considered by Meek, Psycharis, Yim and Chopra. Equations of motion had been formulated by using appropriate Lagrangian coordinates which led to a simple form and to a physical interpretation of the main characteristics of the dynamical behavior. The conditions for uplift had been expressed in terms of a critical displacement and of the correspondent velocity. The critical displacement turned out to be smaller for stiff structures and larger for flexible ones and was greatly affected by the vertical acceleration especially for flexible system. In particular, it increased when the vertical ground acceleration was directed upwards and decreases when was directed downwards. It had also been shown that the damping has the effect of reducing the critical displacement. Results led to the conclusion that the uplift has the effect of reducing the structural response and of modifying the frequency of the elastic oscillation. A scale effect had been observed showing that, when comparing two structures with the same geometrical ratio h/b and the same dynamic characteristics but different height of the mass center, the shorter one is more prone to uplift and overturning than the taller. It was shown that the minimum overturning impulse of a flexible system was always smaller than the corresponding impulse for the rigid system. Moreover, low and flexible structures overturn for an impulse only slightly larger than the uplifting one, while stiff and tall structures require an impulse several times larger. These latter structures may, therefore, benefit considerably from uplifting without a real danger of overturning. On the contrary, low and flexible structures were very resilient to uplift but they may overturn soon after they had uplifted thus canceling out the beneficial effects.

Acikgoz and Dejong [51], investigated fundamental dynamics of flexible rocking structures. Based on the analytical model proposed earlier [50], they derived nonlinear equations of motion, using a Lagrangian formulation for large rotations. Particular attention was devoted to the transition between successive phases; a physically consistent classical impact framework was utilized alongside an energy approach. The fundamental dynamic properties of the flexible rocking system were compared with those of similar linear elastic oscillators and rigid rocking structures, revealing the distinct characteristics of flexible rocking structures. In particular, parametric analysis was performed to quantify the effect of elasticity on uplift, overturning instability, and harmonic response. Invariably, rigid rocking structures uplift when the excitation amplitude exceeds g tanα. On the contrary, flexible rocking structures behave like linear elastic oscillators until uplift occurs. Therefore, the minimum amplitude required for uplift depends on the respective vibration characteristics of the system and the ground motion, and the geometry of the structure. They noted that until uplift occurs, the behavior of the system is governed by resonance and the scale and slenderness of the structure have no influence on this behavior. They carried out dimensional analysis which indicated importance of dimensionless term $\omega/\omega_n$ over $\omega/p$ and $\omega_n/p$. They observed that the minimum excitation amplitude required for uplift of a flexible structure may be much lower than what is required for a rigid structure, particularly when $\omega/\omega_n$ is close to unity. Alternatively, for high ratios of $\omega/\omega_n$, flexible structures require high amplitudes to uplift. In these cases, a rigid body will uplift when a flexible rocking structure may not.All these findings suggested that the interaction of rocking and elasticity cause an altogether distinct response, which demands meticulous attention.

More recently, Vassiliou et.al [52]investigated rocking response of a deformable cantilever structure. They extended previously developed analytical models to account for the influence of the column and the foundation masses on the behavior of top-heavy deformable elastic cantilever columns rocking on a rigid support surface. The column was treated as a continuous dynamic system with uniformly distributed stiffness EI and mass, and a concentrated mass on the top and bottom of the cantilever. Rocking uplift and overturning spectra for the deformable elastic cantilever model excited by sinusoidal ground motions were constructed. The presence of the column and base masses decreased the uplifted frequency (compared to the model with a single mass at the top) and therefore emphasized the effect of column flexibility. However, it was shown that for large structures or relatively high- frequency sinusoidal pulses, the effect of flexibility was still not detrimental to the stability of the structure. Thus, large deformable cantilever structures, such as tall bridge columns, chimneys and wind turbines, uplift and rock without overturning under dynamic ground motion excitation. This remarkable property can be used to limit the design bending moments and shear forces at the base of large deformable structures, thus making them more economical to construct while keeping the risk of overturning less than or equal to the risk of collapse of the corresponding fixed base structures.

In a companion paper, Truniger et.al. [53] presented experimental validation of the analytical results obtained earlier by Vassiliou et.al [52]. A series of experiments were performed to validate analytical models for rocking of deformable cantilever structures with massive columns and concentrated masses at the base and the top of the cantilever developed in a companion paper [52]. Specimens with four different fundamental vibration frequencies, mounted on two different uplifting bases, were excited by analytical pulses and real ground motions using a shaking table. The increase of viscous damping during flexural vibrations of the column in the uplifted configuration as observed by Acikgoz and Dejong [51], was not experimentally observed. Instead, a very small damping value (smaller than the fixed base damping value, but consistent with experimental observations) was used.

### 2.3.2 Combination of Sliding and Rocking Mode of Motion

There is absolute dearth of generic research available on fundamental dynamics of a flexible free-standing structure allowed to undergo all possible modes of motion. Most of the studies mentioned above focused only on the rocking mode of motion assuming sufficient frictional resistance to avoid sliding mode of motion.

In an effort to study effectiveness of base isolation system of a flexible structure, Wang and Guild [54] performed numerical analysis. They had investigated behavior of a structure incorporating the mechanism of uplift in the base mat and the foundation and the mechanism of sliding between the superstructure and the basement. The idea was to study the possible beneficial effects, as compared to a structure permitting partial base uplift only. A two-mass model of system uplift with sliding was proposed. The equations of motion for the phase of full contact, phase of base uplift and transformation of these two phases were derived. The numerical integration of the equations of motion was carried out. The time history of the top floor displacement of the proposed system, as compared with that of a conventional system with uplift but no sliding mechanism, showed that no sharp peak and high-frequency responses occurred. Both the time history and response spectrum results showed that the total displacement of the top floor for the proposed system was considerably reduced, as compared with that of the conventional system allowing partial base uplift only. Both analyses also show that the maximum amount of uplift for the proposed system is greatly reduced as compared with that of the conventional system. They concluded that the structure with both uplift and sliding mechanisms was superior to that with only the uplift mechanism. Not only is the response of the structure reduced, but also the amount of uplift was greatly reduced because of the added sliding mechanism.

Apart from the above-mentioned research carried out by Wang and Guild [54], we could not find any more research on this subject. Hence a generic research is necessary which can highlight effects of flexibility on all possible modes of motion of a free-standing structure subjected to base excitations.

## 2.4 Glove Boxes Shake Table Test Data

Full-scale shake table testing of glove boxes was carried out in Japan. Fujita et. al. [55] and Miura et. al. [56] conducted tests on glove boxes fixed to the floor and it was concluded from the tests that the glove boxes kept working when subjected to design basis earthquake acceleration. It is important to note that these boxes were not free-standing and hence these results are not relevant to the case presented in this thesis. To evaluate seismic stability and integrity of a free-standing glove box system, it was decided to carry out full-scale shake table testing of the glove boxes used in nuclear facilities across India. In supervision of my guides, a task force was formed including engineers from Bhabha Atomic Research Centre (BARC) and Central Power Research Institute (CPRI) [57]. The objective of these tests were to qualify glove boxes for design basis earthquake loading. Three possible configurations of glove boxes were evaluated. In the first case, seismic stability of a single glove box (with mass of machinery and radiation shielding) was analyzed. In the second case, seismic stability of two glove boxes interconnected through a flexible transfer tunnel was analyzed. In the third case, seismic stability of two glove boxes interconnected with rigid cross bracings in addition to flexible transfer tunnel was analyzed. Test results obtained, were provided to carry out this research. They were utilized for validating finite element models of glove boxes being developed later in Chapter-5, 6 and 7. Test setup and procedure is discussed briefly in the next section for the three configurations.

### 2.4.1 Shake Table Testing of a Single Glove box

#### *2.4.1.1Test Setup and Procedure*

To determine seismic stability of a freestanding glove box structure for various configurations extensive shake table testing was carried out on the full-scale glove box structure. The objective of these tests was to observe and evaluate effect of seismic excitation on various operational and functional parameters related to safe handling of radioactive material inside the glove box. Critical parameters observed were leak tightness, sliding displacement and rocking. The leak tightness was important from the viewpoint of containment of radioactivity.

For testing, actual laboratory conditions were simulated. Such as, test floor was prepared in a way that it represents the actual laboratory conditions in which the glove box is generally used. The glove box was subjected to a number of pseudo base acceleration time histories synthetically generated from the ground design response spectrum of an Indian nuclear power plant. The peak base acceleration was varied from 0.1g to 0.4 g in steps of 0.1g in all the three directions. The applied vertical acceleration was 2/3rd of the horizontal acceleration.

The required response spectra was the 5% damping response spectra for safe shutdown earthquake for the plant site [58] and evaluated according to the regulatory requirements [59].

Required response spectrum and test response spectrum used for testing are shown in Fig.2-3.

The glove box was mounted on tri-axis shake table and preliminary dynamic test (Sine sweep test) was carried out to determine natural frequency of the structure. Low amplitude base excitation (0.05g) was given to simulate fixed base boundary conditions for the glove box. Fundamental frequency evaluated for fixed base condition was 7.5Hz. Before carrying out shake table testing static friction coefficient was determined between floor and GBs. Different amplitude base excitations were given to the glove box system. It was observed that glove box train started moving after overcoming sliding friction at 0.15g peak base acceleration. Hence, coefficient of friction value was considered as 0.15. After preliminary testing, shake table tests were conducted simulating earthquake, corresponding to the required response spectrum as mentioned above. The response of the structure in terms of accelerations, displacements, and strains at various identified locations was monitored. Fig.2-4 shows the locations of fifteen numbers of accelerometers (A1-A15) and two number of displacement sensors (D31-D32). Accelerometer number (A12) was not working and hence removed. Shake table time history signals were filtered by band pass filter with a range of 0.5 to 50 Hz. Response signals recorded from accelerometers mounted on glove box were unfiltered. Accelerometers used were of force-balanced type (FGP instrumentation, France) with a sensitivity of 20mV/g and a frequency range of 0.1 to 500 Hz. While the data acquisition system used was from M/s Servotest, UK with a data collection rate of 1,00,000/- samples per second.

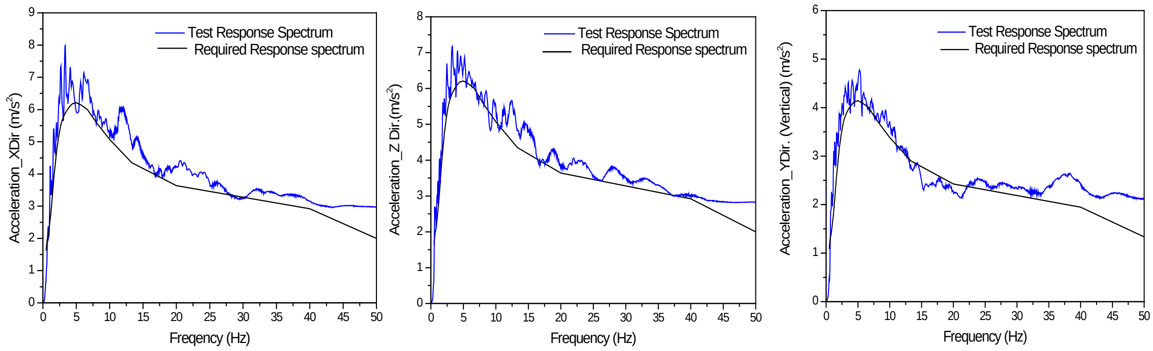


**Figure 2-3 Test and required response spectrum for shake table testing**

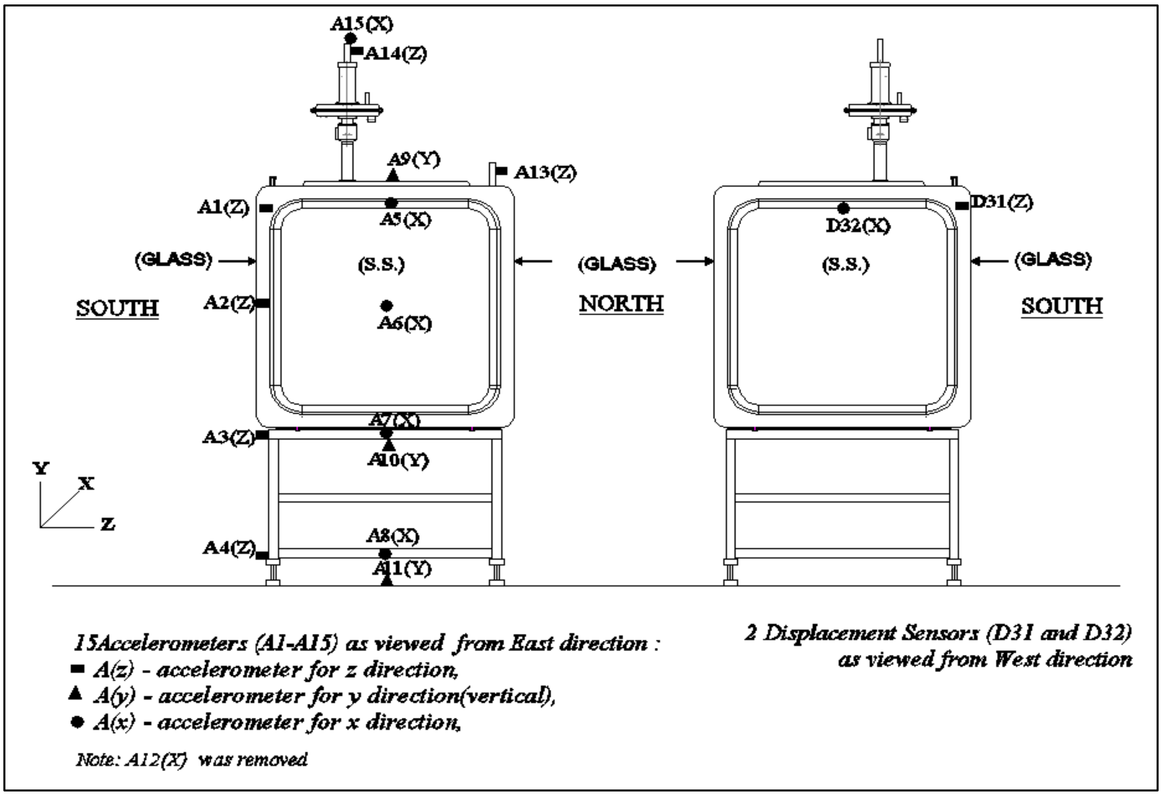


**Figure 2-4 Schematic showing positions of various sensors during shake table testing**

Single GB structure is generally used in mainly three types of operating conditions in laboratory. In the first case, it is used as a maintenance or storage box to store various tools or in process inventory. To simulate this case in testing, it was assumed that mass of tools/in process inventory is very less than the mass of GB structure and hence can be safely ignored. In the second case, GB houses process equipment of considerable weight. To simulate this case in testing, a dead load of 250Kgs in form of a solid box was bolted to the GB base. In the third case, GB can have a radiation lead shield fastened on one side glass panel. To simulate this case, actual lead shield 96Kg load was bolted to the GB front panel. Then shake table tests were carried out for the above-mentioned three cases as given below:

1. *Case 1:* Single glove box structure. See Fig.2-5(a)
2. *Case 2:* Single glove box structure with dead load of 2.5 KN. See Fig.2-5(b)
3. *Case 3:* Single glove box structure with eccentric load of 0.96 KN. See Fig.2-5(c).

For each of the above-mentioned cases the glove box was tested for two conditions; In one condition one-inch ventilation pipe connected at the top of the box was kept free to move ,while in other condition ventilation pipe was fixed to a rigid frame mounted(fixed) on the shake table. These two conditions simulate the actual two field conditions, one in which the glove box is having long flexible ventilation system attached to it and the other in which the ventilation system is of small length and rigidly connected to a support. The integrity of pressure boundary was checked during tests by actually monitoring the pressure changes inside the box during and after shake table testing. Leak testing was carried out after each test for two hours at the pressure of -250 Pa and then again for two hours at -750 Pa, as per the regulatory guidelines [60] [61] [2].

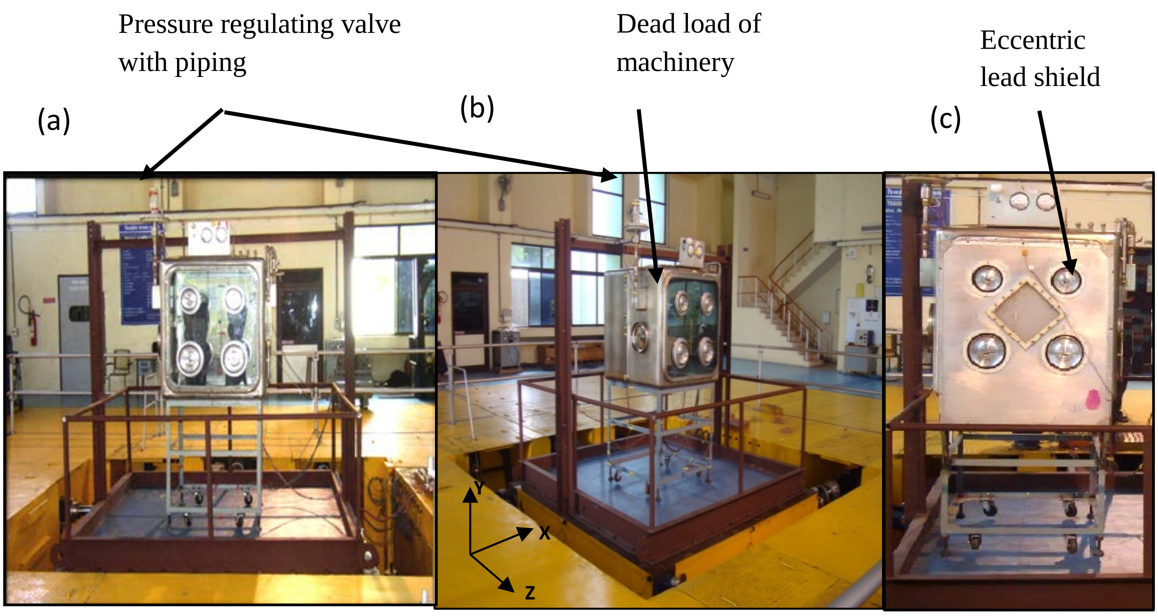


**Figure 2-5 Shake table test setup. (a) Single standalone Glove box, (b) Glove box with central mass, (c) Glove box with eccentric mass**

#### *2.4.1.2 Test Results*

During shake table testing various parameters were observed and recorded viz. sliding displacement of the structure, accelerations, and strains at different locations and leak rate during and after testing. Leak rate and sliding displacement were the most critical parameters from the radiological safety considerations. It was observed during testing that rigid body motions were predominant. Strains recorded by strain gauges were of very low magnitude (< 240µm/m). Glove box sustained design basis ground motion of 0.2g PGA.

### 2.4.2 Shake Table Testing of Flexibly Interconnected Glove Boxes

#### *2.4.2.1Test Set Up*

Shake table tests were carried out on two freestanding glove boxes (1m x 1m x 1m, 370 Kg each) interconnected to each other by a material transfer tunnel (see Fig.2-6 and Table.2-1). The test floor was prepared such that it represents the actual laboratory conditions in which the GBs are used. The response of the structure in terms of acceleration, displacement, and strain at different locations was monitored during testing. Seventeen numbers of accelerometers (A1-

A17), two numbers of displacement sensors (D1-D2) and twenty-six numbers of strain gauges (S1-S26) were mounted on GBs as shown in Fig.2-7. To avoid clutter, locations of strain gauges are not shown.

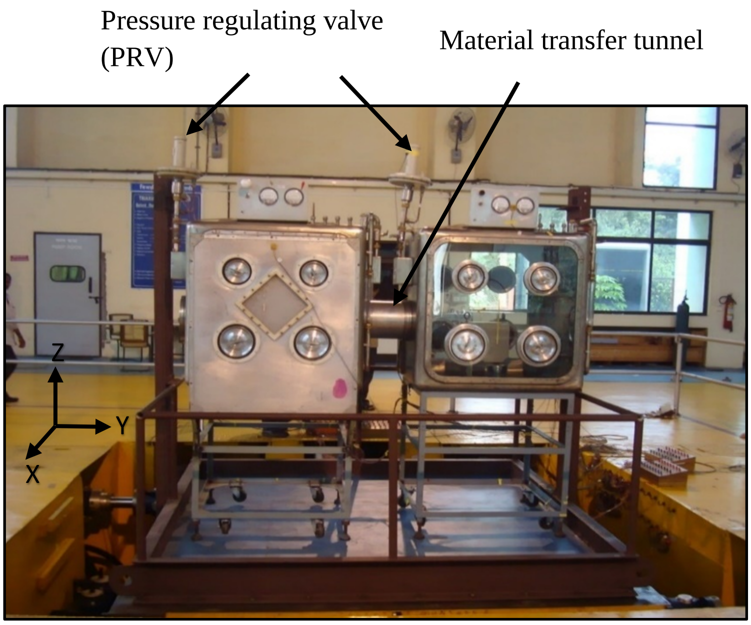


**Figure 2-6 Test set of interconnected glove boxes with a flexible transfer tunnel**

**Table 2-1 Dimensions and properties of interconnected glove boxes**

| | | | | |
|---|---|---|---|---|
| **Glove box shell(top structure)** | | | | |
| Length(m) | Width(m) | Height (m) | Thickness(m) | Material of construction |
| 1 | 1 | 1 | 0.003 | Stainless steel (304) |
| **Bottom supporting plate** | | | | |
| Length(m) | Width(m) | Thickness(m) | | Material of construction |
| 0.96 | 0.96 | 0.009 | | Mild steel |
| **Carriage (stand)** | | | | |
| Length(m) | Width(m) | Height (m) | Thickness(m) | Material of construction |
| 1 | 1 | 1 | 0.006 | Mild steel |
| | | | | |
| **Material transfer tunnel** | | | | |
| Length(m) | Outer Diameter(m) | | Thickness(m) | Material of construction |
| 0.3 | 0.25 | | 0.003 | Stainless steel(304) |

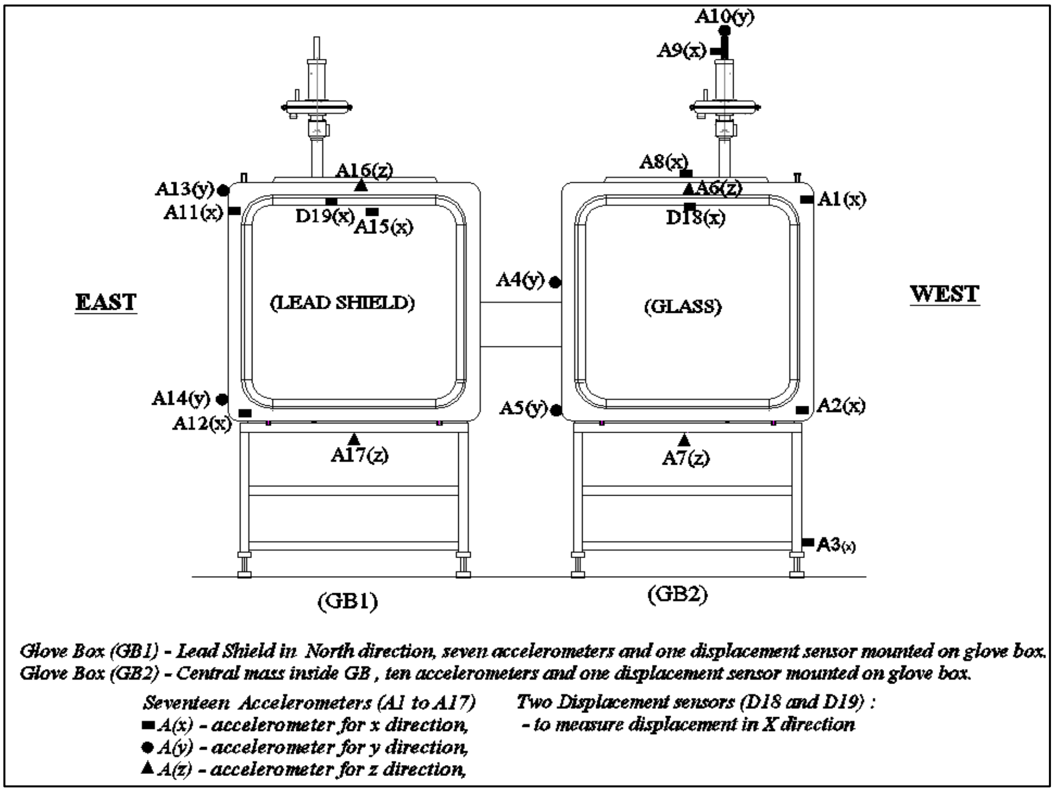


**Figure 2-7Acceleration and Displacement sensors mounted on glove boxes as viewed from North direction**

Interconnected GBs were subjected to a number of base acceleration time histories synthetically generated from the design response spectrum of an Indian nuclear power plant. The peak base acceleration was varied from 0.1g to 0.4 g in steps of 0.1g in all the three directions. The applied vertical acceleration was 2/3rd of the horizontal acceleration. The required response spectra was same as given earlier in Section 2.4.1.1.

#### *2.4.2.2Test Results*

Two glove boxes interconnected through a material transfer tunnel were initially subjected to base excitations up to 0.2g peak base acceleration (design value). Generally, when GBs are mounted at higher floors they can be subjected to floor acceleration values closer to 0.4g. To simulate this condition, GBs were also subjected to higher base excitations up to 0.4g peak base acceleration (PBA) values.  The natural frequency of interconnected GBs was evaluated to be 8.0Hz in lateral flexure in X and Z direction. One of the glove boxes had an eccentric mass of 96 kg simulating lead shielding while other glove box had 250 Kg fixed central mass simulating static load of machinery kept inside. The material transfer port was fixed between the two glove boxes with the help of O-rings. It functioned as a flexible leak tight connection between the two boxes. Due to the space constraints, interconnected GBs were tested by applying simultaneous motion along three directions up to 0.2g PBA value. For 0.3 g and 0.4g pba values, two motions one horizontal motion along the transverse direction (X direction) of the train and one vertical motion were applied.

The integrity of pressure boundary was checked during tests by actually monitoring the pressure changes inside the box during and after shake table testing. Leak testing was carried out after each test run, for two hours at the negative pressure of 250 $N/m^2$ and then, again for two hours at a negative pressure of 750 $N/m^2$, as per the regulatory guidelines [61] [60] [2]. Leak rates were recorded as air leakage volume fraction as a percentage of glove box volume per hour and given in Table2-2.

**Table 2-2 Measured leak rate after shake table testing**

| S.No | Peak base acceleration value (in g) | Leak rate (% of GB volume per hour) |
|---|---|---|
| 1 | 0.1 | No leakage * |
| 2 | 0.2 | No leakage* |
| 3 | 0.3 | 0.040 |
| 4 | 0.4 | 0.054 |

*No measurable change in manometer reading observed during leak testing

Like the case of a single box, here also rigid body motions like sliding and rocking dominated the response. Strains recorded by the strain gauges were of very low value. Max strain observed was only 240µm/m. Hence these test results indicated low deformations and large displacements (slip/rocking).

### 2.4.3 Shake Table Testing of Rigidly Interconnected Glove Boxes

Previous results of shake table experiments for two glove boxes interconnected by a flexible material transfer tunnel highlighted inherent limitations in design. At higher peak ground accelerations, relative sliding and rotational motions between both the boxes caused breach of integrity and leak tightness of the system could not be retained. On the basis of experimental findings, it was decided to modify design to improve seismic stability. Both the carriages (stands) of glove boxes were rigidly fixed to each other using structural members as shown in Fig.2-8. This cross bracing using L-shaped angles was done to constrain relative movement between both the boxes. Horizontal angles for cross and diagonal members (size 40x40x5mm thick) were chosen and interconnected at two locations. No modification was done in material transfer tunnel connection with the boxes. It was still flexibly connected to the boxes using O-rings. After performing these design modifications, shake table experiments were carried out to investigate seismic performance of interconnected GBs. The objective of testing was to observe predominant modes of motion of GB system and there effect on stability. Critical parameters of GB system like the leak tightness, negative pressure and structural integrity were checked during and after the shake table testing.

#### *2.4.3.1Test Set Up*

Two freestanding glove boxes (1m x 1m x 1m, 370 Kg each), interconnected to each other by a material transfer tunnel and cross bracing were placed on the tri-axial shake table for testing as shown in Fig.2-9. Test floor was also prepared similar to laboratory conditions in which the GBs are used. The response of the structure in terms of accelerations, displacements, and strains at different locations was monitored during testing. Seventeen numbers of accelerometers (A1-A17), two numbers of displacement sensors (D1-D2) and twenty-six numbers of strain gauges

(S1-S26) were mounted on GBs. Locations of various sensors are shown in Fig.2-10. To avoid clutter, location of strain gauges is not shown in the figure. Input base motions were same as used earlier.

#### *2.4.3.2Test Results and Observations*

Initially, glove boxes were subjected to base excitations up to 0.2g peak ground acceleration (design value). Subsequently, they were subjected to floor acceleration values up to 0.4g.

Leak testing was carried out after each test run, for two hours at the negative pressure of 250 Pa and then, again for two hours at a negative pressure of 750 Pa. Strains recorded throughout testing were of very low magnitude. Maximum strain value recorded during testing was 220µm per meter.

It was observed that interconnected glove boxes could retain leak tightness and integrity up to 0.4g pba value of seismic excitation.

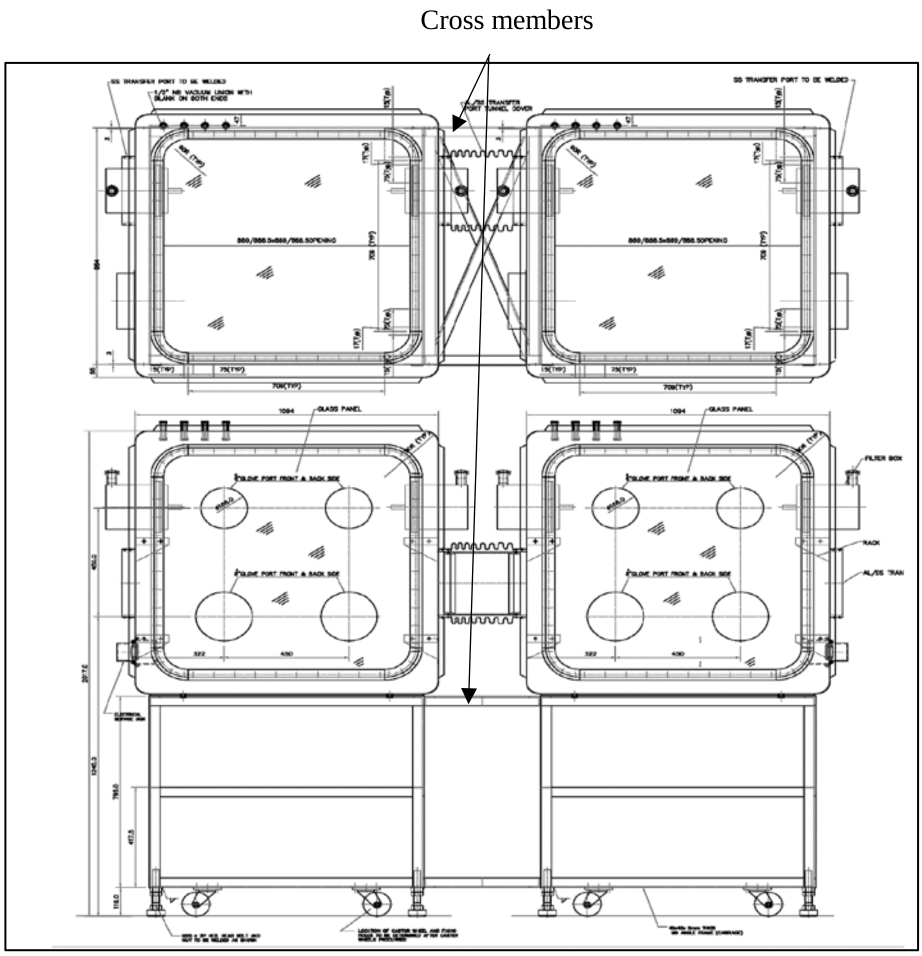


**Figure 2-8 Modified design of interconnected glove boxes (Plan and Elevation view), carriages are connected with cross members**

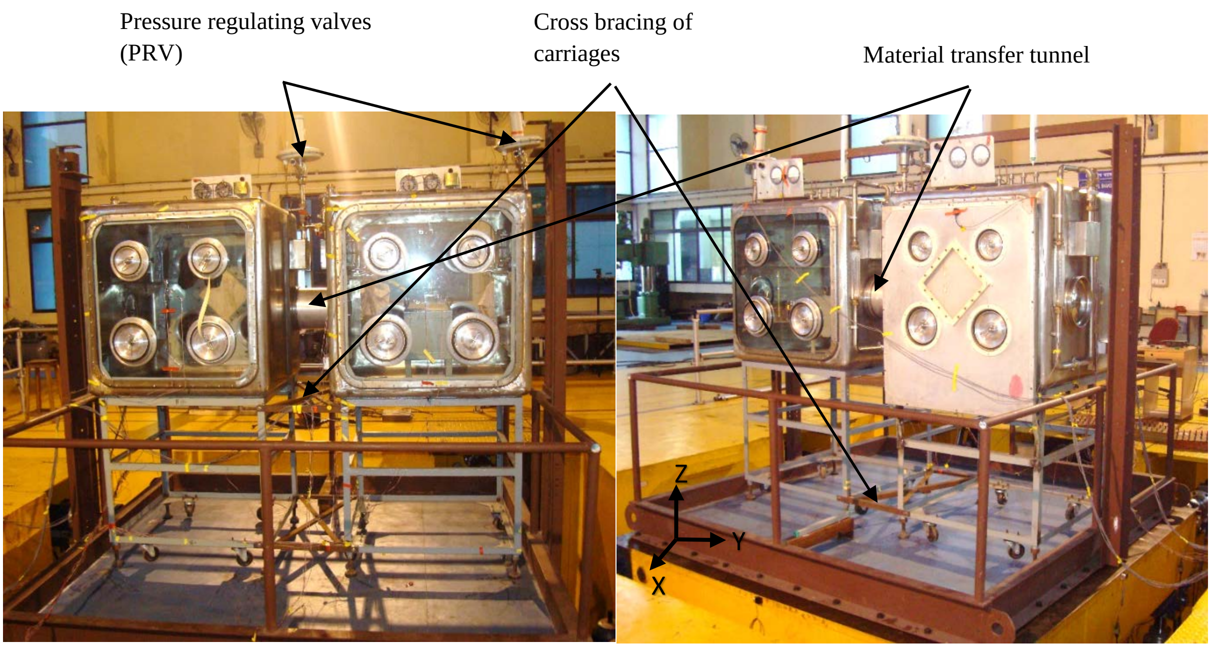


South view North view

**Figure 2-9 Experimental set up of two glove boxes with carriages connected through structural members (cross bracings) at two locations**

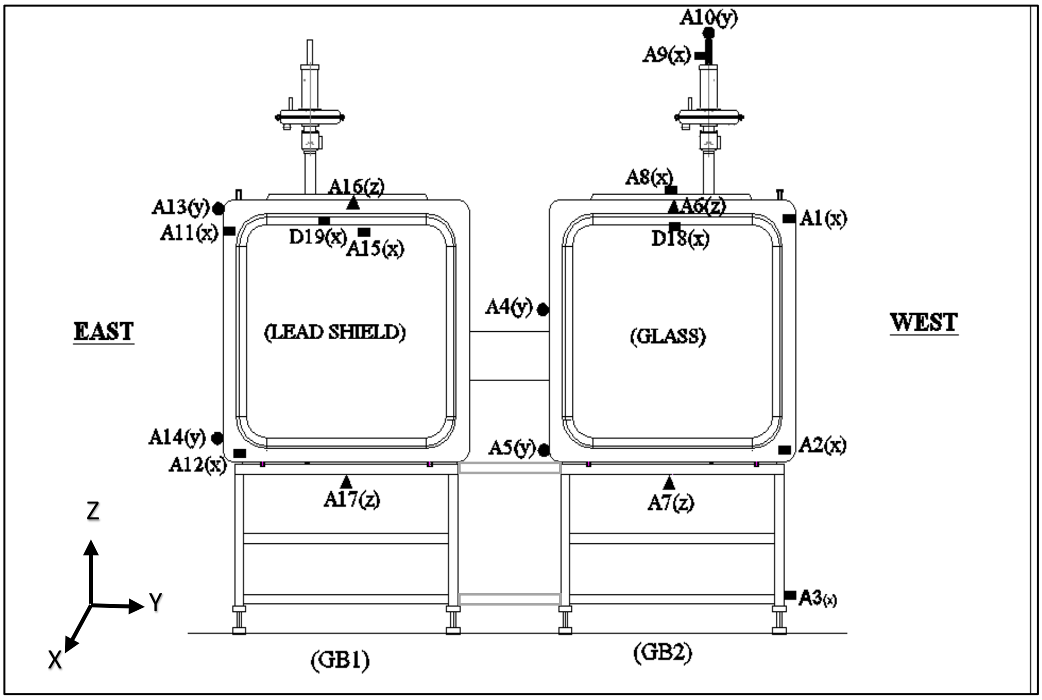


**Figure 2-10 Acceleration and Displacement sensors mounted on glove boxes as viewed from North direction**

## 2.5 Gap Areas and Directions for Research

As described earlier, majority of research on the dynamics of freestanding components is restricted, either to the overall dynamic behavior of a rigid body (as given in Section2.2), or to the limited extent on rocking behavior of a flexible body (as given in Section2.3).

The paucity of available literature on the dynamics of freestanding flexible bodies, signifies a need, of a more comprehensive research.

As described in Section.2.2.3, Shenton and Jones [62] proposed motion initiation criteria diagrams for free-standing rigid blocks. These diagrams are regularly followed and referred in the literature [36] [39] [40]. These plots highlight dependence of initiation of any mode of motion of a free-standing component on three main parameters which are aspect ratio (A.R.), coefficient of friction ($\mu_s$) and peak amplitude of base excitations ($A_g$). However, there are other three important parameters viz. frequency of base excitation, stiffness (flexibility) and natural frequency of a component. Effect of these parameters on initiation of a mode of motion requires further investigation. Hence, it is planned to study effect of additional parameters on motion initiation and highlight the missing linkages. Moreover, study of dynamics of freestanding flexible body under planar modes of motion like sliding, rocking and combination of these two, requires thorough investigation.

In addition to that, overall dynamics of flexible structure was not studied. Acikgoj and Dejong [51] investigated rocking stability of a flexible body. Proposed cantilever beam model was developed using single mass lumped at the center of gravity. Bending stiffness of the beam was considered. Vassiliou et.al. [52] improved model proposed by Acikgoj and Dejong. They proposed cantilever model using continuous beam and consistent mass formulation. Mass was lumped at top and bottom locations. Both these studies were based on the assumption of no sliding motion that means considering pure rocking motion only. Hence a generic study including effects of sliding, rocking and combination of two on the dynamics of a freestanding flexible body is required.

Hence, the present research shall include systematic study of effects of various parameters on all possible planar modes of motion of a rigid and flexible bodies. In addition to that, effect of these parameters on initiation, termination, and sustenance of any mode of motion and hence on overall seismic stability shall be reconnoitered. Reflective investigation of interaction of elastic and rigid body motions of a free-standing component, when subjected to base excitation, is contrived. It includes experimental and numerical investigation of test specimens representing geometrically similar rigid and flexible structures. Generalized results, stemming from this investigation will be applied to a more complex case of a glove box, extensively used in nuclear facilities. This nonstructural component is a leak tight structure which works under negative pressure. It is a safety-related mechanical component, whose integrity and functionality is very critical for any nuclear fuel fabrication/reprocessing facility. In lieu of available findings of shake table testing, detailed assessment of seismic stability of the glove boxes is envisaged. Further, it is planned to carry out extensive numerical analysis to evaluate seismic stability of series of interconnected glove boxes for various possible operational configurations. It is also envisaged to develop a generic methodology to ascertain requirement of anchoring (fixing to the base) of a glove box.

# CHAPTER 3 DYNAMICS OF FREE-STANDING RIGID BODIES SUBJECTED TO BASE EXCITATIONS

## 3.1 Introduction and Outline

Generally, many freestanding components like office and laboratory furniture, mechanical and electrical equipment, art objects in a museum, vending machines etc. behave rigidly when subjected to base excitations. Although, most of these systems may have flexibility, however, their seismic response is largely governed by rigid body motions with low strains. This hypothesis is deeply rooted in historical real life failures of free-standing systems. As discussed in Chapter-1, the majority of seismic failures of freestanding systems were due to either overturning or excessive sliding motion. Hence, seismic stability is largely controlled by rigid body behavior of these systems.

To the best of author's knowledge, effects of base excitation frequency on initiation, termination, and amplification of any mode of motion of a free-standing rigid component has not been studied. Here, a functional relationship between the frequency of excitation and initiation and sustenance of any particular mode of motion from rest state for a parallelopiped rigid block is developed and demonstrated using shake table experiments.

In this chapter, rigid body assumption is retained in all the formulations and numerical solutions. Section 3.2 presents fundamental dynamics of a free-standing rigid body. Mathematical formulation of the problem, with underlying rigid body assumption, is presented. To determine critical parameters influencing stability, experimental studies were carried out and presented in Section 3.3. Further to that, numerical results, obtained from time integration of the nonlinear equations of motion and finite element solution of test models are presented in Section 3.4. Then, Section 3.5 presents a novel three-dimensional motion initiation criteria diagram developed for a rigid body. At the end of the chapter, significant contributions of this research, adding to the existing knowledge base are highlighted in Section 3.6.

## 3.2 Two-dimensional Analytical Model

In this section, equations of motion for possible planar modes of motion like pure rocking, pure sliding and a combination of both are derived. Equations of motion and conditions for initiation & termination of pure sliding and rocking mode of motion are presented; Further equations of motion for the simultaneous occurrence of sliding and rocking mode of motions are derived. Finally, generic equations of motion, governing all possible planar modes of motion for a rigid body are presented. These equations can be used to determine the position of a rectangular rigid body when subjected to one/two-dimensional base excitations.

### 3.2.1 Sliding Mode of Motion

Consider a symmetric rectangular rigid block at rest relative to a moving base, as shown in Fig.3-1. The block has mass (M), Mass moment of inertia (I) about either edge $O_L$ or $O_R$, width (2B), height (2H), and aspect ratio A.R. = H/B. The bottom of the block is in surface contact with the ground. The normal reaction at the base is denoted by $F_N$. The coefficient of Coulomb friction: Static and dynamic coefficients-μ (assumed as same). The Friction force is given by $F_f$. Slip displacements of the block relative to the base are denoted by X and Y. The horizontal and vertical base accelerations are denoted by $\ddot{X}_g$ and $\ddot{Y}_g$ with respect to fixed frame of reference and are assumed to be a function of time.

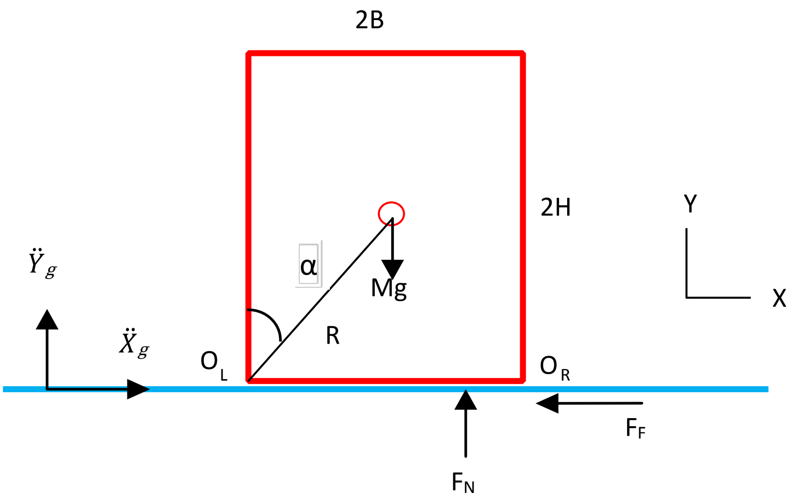


**Figure 3-1 Free body diagram of a rigid block undergoing pure sliding motion**

Equation of motion governing the slip displacement (X) of the body on base is derived by using equilibrium of forces (Newton's Law) in X direction. Here, equations of motion and conditions for initiation and termination of sliding mode of motion are established and are given below:

1. Equations of motion

   a) Slide initiation from rest state

   The block starts slipping, when the horizontal inertia force due to base motion exceeds the static frictional force at the contact surface as given below:

$$M\ddot{X}_g(t) > \mu_s M (g+\ddot{Y}_g(t)) \qquad 3.1$$

   b) While sliding

   Equation of motion during sliding mode of motion can be written as below:

$$M\ddot{X}_g(t) + M\,\ddot{X}(t) + F_F = 0 \qquad 3.2$$

Where, $F_F = \mu\ \mathrm{Sgn}(\dot{X})\ M\ (g+\ddot{Y}_g(t))$

Here Sgn($\dot{X}$) is the Signum function which gives the sign of variables, defined by: Sgn($\dot{X}$)= +1 for $\dot{X}$ >0 , Sgn($\dot{X}$)= -1 for $\dot{X}$ < 0 ,

Now, derived equations of motion for sliding motion may further be simplified by assuming harmonic base excitations as given below:

$$\ddot{X}_g(t) = A_g\, g \sin(\frac{2\pi}{T} t),\ \ddot{Y}_g(t) = A_Y\, g \sin(\frac{2\pi}{T} t) \qquad 3.3$$

Where T- Time period of input motion (assuming same for both the directions), $A_g$, $A_Y$ –non dimensional parameters indicating Amplitude of input acceleration in X and Y direction respectively. On replacing values of $\ddot{X}_g(t)$and $\ddot{Y}_g(t)$ in Eqn. 3.2, we get:

$$A_g\, g \sin(\frac{2\pi}{T} t) + \ddot{X}(t) + \mathrm{Sgn}(\dot{X})\, \mu\, g\, (1 + A_Y \sin(\frac{2\pi}{T} t)) = 0$$

Or $$\ddot{X}(t) = -\, g\, \{A_g \sin(\frac{2\pi}{T} t) + \mathrm{Sgn}(\dot{X})\, \mu\, (1 + A_Y \sin(\frac{2\pi}{T} t))\} \qquad 3.4$$

Further, the equations can be normalized using following substitutions:

$$U = X / gT^2 \text{ and } \tau = t/T.$$

On substituting these values in Eqn.3.4, we get equation of motion in non-dimensional form as below:

$$\ddot{U}(\tau) = -\,\{ A_g \sin(2\pi\tau) + \mu\, \mathrm{Sgn}(\dot{U})\, (1 + A_Y \sin(2\pi\tau)) \} \qquad 3.5$$

In this equation all the derivative are with respect to non-dimensional time parameter $\tau$.

c) Slide termination condition

The sliding motion continues until the relative velocity between the body and base becomes zero. Hence the condition is given below:

$$\dot{X}(t) = 0 \text{ or } \dot{U}(t) = 0 \qquad 3.6$$

The slide motion initiates from the rest mode when the condition in Eqn. 3.1 is satisfied and the condition given by Eqn.3.13 should not be satisfied; otherwise, rocking will start before sliding. Once sliding starts the body follows Eqn.3.2, until the condition in Eqn. 3.6 is satisfied. A slide mode is valid provided the normal reaction is greater than zero ($F_N$ >0).Moreover, during each cycle of harmonic base excitation, slip starts only after a certain threshold amplitude of the wave is reached given by Eqn.3.1.

2. Analytical solution

The equation of motion derived for sliding mode of motion is nonlinear and hence calls for a numerical solution. This can be solved by numerical integration methods (e.g. Newmark-beta and Runge kutta time integration methods) by considering equilibrium of forces at every small time steps.

However, an attempt is made to solve the equation analytically for a particular case of half sinusoidal horizontal base excitation [32].

Vertical excitation is assumed to be zero. Hence Eqn.3.5 can be written in simplified form as:

$$\ddot{U}(\tau) = -(A_g \sin(2\pi\tau) + \mu \, Sgn(\dot{U})) \qquad 3.7$$

Eqn.3.7 is valid from the time of onset of slip determined from Eqn.3.1 up to the time of slip termination to be calculated. Time of onset of slip can be calculated from Eqn.3.1 and is given below:

$$\tau_0 = \frac{1}{2\pi}\sin^{-1}\frac{\mu}{A_g} \qquad 3.8$$

For determining the time of slip termination, we use Eqn.3.6.On integrating with time, slip velocity can be given as below:

$$\dot{U}(\tau) = -\int \left(A_g \sin(2\pi\tau) + Sgn(\dot{U})\mu\right). d\tau \qquad 3.9$$

Now, the time of slip termination ($\tau_1$) is calculated by equating Eqn.3.9 to zero

$$\frac{A_g}{2\pi}\cos(2\pi\tau_1) + Sgn(\dot{U})\mu\tau_1 + C = 0 \qquad 3.10$$

Where, C is the constant of integration which is given by:

$$C = -\frac{A_g}{2\pi}\cos(2\pi\tau_1) - Sgn(\dot{U})\mu\tau_1 \qquad 3.11$$

Hence slip displacement can be determined by integrating $\dot{U}(t)$ again, from time $\tau_0$to $\tau_1$ as given below:

$$U(\tau) = \int_{\tau_0}^{\tau_1}\left(\frac{A_g}{2\pi}\cos(2\pi\tau_1) + Sgn(\dot{U})\mu\tau_1 + C\right).d\tau \qquad 3.12$$

### 3.2.2 Rocking Mode of Motion

Consider same rectangular block subjected to base motion in both horizontal and vertical directions. In this case, it is assumed that coefficient of friction is sufficiently high such that static friction is not overcome by inertial force. The block will rotate about either of the edges $O_R$ or $O_L$ depending upon the base motion as shown in Fig.3-2 below. It is further assumed that there is no bouncing of the block and impact of the block with the base during the transition of rocking from one edge to another is not considered.

The block is assumed to be rigid and uniform so that its centre of gravity coincides with the geometric center, which is at a distance R from any corner. The angle α of the block is given by tan (α) = *B/H* .The base accelerations ($\ddot{X}_g$ & $\ddot{Y}_g$) with respect to fixed frame of reference are assumed to be a function of time.

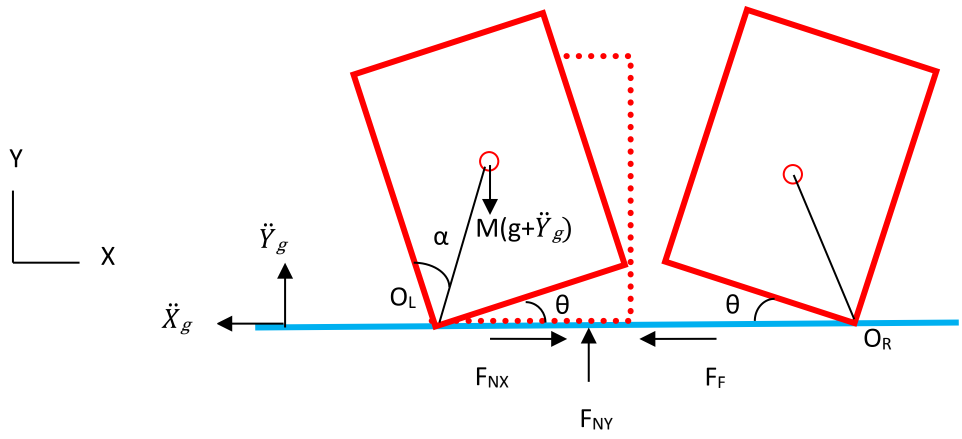


**Figure 3-2 Free body diagram of a rigid block undergoing pure rocking motion**

1. *Equations of motion*

a) *Rocking initiation condition from rest state*

The rocking initiation condition from rest for a rectangular rigid body subjected to base accelerations are derived from the equilibrium of the overturning moment and the resisting moment around a pivoting vertex.

$$M\,(\ddot{X}_g)\,R\,\mathrm{Cos}\,\alpha > M\,(g + \ddot{Y}_g)\,R\,\mathrm{Sin}\,\alpha \qquad 3.13$$

*b) While Rocking about an edge*

Once rocking starts, the block will start rotating about either of the edge depending on the base acceleration. While rocking, the equations of motion are derived by taking moment equilibrium about either of the edge (See Fig.3-2). When there is a rotation, the angular displacement is denoted by θ; Here the positive value of θ corresponds to rotation about vertex $O_R$ and its negative value corresponds to rotation about $O_L$. For the rotation about vertex $O_R$ , where θ >0, the equation of motion is given below:

$$I_o\,\ddot{\theta}(t) + M\,(g + \ddot{Y}_g)\,R\sin(\alpha - \theta(t)) - M\,(\ddot{X}_g)\,R\cos(\alpha - \theta(t)) = 0$$

3.14

Similarly for rotation about vertex $O_L$, where $\theta(t) < 0$ ,we have:

$$I_o\,\ddot{\theta}(t) - M\,(g + \ddot{Y}_g)\,R\,\mathrm{Sin}(\alpha + \theta(t)) - M\,(\ddot{X}_g)\,R\,\mathrm{Cos}(\alpha + \theta(t)) = 0$$

3.15

These equations are piecewise continuous. Block rotates about any one edge due to base excitation and may come back and hit the base and then again start rocking about other edge or the same edge depending on the base motion. Every impact with the base leads to energy dissipation and hence variables have to be adjusted accordingly. This is a nonlinear problem where the impact has to be accounted properly to know the response of block with time. Hence, energy dissipation considering inelastic collision can be derived by conservation of energy before and after impact. Post-impact velocity is lesser than pre-impact velocity by a factor known as coefficient of restitution as given below:

$$\dot{\theta}(t)\ postimpact = r.\dot{\theta}(t)\ preimpact \qquad 3.16$$

On further simplifying Eqn.3.14, we obtain:

$$\mathbf{I_o}\,\ddot{\theta}(t) = M\,(\ddot{X}_g)\,R\cos(\alpha - \theta)\ \mathbf{-}\ M\,(g + \ddot{Y}_g)\,R\sin(\alpha - \theta(t))$$

3.17

On expanding $\sin(\alpha - \theta)$ and $\cos(\alpha - \theta)$ ,assuming small values of rocking angle($\theta$) and considering only the first term of Taylor Series expansion of Sine and Cosine functions, we get the linearized equation of motion as given below:

$$\ddot{\theta}(t) = p^2\,\{A_g\,\mathrm{Sin}\,\alpha + (1+A_y)\,\mathrm{Cos}\,\alpha\}\,\theta(t) + p^2\,\{A_g\,\mathrm{Cos}\,\alpha + (1+A_y)\,\mathrm{Sin}\,\alpha\}$$

3.18

Here $\alpha$ is the critical angle. If $\theta(t) > \alpha$ , then the body will topple due to gravity alone under static conditions. p is the system frequency given by $p^2= MgR/I_o$ .Where $\ddot{X}_g=A_g g$ and $\ddot{Y}_g=A_y g$. Where, $A_g$ and $A_y$ represent time-varying amplitude of horizontal and vertical ground motion respectively.

Now, Eqn.3.18 can be non-dimensionalised by the following change of variables:

$$\emptyset= \theta /\alpha \quad \text{and} \quad \tau= p\, t$$

On making the substitutions we get the non dimensionalized form as:

$$\ddot{\emptyset} - \{A_g \sin \alpha + (1+A_y) \cos \alpha\} \emptyset = 1/ \alpha \{A_g \cos \alpha - (1+A_y) \sin \alpha\} \qquad 3.19$$

c) Rocking termination condition

Rocking motion continues to sustain till net overturning moment arising due to effective inertial forces are overcome by net restoring moment arising due to vertically downward normal forces. In the absence of inertial forces, rocking motion slowly decays down due to energy dissipation in multiple impacts with the base. The condition for rocking termination can be given as:

$$M (\ddot{X}(t)) R \cos \alpha < F_N(t) R \sin \alpha \qquad 3.20$$

*2. Analytical Solution*

It is possible to obtain an analytical solution of Eqn.3.19 for a limited case of rocking about a vertex without considering changes in direction of motion and associated impacts. Here we shall present analytical solution from the time of starting of rocking about one edge up to the time of termination of a half cycle when the block hits back the base, indicated by the condition $\theta = 0$ . Following parameters are considered for obtaining a solution:

Constant horizontal acceleration ($\ddot{X}g$) and vertical acceleration ($\ddot{Y}g$), $A_g$=0.5, $A_y$= 0.1, B=150, H=600, $\alpha$ = 0.245, R=618, p = 3.45, $I_0$= $4/3MR^2$, μ=0.6

It is important to check that sliding should not start before rocking using Eqn.3.1. It is clear from the parameters that slipping doesn't start and the block goes directly into the rocking mode because it satisfies the condition given by Eqn.3.1.On substituting these values in Eqn.3.19, we get:

$$\ddot{\emptyset} = 1.2\emptyset + 0.894 \qquad 3.21$$

On solving Eqn.3.21, for both homogenous and forcing function and using initial conditions as, $\emptyset$= 0 at $\tau$ =0 and $\dot{\emptyset}$ =0 at $\tau$ =0, we finally get:

$$\emptyset = 0.745 \{\text{Cosh}\, \tau - 1\} \qquad 3.22$$

This is a hyperbolic equation indicating the lifting of the block from the base. It is a well-known solution available in the literature [7] [39] .Similarly, on solving Eqn.3.19 using following parameters: sinusoidal horizontal acceleration [$\ddot{X}g = A_g\, g \sin(2\pi\omega t)$] and constant vertical acceleration ($\ddot{Y}g$)

On simplification, we get a final equation in the following form:

$$\ddot{\emptyset} = A_g/\alpha\ \text{Sin}\,(2\pi\,\xi\, t) - (1+A_y)\,(1- \emptyset)$$

3.23

Here, $\xi$ is frequency ratio given by the ratio of applied base excitation frequency to system natural frequency of free vibration. On solving the Eqn.3.23, we get:

$$\emptyset = A\, e^{\sqrt{1+Ay}}\tau + B\, e^{-\sqrt{1+Ay}}\tau - \{A_g\ \text{Sin}\ (2\pi\ \xi\ \tau)\ /\ \alpha\ (4\pi^2\, \xi^2 + 1+ A_y)\} + 1$$

3.24

Where A and B are constants and determined by the initial conditions. For $A_g$= 0.5, $A_y$=0.1, B=150, H=600, $\alpha$ = 0.245, R=618, p = 3.45, $I_0$= 4/3M$R^2$, μ=0.6, $\xi$ =1, we get:

$$\emptyset(\tau) = 1 - 0.35\, e^{1.05\tau} - 0.65\, e^{-1.05\tau} - 0.005 \sin(2\,\pi\,\tau) \qquad 3.25$$

It is interesting to observe that solution obtained for the equation of motion as given in Eqn.3.25, exhibits an exponential increase in rocking angle with time. However, it is also observed that low- amplitude harmonic component is present in the solution due to the forcing function. This result could be interpreted by the reader that responses of two rigid blocks with the same aspect ratio are identical. This is not the case because the size of the block (not its aspect ratio) is hidden in $\tau$ (the non-dimensional time) through the frequency parameter p.

Therefore it should be noted that the rocking response is not only aspect-ratio dependent, but also size dependent for a given aspect ratio. [63]

### 3.2.3 Combination of Sliding and Rocking Mode of Motion

For a particular combination of system parameters, a rigid body can simultaneously undergo sliding and rocking mode of motions. In this section, firstly transition conditions from one mode of motion to the other are derived. Then, equations of motion are written for a generic case of rigid block undergoing any possible planar mode of motion.

1) Analytical formulation

The equation of motion for a rigid rectangular block of mass (M) and mass moment of inertia ($I_o$) about an edge, subjected to base motion can be obtained by taking equilibrium of various forces and moments acting on the body at any instant of time. As shown in Fig.3-3, various forces acting on a block undergoing sliding and rocking rigid body motions, can be categorized as below:

a) Inertial force

These forces arise due to net effective acceleration, due to the resultant of all forces acting on the block. It is given as $\overrightarrow{F_I}$(t), which is a time-varying vector corresponding to net inertial forces acting on the block. Its value can be given as in Eqn.3.26 below:

$$\overrightarrow{F_I}(t) = M\,\ddot{X} \qquad 3.26$$

Here, M is the mass of the block and $\ddot{X}$ is the net resultant acceleration of the block due to all acting forces.

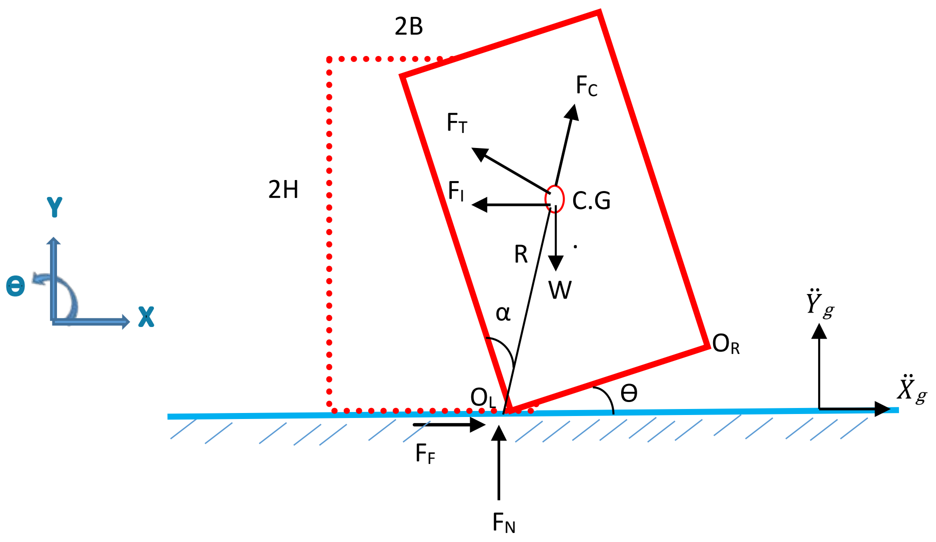


**Figure 3-3 Rectangular rigid block subjected to various forces during rocking and sliding motions**

b) Contact forces

At the line of contact between the block and base, there will be contact forces which can be divided into two categories viz. a normal force acting perpendicular to the contact surface known as a normal reaction and a horizontal force acting tangentially to the normal direction known as frictional force. A time-varying frictional force given as $\overrightarrow{F_F}$(t), will act at the contact interface between body and base as given in Eqn.3.27 and Fig.3-3. During pure sliding motion, a line of action of frictional force will be at the bottom edge of the block. However, this will change to almost a point contact about either of the left/right vertices, as rocking initiates. The direction of frictional force will be opposite to the direction of motion (velocity) as given by a Signum function. Time-varying normal force ($\overrightarrow{F_N}$(t)) will be acting at contact interface as given by Eqn.3.28. In addition to these forces, there will be an impact force arising due to change in direction of rotation of the block. This force is intermittent in nature and its magnitude can be obtained by using conservation of momentum principle.

$$\overrightarrow{F_F}(t) = Sgn(\dot{X})\ \mu\ \overrightarrow{F_N}(t) \tag{3.27}$$

$$\overrightarrow{F_N}(t) = M\ (g \pm \ddot{Y}_g) \tag{3.28}$$

c) Rotational forces

During rocking or a combination of rocking- sliding motion, rotational forces will be acting on the block. Two forces namely centrifugal ($\overrightarrow{F_C}$(t)) and tangential force ($\overrightarrow{F_T}$(t)) are acting at center of gravity (C.G) of the block. The direction of centrifugal and tangential forces will be normal and tangential to the line joining C.G. with the center of rotation respectively as shown in Fig.3-3. They are given by Eqn. 3.29 &3.30 respectively.

$$\overrightarrow{F_C}(t) = M.R.\dot{\theta}(t)^2 \tag{3.29}$$

$$\overrightarrow{F_T}(t) = M.R.\ddot{\theta}(t) \tag{3.30}$$

d) Body force

As the block is having a finite volume and density, hence gravitational force will act at the C.G. of the block. Its direction is vertically downwards and magnitude is equaled to mass times gravitational acceleration as given by W in Eqn.3.31.

$$W = M.g \tag{3.31}$$

Please note the sign conventions as given in Fig.3-3. Anticlockwise rotation is considered as positive. All the forces described above shall be present in case motion of the block is a combination of sliding and rocking. In the next sections, we shall initially derive equations of motion for individual modes of motion, then these equations will be suitably transformed into a generic equation of motion applicable to all possible modes of motion.

2) Initiation of sliding motion from rocking motion

The sliding mode can also start from rocking mode of motion, provided that the dynamic frictional force at the interface is overcome by a net horizontal force acting on the block at that instant of time. The frictional force is derived from the instantaneous dynamic normal reaction acting at the rocking corner of the block (See Fig.3-3 for free block diagram). The equation of motion can be written as:

$$F_F(t) < M\,\ddot{X}(t) \qquad 3.32$$

Where $F_F$ is a frictional force at a particular instant when the block is in a rotational motion with an effective net horizontal acceleration value of $\ddot{X}$. Here frictional force is evaluated by a dynamic normal reaction $F_N$ at a particular instant.

$$F_F(t) = \mu_s\, F_N(t) \qquad 3.33$$

$$F_N(t) = M(g + \ddot{Y}_g(t)) - F_T(t)\,\mathrm{Sin}(\alpha-\theta(t)) - F_C(t)\,\mathrm{Cos}(\alpha-\theta(t)) \qquad 3.34$$

Where $\alpha$ is the critical angle. $\theta(t)$ is angle of rotation of the block from base. $F_T(t)$ is the tangential force due to rotation and $F_C(t)$ is the centrifugal force.

3) Initiation of rocking motion from sliding motion

There is a possibility that rocking may initiate while the block is sliding. This is possible if overturning moment arising due to the net horizontal acceleration of the block overcomes restoring moment due to net vertical force at a particular instant.

$$M\,(\ddot{X}(t))\,R\cos\alpha > M\,(g + \ddot{Y}g(t))\,R\sin\alpha \qquad 3.35$$

4) Generic equations of motion

After deriving boundary conditions, for initiation, transition and termination of the different planar mode of motion, generic equations of motion required to be solved to obtain position and state of the rectangular block at any instant of time are presented. They are given below:

$$M\,\ddot{X}(t) + \mathrm{Sgn}(\dot{X}(t))\,F_F(t) = M\,\ddot{X}_g(t) \qquad 3.36$$

$$I_o\,\ddot{\theta}(t) = M\,\ddot{X}_g\,(t).\,R\,\mathrm{Cos}\,(\alpha \pm \theta\,(t)) - \lambda\,F_N\,(t).\,\mathrm{Sin}\,(\alpha \pm \theta\,(t))$$

3.37

Where, λ is a parameter determining the direction of rocking of the body. Position of CG from either of the left edge can be calculated using Eqn. 3.38.

$$X_{CG} = X_{OL} + R.\mathrm{Sin}(\alpha - \theta) \qquad 3.38$$

Where, $X_{CG}$ and $X_{OL}$ are the position of center of gravity and left edge at any point of time. Eqns. 3.36 and 3.37 can be solved numerically using suitable time integration scheme.

### 3.2.4 Numerical Solution

The equations of motion Eqn.3.38 and Eqn.3.39 are second order Ordinary Differential Equations (ODE’s). A free-standing rectangular block subjected to base excitations has two degrees of freedom given by sliding displacement(X) and rocking angle (θ). Hence these equations of motion shall be solved simultaneously using numerical time integration scheme appropriate for the single degree of freedom systems.

In the present case, central difference method was used to compute the response of a rigid rectangular block subjected to base excitations. A numerical code in FORTRAN language was developed which can integrate equations of motion given by Eqns.3.36 and 3.37. It checks for initiation and termination of any mode of motion using boundary conditions defined earlier and calculates the position of the block in terms of sliding displacement(X) and angular rotation ($\theta$). Central difference scheme was utilized for time integration with a fixed time step of 1e-4 Sec. Experimentally evaluated values of coefficient of restitution and friction were used in numerical solution. Since, experiments were carried out on a unidirectional shake table, only horizontal component of base excitation was utilized for numerical studies neglecting vertical component. Comparison of results for a two-dimensional rigid body numerical model and shake table experiments are presented in Section 3.4.5.

## 3.3 Experimental Investigation

### 3.3.1 Objectives and Introduction

Experiments were carried out to evaluate the influence of various system parameters on the dynamic stability of a freestanding rigid body. Three different test specimens were fabricated to simulate rigid body behavior. These specimens were considered as a rigid body for the range of frequencies encountered in seismic response (0-33Hz). All the specimens had fundamental deformation frequency higher that 33Hz. Hence they were practically rigid for seismic studies. Objectives of testing were twofold: firstly, to determine the fundamental dynamic behavior of free-standing test specimens when subjected to base excitations and secondly, to analyze effects of variation in system parameters like contact properties, base excitation characteristics and slenderness on the overall seismic stability. A variation in slenderness was achieved by keeping the base dimensions same and varying heights to obtain three different aspect ratios of two, three and four. Similarly, a variation in contact properties was achieved by using four different surfaces as a base material. Further, base excitation properties like peak amplitude and frequency were varied by simulating different harmonic and seismic excitations. It shall be noted that the interest of studying responses under harmonic excitations is in the analysis of the stationary part of the response. The transient phase, which is due to the at rest initial conditions, is of little interest. As a consequence, the amplitude of the stationary part of the sliding response shall be regarded as the output of interest [63]. The objective of the present research was initiated with the interest of determining seismic stability of free standing critical nuclear components like glove boxes. Any movement due to sliding or rocking may cause undesirable interaction with the adjacent structure or breach of integrity/leak tightness. Hence, it was utmost important to check the damage if any, due to peak values of sliding displacement and rocking. Hence, with this objective in mind, output of interest is selected as peak values of sliding displacement and rocking angle.

Details of test setup/facility are given below:

### 3.3.2 Test Set up and Specimens

A uni-axial hydraulic shake table, available at Bhabha Atomic Research Centre (BARC) was utilized for carrying out various experiments on test specimens. This facility uses a double-acting, double-ended, heavy-duty actuator that operates under a precision servo valve control in closed-loop servo hydraulic systems. Table.3-1 provides important details of the shake table.

**Table 3-1 Technical specifications of the Shake Table**

| Capacity (Kg) | Maximum Force (KN) | Displacement range (m) | Dimensions (m) |
|---|---|---|---|
| 500 | 250 | ±0.075 | 1X1 |

This actuator was connected to one end of the shaking table using swivels and fixtures. Uni-directional piezoelectric accelerometers were used for recording accelerations at various desired locations. Three parallelepiped rigid box type specimens were fabricated for experiments. Details of specimens are given in Table 3-2 Typical test setup for a test specimen (TS1), having an aspect ratio of four is shown in the Fig.3-4 (a). The position of various accelerometers can also be seen in the figure. Fig.3-4(b) shows other two test specimens having an aspect ratio of three (TS2) and two (TS3). The direction of the table movement was along X-axis as shown in Fig.3-4(a). Accelerometers A1, A2 & A4, A3 were mounted on the specimens to record accelerations in Z, X and Y direction respectively. Physical and mechanical properties of three test specimens are also given in the Table.3-2. Data acquisition and processing system were used to analyze accelerometer readings.  From the accelerometer readings, displacement and rocking angle values were calculated using numerical integration and simple mathematic formulas. [63]

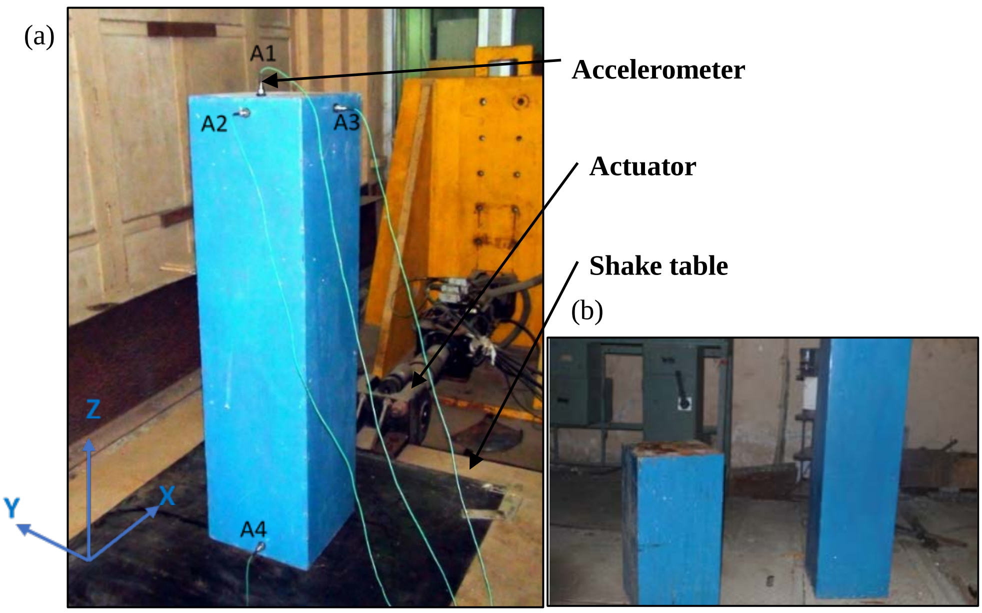

**Figure 3-4 (a) Test set up showing test specimen with aspect ratio of four (TS1) with the accelerometers, (b) test specimens with aspect ratios of three and two (TS2, TS3)**

### 3.3.3 Preliminary Dynamic Characteristics

Before carrying out actual testing, various dynamic characteristics of the specimens were evaluated. These were free rocking frequency (henceforth denoted by $\omega_r$), critical angle (henceforth denoted by $\alpha$), fundamental frequency in flexure with fixed base conditions (henceforth denoted by $\omega_n$), the damping ratio ($\xi$) and coefficients of friction ($\mu$) between the specimen and different materials to be used as a base surface. Please note that $\omega$ in this thesis refers to cyclic frequency with a unit of cycles/sec or Hz. it shall not be confused with the circular frequency (Rad/sec)

#### *3.3.3.1 Free rocking frequencies and critical angle*

The critical angle is the angle of rotation about an edge above which a freestanding structure overturns by gravity itself. This can be easily computed from the geometry of the specimen. However, this was experimentally determined by uplifting the specimens to remove errors if any, arising due to manufacturing processes. Similarly, $\omega_r$ of the test specimens for different values of initial uplift (angular displacement about an edge) was evaluated. Experiments were performed for different values of initial uplift starting from 1mm up to the 20mm and finally for the critical value of uplift corresponding to the critical angle of each test specimen. Uplift was physically realized by lifting the specimen from one edge by pivoting it on diagonally opposite edge. Accelerometers readings obtained from accelerometer-A2, mounted on the test specimens, were analyzed using Fast Fourier Transform (FFT). From the FFT, the frequency corresponding to the highest peak in Fourier spectra was selected as free rocking frequency corresponding to a particular value of initial uplift. All the three specimens were tested sequentially to obtain values for rocking frequencies. Approximate analytical evaluation of rocking frequency can be carried out by using the below- mentioned formula for the natural time period [7]:

$$T = \frac{4}{p} \cosh^{-1}\left(\frac{1}{1 - \frac{\theta}{\alpha}}\right) \qquad 3.39$$

Where T is the natural time period of rocking, p is a geometrical parameter given by Eqn. 3.39, $\alpha$ is critical angle and $\theta$ is the angle of rotation about either corner in a vertical plane. This equation is valid only for a slender block and small rotations ($\theta$).

$$p = \sqrt{\frac{M\,g\,R}{I}} \qquad 3.40$$

Here M is the mass, I is the corresponding mass moment of inertia (defined with respect to either edge) and R is defined as $R^2=b^2+h^2$ , where 2b is the width and 2h is the height of the block.

Experimentally determined values of $\alpha$ and $\omega_r$ for different specimens are given in Table.3-2 and Fig.3-5 respectively. Critical values of rocking frequencies ($\omega_{rc}$) for each specimen is also given in the parenthesis in the same column of Table.3-2. As expected, $\omega_r$ decreased non-linearly with increasing amplitude of rocking. All of these properties are listed in Table.3-2.

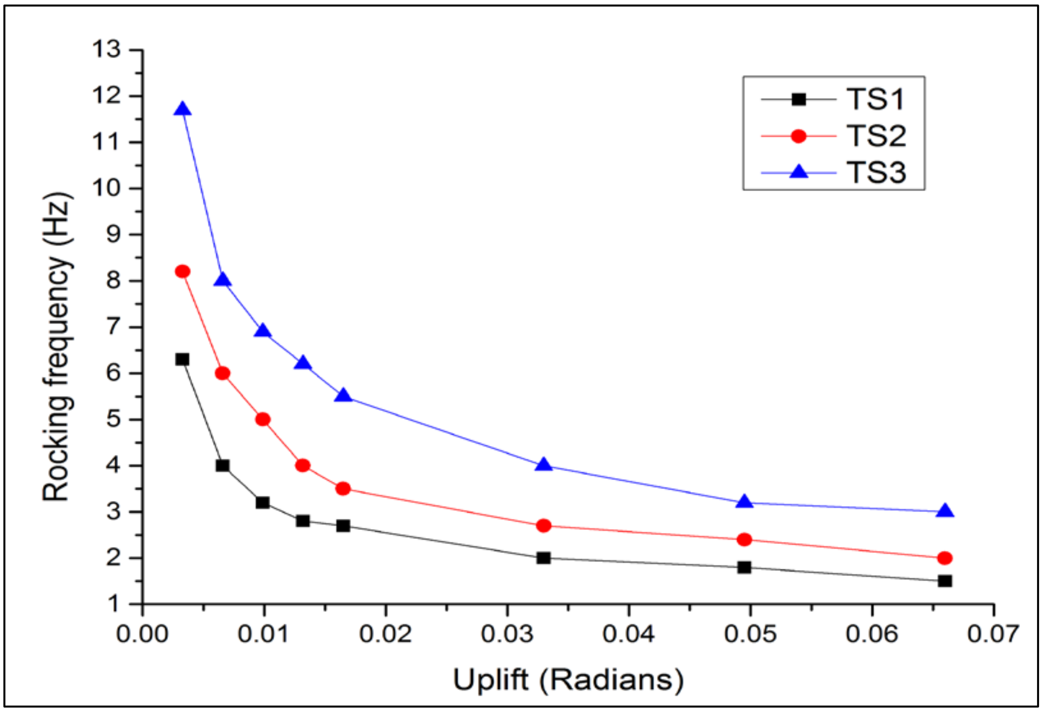


**Figure 3-5 Variation of Free rocking frequencies with amount of uplift for test specimens (TS1, TS2 & TS3)**

**Table 3-2 Physical and Material properties of test specimens**

<table>
<tr><td colspan="11">TS- Test Specimen, AR- Aspect ratio, D- Dimension (length, width, height), t-sectional thickness, p-frequency parameter, α -critical angle, R- diagonal length, M-mass, $\omega_r$ – free rocking frequency, , $\omega_{rc}$ – critical rocking frequency C.G.- relative position of centre of gravity from any vertex (x,y),</td></tr>
<tr><td>TS</td><td>AR</td><td>D<br>(m)</td><td>t<br>(m)</td><td>p<br>(Hz)</td><td>α<br>(Rad)</td><td>R<br>(m)</td><td>M<br>(Kg)</td><td>$\omega_r$<br>($\omega_{rc}$)<br>Hz</td><td>C.G<br>(x,y)<br>(m)</td><td>Material<br>properties</td></tr>
<tr><td>TS1</td><td>4</td><td>(0.3,<br>0.3,</td><td>0.003</td><td>3.34</td><td>0.245</td><td>0.62</td><td>38</td><td>1.5-<br>6.3</td><td>0.15,0.6</td><td>Mild Steel<br>E= 210GPa,</td></tr>
</table>

| | | | | | | | | | | |
|---|---|---|---|---|---|---|---|---|---|---|
| | | 1.2) | | | | | | (0.9) | | $\rho$ = 7800Kg/m$^3$ $\nu$ = 0.3 |
| TS2 | 3 | (0.3, 0.3, 0.9) | 0.004 | 3.77 | 0.322 | 0.47 | 38 | 2-8.2 (1.2) | 0.15,0.45 | Same as above |
| TS3 | 2 | (0.3, 0.3, 0.6) | 0.005 | 4.42 | 0.463 | 0.34 | 35 | 3-11.7 (1.8) | 0.15,0.30 | Same as above |

#### *3.3.3.2 Evaluation of coefficient of friction*

A simple pull test was carried out to determine values of coefficient of friction between the steel test specimen (TS1) and various surfaces used for experiments. Four surfaces used were plywood, high-density polyethylene (HDPE), aluminum and steel. They were selected in such a way that different modes of motion from rest could be simulated when excited by a base excitation. As per the available literature, plywood generally has a low coefficient of friction ($\mu$) (between 0.1-0.3) with a steel structure. This can be used to simulate sliding mode from the rest when excited by base excitation above a predefined amplitude. Similarly, HDPE has $\mu$ value between 0.2-0.4 with a steel surface. This can be used to simulate sliding-rocking motion from the rest state. Further, aluminum and mild steel have higher values of $\mu$ between 0.3-0.5 and 0.7-0.8 respectively, which can be utilized to simulate rocking motion from rest. By suitable selection of base material, it is possible to simulate all possible modes of motion, which a rigid block can undergo when excited by a base motion. In addition to that, it is possible to examine effects of the base excitation frequency on these modes. A simple fixture for manually pulling the block with the load cell was arranged and readings were recorded to a data recorder.

Fig.3-6 shows the plot of load versus time. Peak value of load before starting of slip was considered for evaluation of coefficient of friction value for a particular base material. Experimentally determined values of static coefficient of friction of test specimen with plywood, HDPE, aluminum, and steel were 0.15, 0.32, 0.48 and 0.72 respectively. After evaluating coefficient of friction values, free rocking experiments were performed to study impact damping property of the specimens given by the coefficient of restitution.

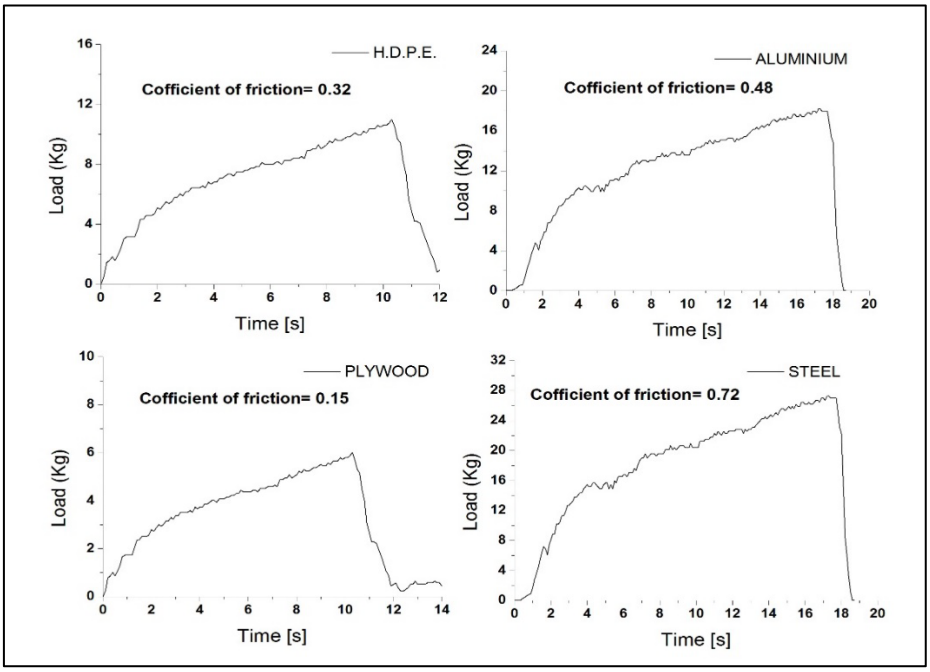


**Figure 3-6 Coefficient of friction of test specimen with different base materials**

### *3.3.3.3 Evaluation of coefficient of restitution*

When a body is undergoing rocking motion, every change in direction of rotation is associated with impacts at edges. Due to this impact, instantaneous reduction in angular velocity of the block takes place. To account for this reduction in velocity and subsequent loss of energy, the coefficient of restitution is utilized. Hence, two-dimensional rigid body analytical model described in Section3.2 requires coefficient of restitution value as an input. Numerical solution of equations of motion derived for pure rocking and combination of rocking and sliding mode of motion requires coefficient of restitution value to modify angular velocity after impact. Hence, the coefficient of restitution was evaluated as a ratio of angular velocities before and after impact. Experimental data obtained from the free rocking experiments (Section3.3.3.1) was utilized to calculate the coefficient of restitution. Numerical integration was carried out to obtain velocities from recorder accelerometer (A4) reading located on the bottom edge of the specimen. Then, using distance of the accelerometer from the rocking edge, angular velocities were calculated. For every instant of impact, identified from change of rocking angle, reduction in velocity was determined as a ratio given by coefficient of restitution. For each experimental case, multiple readings were taken to improve the accuracy of the results. Average of the calculated values obtained for different experimental cases is tabulated in Table.3-3. These values were then utilized for numerical calculations (Eqn.3.16).

**Table 3-3 Coefficient of restitution values for different base materials used in experiments**

| Base material | Coefficient of restitution (average value) |
|---|---|
| Steel | 0.98 |
| Aluminum | 0.97 |
| HDPE | 0.95 |
| Wood | 0.94 |

### 3.3.4 Dynamics of a Pure Rocking Motion

After carrying out preliminary dynamic investigations, rocking dynamics of the test specimens was examined. All the three test specimens (TS1, TS2 and TS3) were kept on a steel plate fixed to the shaking table. Steel surface was selected because of its evaluated higher value of coefficient of friction ($\mu_s$=0.72), which favors pure rocking motion without slipping. Synthetic time history corresponding to design response spectra of a nuclear power plant site in India was used as a base motion [59] [58]. Test response spectra used was same as given in Fig.2-3. To find out, synthetic time history corresponding to 0.8g PGA value, synthetic time history at 0.3g was suitably scaled up and used as shown in Fig.3.7 (a). [63] Details of procedure used for generation of design response spectra and its compatible time history were already discussed in Section 2.4.1.1.

The objective of testing was to observe the response of three different test specimens to seismic base excitation. The input base excitation is shown in Fig.3-7(a) and frequency contents of input signal, extracted using FFT are shown in Fig.3-7(b).

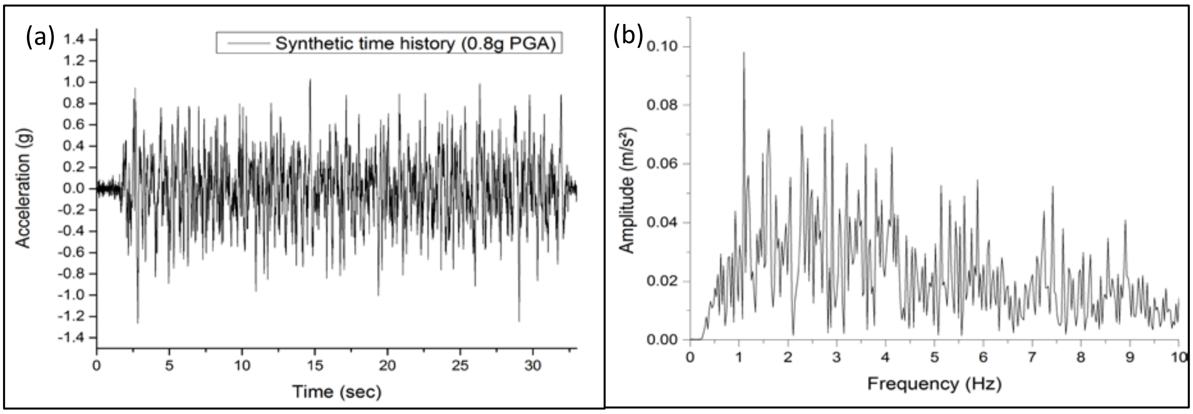


**Figure 3-7 (a)Time variation of input base excitation at 0.8g PGA and (b) frequency contents on input base excitation**

Input base excitation as shown in Fig. 3-7(a) was given to the test specimens TS1, TS2 and TS3. Acceleration time history recorded by A2 accelerometer located at the top of the specimens are plotted in Fig.3-8. Similarly, variation of rocking angle of the specimens with time is shown in Fig.3-9. TS1 and TS2 overturned by the base excitation and hence rocking angle time history only up to the overturning is plotted. These results indicated following important behavior of test specimens:

1. Acceleration response recorded on top of all the specimens indicated higher values compared to the base excitation. Acceleration values observed were 1.3 times the

excitation for TS1 (Refer Fig.3-8 (a), (b)), three times for TS2 (Refer Fig.3-8 (a), (c)) and six times for TS3 (Refer Fig.3-8 (a), (d)). These observations indicated amplification of accelerations. This point would be further discussed in Section 3.3.4.2.

2. Test specimens TS1 and TS2 overturned due to base excitation as shown in Fig.3-9. However, TS3 could sustain the effect of ground shaking. This observation highlighted effect of slenderness for specimens of same base dimensions. This observation requires thorough investigation on overturning behavior of the specimens which is carried out in Section3.3.4.4.
3. Fast Fourier Transform of acceleration time histories shown in Fig3-8 was carried out to find out frequency contents of response. Same is plotted in Fig.3-10. Frequency contents of all the specimens were dissimilar. TS1 and TS2 had lower number of frequencies in the response and peaking was observed at around 1Hz. On the other side, TS3 had wider frequency spectrum with multiple frequency peaking. It would be interesting to observe effects of individual frequencies on the response of the specimens. This aspect would be further studied in Sections 3.3.41 to 3.3.4.3.

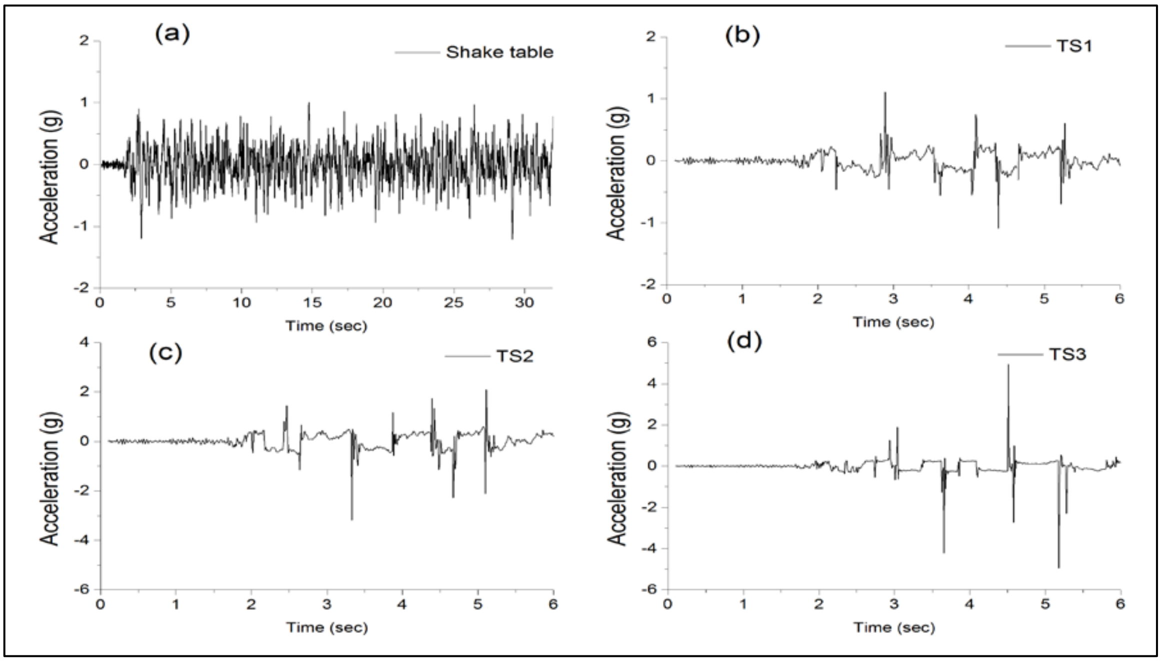


**Figure 3-8 Time variation of accelerations recorded on, (a) shake table and A2 accelerometer for specimens (b)TS1, (c)TS2 and (d)TS3**

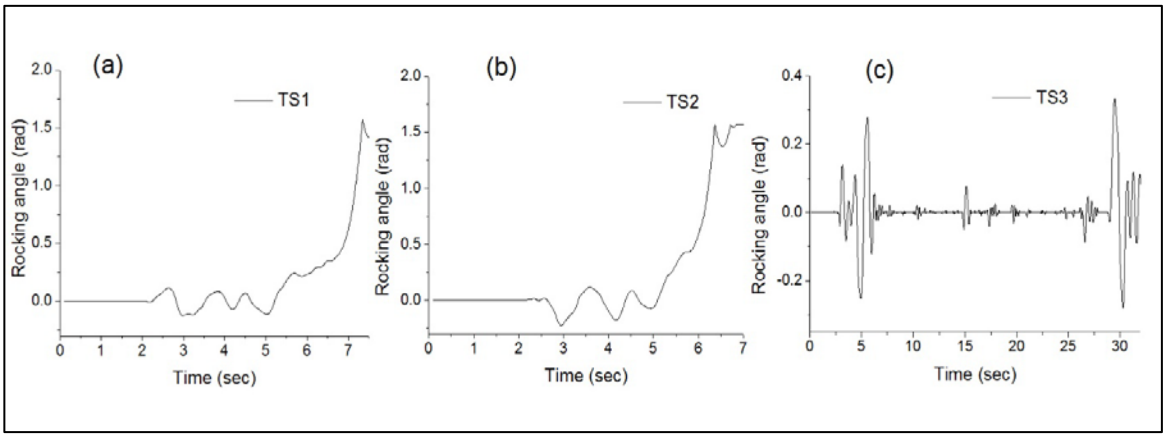


**Figure 3-9 Rocking angle time histories for specimens, (a) TS1, (b) TS2 and (c) TS3**

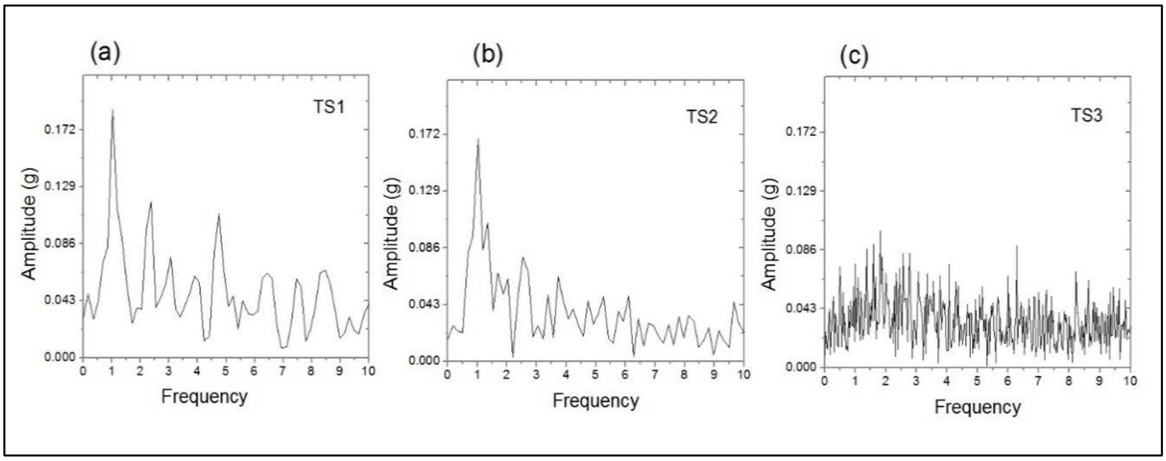


**Figure 3-10 FFT of acceleration responses of (a) TS1, (b) TS2 and (c) TS3**

After carrying our random motion testing, specimens were subjected to harmonic base excitations. The objective was to examine effects of base motion characteristics, slenderness and contact properties on the rocking response. Sine waves of varying frequencies (ω) were given as a base acceleration. Values of $X_g$ and $\mu_s$ were selected in such a way to simulate pure rocking motion without any sliding.

Effects of frequencies and slenderness on various important parameters like initiation of motion, overturning instability, response amplification and peak response characteristics of the specimens were examined.

### *3.3.4.1 Rocking Motion Initiation*

For a free-standing body, it is vital to know the initiating mode of motion from rest state, when excited by a base excitation. It is widely observed that initial mode of motion dominates general dynamic response of a free-standing body and plays an important role in determining overall stability of a free-standing body. During testing, the objective was to examine effects of variation in excitation frequency on initiation of rocking motion. Specimens were excited by amplitudes lesser than what is statically required for rocking initiation. For example, specimen TS1 was excited by a harmonic base excitation of peak amplitude ($X_g$ = 0.25g). This value of acceleration is transition value above which TS1 should initiate rocking motion. Amplitude values corresponding to the initiation condition above which specimens are expected to go into the rocking motion are given in Table.3-4. Conditions derived earlier were utilized for checking initiation of rocking and sliding motion for these values. In this case, for $X_g$ = 0.25g and $\mu_s$=0.72, using Eqns. 3.1 and 3.13, one can check that $X_g < \mu_s$ (no sliding condition) and $X_g < g \tan \alpha$= 0.25(no rocking condition). Similarly, rocking initiation conditions can be estimated for other two test specimens (TS2 and TS3) using Eqns.3.1 and 3.13. We get, $X_g \leq g \tan \alpha$= 0.33g for TS2 and $X_g \leq g \tan \alpha$= 0.5g for TS3. It is still easier to check initiation of any mode of motion by using motion initiation criteria diagrams developed by Shenton and Jones [35] as shown in Fig.2-2, for an aspect ratio of four.

For all the experiments, sinusoidal waves of different frequencies varying from 0.5Hz to 10 Hz were given as base excitations. Input base excitations and test matrix are shown in Fig.3-11 and Table.3-4 respectively. For brevity, only one case of harmonic base excitation of 2Hz for each amplitude is plotted. That means out of total 66 test cases, input base excitations corresponding to 6 (i.e. only one frequency for one amplitude) are plotted.

All the test runs corresponding to Table.3-4 resulted in no rocking initiation, which means rest region bounded by the vertical line $A_g$= B/H and inclined line $A_g = \mu_s$ in Fig.2-2, was observed to be unconditionally stable to any variation of base excitation characteristics. In other words, statically estimated rest region of Fig.2-2 is valid for all the cases of dynamic excitations as well.

**Table 3-4 Experiments performed to observe effect of base motion characteristics on the test specimens in the rest state**

| Test Run | Specimen | Xs* (g) | Input Base excitations | Output/ Results |
| --- | --- | --- | --- | --- |

| | | | Peak Amplitude(g) | Frequencies(Hz) | |
|---|---|---|---|---|---|
| **1** | TS1 | 0.25 | 0.25 | 0.5,1,2,3,4,5,6,7,8,9,10 | Rest state |
| **2** | TS1 | 0.25 | 0.2 | 0.5,1,2,3,4,5,6,7,8,9,10 | Rest state |
| **3** | TS2 | 0.33 | 0.33 | 0.5,1,2,3,4,5,6,7,8,9,10 | Rest state |
| **4** | TS2 | 0.33 | 0.3 | 0.5,1,2,3,4,5,6,7,8,9,10 | Rest state |
| **5** | TS3 | 0.5 | 0.5 | 0.5,1,2,3,4,5,6,7,8,9,10 | Rest state |
| **6** | TS3 | 0.5 | 0.45 | 0.5,1,2,3,4,5,6,7,8,9,10 | Rest state |
| ***Xs = g. tan $\alpha$,statically determined minimum base amplitude required for uplift initiation** | | | | | |

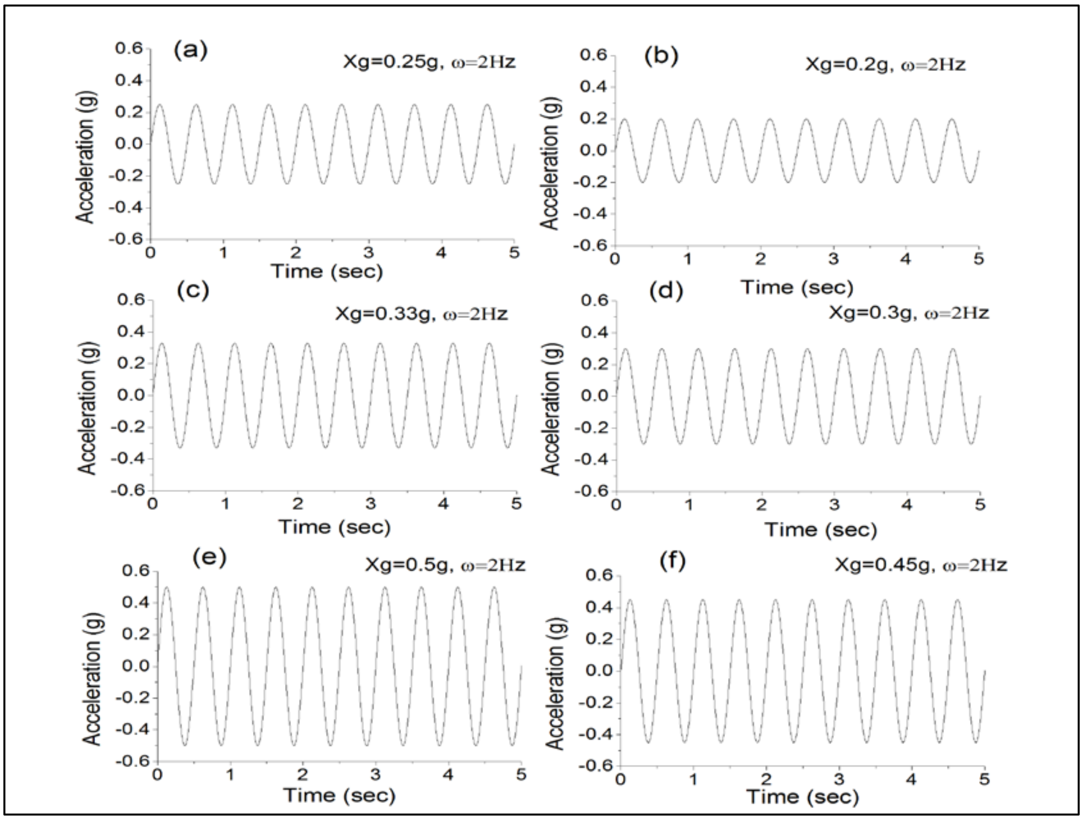


**Figure 3-11 Input time histories for six test cases: a) $X_g$=0.25g, 2Hz, b) $X_g$=0.2g, 2Hz, c) $X_g$=0.33g, 2Hz, d) $X_g$=0.3g, 2Hz, e) $X_g$=0.5g, 2Hz, f) $X_g$=0.45g, 2Hz**

Now after carrying out an investigation in the rest region for a rigid body, experiments were again performed to investigate effects of base motion characteristics on rocking mode of motion. Sets of experiments carried out for the rest state were repeated again with the fixed value of amplitude equals to 0.8g. This amplitude was selected because it can initiate rocking mode of motion for all the three test specimens. Test point corresponding to $A_g$=0.8 and $\mu_s$=0.72 can be located in Fig.2-2, lying in the region corresponding to rocking mode of motion. Input base excitations for only two test cases corresponding 2Hz and 10Hz out of total 11 are shown in Fig.3-12. Details of performed experiments are given in Table.3-5.

**Table 3-5 Details of various experiments performed to observe effects of base motion characteristics on the rocking response of test specimens**

| Test Run | Specimen | Input Base excitations Peak Amplitude(g) | Frequencies(Hz) | Coefficient of friction (μ) | Output/ Results |
|---|---|---|---|---|---|
| **1** | TS1 | 0.8 | 0.5,1,2,3,4,5,6,7,8,9,10 | 0.72 | Rocking initiation only for lower frequencies |
| **2** | TS2 | 0.8 | 0.5,1,2,3,4,5,6,7,8,9,10 | 0.72 | Rocking initiation only for lower frequencies |
| **3** | TS3 | 0.8 | 0.5,1,2,3,4,5,6,7,8,9,10 | 0.72 | Rocking initiation only for lower frequencies |

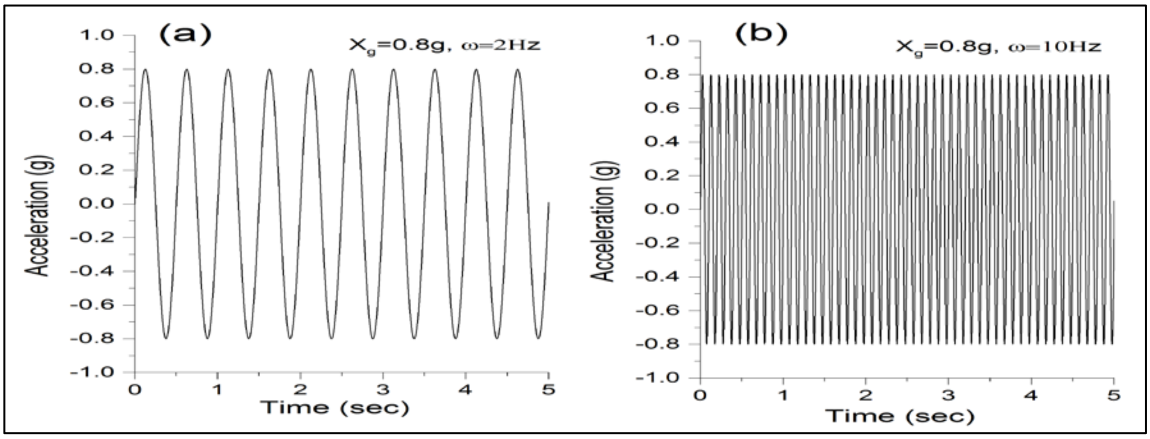


**Figure 3-12 Input base excitations. a) $X_g$=0.8g, 2Hz, b) $X_g$=0.8g, 10Hz**

The rocking response of specimens for different harmonic frequencies is given in Fig. 3-13. Test specimens TS1, TS2 and TS3 overturned for frequencies lesser than 2Hz, hence these points are excluded from the graph. However, at 2Hz, TS1 and TS2 overturned while TS3 remained in the rocking phase of motion. For a frequency of 2Hz, less slender specimen (TS3) was observed to be stable and prevented overturning. However, more slender specimens (TS1, TS2) overturned. Two factors govern the overturning of a body subjected to harmonic excitation viz. peak value of acceleration and velocity. While peak acceleration value determines uplift of a body, peak velocity determines overturning of the body. Peak velocity (Vpeak) is the lower limit of the maximum velocity required to overturn a rectangular rigid body subjected to harmonic excitation is given by Eq. 3.41. [10]

$$Vpeak = 0.4\sqrt{\frac{8gr(1-\cos\alpha)}{3\ \cos\alpha}} \qquad 3.41$$

Using Eqn.3.41, Vpeak for TS1, TS2 and TS3 was calculated and compared with different test cases shown earlier in Table 3.5, where overturning happened. Comparison is shown in Table.3-6. Maximum velocity of the shake table (excitation) in Table.3-6 was calculated by the numerical integration of recorded acceleration time history. It can be observed from the table that slender specimens (TS1 and TS2) overturned at 2Hz frequency while TS3 retained rocking motion [63].

**Table 3-6 Table showing minimum velocities required to overturn a specimen versus recorded peak values of velocities for different test runs**

| Test Specimen | Vpeak (m/sec) | Test Run 1 | | | Test Run 2 | | | Test Run 3 | | |
|---|---|---|---|---|---|---|---|---|---|---|
| | | 0.5Hz | 1Hz | 2Hz | 0.5Hz | 1Hz | 2Hz | 0.5Hz | 1Hz | 2Hz |
| | | Maximum velocity of excitation (m/sec) | | | | | | | | |
| TS1 | 0.283 | 1.75 | 0.875 | 0.436 | | | | | | |
| TS2 | 0.326 | | | | 1.765 | 0.884 | 0.421 | | | |
| TS3 | 0.499 | | | | | | | 1.77 | 0.88 | 0.431 |

Further to that, slenderness has an insignificant effect on peak rocking angles at higher frequencies (frequencies higher than required for overturning) as shown in Fig.3-13.

The Figure indicates a gradual decrease in peak rocking angles with increase of base excitation frequency. Irrespective of the value of slenderness, rocking angles decreased with increasing frequencies. The Physical explanation behind this behavior can be given by the fact that as the frequency of harmonic excitation increases, effective time span available to cause uplift decreases thereby decreasing rocking angles. Moreover, one of the cause of the reduced effect of higher frequency input motion is that, for a given acceleration, the higher the frequency the lower the velocity of input motion [63].

Hence, it can be concluded that base motion characteristics have a significant effect on initiation of rocking mode of motion from the rest state. The frequency of base excitation affected rocking motion initiation; while lower harmonic frequencies aided uplifting, higher frequencies diminished rocking motion to a virtual zero value. These results highlighted an interesting fact that even for a sufficiently high amplitude (more than what is statically required for uplift), it is possible to have a rest state (no motion). These findings have also raised questions about the validity of Fig.2-2. The prevalent hypothesis that initiation of any mode of motion from rest state depends only on three parameters ($A_g$, $\mu_s$ and B/H) is not adequate.

Hence, an addition of an extra parameter known as base excitation frequency (ω) is required to complete and correct Fig.2-2. Section 3.5 discusses details of numerical calculations carried out to redevelop motion initiation criteria maps (Fig.2-2) into three-dimensional map incorporating effects of frequency of base excitation. Next Subsection 3.3.4.2 discusses details about the response amplification and Amplification factor.

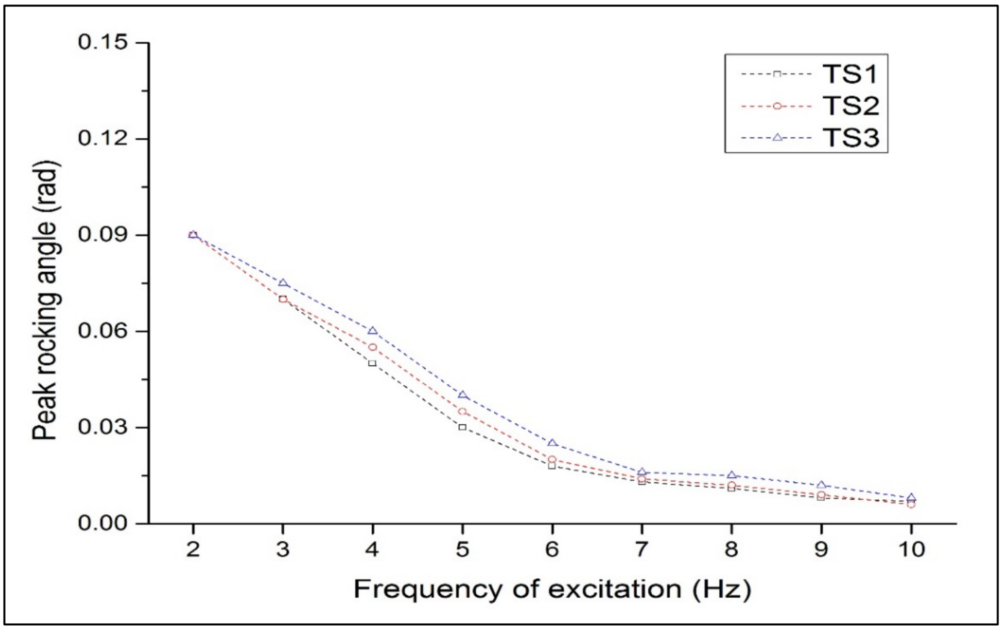


**Figure 3-13 Variation of peak rocking angles of test specimens TS1, TS2 and TS3 with frequency of base excitation for Xg=0.8g**

### *3.3.4.2 Response Amplification*

For a free-standing body, it's important to understand and evaluate response of the body relative to the applied forcing function. In this case, base acceleration acted as a forcing function. Hence, it is imperative to establish a relation between applied forcing function and response of the body with respect to parameter like base acceleration. Any amplification or reduction in this parameter shall be of special interest to the designers. As observed in random motion test (seismic base excitation) performed earlier, amplification of acceleration takes place in rocking mode of motion. To further investigate the cause of this amplification and establish a relation between frequencies of base excitations and acceleration amplification, harmonic motion test were carried out. The objective of testing was to independently evaluate the role of each frequency on acceleration amplification. Applied input base accelerations were same as already given in Table.3-5 and Fig.3-12. For brevity, accelerometers readings (A1, A2 & A4) are plotted for two cases; firstly for 2Hz as shown in Fig.3-14 (a, c, e, g, i) and secondly for 10 Hz base excitation frequency as shown in Fig.3-14 (b, d, f, h, j). Following are the important observations:

1. Peak acceleration amplitude recorded on top of the block by accelerometer A2 for 2Hz frequency was around 2g [see Fig.3-14(c)] .It was 2.4 times the acceleration value recorded at the shake table (input motion). Similarly, values recorded by A1 for 2Hz frequency were of high amplitude [see Fig.3-14 (a)]. The reason for such an amplification stems from the fact that every rocking cycle, invariably had multiple impacts with the base, which led to a sudden rise in angular as well as linear acceleration. These impacts can be identified from Fig.3-14(a) by observing peaks of acceleration time histories. Time of impacts can also be obtained from rocking angle time histories corresponding to change in rocking angle from positive to a negative value or vice versa [refer Fig.3-14(i,j)]. For that time instant, a sharp jump in acceleration shall be observed in Fig.3-14(a). This signifies impact corresponding to change of rotational motion.

2. Results highlighted an inherent property of rocking motion, where the impact was considered as an energy-dissipating phenomenon, but at the same time resulted in transmitting higher accelerations at top of the block. This behavior would be further discussed in Section.3.3.6 on contact-impact behavior.

3. Acceleration values recorded by A1 and A2 for a frequency of 10Hz were around 0.8g [see Fig.3-14(b, d)]. These values were of the same amplitude as the base

acceleration (0.8g).Hence, there was no amplification of base motion at 10 Hz frequency.

4. Peak acceleration recorded in lateral direction (along Y-axis) by A3 for 2Hz frequency was 0.6g [see Fig.3-14 (e)]. The presence of motion in the third direction was recorded during experiments. This was expected because of square base of the specimens. The third directional motion would have been much lower had the third dimension be significantly larger than the width of the blocks. However, the scope of present research was not to study the three-dimensional effects arising due to two-dimensional planar motion. Hence, we would not discuss it further.

Experimental results plotted in Fig.3-14 highlights few important properties of pure rocking motion of a rigid rectangular body. Foremost of them is an amplification of base motion and its dependence on base excitation frequencies. In the next subsection, a term amplification factor is defined which can be used to quantify amplification of base motion in a rocking mode of motion.

#### *3.3.4.3 Amplification Factor*

Amplification factor (AF) is defined as a dimensionless number given as ratio of output quantity to input quantity. This quantity can be given by a parameters like acceleration or velocity. There may be two main reasons for the failure of a freely standing nonstructural component; firstly, it may fail due to overturning Instability and secondly, it may fail due to high accelerations at certain locations. Hence, acceleration amplification is an important stability parameter which needs discussion. Experimental results revealed that rocking motion is associated with sudden jumps in acceleration values at discrete time intervals (refer Fig3-14(c) and Section 3.3.4.2). These high acceleration jumps may be a concern for a designer/user of a facility as it may endanger integrity or functionality of a component. Variation of acceleration AF, with frequencies of base excitation for a constant amplitude of base excitation, is evaluated using shake table testing results. These are shown for all the three test specimens (TS1, TS2 and TS3) in Fig.3-15. In the figure, some of the points corresponding to low frequencies are missing because they correspond to the overturning of the test specimen. The case of overturning is treated separately in the next section. Experimental results revealed few important properties of free-standing nonstructural components as given below:

1) AF for all the specimens TS1, TS2 and TS3 was greater than unity for all frequencies varying from 2 Hz to 10 Hz. This indicated significant amplification of base acceleration when recorded at top of the specimens.
2) There was a consistent nonlinear decrease in the AF from 2 Hz up to 10 Hz and thereafter AF attained a finite value greater than unity. As observed from Fig.3.14 (i) and Fig.3.14 (j), low-frequency excitation of 2Hz resulted in higher rocking angles compared to 10Hz frequency excitation. Hence associated impacts and subsequent acceleration jumps (AF) were higher at low frequency excitations.
3) As the slenderness of the specimen has decreased from TS1 to TS3, AF has increased. The reason for this change was a decrease in coefficient of restitution or increase of energy dissipation with a decrease of slenderness. Moreover, for a shorter specimen (TS3), acceleration peak due to impact was transferred faster to the top. While for the case of the larger specimen (TS1), attenuation effect arising due to structural vibrations reduces acceleration peaking at the top and hence AF. Hence, AF for a more slender component (TS1) was lower than that of a less slender component (TS3), for a given excitation frequency.

These results are generic in nature and are equally applicable to a seismic base excitation also as seen earlier in this section.

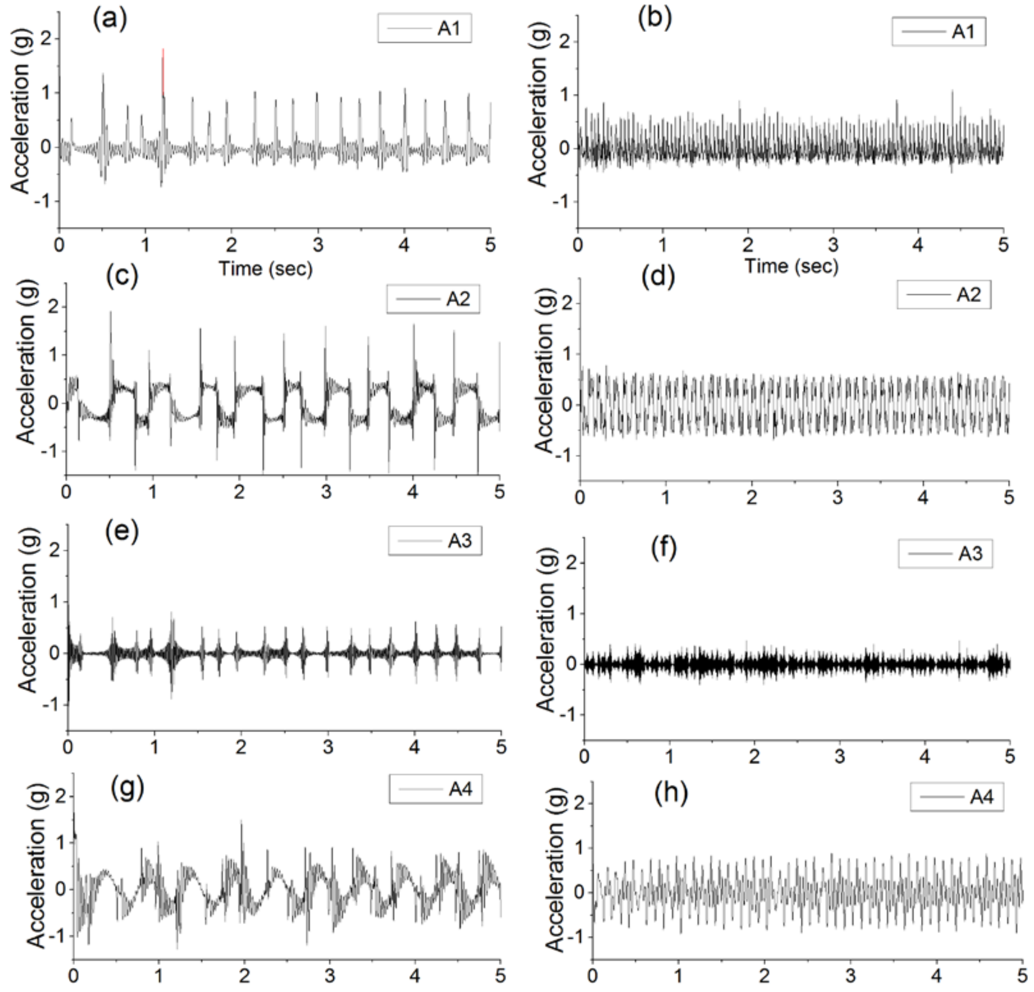


**Figure 3-14 Acceleration and rocking angle time histories recorded by various accelerometers for the test specimen TS1. (a, c, e. g,i) represents a response to harmonic base excitation of Xg=0.8g, ω=2Hz and (b, d, f, h,j) represents a response to harmonic base excitation of Xg=0.8g, 10Hz**

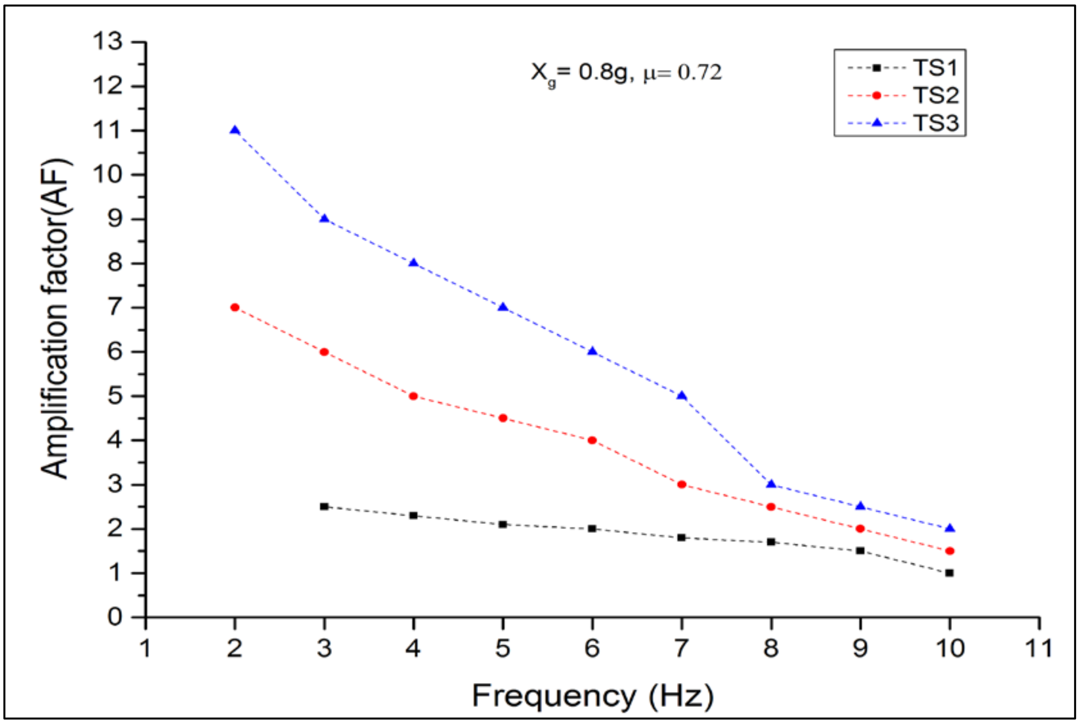


**Figure 3-15 Variation of amplification factors of test specimens TS1, TS2 &TS3 with base excitation frequencies**

### *3.3.4.4 Overturning Instability*

As stated earlier, one of the prime cause of failure of a NSC is by overturning. Experiments were performed on test specimen TS1, to evaluate effects of base motions characteristics on the overturning instability. The test specimen was subjected to sinusoidal pulses of 1sec duration given by $\ddot{X}_g$= A. Sin (2πωt). A systematic variation in amplitude (A) and frequency (ω) of pulse was done to investigate different possible modes of overturning failures. Two modes of overturning failures are possible for a rigid body [64] [22]. Mode-1 is defined as overturning in the direction opposite to initial motion with impacts (single or multiple), whereas Mode-2 is defined as overturning in the initial direction of motion without an impact as shown in Figure 3-16 below. The curve was plotted mainly with the help of the experimental data. However, due to limitations of the available shake table facility, numerical simulation was also used. As stated earlier, the shake table utilized for testing can generate a maximum displacement of ±0.075 m; hence only possible combinations of $X_g$ and ω were such that

$$\left|\frac{Xg}{\omega^2}\right| \leq 0.075\, m \qquad 3.42$$

Base excitation values which were outside the range given in Eqn.3.55 were generated numerically using finite element (FE) software. Three-dimensional model of the test specimen was developed and benchmarked using available experimental results and then utilized for generating overturning curves for the test specimen. Detailed discussion on finite element solution is provided in Section.3.4.

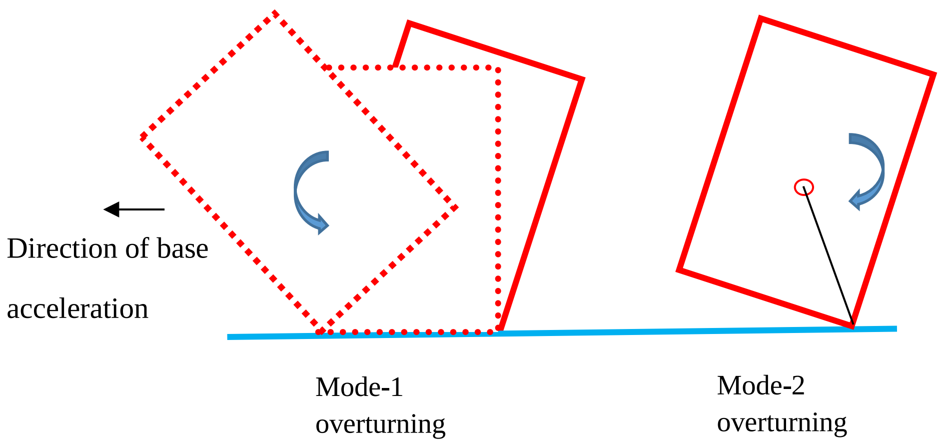


**Figure 3-16 Schematic showing two possible modes of overturning**

The dimensionless overturning curve plotted for the test specimen TS1 identifies various zones corresponding to Mode1 and Mode2 overturning failures as shown in Fig.3-17. It also identifies safe zone where there is no possibility of the overturning of the structure. Following important conclusions about the behavior of the specimen can be drawn as below:

1. In the amplitude/frequency space, two different modes of overturning failures and three different regions exist for a rigid rocking body. Lower frequencies (ω/p) of excitations starting from zero up to 0.3 correspond to a region where a rigid body transforms from

stable rocking phase to overturning without any impact (Mode2 failure) with the increase of amplitude value. This region is shown as R1 in Fig.3-17. In the mid frequency region (0.3 to 3.3), with the increase of amplitude, a rigid body TS1 first transforms from a stable rocking motion to overturning with one or more impacts; then with further increase of amplitude finally overturns without any impact. This frequency region (0.3-3.3) is given by R2 in Fig.3-17. High-frequency region ($\omega/p>3.3$), R3 has similar attributes as that of the R1 region.

2. Mode1 failure was observed to be a complex behavior, in which for a certain combination of frequency and amplitude the specimen had multiple impacts with the base before overturning. This also affected the total time required for overturning. Mode2 failures were prompt taking less than a second, while on the other side Mode1 failures were slow and even for some cases it took the specimen around 7 seconds to overturn. More investigation is required on this subject.

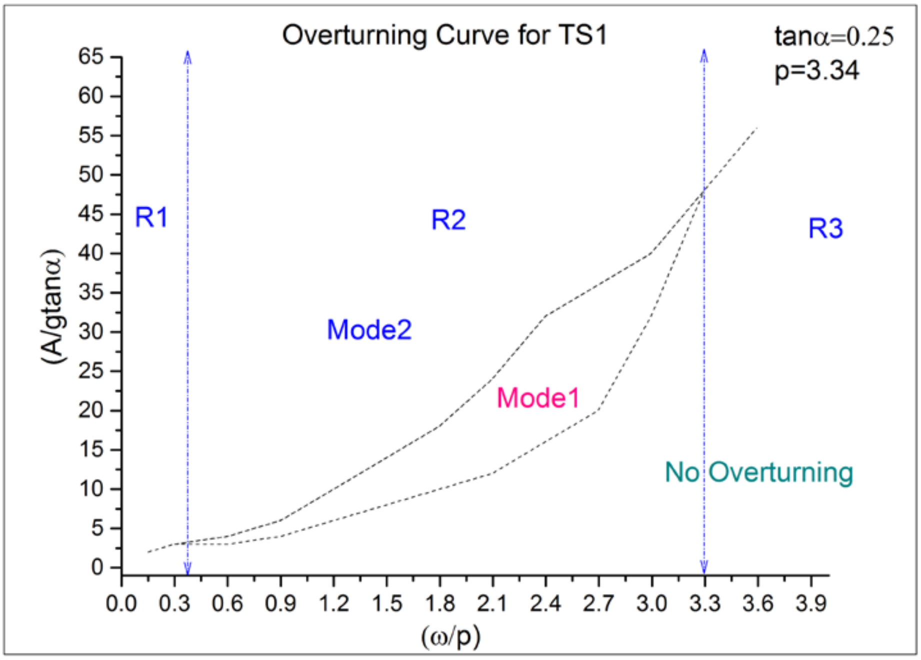


**Figure 3-17 Dimensionless overturning curve for TS1 showing various regions of Mode1, Mode2 failures with the variation in frequency and amplitude parameters**

### 3.3.5 Dynamics of a Pure Sliding Motion

After studying the rocking response of a rigid body and effects of various parameters on it, it is planned to investigate the case of a pure sliding motion. Generally, sliding is a prevalent mode of motion in low grip bases. In a case of a freestanding body, sliding may be sometimes beneficial from the point of view of input energy dissipation; however, excessive sliding may be dangerous for integrity and stability of the body and its nearby objects. The amplitude of the stationary part of the sliding response is regarded as the output of interest and hence compared for different frequencies.

Similar to the case of pure rocking motion discussed in the last section, here also basic dynamics of sliding motion is evaluated.

All the three test specimens (TS1, TS2 and TS3) were kept on a plywood plate fixed to the shaking table. Plywood surface was selected because of its evaluated lower value of the coefficient of friction ($\mu_s$=0.15), which favors pure sliding motion. Synthetic time history corresponding to a nuclear power plant site in India was used as a base motion [58] [59]. Test response spectrum was shown in Fig.2-3.The objective of testing was to observe the response of test specimens to seismic base excitation. Input base excitation was same as earlier, as shown in Fig.3-7(a) and frequency contents of the input signal, extracted using FFT are shown in Fig.3-7(b). Acceleration time history recorded by the A2 accelerometer located at the top of the specimens are plotted in Fig.3-18. Similarly, variation of slip with time for the specimens is shown in Fig.3-19. Slip displacements were calculated by using numerical integration of acceleration values of suitable accelerometers. It shall be noted that henceforth, all the values of sliding displacements were calculated with reference to the shake table, unless otherwise specified. [63]

Test results indicated following important behavior of test specimens:

1) Acceleration time histories recorded at top of the specimens by A2 indicated a significant reduction in accelerations. This signifies response reduction in the specimens. In quantitative terms, peak accelerations recorded for TS1, TS2 and TS3 were same at 0.15g. This indicates a fivefold reduction in accelerations.
2) There was no effect of the slenderness of the specimens on peak acceleration response. All the specimens had same peak acceleration values (0.15g) despite variation in slenderness. The reason for this peak at a constant value is connected to coefficient of friction value between the specimens and the base. As evaluated earlier, contact surface used had $\mu$=0.15. Once base excitation exceeds this value (0.15g), slip motion initiates. This point requires further investigation and hence shall be elaborated in the Section 3.3.5.1.
3) Despite random nature of input seismic excitation, response recorded was symmetric and ordered. The response followed the base motion till the time slip starts i.e. up to 2secs of excitation. This can be easily observed from comparison of Fig.3-19 and Fig.3-18. After initiation of slip motion, the response was largely ordered with the uniform peaks and symmetric behavior along X-axis. This is quite interesting and requires further studies which are carried out in Sections 3.3.5.1.
4) Despite variation of slenderness and other physical properties like mass and moment of inertia, slip displacement of all the test specimens followed a single path. In other words, slip displacements of all the specimens were exactly the same as shown in Fig.3-19. This independence of slip displacement can be well explained by referring to equations of motion of a rigid body during sliding phase as derived in Section3.2.1. Eqn.3.2 derived earlier for slip motion is

independent of mass, moment of inertia and slenderness of the rigid body, hence slip motion doesn't depends on these physical parameters.

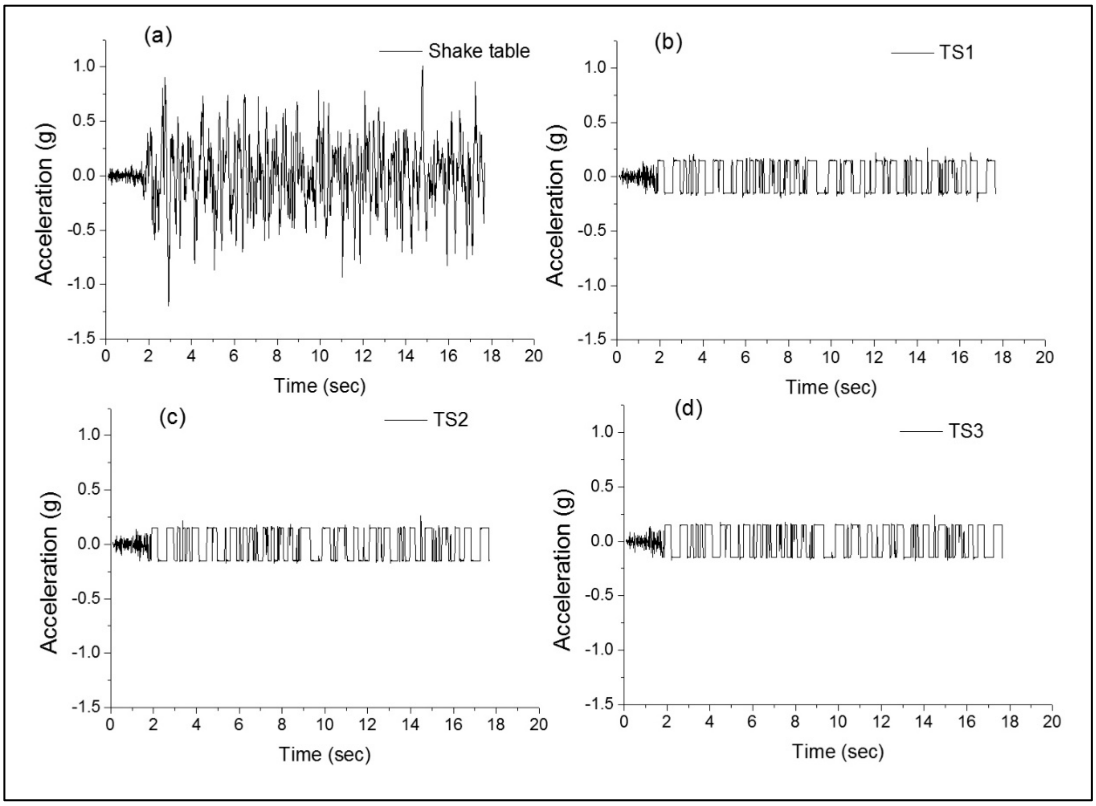


**Figure 3-18 Acceleration time histories recorded at, (a) shake table and (b, c, d) TS1, TS2 and TS3 by accelerometer A2**

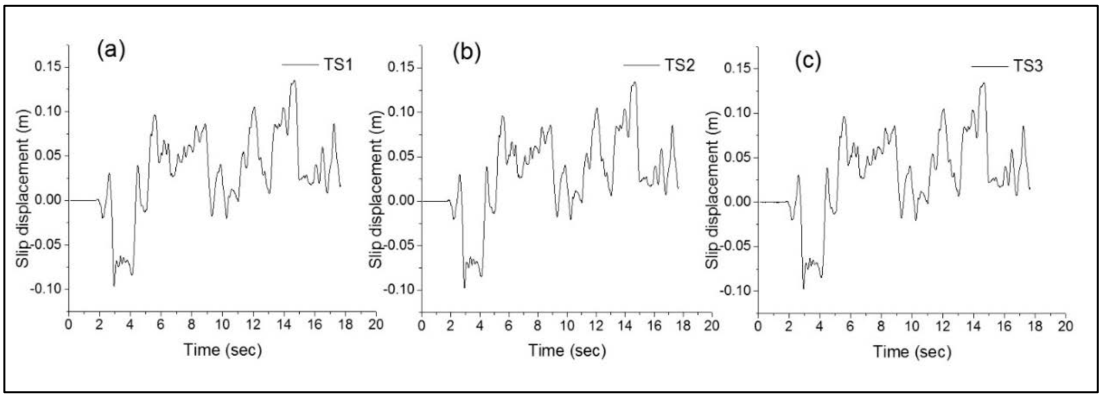


**Figure 3-19 Slip displacements of test specimens (a) TS1, (b) TS2 and (c) TS3**

#### *3.3.5.1 Slip behavior*

After carrying out random motion testing, experiments were carried out with harmonic excitations to study behavior of sliding motion for individual frequencies. Test matrix for these experiments is given in Table.3-6. Same base material (plywood) was used to carry out experiments. Similar to the case of pure rocking discussed in Section3.3.4, tests were carried out using sine waves of varying frequencies ($\omega$) as base accelerations for a duration of 5secs. Values of $X_g$= 0.8g and $\mu_s$=0.15 were selected in such a way to simulate pure sliding motion without any uplift. Here, objective of testing was to observe stability parameters like response amplification and peak sliding response of the specimens. Effects of variation of base excitation frequency ($\omega$) and slenderness value on these parameters, were studied. Acceleration time histories at various locations were recorded by the accelerometers mounted on the test specimens as shown in Fig.3-4(a).Accelerometers recordings of A1 and A3 were of very low amplitude and hence insignificant to be reported. Values of accelerometers A2, A4, and sliding displacement for the frequency of 2Hz are shown in Figs.3-20 (a), (c) and (e) respectively. Similar values for 10Hz are shown in Figs.3-20 (b), (d), and (f). Following are the observations:

1. Peak acceleration values recoded by accelerometer A2 at 2Hz and 10Hz were around 0.16g (see Fig.3-20 (a, b). This indicated a fivefold reduction of amplitude when compared with the shake table excitation (0.8g). Moreover, it can also be observed that frequency of base excitation has no effect on acceleration response recorded by A2.
2. It is interesting to note that for a sinusoidal input base excitation, output acceleration appears to be in form of a rectangular pulse. During a harmonic cycle, as base excitation force overcomes limiting static frictional force, sliding initiates (See Fig.3-20). Once sliding starts, the body continues to move with a virtual

constant acceleration, giving a rectangular pulse look to the acceleration profile. This state of constant acceleration continues, till the point input sine wave reverses its direction and its magnitude grows more than that of frictional resistance. This process repeats itself for every stick-slip cycle.

3. There was insignificant variation in response acceleration time histories recorded on the specimens with frequency of the base excitation. The basic shape of the profile remained same with the only change in the duration of a cycle.
4. Maximum sliding displacement observed was 26mm at 2Hz frequency [see Fig.3-20 (e)] and 1.6mm at 10Hz frequency [see Fig.3-20 (f)]. These readings highlighted a substantial reduction (around 16 times) in displacement amplitude with increasing frequency of excitation. It shall be noted that the input shake table displacement was divided by a factor 25 resulting in the reduced slip. The same reason is valid for the root cause of the reduced effect of high frequency input motions, with displacement in place of velocity. [63]
5. There was a large reduction observed in the amplitude of the sliding displacement with the frequency of base excitation. The physical explanation for the same can be obtained by comparing the time available to the input excitation in initiating and sustaining sliding motion. As the frequency of excitation increases, time available for the net sliding force to cause slip reduces, which in turn reduces slip displacement significantly as quantified in the earlier point.
6. A shift of sliding displacement centerline was observed as shown in Fig.3-20(e). This indicates a net final displacement after termination of base excitation. Variation of displacement with time was similar to the input excitation with a phase difference between the two. However, centerline shift happened in the initial cycle, signified net final slip from the original position.

7. The maximum value of slip was recorded for a sinusoidal excitation of 1sec. Stationary part of slip values are plotted for various frequencies in Fig.3-21. It can be observed that slip behavior is also dependent on base excitation frequencies. The stationary value of sliding displacement varied from 0.07m at 1Hz to 0.001m at 10Hz frequency as shown in Fig.3-21. Similar to the rocking angle for rocking motion as observed in Section.3.3.4, in this case, response quantity (slip displacement) reduced considerably with an increase of frequency. The reason for such a behavior can again be physically explained by observing the difference in net available time required for slip displacement. As the frequency increases, the effective time of base motion causing slip decreases and hence slip displacement reduces. It is worth noting again that slip displacement is independent of specimen's slenderness value as was recorded earlier during seismic motion testing also.

**Table 3-7 Details of various experiments performed to observe effects of base motion characteristics and slenderness on the sliding response of specimens**

| Test Run | Specimen | Input Base excitations<br>Peak Amplitude(g) | <br>Frequencies(Hz) | Coefficient of friction (μ) |
|---|---|---|---|---|
| **1** | TS1 | 0.8 | 0.5,1,2,3,4,5,6,7,8,9,10 | 0.15 |
| **2** | TS2 | 0.8 | 0.5,1,2,3,4,5,6,7,8,9,10 | 0.15 |
| **3** | TS3 | 0.8 | 0.5,1,2,3,4,5,6,7,8,9,10 | 0.15 |

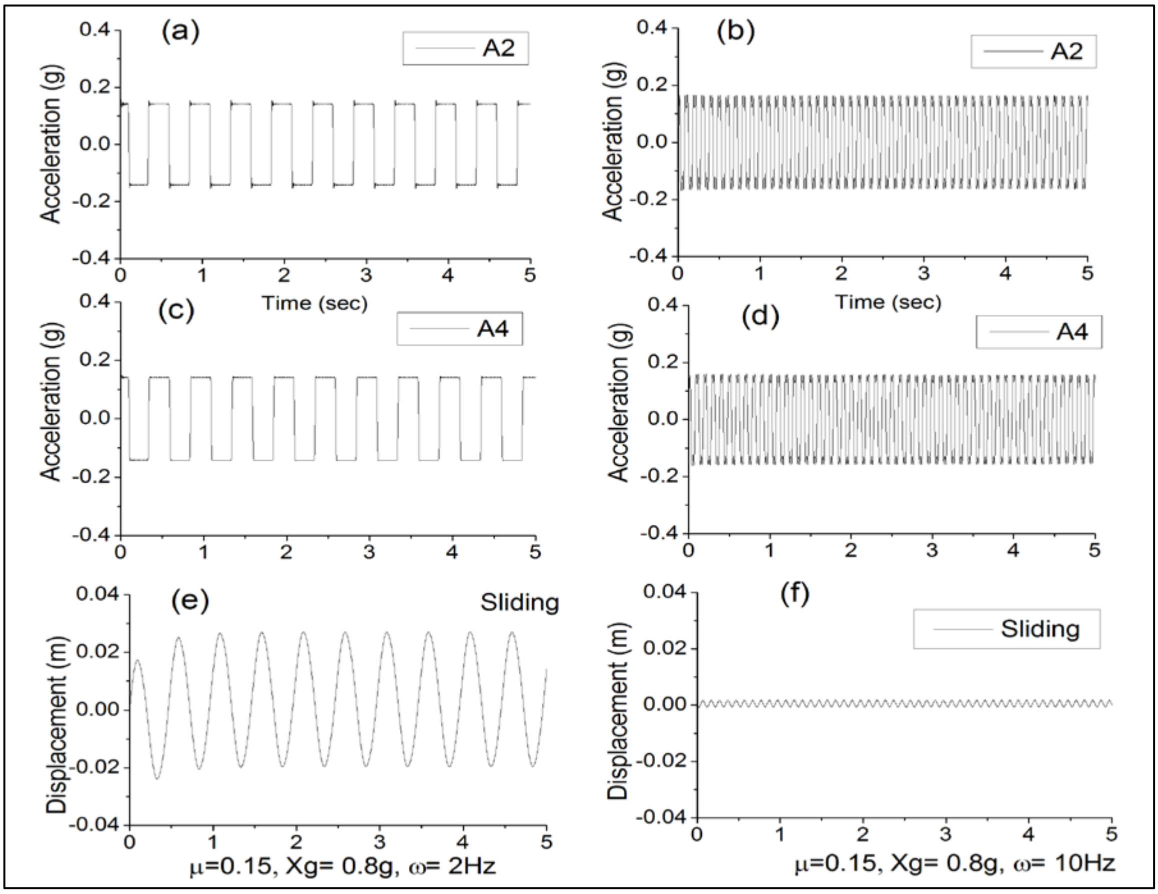


**Figure 3-20 Acceleration time histories recorded by various accelerometers for the test specimen TS1. (a, c, e) represents a response to harmonic base excitation of Xg=0.8g, ω=2Hz and (b, d, e) represents a response to harmonic base excitation of Xg=0.8g, ω=10Hz**

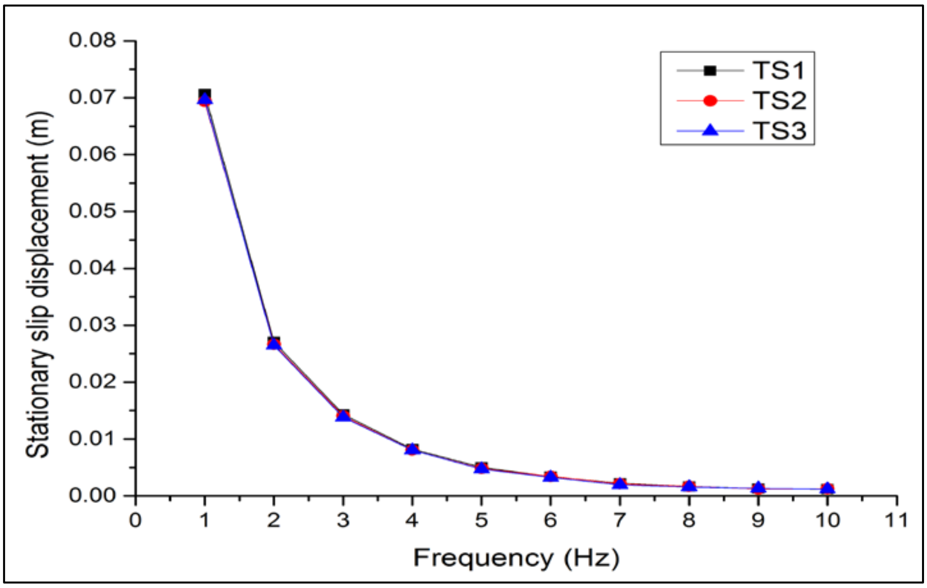


**Figure 3-21 Variation of amplitude of stationary part of slip displacement with frequency of excitation for TS1, TS2 and TS3 (Xg=0.8g, μ=0.15)**

### 3.3.5.2 Response Amplification

Acceleration amplification for sliding motion was evaluated for all the three test specimens. Experimental results highlighted following important points:

1. In general, Acceleration amplification in sliding motion was lesser than rocking motion for similar base excitation parameters. As observed from Fig.3-22, recorded value of AF was around 0.2.

2. AF value was found to be independent of base excitation frequency and was completely defined by the coefficient of friction value. Moreover, the slenderness of the specimens had no effect on the AF. Hence, AF value was observed to be independent of parameters like frequency and amplitude of excitation and slenderness value (aspect ratio) of the specimen.

3. AF value of less than unity makes sliding an attractive alternate over the rocking motion as far as energy dissipation is considered. It can also be generalized that sliding motion substantially reduced acceleration transmitted to the top. Hence, sliding motion could be considered as an effective way of dissipating input energy added into the system by the base excitation without further transmitting it.

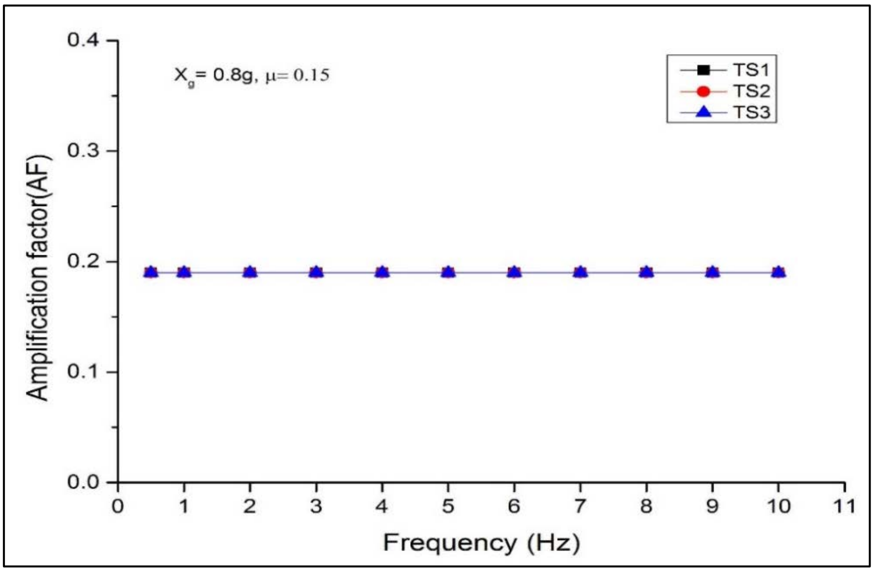


**Figure 3-22 Acceleration amplification factor variation with frequency for TS1, TS2 and TS3**

### 3.3.6 Dynamics of Combination of Rocking and Sliding Motion

After studying dynamics of a free-standing rigid body in pure rocking and sliding motion, it was formulated to test the specimens in a combination of rocking and sliding mode of motion. It is apparent form motion initiation criteria diagram shown in Fig.2-2, that there is a narrow region pertaining to the combination of sliding and rocking motion. In addition to that, it can also be observed that this band reduces in size with the reduction of aspect ratio from four to two. Experimentally, it was difficult to arrange a suitable combination of $\mu_s$ and $A_g$ values which could simulate this mode of motion. However, this combined mode of motion was simulated by using HDPE as a base material which had $\mu_s$=0.32, as determined experimentally, with the steel test specimens. It can be noticed from Fig.2-2, that for a value of $\mu_s$=0.32 and $X_g$>0.5g, it is possible to simulate a combination of rocking and sliding mode of motion for test specimen TS1. Hence it was decided to perform experiments only on the TS1 and study its dynamic behavior. Specimen TS1 was subjected to harmonic base excitations of varied frequencies. Shake table experiments were carried out for the conditions ($\mu_s$=0.32, $X_g$=0.8g and ω=0.5 to 10Hz).

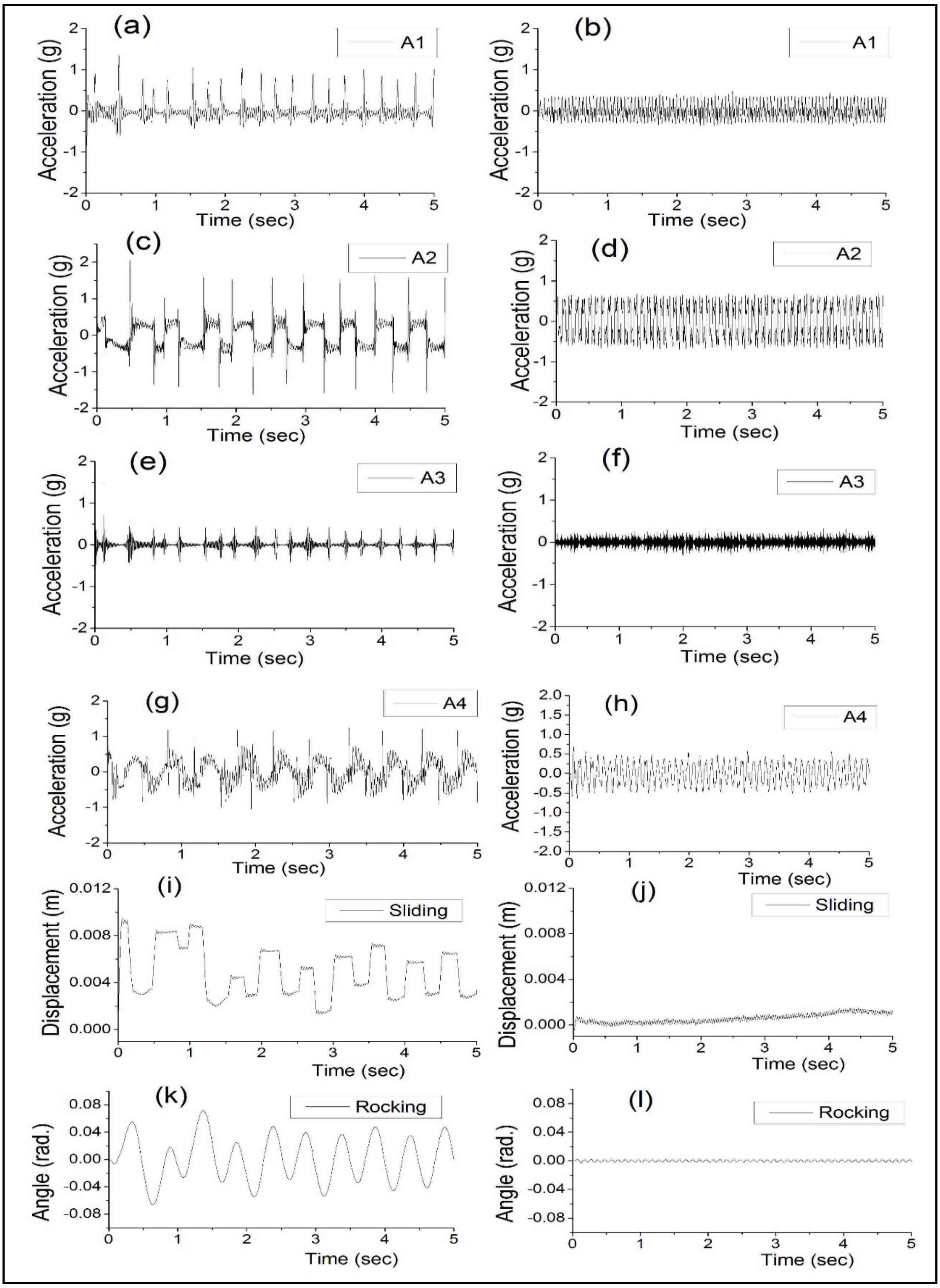


**Figure 3-23 Acceleration, sliding displacement and rocking angle response time histories recorded for test specimen TS1 (f=2Hz, μ=0.32, $X_g$=0.8g)**

A combination of sliding and rocking motion initiated from the rest state. Accelerometer readings (A1, A2, A3 & A4), sliding displacement and rocking angle for frequencies of 2Hz and 10 Hz are plotted in Fig.3-23.(a to l) as shown below. Following were the significant interpretations from Fig.3-23.

1. Similar to rocking motion, here also peak acceleration amplitude recorded on top of the block by A2 for 2Hz frequency was 2g as shown in Fig.3-23(c). Hence, this mode of motion was also characterized by significantly high amplitudes of accelerations at the top [see Fig. 3-23(a, c)]. This indicated a predominance of rocking behavior over sliding motion. Acceleration amplification at the top was of the same order as observed in the pure rocking, thereby overshadowing the effect of reduction in acceleration amplitude observed in pure sliding motion.

2. As the frequency of base excitation increased from 2 Hz to 10 Hz, the amplitude of peak sliding displacement was reduced from 0.009m to 0.0017m [see Fig.3-23(i, j)]. Similarly, the peak value of rocking angle was also decreased from 0.06 radian to 0.002 radian [see Fig.3-23 (k, l)]. In addition to that, peak acceleration recorded at the top was reduced by one-third [see Fig.3-23 (c, d)].

3. Three-dimensional behavior of the block was again observed for the cases of combination of rocking and sliding motion. As shown in Fig.3-23(e,f), significant accelerations were recorded in the lateral direction (along Y-axis). This behavior underlined the need to consider three-dimensional effects while modeling and performing numerical simulations.

Before proceeding to study dynamics of flexible freestanding bodies, it is vital to understand the contact-impact behavior of the problem. Next section deliberates on this intricate phenomenon.

### *3.3.6.1 Contact- Impact behaviour*

For a rocking and combination of sliding rocking motion, impact behavior is significant for the thorough understanding of the motion. It was observed in the experimental results that impact phenomenon dominates characteristics of motion and acceleration amplification takes place in specimens. Recorded data by various accelerometers (A1, A2, A3 and A4), slip displacement and rocking angle for a time period of 5 secs is plotted in Fig.3-24. For better understanding, acceleration, velocity and displacement time histories recorded by the accelerometers located at the shake table, A1 and A2 are plotted for a duration of 1sec in Fig.3-24. In addition to that, Fig.3-25 highlights variation of rocking angle and slip displacement of the specimen TS1, for a duration of 1sec.

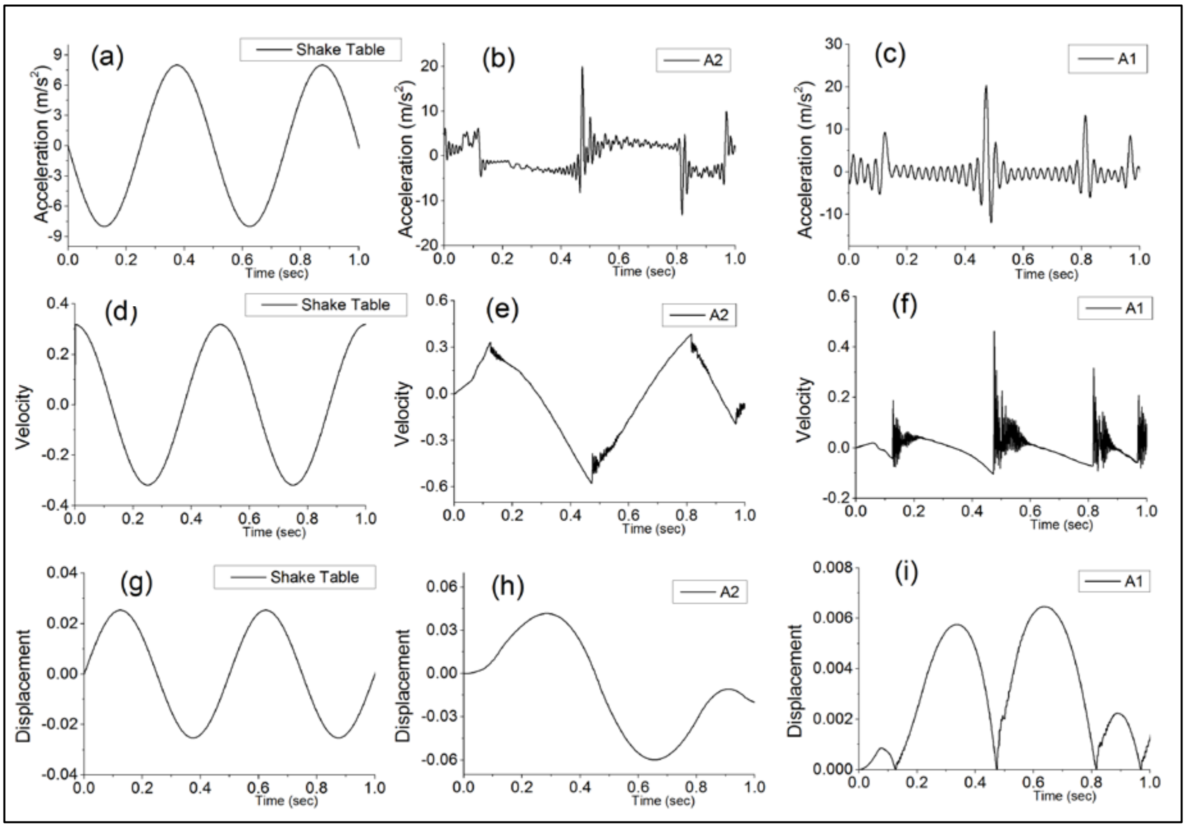


**Figure 3-24 Acceleration, velocity and displacement variations for TS1 as recorded by accelerometers ($f$=2Hz, $\mu$=0.32, $X_g$=0.8g)**

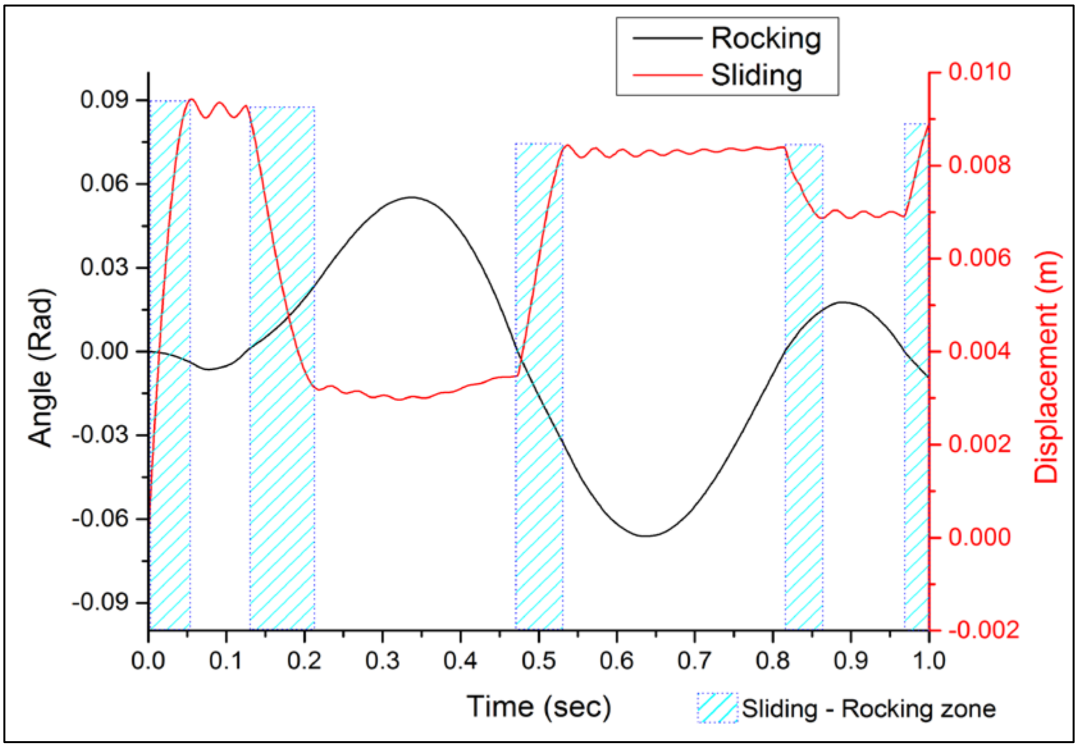


**Figure 3-25 Experimental results for rocking angle and sliding displacement for a duration of 1 sec (f=2Hz, μ=0.32, $X_g$=0.8g)**

Following observations for the contact-impact phenomenon in a combination of sliding-rocking motion are made (refer Fig.3-23, Fig.3-24 and Fig.3-25):

1. Acceleration time histories records highlighted multiple impacts across the contacting surfaces. This was evident in form of multiple jumps in acceleration time histories recorded on the top of the specimen by A2 (horizontal)and A1(vertical) during impacts as shown in Fig.3.23(a and c) for 2Hz frequency of base excitation. This was possible only for the case of a three-dimensional structure having a surface contact with the base.
2. It is interesting to note that impacts were reduced significantly for higher base excitation frequency of 10Hz. This point can be observed on comparing Figs.3-23(a) and 3-23(b). Reason for this is similar to the case of pure rocking, where lower frequencies of base excitations were observed to cause higher uplift and subsequent increase of acceleration

jumps during impacts. This led to the reduction of amplification factor with the increase of frequency.

3. Specimen exhibited simultaneous slip and rocking motion during experiments as observed from Figs.3-23(i) and 3-23(k). Magnitude of slip displacement and rocking angle was found to be a decreasing function of base excitation frequency. With the increase of frequency from 2Hz to 10Hz, peak values of slip displacements and rocking angles reduced from 9mm and 0.07radians to 1mm and 0.005radians respectively.
4. For a harmonic base excitation of 2Hz frequency and $\mu=0.32$, impacts occurred at 0.12, 0.47, 0.81 and 0.96secs in a time of 1 sec [see Fig.3-24(i) or Fig.3-25]. The frequency of impact observed was twice of that of the excitation frequency. That means every cycle of excitation involved two impacts of the block with the base.
5. For particular time instants, corresponding to impact, a sharp peak in acceleration was recorded. It was also noted that pre-impact (prior to edge contact) and post peaks (after edge contact) were significant. This owed to surface contact prior and after actual edge contact with the base.
6. It was examined in a sliding-rocking motion that in certain regions of the rocking time history, combination of sliding-rocking motion was predominant; while in other regions, pure rocking motion was observed as shown in Fig.3-25. Hatched regions in the figure correspond to a combination of sliding and rocking motion. However, intermediate regions correspond to pure rocking motion with almost no sliding displacement i.e. maximum variation in calculated sliding displacement was less than 0.0004mm.

Since, presence of three-dimensional motion has been experimentally observed during shake table testing, a three-dimensional numerical model of the specimen is required for carrying out numerical studies. It is proposed to develop a three-dimensional model which can accurately predict the dynamics of a free-standing rigid body subjected to base excitations. The developed generic model will be benchmarked with the existing experimental data. Next section gives the details of development and benchmarking of a three-dimensional finite element model.

## 3.4 Finite Element Modelling and Analysis

While performing experiments on the rigid parallelepiped test specimens, significant lateral accelerations (perpendicular to the line of action of base excitations) and movement was observed. Test results highlighted the importance of considering three-dimensional effects while accurately analyzing a parallelepiped block. Earlier research carried out by Egidio [65] and Pena [20] highlighted that for a square base parallelepiped structure three-dimensional effects cannot be neglected. Hence, to accurately predict dynamic response of a three-dimensional rigid parallelepiped structure, three-dimensional finite element model of test specimens was developed. Modelling and analysis procedure used for carrying out numerical calculations is presented. Three-dimensional finite element model of the test specimens (TS1, TS2 and TS3) were prepared in FE software. They were kept free-standing on the floor and the floor was subjected to different types of base excitations. In the coming sections, details of modelling and meshing techniques, boundary conditions, and contact interactions are provided.

### 3.4.1 Part modelling

All the test specimens were fabricated out of mild steel material. Sectional thickness was 3, 4 and 5mm respectively for TS1, TS2 and TS3. As the thickness was very less in comparison with longitudinal and lateral dimensions, shell elements were used for modelling. Here, a four node general-purpose shell element (S4R) with reduced integration and hourglass control was chosen. This element is capable of taking finite membrane strains. This element is suitable for analysing thin to moderately-thick shell structures. The element has four nodes with six degrees of freedom at each node (i.e. translations in the x, y, and z-axes, and rotations about the x, y, and z-axes). This element allow transverse shear deformation. This element uses thick shell theory as the shell thickness increases and become discrete Kirchhoff thin shell elements as the thickness decreases; the transverse shear deformation becomes very small as the shell thickness decreases. Hence this is a versatile shell element which is best suited for a contact analysis. In the present case, the shake table was very stiff in comparison with the test specimens. Moreover, stresses and strains in the shake table were of no research interest to us, hence it was modelled as a rigid body. Rigid element R3D4, which is a three-dimensional, 4-noded bilinear quadrilateral element was selected for analysis. This element doesn't have any mass properties and is defined with the help of a reference point. All the boundary condition were applied at the reference point because only the rigid body reference node has independent degrees of freedom. For a three-dimensional element, the reference node has three translational and three rotational degrees of freedom; for planar and axisymmetric elements the reference node has degrees of freedom 1, 2, and 6 (rotation about the 3-axis).The nodes attached to rigid elements have only slave degrees of freedom. The motion of these nodes is determined entirely by the motion of the rigid body reference node. For planar and three-dimensional rigid elements the only slave degrees of freedom are translations.

Since the rigid elements are not deformable, they do not use numerical integration points, and there are no optional formulations. In addition to this, there are no element output variables. The only output from rigid elements is the motion of the nodes. Reaction forces and reaction moments are available at the rigid body reference node. Details of various material properties are given in Table.3-8

Table 3-8 Properties of various materials used in finite element analysis

| Material | Density ($Kg/m^3$) | Modulus of Elasticity (GPa) | Poisson ratio |
|---|---|---|---|
| Aluminum | 2100 | 70 | 0.3 |
| Steel | 7800 | 210 | 0.3 |
| HDPE | 970 | 1 | 0.1 |
| Wood | 500 | 12 | 0.05 |

All the three test specimens were assembled on top of the rigid floor as shown in Fig.3-26. Contact constraints were applied at the contacting surfaces between floor and specimens. Next section describes more about the interactions and boundary conditions applied.

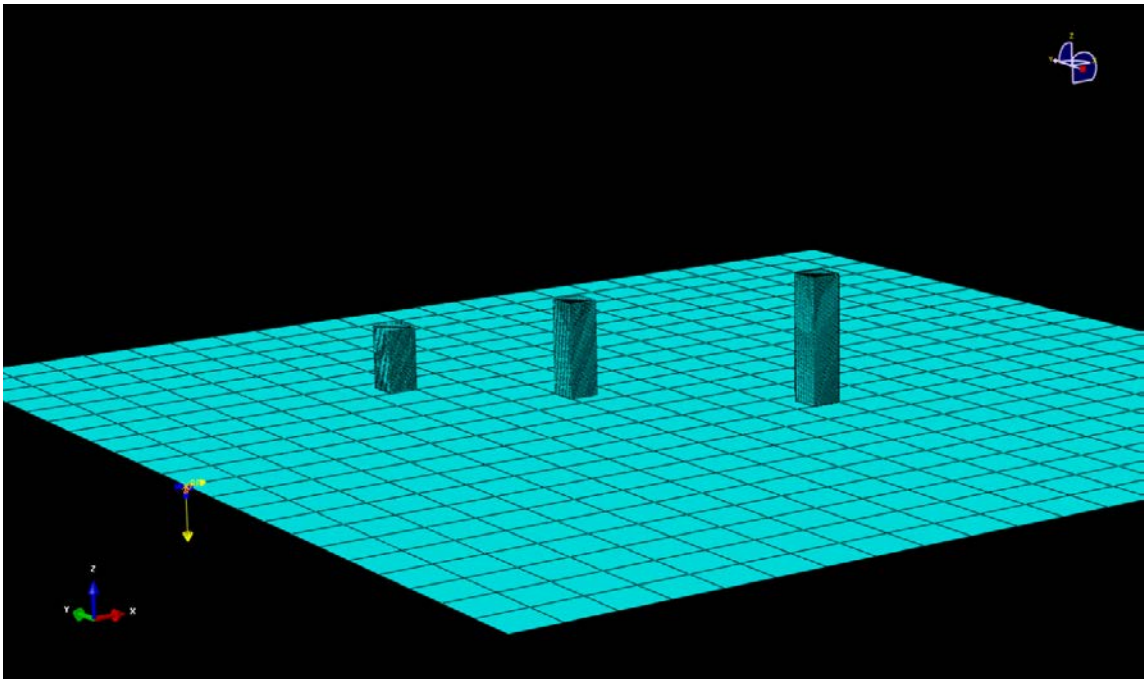

**Figure 3-26 Finite element assembly of the three test specimens (TS1, TS2, TS3) mounted on the top of a rigid shake table**

### 3.4.2 Contact interactions and boundary conditions

While creating an assembly of three test specimens and rigid floor, contact constraint was defined. In the present case, surface based contact formulation was used for defining the contact. The rigid floor was selected as a master surface and contacting surfaces on the specimens were selected as slave surfaces. In addition to the contacting surfaces between the floor and the test specimens, other surfaces perpendicular to the direction of base excitation (i.e. X-axis), lying in the YZ plane, were also selected as slave surfaces. They were selected because of the possibility of contact with the master surface in case of overturning of the specimens. Contacting surfaces are shown with dots in the Fig.3-27.

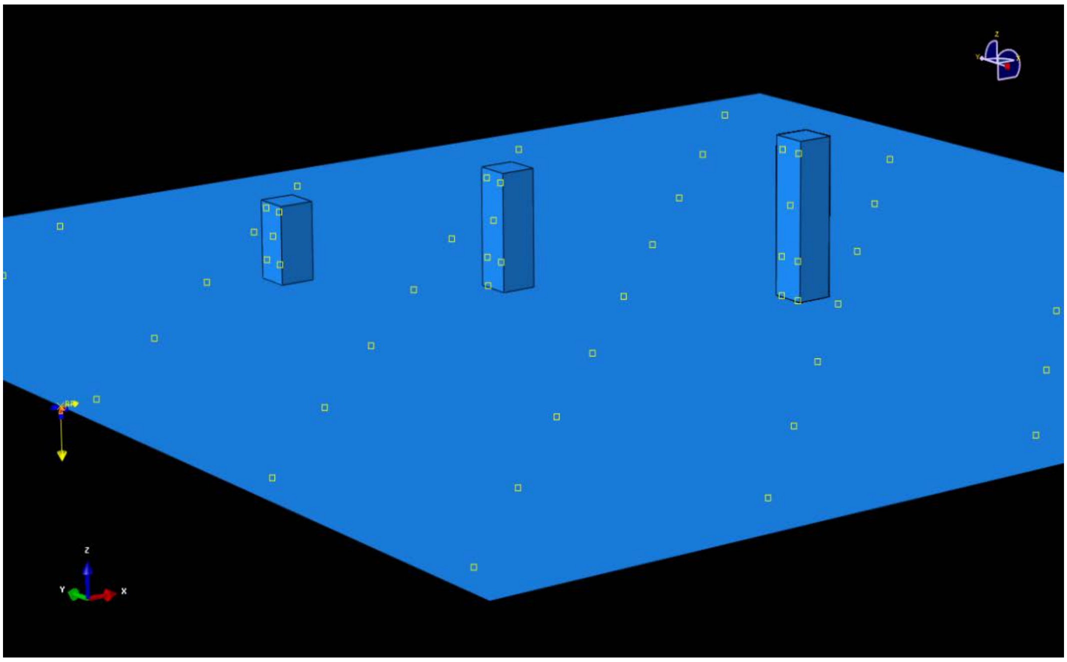

**Figure 3-27 Contact interaction between the master surface (floor) and slave surfaces (on the specimens)**

Contact properties were defined in the normal and tangential directions. In tangential directions, Coulomb friction model was used to relate the maximum allowable frictional (shear) stress across an interface to contact pressure between contacting bodies. The Coulomb friction model defines critical shear stress, ($\tau_{crit}$) at which sliding of the surfaces starts as a fraction of the contact pressure (p), between the surfaces. ($\tau_{crit} = \mu p$) The stick/slip calculations determine when a point transitions from sticking to slipping or from slipping to sticking. This friction model assumes that μ is the same in all directions (isotropic friction).

Similarly, in the normal direction, hard contact was selected to account for normal pressure/over closure relationship. For numerical enforcement of contact constraints in tangential and normal direction, Penalty algorithm was used. [66] [67] [68] [69] [70]. Two configurations (path) based contact tracking scheme was used in a finite sliding formulation with surface to surface discretization. All the rigid body rotational motions of the floor were constrained and actual recorded time histories of base excitations were applied at reference node of the floor.

### 3.4.3 Modal Frequency Analysis

Before carrying out dynamic analysis of test specimens, it is important to understand fundamental dynamics characteristics of the specimens. Natural frequencies of the test specimens in the fixed based boundary condition were evaluated using FE software. Lanczos solver was used for eigenvalue extraction. The fundamental frequencies of TS1, TS2 and TS3 are tabulated in Table.3-9. First three fundamental mode shapes for test specimens TS1, TS2 and TS3 are shown in Fig.3-28, Fig.3-29 and Fig.3-30 respectively. Displacement gradients are shown by color scheme, whereas blue color indicates lowest displacement value and red color indicates the highest.

It can be observed from Fig.3-28, Fig.3-29 and Fig.3-30 that fundamental mode of deformation of these rigid structures does not include bending of the complete structure about fixed end. This is a typical behavior of a box type of rigid block which in fundamental mode undergoes deformations of individual panels (sides), but not bending of the entire structure about the centroidal axis.

**Table 3-9 First three modal frequencies of the test specimens**

| Mode | Modal Frequencies(Hz) | | |
|---|---|---|---|
| | TS1 | TS2 | TS3 |
| 1 | 93 | 94 | 186 |
| 2 | 121 | 127 | 248 |
| 3 | 131 | 134 | 248 |

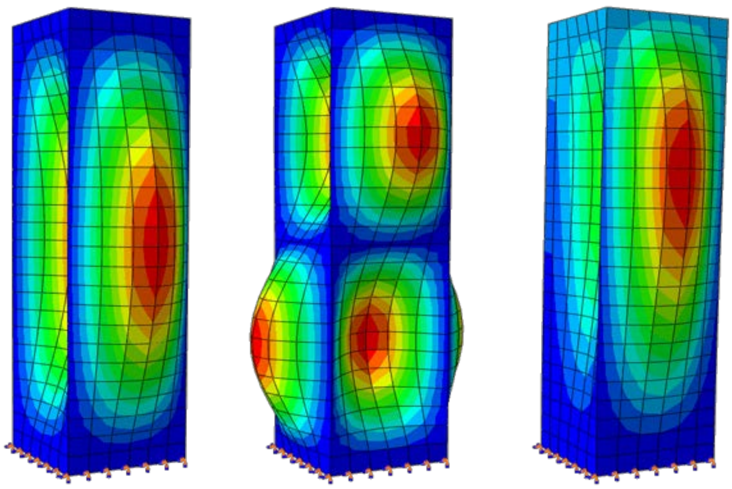

(a) (b) (c) (d)

**Figure 3-28 Fundamental modal shapes of test specimen TS1 in fixed base boundary condition, (a) Un-deformed shape, (b) Mode1, (c) Mode2 & (d) Mode3**

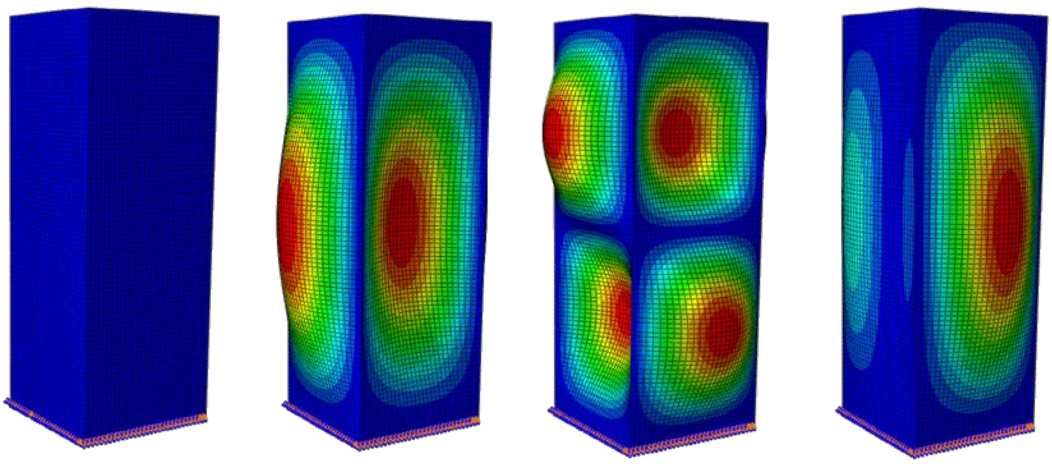

(a) (b) (c) (d)

**Figure 3-29 Fundamental modal shapes of test specimen TS2 in fixed base boundary condition, (a) Un-deformed shape, (b) Mode1, (c) Mode2 & (d) Mode3**

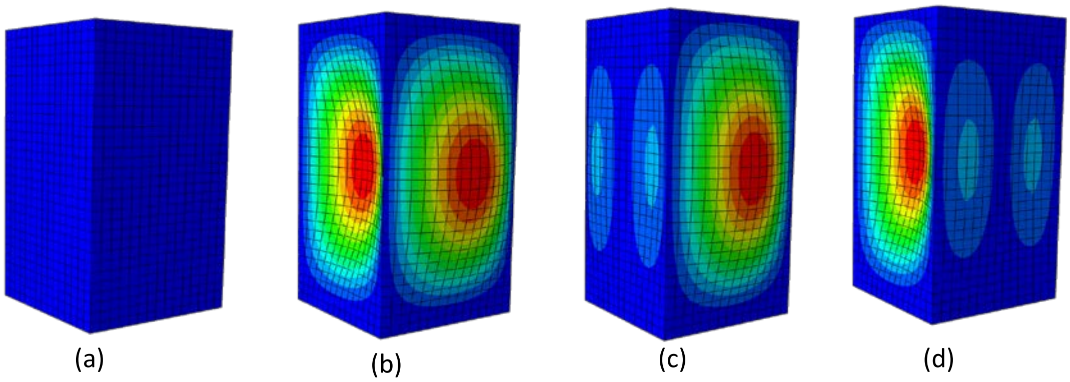


**Figure 3-30 Fundamental modal shapes of test specimen TS3 in fixed base boundary condition, (a) Un-deformed shape, (b) Mode1, (c) Mode2 & (d) Mode3**

### 3.4.4 Numerical solution

Implicit solver was used to carry out numerical solution. Solver uses the Hilber-Hughes-Taylor [71] time integration scheme for a numerical integration. The Hilber-Hughes-Taylor operator is an extension of the Newmark beta-method. Numerical parameters associated with the Hilber-Hughes-Taylor operator were tuned differently for moderate dissipation and transient fidelity applications. This time integration operator is implicit, which means that the operator matrix must be inverted and a set of simultaneous nonlinear dynamic equilibrium equations must be solved at each time increment. The solution was done iteratively using Newton's Raphson method. [66]. The principal advantage of this operator is that it is unconditionally stable for linear systems; there is no mathematical limit on the size of the time increment that can be used to integrate a linear system. Nodal accelerations and displacements at locations where actually sensors were installed during shake table experiments were obtained. Next section compares results obtained from the numerical models presented in this chapter with the experimental results.

### 3.4.5 Validation of Numerical Models

In the present chapter, two types of numerical models were presented. Firstly, a two-dimensional analytical mode was presented in Section3.2 and then a three-dimensional finite element model was presented in Section3.4. It is important to validate these models using generated experimental data. Test specimen TS1 is selected for validation of numerical models. Numerical results for sliding and rocking mode of motions is compared with the corresponding test results. In addition to that, amplification factors for all the three modes of motion of TS1 are compared. This comparison shall be valid for other two specimens also because of similarity in modelling and analysis methodology. Comparison of experimental results with two-dimensional and three-dimensional model is presented below. Comparison of results for amplification factors in sliding, rocking and sliding-rocking mode is presented in Fig.3-31, Fig.3-32and Fig.3-33 respectively. Comparison of sliding displacements and rocking angles are presented in Fig.3-34 and Fig.3-35 respectively.

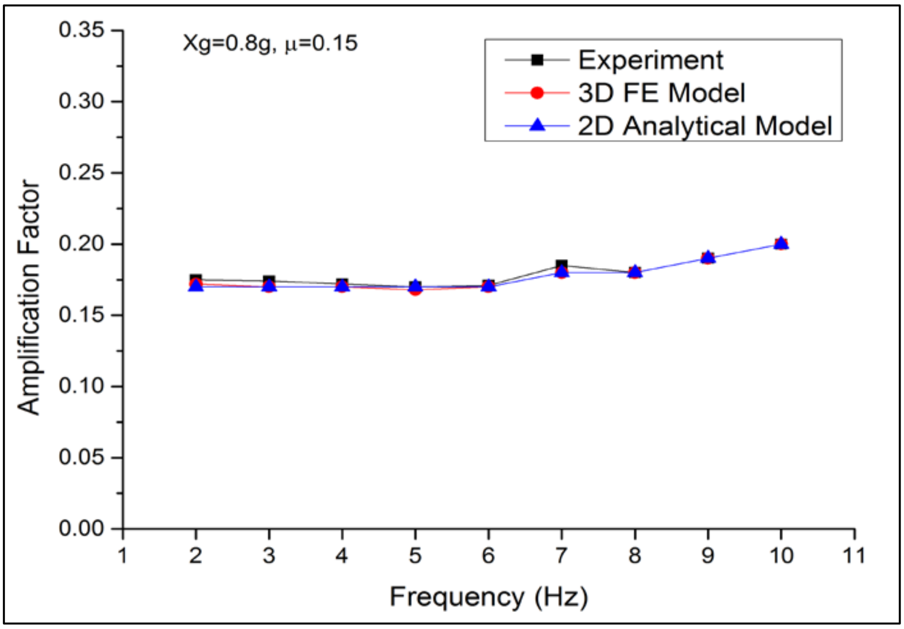


**Figure 3-31 Comparison of acceleration AF obtained by experiments, 3D FEA model and 2D analytical model of TS1 in sliding motion**

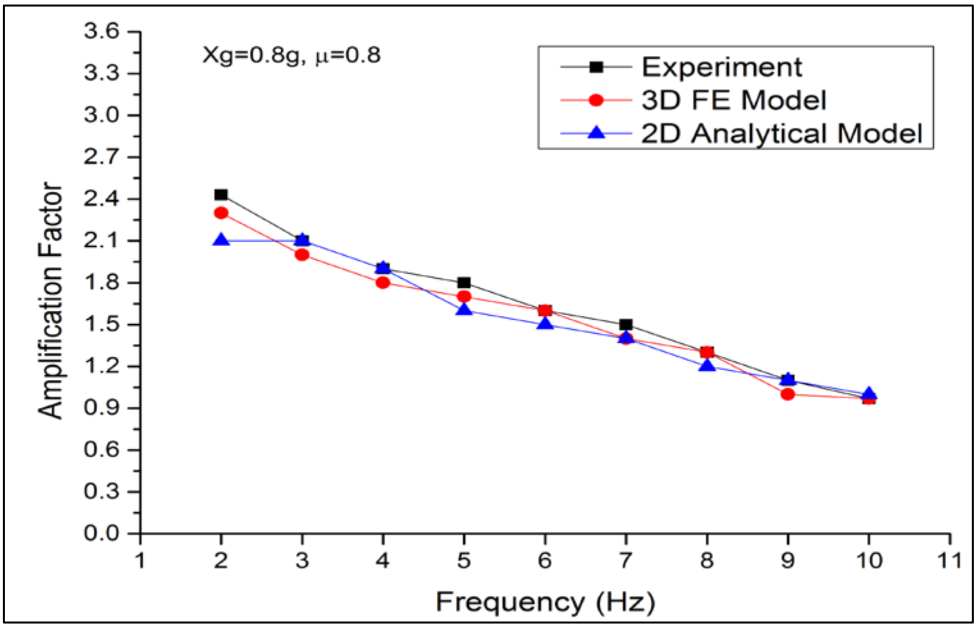


**Figure 3-32 Comparison of acceleration AF obtained by experiments, 3D FEA model and 2D analytical model of TS1 in rocking motion**

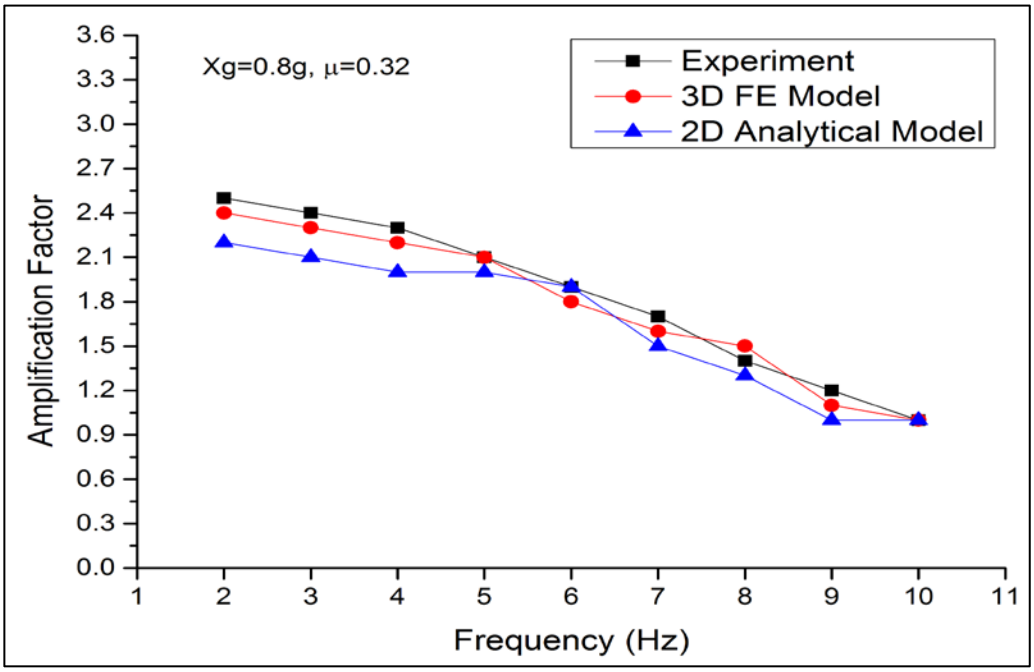


**Figure 3-33 Comparison of acceleration AF obtained by experiments, 3D FEA model and 2D analytical model of TS1 in sliding-rocking motion**

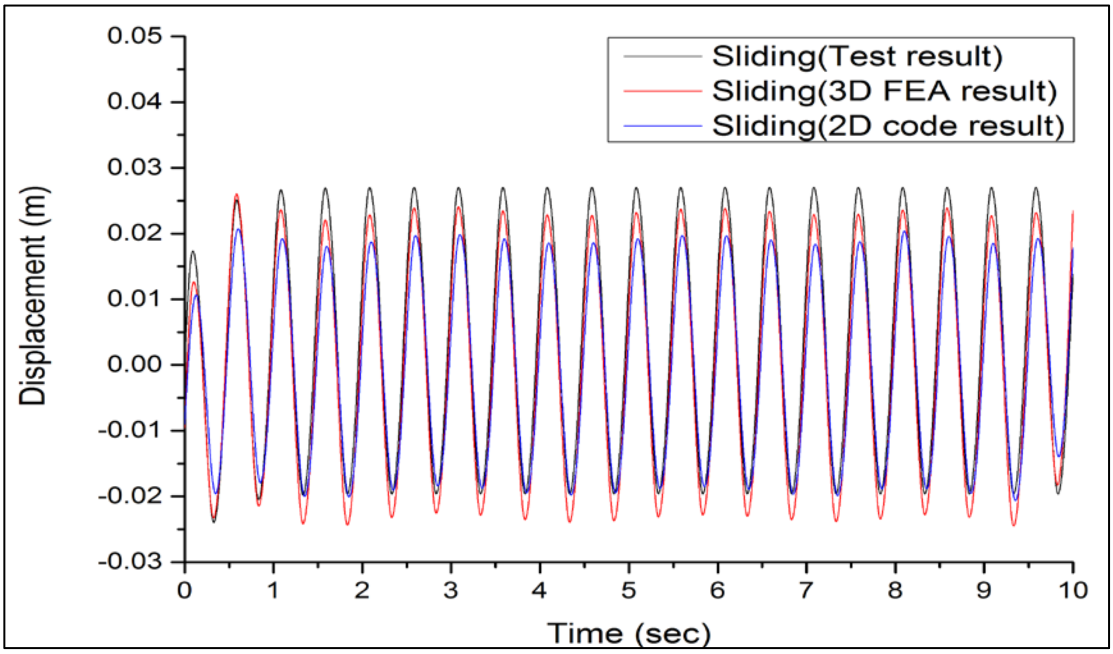


**Figure 3-34 Comparison of sliding displacement obtained by test, FEA and numerical code for TS1 (μ=0.15 and ω=2Hz)**

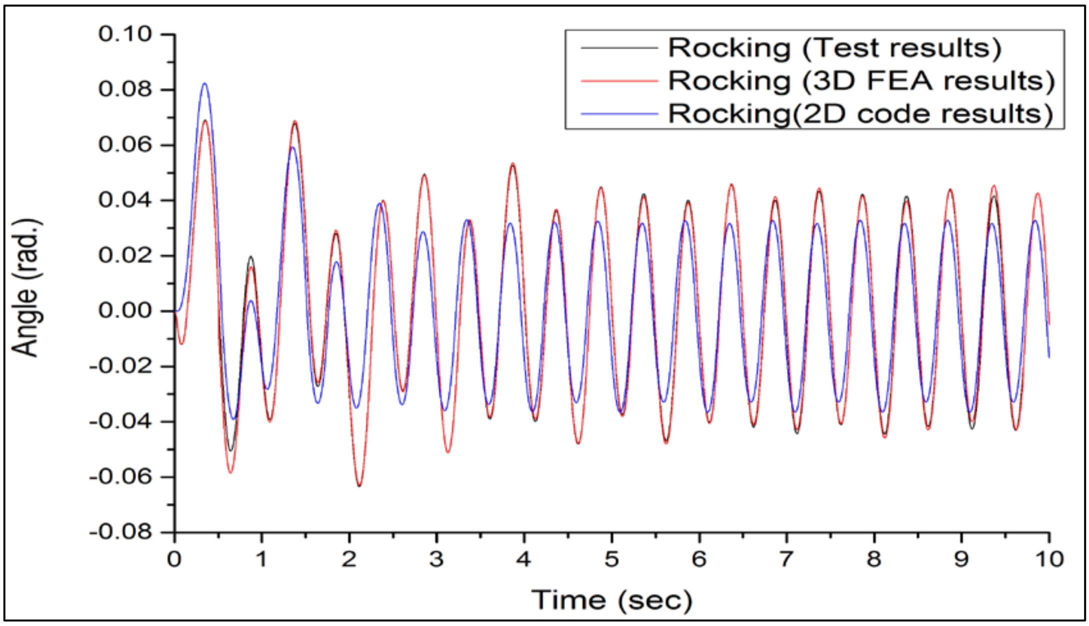


**Figure 3-35Comparison of rocking angle obtained by test, FEA and numerical code forTS1 (μ=0.72 and ω=2Hz)**

Following points can be observed from Fig3-31 to Fig.3-35:

1. In general, three-dimensional FEA, two-dimensional numerical code and shake table experiment results were in good agreement and indicated similar trends.
2. Maximum variation in amplification factor for sliding mode was 2.7% between experiment and FE results and 2.9% between experiment and numerical results as shown in Fig.3-31. Similarly, for rocking motion maximum variation was 9% between experiment and FE results and 7.6% between experiment and numerical results as shown in Fig.3-32. For the sliding-rocking motion maximum variation was 8.3% between experiment and FE results and 7.8% between experiment and numerical results as shown in Fig.3-33.
3. For sliding displacements, the maximum difference between experiment and FEA result was 12 percent of experiment value as shown in Fig.3-34. This difference occurred only near the peaks of the curve, while at other places difference was less than 1 percent. On the other side, the maximum difference between experimental and numerical code results was 31 percent of experiment value. Again, this happened only near the peaks, whereas at other places difference was insignificant.
4. For the rocking angle, the maximum difference between experimental and FEA result was 13 percent of the experimental value, which occurred at t=0.6sec as shown in Fig.3-35. Rest of the time difference was insignificant to mention. However, the difference between experimental and 2D code result was around 47 percent of experiment value for a peak at t= 2.1sec, whereas it was lesser than this values at rest of the peaks. At other places, 2D code results accurately matched with the experiment values.
5. Three-dimensional model FEA results were coherent with the corresponding experiment results. Variation of various parameters like amplification factor,

sliding displacement and rocking angle was accurately predicted by analysis. However, some variations were observed due to inevitable errors in modelling and contact properties input.

6. Two-dimensional numerical code results were also coherent with the experiment values. Code results satisfactorily predicted the response of three-dimensional parallelepiped block. Errors in estimation of rocking angles were attributed to three-dimensional effects and errors in estimating values of input contact parameters like coefficient of friction and restitution. Hence, it can be concluded that F.E. analysis could be utilized in study of behavior of a freestanding structure.

## 3.5 Three-dimensional Motion Initiation Criteria Diagram

Experimental and numerical results presented in Section3.3.4.1 signified the importance of frequency of base excitation for determining initiation of any mode of motion from the rest state. The frequency of excitation whether it was harmonic or random was observed to have a pivotal role in exciting different modes of motion for a rigid test specimens. It can be easily understood, that generally initial mode of motion dominates the response unless there is a variation in amplitude or frequency content of the base excitation. To introduce effects of base excitation frequencies in 2D motion initiation criteria diagram as shown in Fig.2-2, it is redeveloped into 3D diagrams.

Numerical calculations were carried out using FE model of test specimen TS1, for different values of the parameters like $A_g$, $\mu_s$ and $\omega$. FE results were used to redraw Fig.2-2, with the frequency of excitation as one of the parameters. This is named as initiation criteria diagram as shown in Fig.3-36. In addition to that a 2D projection of these plots on YZ and XY axis has been taken and shown in Fig. 3-37 and Fig.3-38 respectively. These diagrams identify various regions corresponding to different modes of motion.

Developed motion initiation criteria diagrams accentuate following important characteristics of a freestanding rigid block subjected to base excitations.

1. For any combination of parameters (μ, $A_g$ and AR), lies a value of frequency above which a freestanding structure subjected to harmonic/periodic base excitation shall practically be in a state with very low motion. The state of low motion is shown in the diagrams by the points, given by following conditions:

    a. Maximum value of the angle of rotation (rocking angle) calculated during numerical simulation should be less than 0.003 radians.

    b. Maximum sliding displacement calculated during numerical simulation should be less than 1mm.

2. It was observed that with the increase of frequency, motion of the body (rocking, sliding or slide/rock) reduces significantly. For example, for an amplitude of 0.8g and c.o.f of 0.2, sliding displacement was as large as 70mm which reduced to 0.7mm for a frequency of 10Hz. Hence this value of frequency which reduced the amplitude below a defined value given above is termed as cut off frequency.

3. In the sliding region and sliding-rocking region, cut off frequency increased as a nonlinear function of peak base acceleration amplitude. While In the rocking region, it increased linearly with the peak base excitation amplitude.

4. For a fixed value of amplitude, cut off frequency decreased non-linearly with increasing μ, until structure was lying in slide-rock zone ($\mu < 0.4$). Afterwards, as the value of coefficient of friction was increased up to rocking zone cut off frequency attained a constant value.

5. It was noted in the rocking zone, for a fixed value of amplitude, cut off frequency was independent of coefficient of friction.

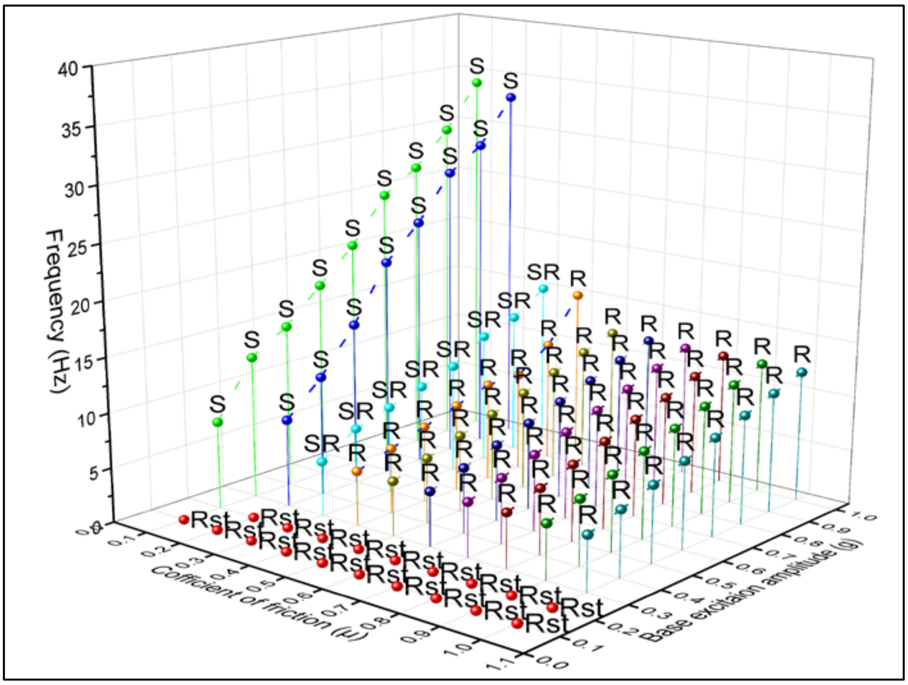


**Figure 3-36 Initiation criteria diagram (Fig.3-7) replotted with frequency as an axis, showing various possible modes of motion for a rigid block of four aspect ratio (S-sliding, R-rocking, SR-slide/rock, Rst-rest state)**

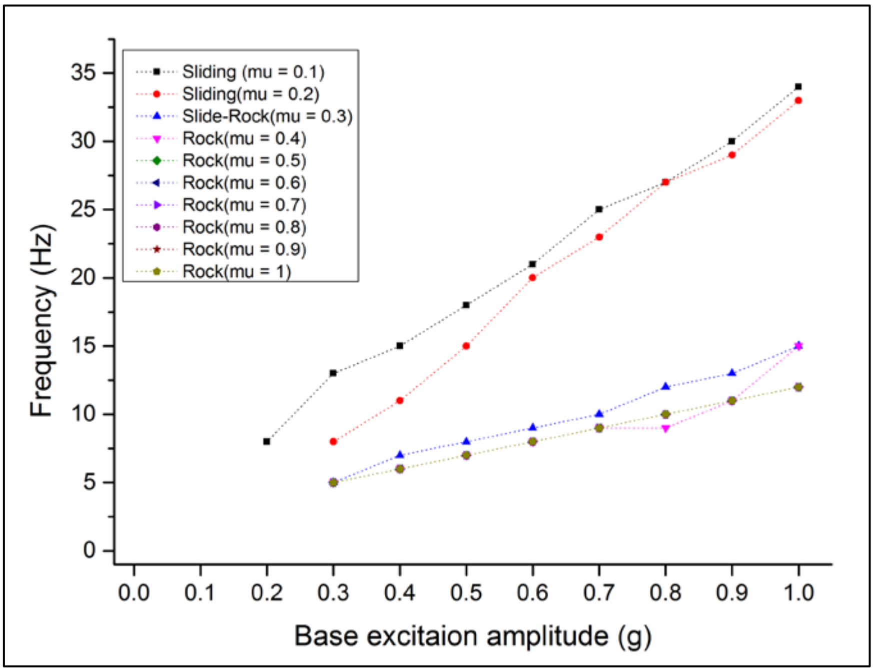


**Figure 3-37 YZ plane projection of 3D motion initiation diagram**

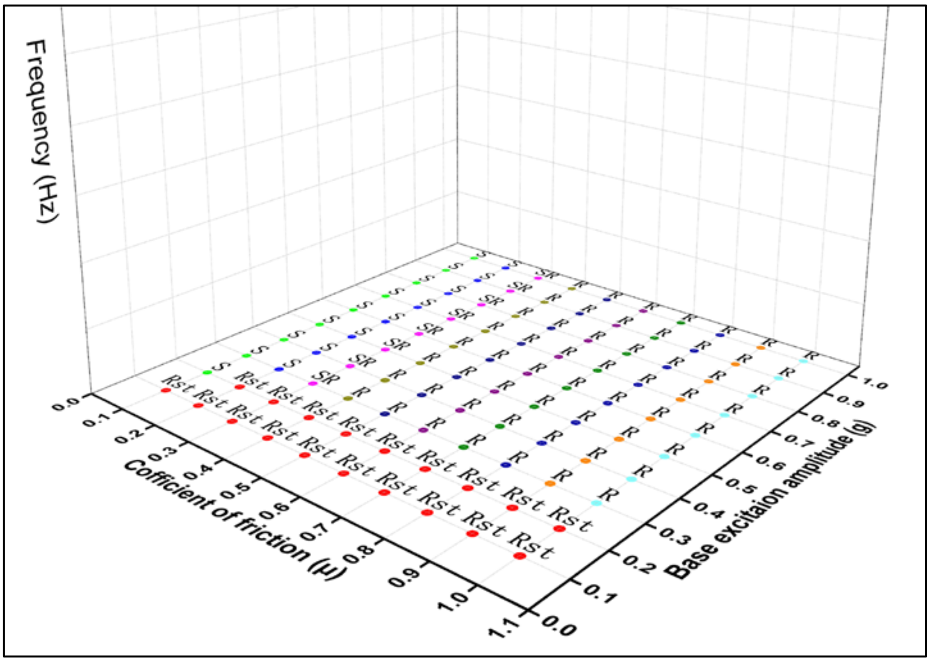


**Figure 3-38 XY plane projection of 3D motion initiation diagram**

## 3.6 Outcomes and Discussions

The behavior of a three-dimensional parallelepiped structure subjected to base excitation is highly nonlinear. When subjected to periodic, harmonic or seismic base excitation, it can undergo different modes of motion. Initiation of any particular mode from rest and hence stability is governed by various parameters including frequency of base excitation. It was observed that for any given value of other parameters, there exists a frequency above which structure remains in the rest state and is completely stable. For the designers of the freestanding systems, this could be a useful information in selection and optimization of operating parameters for inherent safety of the structures from base excitation. We observed that cutoff frequencies for the sliding mode of motion were higher compared to other two modes of motion making it inherently unstable. Nevertheless, amplification factor was observed to be below unity irrespective of the frequency of base excitation. Hence, a sliding freestanding system does not amplify base motion; however, the prime concern is sliding displacement. If there is no safety concern from the sliding displacement, then the designers can allow calculated slip to dissipate energy input into the system by base excitation. Generally, designers have a very little control over the base motion characteristics especially in the case of seismic excitation. Nonetheless, they can have some flexibility in selecting coefficient of friction by appropriate selection of base material.

Rocking and combination of sliding and rocking mode of motion are predominant in low-frequency range. Especially frequencies pertaining to free rocking frequencies of a structure has a tendency to cause uplift, even at an amplitude lower then statically required for it. Base isolation can be quite effective to filter off these low frequencies of base excitation and hence enhancing the stability of the system by limiting rocking motion. The rocking mode is not inherently safe for a structure because it not only amplifies base motion but also may lead to overturning of the structure. In the case of a seismic excitation, low frequency and high amplitude waves are more dangerous for the stability of a structure. It was observed that for a rocking mode amplification factor was always above unity, irrespective of the cutoff frequency. Hence input energy dissipation via frictional sliding is more efficient and safer than via impact in the rocking motion. As the frequency of impact increases, more amplification takes place making any system located on top part of the structure vulnerable to damage. After studying the dynamic behavior of a rigid body, dynamics of a flexible body is explored in the next chapter.

# CHAPTER 4 DYNAMICS OF A FREE-STANDING FLEXIBLE BODY SUBJECTED TO BASE EXCITATIONS

## 4.1 Introduction and Outline

In the last chapter, the fundamental dynamic behavior of a free-standing rigid body subjected to base excitations was presented. Analytical formulation and numerical solutions were presented on the basic premise of rigid body motions. In this chapter, basic assumption of the predominance of rigid body motions is removed and comprehensive studies are performed, considering possible elastic motions of a flexible free-standing bodies subjected to base excitations. As discussed earlier in Section 2.3, the majority of available research on the subject is focused on a single degree of freedom cantilever type of model, which has a limited applicability.

In this chapter, extensive experiments were carried out on flexible test specimens, geometrically similar to rigid specimens discussed in Chapter-3. Effect of body's flexibility on initiation of any particular mode of motion from rest was investigated. In addition to that, overall stability of body in terms of overturning potential for rocking motion or maximum allowable slip for sliding motion was studied. Further, the effect of flexibility on amplification factor was examined.

Section 4.2 of this chapter present details of experiments carried out on flexible free-standing bodies. Then, Section 4.3 presents a numerical investigation and provides in-depth analysis of behavior. Section.4.4 of the chapter highlights important findings of the research carried out and finally Section.4.5 summarizes the chapter with final conclusions.

## 4.2 Experimental Investigation

### 4.2.1 Objectives and Introduction

Flexible test specimens of three different aspect ratios were tested on a uni-directional shake table. The objective of this testing was to observe dynamic behavior of flexible freestanding bodies when subjected to base excitations. Experiments carried out were similar to those performed earlier for the geometrically similar rigid specimens (TS1, TS2 & TS3). The intent was twofold; firstly to observe overall dynamics of a flexible body and secondly, to investigate effect and interaction of elastic motions on rigid body motions and overall dynamics of the problem. The aim was also to observe differences in the response of geometrically similar flexible and rigid test specimens when subjected to identical loading and boundary conditions.

### 4.2.2 Test Set up and Specimens

A uniaxial hydraulic shake table available at Bhabha Atomic Research Centre (BARC) having dimensions of 1m x 1m was used for testing. Details of the shake table were already provided in the last chapter in Table.3-1. Three flexible test specimens TS4, TS5 and TS6 of aspect ratios four, three and two respectively were fabricated in such a way that they were geometrically similar to the three rigid specimens TS1, TS2 and TS3 tested earlier. These specimens had top and bottom plates which were bolted to each other through four columns. Using a single set of plates, three different specimens can be created by interchangeably using channels of different lengths. Details of the specimens are provided in Table.4-1. Three different base materials were bolted sequentially to the shake table to generate three different values of coefficient of friction (μ) with the specimens. This was to simulate three possible modes of motion viz. sliding, rocking, and combination of them. The test set up and specimens are shown in Fig.4-1. Five accelerometers (A1 to A5) were mounted on the test specimens at the locations exactly similar to earlier cases as shown in Fig.3-4. A5 was mounted on the shake table.


**Figure 4-1 Test set up showing different test specimens.(a) TS4, (b) TS5, (c) TS6 and (d) high-speed videography arrangement**

### 4.2.3 Preliminary Dynamic Characteristics

Before carrying out shake table testing, important dynamic properties of the specimens were evaluated. These were free rocking frequency (henceforth denoted by $\omega_r$), critical angle (henceforth denoted by $\alpha$), fundamental frequency in fixed base conditions (henceforth denoted by $\omega_n$) and coefficients of friction ($\mu$) between the specimen and different materials to be used as a base material. Various dynamic properties of test specimens are given in Table.4-1.

### 4.2.3.1 Free rocking frequencies and critical angle

To rule out any deviation from the theoretical value, critical angle was experimentally determined by uplifting the specimens up to the point of self-overturning. Similarly, free rocking frequencies ($\omega_r$) of the test specimens were evaluated for different values of initial uplift. Uplift was simulated by providing angular displacement about a pivoting edge. Experiments were performed for different values of initial uplift starting from 0.001m up to 0.020m of uplift and finally just below the value of critical uplift corresponding to critical angles. Accelerometers readings obtained from accelerometer-A2, mounted on the test specimens, were analyzed using Fast Fourier Transform (FFT), to obtain free rocking frequencies. All the three specimens were tested sequentially to obtain values for rocking frequencies. Fig.4-2 displays variation of free rocking frequencies with initial uplift for flexible test specimens. Experimentally evaluated values of rocking frequencies are given in Table.4-1. For each specimen, the frequency corresponding to a critical value of uplift is also given in a bracket under the same column.

### 4.2.3.2 Evaluation of coefficient of friction

A simple pull test was carried out to determine values of coefficient of friction between rigid block and various surfaces used for experiments. Four surfaces used were plywood, high-density polyethylene (HDPE), aluminum and steel. They were selected in such a way that different modes of motion of the block from rest state could be simulated when excited by a base excitation. Evaluated values of coefficients of friction were same as estimated earlier and given in Section.3.3.3.2.

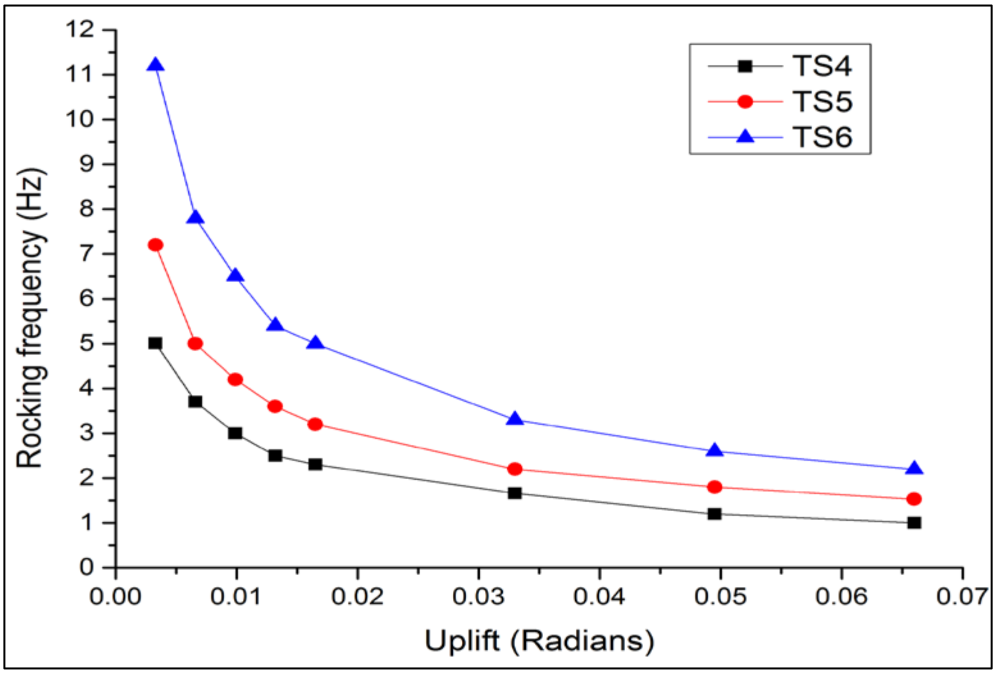


**Figure 4-2 Free rocking frequencies of flexible test specimens TS4, TS5 and TS6**

**Table 4-1 Physical and geometrical details of test specimens**

| TS | AR | D (m) | Sectional Details (m) | p (Hz) | α (rad) | R (m) | M (kg) | $\omega_r$ ($\omega_{rc}$) Hz | $\omega_n$ (Hz) |
|---|---|---|---|---|---|---|---|---|---|
| TS4 | 4 | 0.3X0.3 X1.2 | Top & bottom plate- 0.023 Columns (L shaped)- 0.025X0.025X 0.003 | 2.91 | 0.24 | 0.62 | 38 | 1-5 (0.63) | 7.8 |
| TS5 | 3 | 0.3X0.3 X0.9 | Same as above | 3.33 | 0.32 | 0.47 | 36 | 1.5-7.2 (0.8) | 11.8 |
| TS6 | 2 | 0.3X0.3 X0.6 | Same as above | 3.99 | 0.46 | 0.34 | 35 | 2.2-11.2 (1.1) | 21.4 |

TS- Test Specimen, AR- Aspect ratio, D- Dimension (length, width, height), p-frequency parameter, $\alpha$ -critical angle, R- diagonal length, M-mass, $\omega_r$ – free rocking frequency, $\omega_{rc}$ – critical rocking frequency, C.G.- relative position of centre of gravity from any vertex (x,y), $\omega_n$ – fundamental frequency

### 4.2.4 Dynamics of a Pure Rocking Motion

After carrying out preliminary dynamic investigations, rocking dynamics of the test specimens was examined. All the three test specimens viz. TS4, TS5 and TS6 were kept on a steel plate which was fixed to the shake table. Steel surface was selected because of its evaluated higher value of coefficient of friction ($\mu_s$=0.72), which may favour pure rocking motion without slipping. Synthetic time history corresponding to a nuclear power plant site in India was used as a base motion. [59] [58].The objective of testing was to observe response of test specimens to seismic base excitation. Input base excitation is shown in Fig.4-3(a) and frequency contents of an input signal, extracted using FFT are shown in Fig.4-3(b). Input base excitation as shown in Fig.4-3(a) was given to the test specimens TS4, TS5 and TS6. Acceleration time histories recorded by A2 accelerometer located at the top of the specimens are plotted in Fig.4-4. Similarly, a variation of rocking angle of the specimens with time is shown in Fig.4-5. Both the figures are plotted, only up to the time of overturning. Fig.4-6 plots FFT of acceleration history recorded by A2 for TS4, TS5 and TS6.

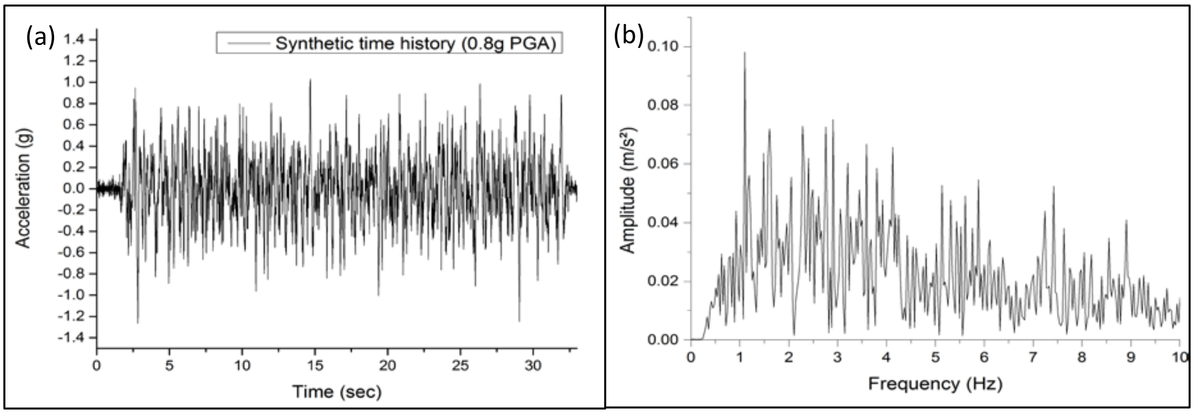


**Figure 4-3 (a)Time variation of input base excitation at 0.8g PGA and (b) frequency contents on input base excitation**

**Figure 4-4 Time variation of accelerations recorded by A2 accelerometer for specimens (a)TS4, (b)TS5 and (c)TS6**

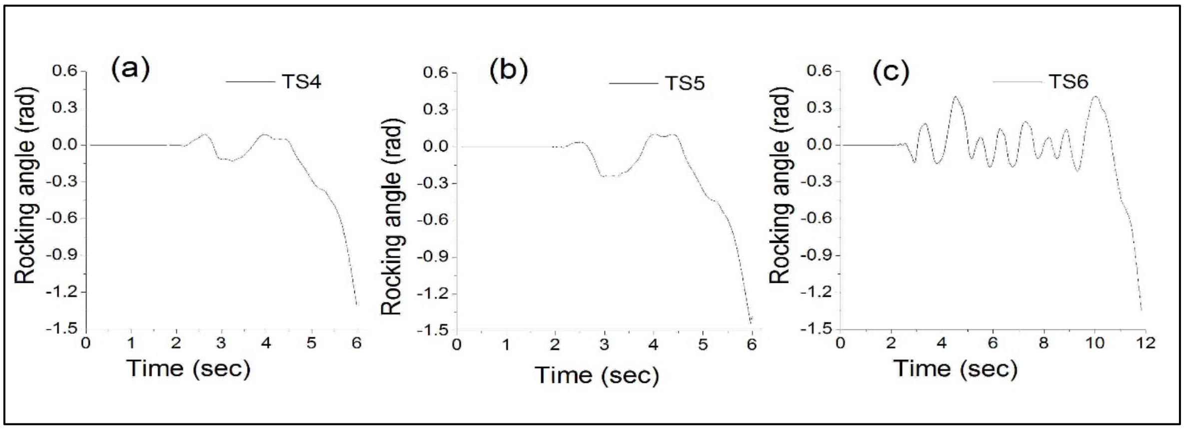


**Figure 4-5 Rocking angle time histories for specimens, (a) TS4, (b) TS5 and (c) TS6**

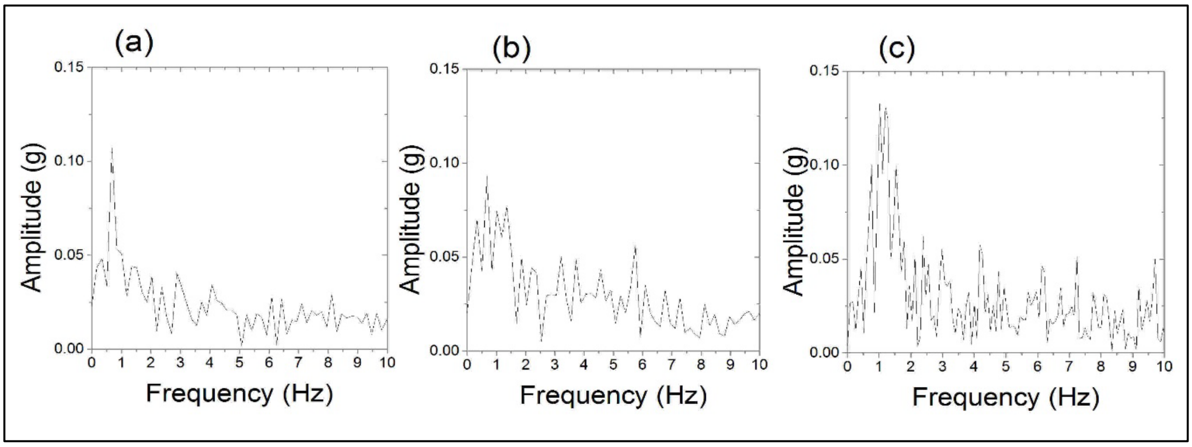


**Figure 4-6 Fast Fourier Transform of acceleration signal recorded by A2 for, (a) TS4, (b) TS5 and (c) TS6**

These results indicate following important behavior of test specimens:

1. All the acceleration time histories for specimens TS4, TS5 and TS6 featured amplifications from the base values. Amplification values were 1.25 for TS4, 2 for TS5 and 2.5 for TS6 as shown in Fig.4-4. This would be further explored by performing more experiments in coming sections. Effects of slenderness were also observed in the response. TS6 (less slender) specimen exhibited more number of peaks in acceleration time histories when compared with TS4 and TS5 as shown in Fig.4-4. The reason for the same would be clear in next few points.
2. Rocking angle time histories for the specimens showed few significant observations. More slender specimens TS4 and TS5 overturned in just 6secs, while less slender specimen TS6 took almost double the time (12 secs) to overturn. Moreover, it can also be observed that a number of times TS6 impacted with the floor is much higher than the number of impacts made by TS4 and TS5. This is clearly visible from Fig.4-4 and Fig.4-5. Sudden spikes in acceleration time histories can be attributed to impacts associated with the change of rocking directions. Every reversal of rocking direction as shown in Fig.4-5 corresponds to a peak in acceleration time history as observed in Fig.4-5.

3. FFT of output response for all the three specimens contains low-frequency contents. The highest peak in FFT of TS4 is at 0.68Hz, while that of TS5 is at 0.7Hz.It is interesting to notice that these frequencies resemble critical rocking frequencies of these specimens. On the other side, FFT of TS6 has many distinct peaks varying from 0.7Hz to 1.5 Hz. Here again, these frequencies lie in the range of free rocking frequencies of the specimen. Rocking angle time history (Fig.4-5) indicates a gradual increase in rocking angle with time. Every rocking angle below critical angle has its signature frequency lying in the range of free rocking frequencies of that specimen. Hence, the presence of these frequencies in FFT is technically justified. This point shall be further studied in the next sections.

After carrying out random motion testing, specimens were tested for Sine waves of varying frequencies ($\omega$) and peak amplitudes ($X_g$) given as a base acceleration. Stability parameters like the initiation of motion, overturning instability, response amplification and peak response characteristics of the specimens were examined. Effects of variation of base excitation frequency ($\omega$) and peak amplitude ($X_g$) on these parameters were studied. Detailed discussion on these stability parameters would be followed in the next coming sections. Acceleration time histories at various locations were recorded by accelerometers mounted on the test specimens.

#### *4.2.4.1 Rocking Motion Initiation*

The objective of testing was to explore relationship between base excitation frequencies and initiation of rocking motion of flexible bodies of different slenderness, below a statically determined amplitude of base excitation. A total number of seventeen different experimental runs were performed as shown in Table4-2. For brevity, base input excitations for test runs-1 to 6 are plotted in Fig.4-7. It is easier to understand input base motions for rest of the test cases because they were sinusoidal excitations of 5sec durations. Specimens were excited by amplitudes lesser than what is statically required for rocking initiation. As per the rigid body dynamics, we can determine the value of acceleration which is transition value above which TS4 should initiate rocking motion. We can use equations derived earlier for checking that the rocking and sliding motion shall not initiate for this value. In this case, for $A_g$ = 0.25g and $\mu_s$=0.72, using Eqns. 3.1 and 3.13, we can check that $A_g < \mu_s$ (no sliding condition) and $A_g \leq g \tan\alpha$= 0.25(no rocking condition). Similarly, rocking initiation conditions can be estimated for other two test specimens (TS5 and TS6) using Eqns.3.1 and 3.13. We get, $A_g \leq g \tan\alpha$= 0.33g for TS5 and $A_g \leq g \tan\alpha$= 0.5g for TS6. The minimum value of rocking angle required to satisfy rocking initiation condition was set as 0.003 radians. This angle corresponds to an uplift of 1mm for all the test specimens (TS1 to TS6).

**Table 4-2 Details of tests performed on the flexible test specimens**

| Test Run | Specimen | Xs* (g) | Input Base excitations<br>Peak Amplitude(g) | Frequencies(Hz) | Output/Results |
|---|---|---|---|---|---|
| 1 | TS4 | 0.25 | 0.2 | Earthquake time history | Rocking initiation |
| 2 | TS4 | 0.25 | 0.15 | Earthquake time history | No Rocking initiation |
| 3 | TS5 | 0.33 | 0.3 | Earthquake time history | Rocking initiation |
| 4 | TS5 | 0.33 | 0.25 | Earthquake time history | No Rocking initiation |
| 5 | TS6 | 0.5 | 0.45 | Earthquake time history | Rocking initiation |
| 6 | TS6 | 0.5 | 0.4 | Earthquake time history | No Rocking initiation |
| 7 | TS4 | 0.25 | 0.2 | 1Hz- 20Hz (step size-1Hz) | Rocking initiation for 3Hz-6Hz frequencies |
| 8 | TS4 | 0.25 | 0.15 | 1Hz- 20Hz (step size-1Hz) | Rocking initiation for 4Hz-6Hz frequencies |
| 9 | TS4 | 0.25 | 0.1 | 1Hz- 20Hz (step size-1Hz) | Rocking initiation for 5Hz frequency |
| 10 | TS5 | 0.33 | 0.3 | 1Hz- 20Hz (step size-1Hz) | Rocking initiation for 3Hz-8Hz frequencies |

| | | | | | |
|---|---|---|---|---|---|
| 11 | TS5 | 0.33 | 0.25 | 1Hz- 20Hz (step size-1Hz) | Rocking initiation for 5Hz-8Hz frequencies |
| 12 | TS5 | 0.33 | 0.2 | 1Hz- 20Hz (step size-1Hz) | Rocking initiation for 6Hz-8Hz frequencies |
| 13 | TS5 | 0.33 | 0.15 | 1Hz- 20Hz (step size-1Hz) | Rocking initiation for 7Hz frequency |
| 14 | TS6 | 0.5 | 0.45 | 1Hz- 20Hz (step size-1Hz) | Rocking initiation for 4Hz-12Hz frequencies |
| 15 | TS6 | 0.5 | 0.4 | 1Hz- 20Hz (step size-1Hz) | Rocking initiation for 8Hz-12Hz frequencies |
| 16 | TS6 | 0.5 | 0.3 | 1Hz- 20Hz (step size-1Hz) | Rocking initiation for 9Hz-11Hz frequencies |
| 17 | TS6 | 0.5 | 0.25 | 1Hz- 20Hz (step size-1Hz) | Rocking initiation for 10Hz frequency |
| *Xs = g. $\tan \boldsymbol{\alpha}$ , statically determined minimum base amplitude required for uplift initiation | | | | | |

Initially test specimens were subjected to random seismic motion as shown in test runs from 1 to 6 in Table.4-2.Peak ground acceleration (PGA) values of synthetic time histories were kept below statically determined minimum amplitude ($X_s$) required for rocking initiation. Experimental results for all the three specimens (TS4, TS5 and TS6), as shown in Table.4-2, indicated an unexpected trend of initiation of rocking motion in some test cases (Test runs-1, 3 and 5) at an amplitude below $X_s$ values. It can be observed from Fig.4-8, that the peak value of rocking angle is 0.0035, which indicated 1mm uplift of the specimen. This unusual dynamic behavior was the motivation to carry out further investigation on the role of individual frequencies of base excitations in initiating uplift.

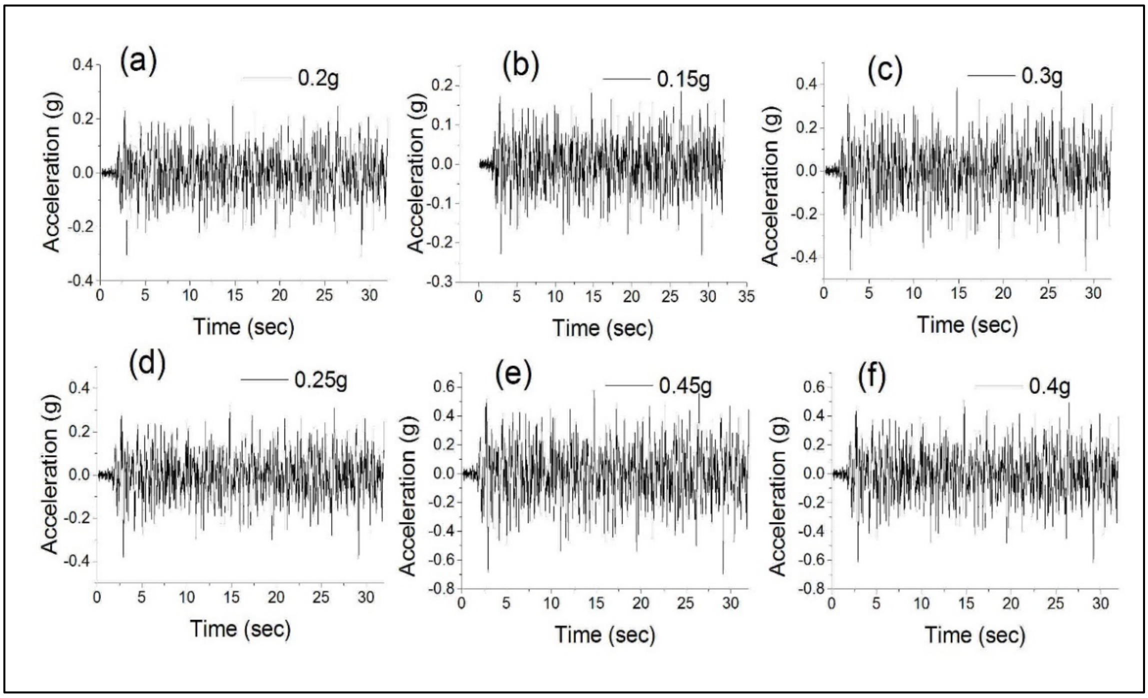


**Figure 4-7 Input seismic base excitations for test runs from 1 to 6 (a-f)**

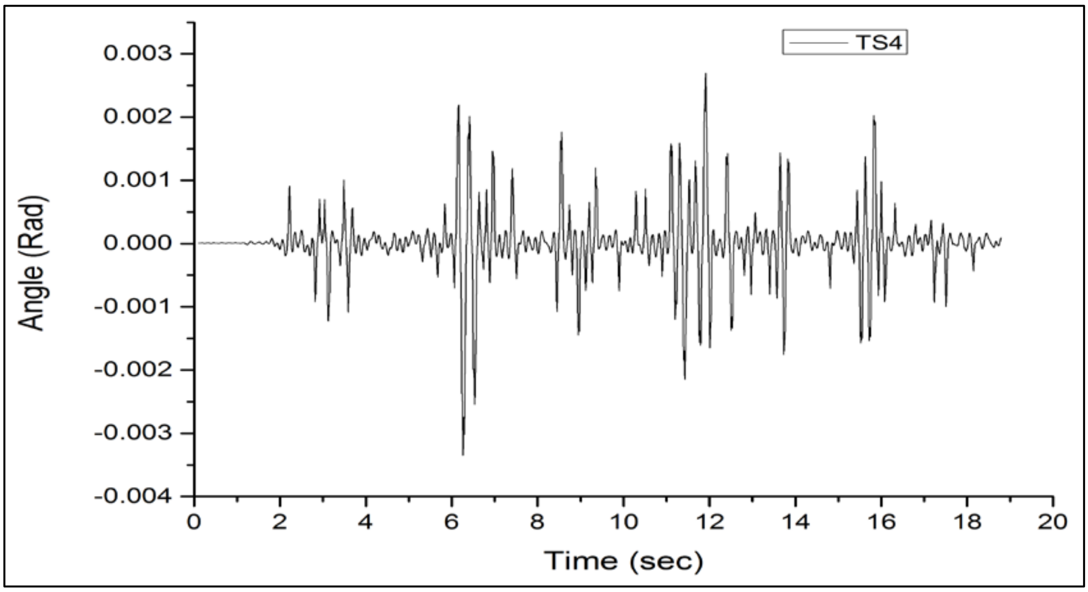


**Figure 4-8 Rocking motion initiation of TS4 for 0.2g PGA seismic base excitation (test run-1)**

Subsequent to seismic motion testing (test runs 1-6), Sinusoidal waves of different frequencies varying from 1Hz up to 20 Hz in a step of 1Hz were given as base excitations. The amplitude of sinusoidal waves were also varied, in steps, from 0.2g to 0.1g for TS4, 0.3g to 0.15g for TS5 and from 0.45g to 0.25g for TS6. Test details are given in Table.4-2 (test runs-7-17). Since there were numerous sinusoidal input base excitations which can be easily visualized, hence not plotted.

Results for all the test cases (Test Runs 7-17) as given in Table.4-2 are plotted in form of normalized curves as shown in Figs.4-9 to 4-11. These curves were plotted by selecting peak value of rocking angle corresponding to every frequency of base excitation. Ordinate of these graphs indicate peak rocking angle values normalized using critical angle, whereas abscissa indicates base excitation frequencies normalized using specimen's fundamental modal frequency. In addition to these figures Fig.4-12 shows the response of all the three specimens in a single plot. This is a dimensional plot of the response. Moreover, Fig.4.13 shows the variation of peak rocking angles and peak sliding displacements for the test specimen TS4 with the frequencies varying from 1Hz to 10Hz for a fixed amplitude of 0.2g.

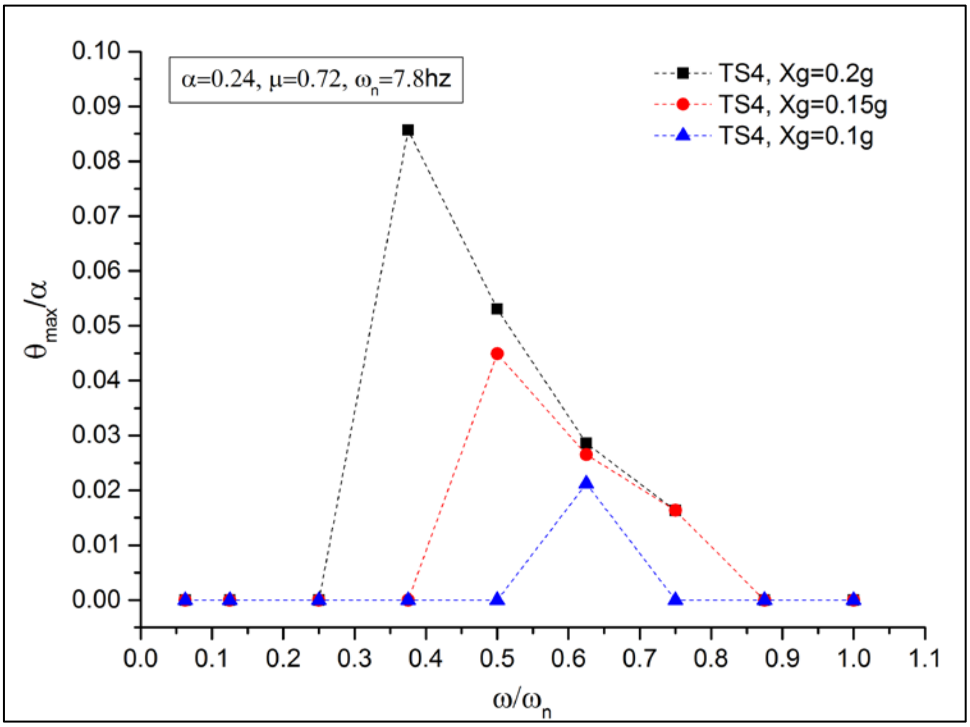


**Figure 4-9 Normalized curves showing variation of peak rocking angle with the frequency of base excitation for different peak amplitude values for specimen TS4**

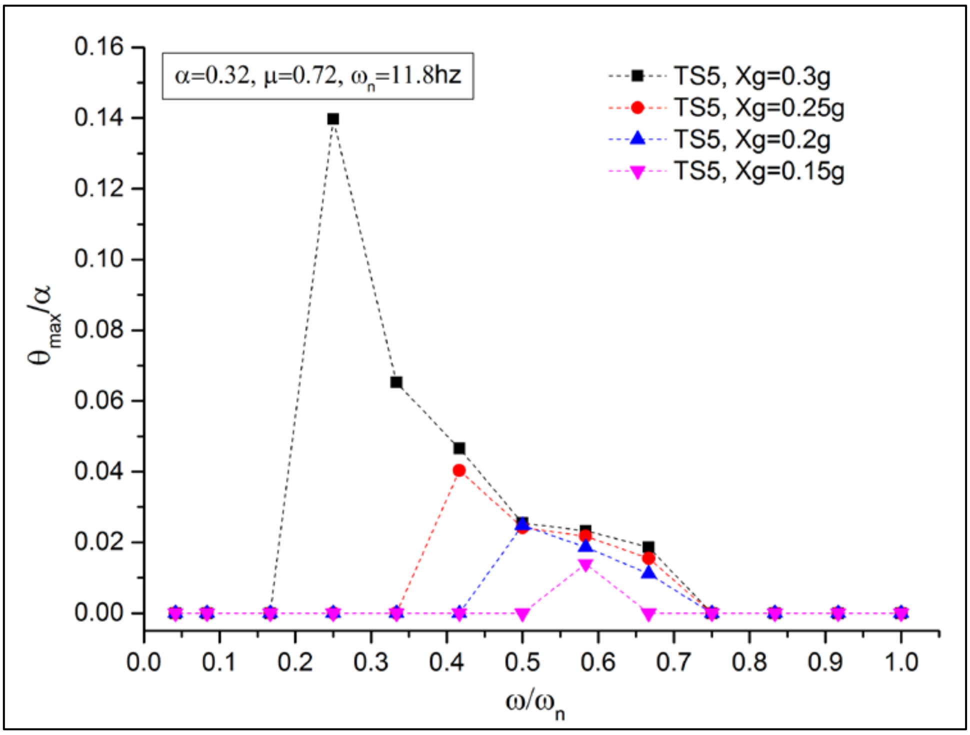


**Figure 4-10 Normalized curves showing variation of peak rocking angle with the frequency of base excitation for different peak amplitude values for specimen TS5**

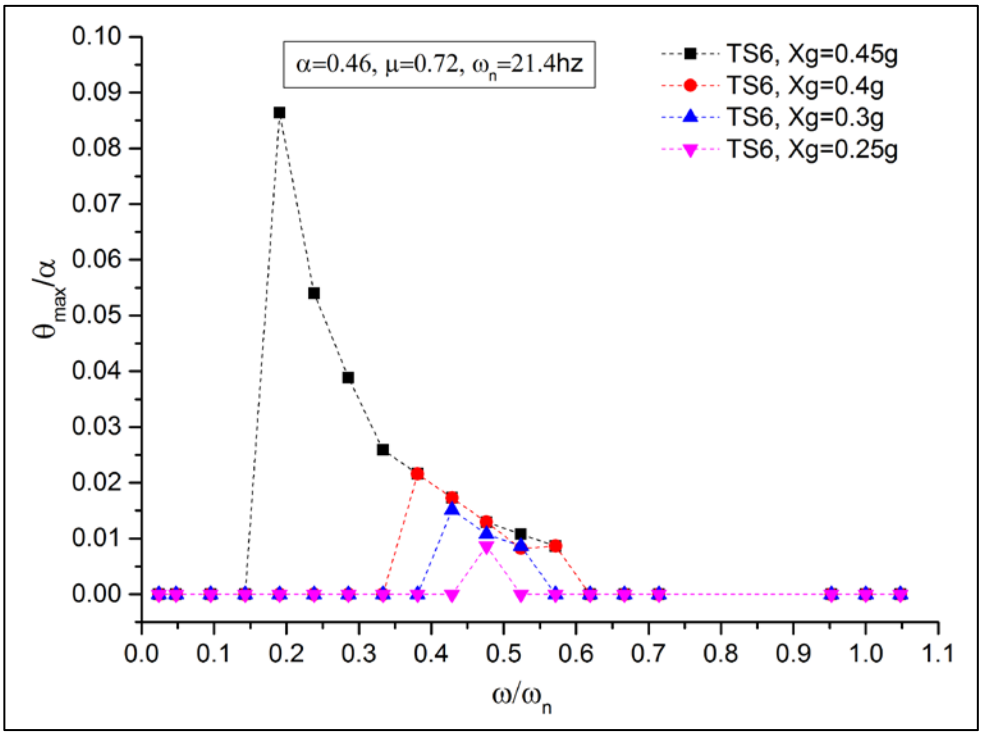


**Figure 4-11 Normalized curves showing variation of peak rocking angle with the frequency of base excitation for different peak amplitude values for specimen TS6**

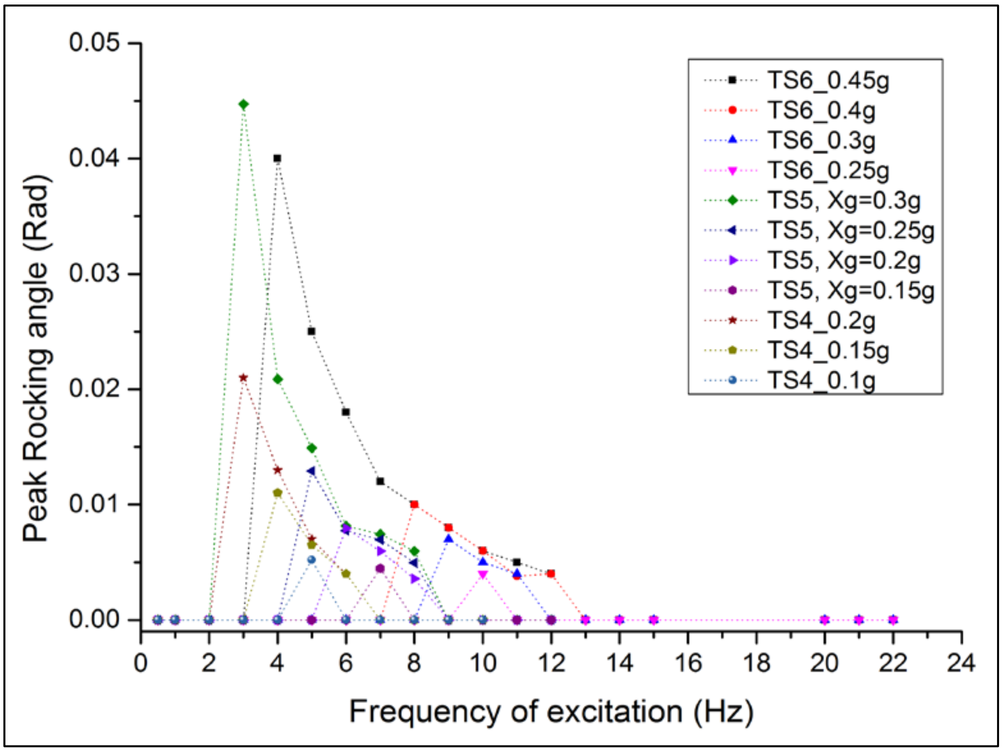


**Figure 4-12 Variation of peak rocking angle with frequency and amplitude of base excitation for different test specimens TS4, TS5 and TS6**

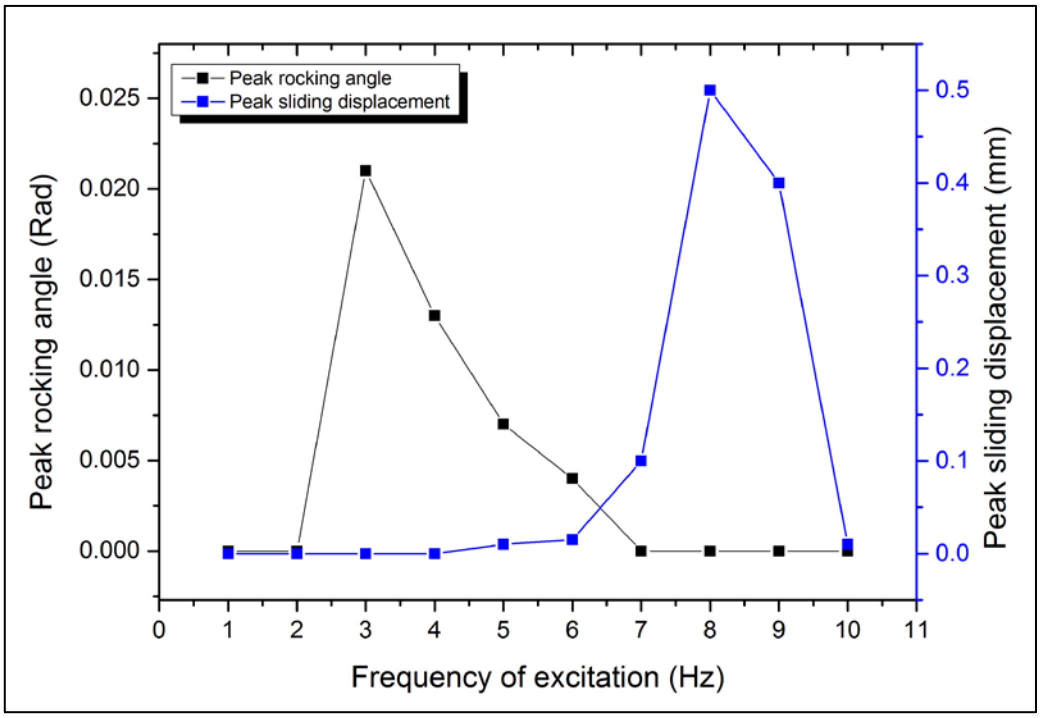


**Figure 4-13 Variation of peak rocking angle and sliding displacement of the specimen TS4 for 0.2g amplitude and varying frequencies**

These results unveiled novel findings of the rocking behavior of the flexible bodies. Important experimental findings are as follows:

1. A strong relationship exhibited between free rocking frequencies of a flexible specimen and amplitude of base excitations required for uplift. Experimental results indicated uplift of flexible specimens TS4, TS5 and TS6, at an amplitude of base excitation, much lower than what is statically required for uplift initiation, as shown in Fig.4-9 to Fig.4-11. This peculiar behavior was present only for the range of frequencies corresponding to $\omega_r$ of TS4, TS5 and TS6 as can be verified from Figs.4-9 to 4-11 with Fig4-2/Table 4-1.

2. The explanation for such a behavior can be due to the capability of low amplitude rocking frequency pulses to excite elastic motions/vibrations in a flexible body and force uplift. Hence, this rocking motion was not only initiated by the amplitude, but by the frequencies of base excitation. This phenomenon of initiation of rocking motion at amplitudes much lesser than statically required to cause uplift in a flexible free-standing body is unique and not reported earlier. It can be asserted that, a flexible structure is vulnerable to uplift, if base excitation frequencies matches structure's free rocking frequencies.

3. There was an observable difference between the response of the specimens to seismic excitations and harmonic excitations of the same amplitude. For example, 0.2g PGA seismic excitation could initiate uplift in TS4 with a peak rocking angle of 0.0035 radians as shown in Fig. 4-8. On the other side, a harmonic excitation of similar amplitude has generated a rocking angle of 0.026 radians for a frequency of 3Hz as interpreted from Fig.4-9, nearly a seven-fold increase in magnitude. This indicates the capability of a harmonic motion to build up and sustain rocking motion. The possible

reason behind this difference could be found in the very nature of seismic and harmonic excitations. On one side, the seismic motion is random in nature with diverse frequency contents. Every frequency in excitation has certain amplitude and signal power associated with it. On the other side harmonic motion has a single frequency associated with it and which has full signal power. Hence, it can be inferred that, where frequency induces rocking motion, effect of harmonic excitation in initiation and building up of motion is maximum.

4. A systematic trend was observed between $X_g$ and $\omega_r$ of all the flexible test specimens (TS4, TS5 &TS6). As $X_g$ decreased, magnitude of peak rocking angle ($\Theta_{max}$) also decreased, as shown in Figs.4-9, 4-10 &4-11. Reduction in rocking angle was attributed to the reduction of inertial disturbing forces responsible for uplift. In addition to that, frequency band responsible for uplift was also reduced. For example, in the case of TS4 as shown in Fig.4-9, frequency ratio ($\omega/\omega_n$) band corresponding to uplift was varying from 0.27 to 0.75, for a value of $X_g$ equals to 0.2g. This band reduced to a single value of $\omega/\omega_n$ = 0.62, for $X_g$ = 0.1g. Moreover, a positive shift was observed in frequency values corresponding to maximum uplift angle with the decrease in values of $X_g$. For example, in Fig.4-9, value of $\omega/\omega_n$ corresponding to $\Theta_{max}/\alpha$ = 0.086 and $X_g$= 0.2g was 0.37, which increased to 0.62 for $\Theta_{max}/\alpha$ = 0.02 and $X_g$= 0.1g. A similar trend was observed for other two cases also as shown in Figs.4-10 & 4-11. This observation can be explained by the fact that rocking frequencies of a body are inversely proportional to the amplitude of uplift. Hence, as the magnitude of peak base excitation decreases, the amplitude of uplift also decreases, hence excitation frequency corresponding to the peak of uplift angle increases. More importantly, for a flexible body, there exists a singular set of values, of minimum amplitude ($X_g$) and frequency of base excitation ($\omega$), which has the potential to initiate uplift. These are termed as $X_f$ and $\omega_f$ .Below the

minimum amplitude value ($X_f$), excitation frequency values has no influence on uplift initiation. It is further shown that there exists a range of values of $X_g$ where $\omega_r$ of a flexible structure dominates the rocking response. This range is bounded on the upper side by the statically determined value of the amplitude of base motion required for uplift ($X_s$) and on the lower side by a value termed as $X_f$ which can be evaluated numerically/experimentally.

5. These observations have a direct effect on the validity of two-dimensional (Fig.2-2) and three-dimensional (developed in Section3.5) motion initiation criteria diagrams developed for a rigid body. Since frequency induced rocking phenomenon exists in a flexible body, these diagrams are not valid for a flexible body. Hence, they are required to be redeveloped for a flexible body. This subject is discussed in more details in Section4.3.

6. It is important to note, that the widely referred two degrees of freedom, lumped mass, cantilever model available in the literature [50], failed to predict the functional relationship between the initiation of rocking motion and free rocking frequencies of a flexible structure. Acikgoz and Dejong [51]presented a graph (Refer Fig.4 of the reference paper) which highlighted that minimum excitation amplitude required for uplift of a flexible structure was lower than what is required for a rigid structure, particularly when base excitation frequency matches with fundamental modal frequency of the structure ($\omega/\omega_n$=1). On the other hand, for high ratios of $\omega/\omega_n$ flexible structure required higher amplitudes to uplift. Experimental findings in our research highlighted the reduction in amplitude required for uplift for a range of frequencies corresponding to ($\omega_r$) but not up to the value of $\omega_n$ (see Fig.4-9, 4-10 &4-11). At base frequencies higher than $\omega_{n,}$ there was practically zero uplift (< 0.1mm) for the flexible

specimen. Hence it is clear, that simplified model used in numerical analysis by Acikgoz and Dejong was unable to correctly predict the dynamic behavior of three-dimensional flexible bodies.

7. The response of flexible specimens exhibited uplift at values of excitation frequencies matching with their free rocking frequencies as shown clearly in Fig.4-12. It was also observed from Fig.4-13 that for the values of frequencies corresponding to free rocking frequencies of TS4 viz. 3Hz to 6Hz rocking initialized. However, with the further increase of frequency up to the specimen's fundamental modal frequency (8Hz) rocking motion vanished and sliding initiated.

#### *4.2.4.2 Response Amplification*

In many critical free-standing equipment, it is important to control accelerations and associated displacements when subjected to base excitations. For example, excessive accelerations at the top of an equipment used for a medical facility may render it unusable. Similarly, some loose items lying on top of shelves may be dislodged due to excessive accelerations and may hit adjacent components. Hence, it is always important to know the response amplification of a free-standing structure/equipment in terms of acceleration applied at the base. In case of a fixed flexible structure, it can be calculated as a transmissibility factor.Here, response amplification factor (AF) for flexible test specimens is evaluated, as the ratio of acceleration obtained at top of the structure to the applied base acceleration. Variation of amplification factor with the frequency of base excitation for rocking mode of motion is plotted in Fig.4-14 below.

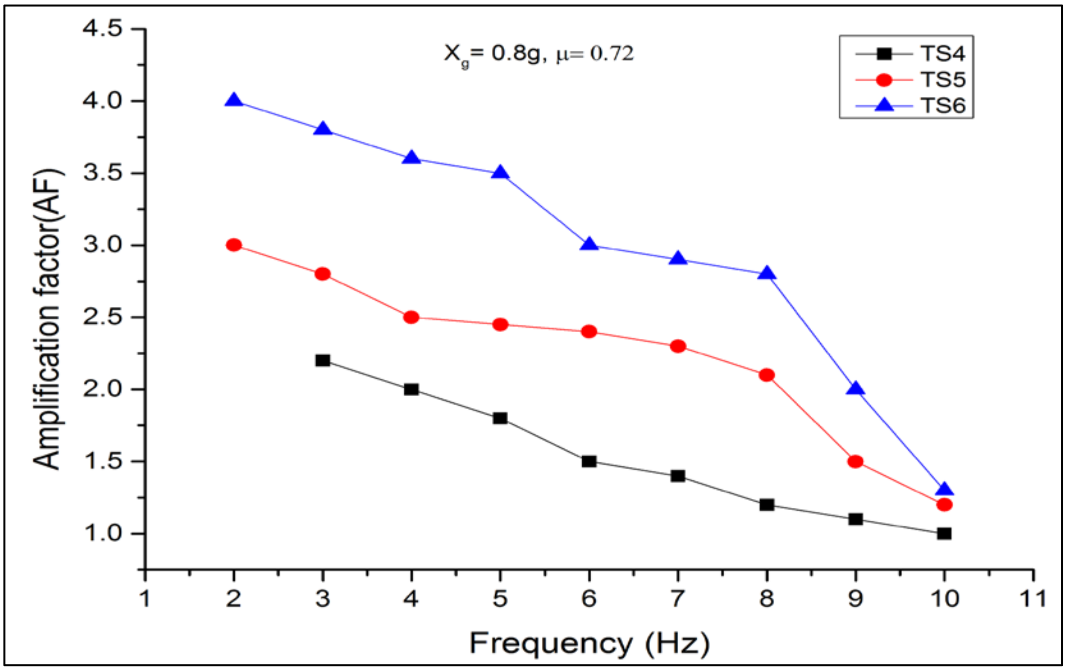


**Figure 4-14 Amplification factors for test specimens TS4, TS5 and TS6 in pure rocking motion**

Following important points were noted:

1. In general, response amplification factors obtained were higher than unity for all the flexible test specimens. However, the minimum value observed was 1 for TS4, 1.2 for TS5 and 1.3 for TS6 at 10 Hz base excitation frequency.
2. Acceleration amplification was observed to be dependent on slenderness of the specimens. With the decrease in slenderness and increase of rigidity of the specimens, amplification of acceleration increased. Less slender bodies (TS6) can easily transmit acceleration peaks generated due to impacts with the base, however, more slender bodies (TS4) reduces acceleration pulses transmission to the top of the body. Higher structural vibrations arising due to impact and better damping properties results in a lower transmission of impact accelerations to the top.
3. Amplification factors for all the specimens reduced with the increase of the frequency of base excitations. Higher frequency of base motion is less effective in uplift initiation

because effective time a specimen sees peak base acceleration reduces drastically thereby reducing overall rocking motion and associated impacts causing lower AF.

#### *4.2.4.3 Overturning instability*

In dynamics of a free-standing rocking structure, it is critical to understand overturning phenomenon. Effect of the flexibility of a structure in determining overturning instability has been investigated. Here the objective was to experimentally evaluate overturning instability of a flexible test specimen TS4 subjected to sine pulse base excitations. As mentioned earlier in Section 3.3.4.1, the overturning curve was plotted partially with the help of the experimental data and rest with the help of FE simulations. Three-dimensional model of the test specimen was developed in a finite element software. FE model was benchmarked using available experimental results and then utilized for generating the overturning curve. Details of FE modelling and analysis along with the benchmarking results are given in Section- 4.4.

The dimensionless overturning curve plotted for the flexible test specimen TS4 identifies various zones corresponding to Mode1 and Mode2 overturning failures as shown in Fig.4-15. It also identifies safe zone where there is no possibility of the overturning of the structure.

In the amplitude/frequency space, two different modes of overturning failures and three different regions exist for a flexible rocking body. Lower frequencies ($\omega/p$) of excitations starting from zero up to 0.35 correspond to a region where with the increase of amplitude value, the specimen transforms from stable rocking phase to overturning without any impact (Mode2 failure). This region is shown as R1 in Fig.4-15. In the mid frequency region (0.35 to 4.1), with the increase of amplitude, a flexible body TS4 first transforms from a stable rocking motion to overturning with one or more impacts; then with further increase of amplitude finally overturns without any impact. This frequency region (0.35-4.1) is given by R2 in Fig.4-15. High-frequency region R3 ($\omega/p>4.1$) has similar attributes as that of the R1 region.

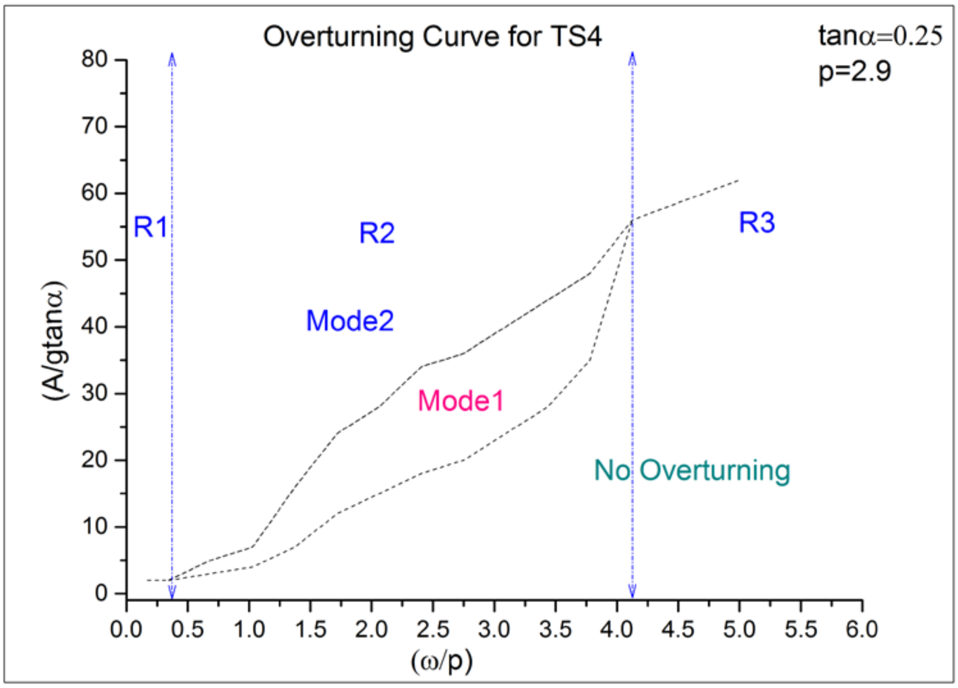


**Figure 4-15 Overturning curve for TS4 showing various regions of failures due to rocking instability**

### 4.2.5 Dynamics of a Pure Sliding Motion

The base material used for the experimental set up was now changed to plywood to simulate sliding mode of motion. Similar to the experiments performed earlier for rigid specimens, a set of experiments were carried out to evaluate sliding behavior of flexible specimens. The objective of testing was to observe sliding dynamics and investigate effects of parameters like base motion characteristics and slenderness value on it.

All the three test specimens (TS4, TS5 and TS6) were kept on a plywood plate fixed to the shaking table. Plywood surface was selected because of its evaluated lower value of the coefficient of friction ($\mu_s$=0.15), which favors pure sliding motion. Synthetic time history used as a base motion was similar to the one used earlier for rigid specimens (TS1, TS2 and TS3) as shown in Fig.3-7. Acceleration time histories recorded by accelerometers located at the top of the specimens and shake table are plotted in Fig.4-16. Variation of slip and rocking angles with time is shown in Fig.4-17 and Fig.4-18 respectively.

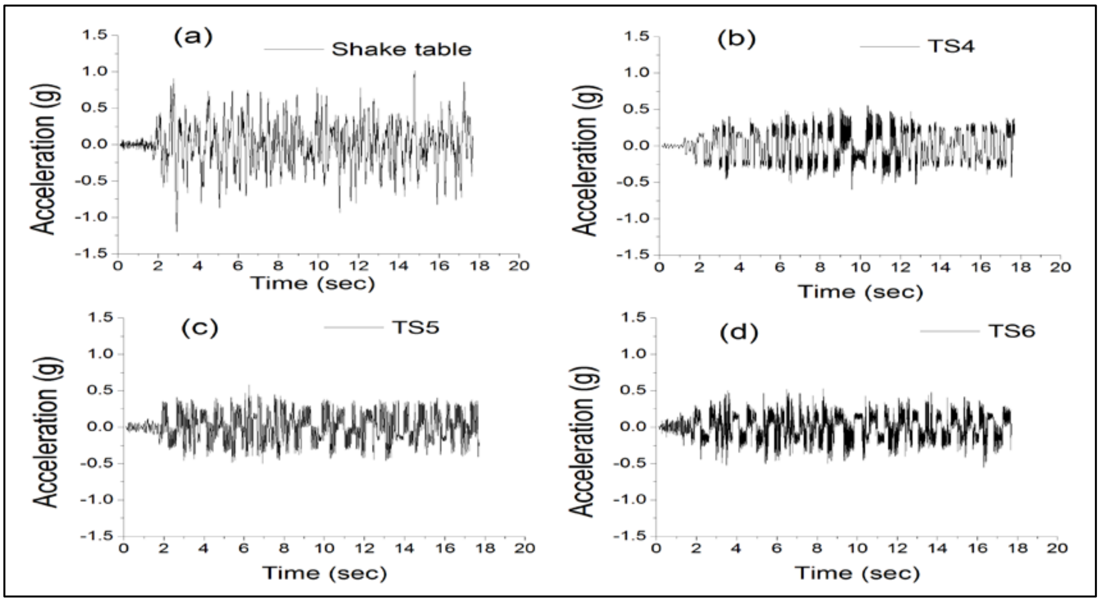


**Figure 4-16 Acceleration response recorded at (a) shake table, top of the specimens (b) TS4, (c) TS5 and (d) TS6**

**Figure 4-17 Variation of sliding displacement with time for (a)TS4, (b)TS5 and (c) TS6**

**Figure 4-18 Rocking angle variation with time for (a)TS4, (b)TS5 and (c)TS6**

These results highlighted following important behavior of test specimens:

1) Acceleration time histories recorded at top of the specimens TS4, TS5 and TS6 indicated a significant reduction in accelerations. This signifies response reduction in the specimens. Quantitatively, peak accelerations recorded for TS4, TS5 and TS6 were around 0.5g. This indicates around one half reduction in accelerations.
2) There was no effect of the slenderness of the specimens on peak acceleration response. All the specimens had same peak acceleration values (0.5g) despite variation in slenderness.
3) Slip displacements for all the three specimens were obtained as shown in Fig.4-17. Slip motion time history was, by and large identical for all the three specimens. However, a slight difference in peak slip displacement values was observed. For example peak slip displacement for TS4 was 0.0017m, TS5 was 0.0012m and TS6 was 0.0015m. In this case, flexibility (stiffness) of the specimens has contributed towards the variation in sliding behavior.
4) A peculiar behavior of the specimens was observed during the experiments. As per the input parameters, $X_g$ =0.8g PGA and $\mu_s$= 0.15, all the specimens were expected to follow pure sliding motion without any uplift. However, specimen TS4 exhibited uplift from the base and sliding cum rocking motion was observed. It can be seen from Fig.4-18 that significant rocking motion is present with the peak rocking angle value of 0.12 radians, which corresponds to an uplift of 36mm. This unexpected behavior requires further investigation. More experiments were carried out to further explore this phenomenon and results and discussions are given in the next section.

### *4.2.5.1 Sliding behaviour*

After initial random motion testing of the specimens, it was decided to subject them to harmonic base excitations. Specimens were subjected to a sinusoidal excitation of peak amplitude ($X_g$) equals to 0.8g and frequencies (ω) varying from 0.5Hz to 10Hz. Duration of harmonic wave was 5 secs. Details of tests performed are given in Table.4-3. Objective of testing was to observe effect of variation of base excitation frequency and slenderness of the specimens on sliding behavior.

**Table 4-3 Experiments performed to observe sliding behavior of test specimens**

| Test Run | Specimen | Xs* (g) | Input Base excitations<br>Peak Amplitude(g)<br>Frequencies(Hz) | Output/Results |
|---|---|---|---|---|
| 1 | TS4 | 0.15 | 0.8<br>0.5,1,2,3,4,5,6,7,8,9,10 | Sliding and rocking motion observed for 1Hz to 7Hz frequencies |
| 2 | TS5 | 0.15 | 0.8<br>0.5,1,2,3,4,5,6,7,8,9,10 | Sliding and rocking motion observed for 7Hz-9Hz frequencies |
| 3 | TS6 | 0.15 | 0.8<br>0.5,1,2,3,4,5,6,7,8,9,10 | Pure Sliding motion observed for all the frequencies |
| Xs – Minimum amplitude required to initiate slip motion | | | | |

**Figure 4-19 Response time histories of test specimen TS4. (a ,c, e, g)- Response recorded for 2Hz and (b, d, f, h) - response recorded for 10Hz base excitation frequencies**

For brevity, experimental results for the specimen TS4 are plotted in Fig.4-19. Whereas, peak rocking angles and slip displacements are plotted in Fig.4-20 and Fig.4-21 respectively. The basic dynamic behavior for all the three specimens was similar and hence plotting response for one out of three is adequate for understanding.

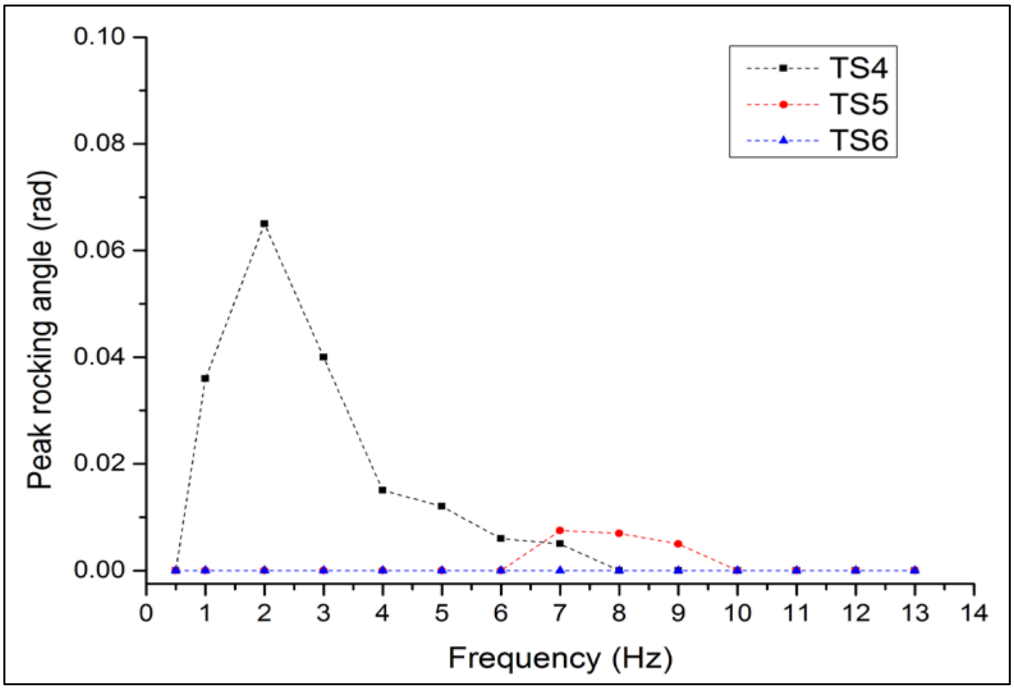


**Figure 4-20 Variation of peak rocking angle of specimens TS4, TS5 and TS6 with base excitation frequencies**

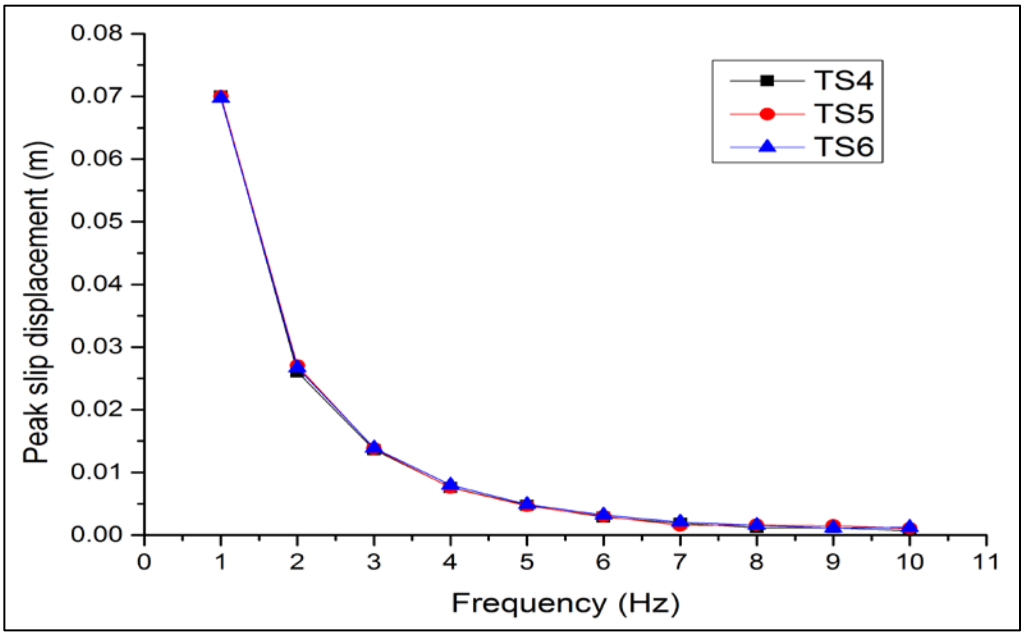


**Figure 4-21 Variation of peak slip displacements of specimens TS4, TS5 and TS6 with base excitation frequencies**

Following were the important findings from Fig.4-19 to Fig.4-21:

1. A peculiar observation was presence of rocking motion in the response. For the given combination of coefficient of friction and amplitude of base motion, expected response was pure sliding motion as observed earlier in case of a rigid specimen in Section 3.3.5. However, a significant rocking motion was observed as shown in Fig.4-19(g) for 2 Hz frequency of excitation. This behavior resembles with the ***rocking*** phenomenon observed earlier in Section-4.2.4. Despite unfavorable conditions for rocking initiation low amplitude rocking motion initiated. To further clarify this phenomenon, refer Fig.4-20. It can be clearly seen from the figure, that for base excitation frequencies corresponding to free rocking frequencies of TS4, rocking motion was observed. Similarly for the test specimen TS5, rocking motion was present in a narrow frequency range of 7 Hz to 9Hz. This frequency range is on the higher side of free rocking frequencies ($\omega_r$) of this specimen. This effect was prominent in specimens of higher slenderness values like TS4 and TS5. However, it was absent in specimen TS6. This indicates that more slender structure is susceptible to frequency induced rocking phenomenon.
2. Similar to the observations of seismic motion testing presented in Fig.4-16, in general, acceleration responses at the top of the specimens were reduced. Acceleration records of accelerometer A2 of TS4 indicated significant reduction for 10Hz frequency as shown in Fig.4-19(d). In quantitative terms peak acceleration reduced to 0.4g which is half of the applied value. However, acceleration response at 2Hz base frequency presented no significant reduction as shown in Fig.4-19(c). Acceleration spikes were observed in Fig.4-19(c). These spikes correspond to impacts arising due to rocking motion. On comparing Fig.4-19(c) with Fig.4-19(g), it can be clearly seen that every

change in rocking direction led to impact and consequently spikes in acceleration time history. It is still interesting to notice, the presence of multiple spikes on every impact. The reason behind them is the free vibrations emanating from the site of impact and transmitting up to top of the specimen. Free vibrations associated with impact is a unique feature of a flexible body and were insignificant in the rigid body as seen earlier in Fig.3-19(c).

3. Slenderness of the specimens has a significant effect on the frequency induced rocking behavior as seen in Fig.4-20, while it has no significance on overall sliding behavior. Slip displacement were observed to be independent of slenderness values as shown in Fig.4-21. However frequency of excitation has an influence on peak slip displacements. Slip value reduces from as high as 0.07m at 1Hz to 0.001m at 10Hz, almost a 70 fold reduction.

#### *4.2.5.2 Response Amplification*

Acceleration amplification for sliding motion was evaluated for all the three test specimens. Experimental results are plotted in Fig.4-22. Following important points can be observed:

1. In general, for flexible specimens, acceleration amplification in sliding motion was lesser than unity. This indicates reduction in acceleration values transmitted to top of the specimens. However, for a single case of 2Hz frequency for TS4, its value reached unity. Reason for it was presence of frequency induced rocking (peak rocking angle = 0.07radians) for that frequency. It can also be observed that AF value was constantly maintained at 0.62 for all the three test specimens. However, variation from this value was observed for particular frequencies where rocking motion in the specimen was observed. For example, for base excitation frequencies varying from 1-7Hz, AF of TS4 was higher than 0.625. Similarly, for base excitation frequencies varying from 7-9Hz,

AF of TS5 was higher than 0.625. The reason for the same was presence of rocking motion, as observed in Fig.4-22, along with the sliding motion for these particular frequencies.

2. Acceleration amplification was observed to be a nonlinear function of base excitation frequencies for all the test specimens.
3. Sliding motion in flexible bodies has an inherent advantage of low response amplification and higher energy dissipation due to friction.

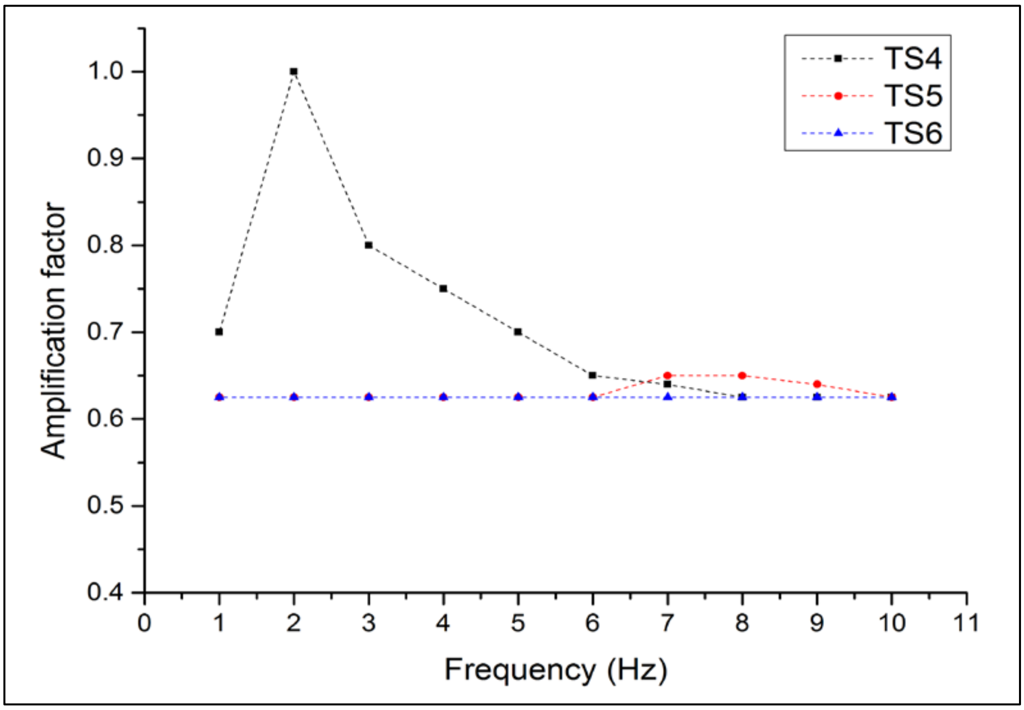


**Figure 4-22 Acceleration amplification factor variation with frequency of base excitation for TS4, TS5 and TS6**

## 4.3 Motion Initiation Criteria Diagram for Flexible Bodies

Experimental results highlighted peculiar behavior of a flexible body. Anomalous presence of rocking motion in the rest and sliding mode of motion, requires development of new motion initiation criteria diagram for a flexible body. As discussed earlier in Section3.5, two-dimensional motion initiation criteria diagram available in literature [62] is valid only for a range of frequencies below cutoff frequency plane of developed three-dimensional diagram (Refer Fig.3-33 and Fig.3-34). It was also observed that cutoff frequencies for any given state of a body, generally have higher values (>10Hz). In the case of a flexible body, it was observed that much below cutoff frequencies, a range of frequency exists (pertaining to free rocking frequencies of the specimen) where rocking phenomenon is predominant. Hence existence of rocking phenomenon as discussed in Sections-4.2.4 to 4.2.5 in rest and sliding state of motion is required to be incorporated in a redeveloped diagram. In the present research, two-dimensional motion initiation criteria map is developed for a test specimen TS4 for a range of frequencies corresponding to free rocking frequencies ($\omega_r$) of the specimen. It is worth mentioning that outside this range of frequencies up to the cutoff frequency plane, motion initiation criteria diagram available in the literature [62] shall be valid. Numerical calculations using FE method were performed to develop motion initiation criteria diagram for a flexible body of four aspect ratio. Numerical simulation was carried out by exciting the specimen with harmonic waves of frequencies covering the range of free rocking frequencies of TS4. In this case, several numerical simulations were carried out for a frequency range of 1Hz to 7Hz, corresponding to $\omega_r$ value of TS4. Position of boundary lines demarcating different zones was evaluated using sinusoidal excitation because it gives a conservative estimate over the seismic/random excitation. Experimental results carried out in Section-4.2.4 and 4.2.5, highlighted the fact that harmonic motion can induce higher uplift than the similar amplitude seismic motion. Various regions corresponding to different modes of motion for a flexible body can be seen in Fig.4-23.

Flowing conclusions can be drawn from Fig.4-23:

1. Developed initiation criteria diagram has significant differences from the existing one. Effect of specimen flexibility can be readily observed from this figure. Boundary line demarcating transition between rest and rock region for a rigid body has moved to the left for a flexible body, thereby increasing effective rocking area. Hence, for a flexible body, rocking motion initiates at a lower amplitude of 0.1g instead of 0.25g for the geometrically similar rigid body.
2. Boundary line demarcating transition between slide and slide/rock state has moved vertically downward thereby increasing effective slide/rock area. Moreover shifting of boundary between slide and slide/rock area indicates higher tendency of a flexible body to undergo a combined rocking and sliding motion than its rigid counterpart. These two observations adversely affect seismic stability of a flexible body because of reduction in available rest area.
3. Developed initiation criteria diagrams bring out two distinct phenomenon. Firstly, amplitude induced sliding or rocking motion and secondly frequency induced rocking motion. The first phenomenon is well known in literature and is observed to be the governing factor in deciding initiation of motion from rest. On the other hand, second phenomenon is a novel outcome of this research. Frequency induced rocking was not known in the past and hence was not considered to effect dynamics of a flexible free-standing body. This phenomenon has a predominant role in rocking initiation even at very low amplitudes. Induced low amplitude rocking motion leads to multiple impacts with the base. It is associated with two counteracting effects. Firstly, multiple impacts lead to energy dissipation via inelastic collisions, radiation damping and thermal effects. Secondly, sudden acceleration jumps arising due to impacts will lead to high value of acceleration amplification factors.

4. Frequency induced rocking leads to low amplitude rocking motion as observed in Fig.4-23 and discussed earlier in Sections 4.2.4 and 4.2.5. It cannot lead a body/structure to overturn. Hence this phenomenon is not a safety concern as far as overturning of the structure is concerned. On the other side, this may be very useful mechanism in dissipating ground energy pumped into the body via ground motions/base excitations. A frequency-controlled rocking can be an attractive and safer mechanism for energy dissipation in earthquake control of flexible structures. This can be a potential candidate for passive control of structures.
5. Significant reduction in the stable region (rest state) of a flexible body is observed. This reduction is attributed to presence of additional frequency induced when compared to the Fig.2-2. Applicability of this diagram is for the frequency range corresponding to free rocking frequencies of the flexible body which are governed by geometrical properties like slenderness (AR), diagonal length(R), moment of inertia (I) and mass of the body.
6. Presence of frequency induced uplift at an amplitude lower than statically required for uplift can have a destabilizing effect on the stability of a flexible body. There is always a possibility of subsequent building up of rocking motion, once initial uplift is available. Even if, this instability doesn't lead to overturning, it can be a cause of higher accelerations at top of the body, arising due to multiple impacts with the base.
7. In the traditional diagram available for a rigid body as shown in Fig.2-2, the horizontal line given by $\mu_s$= B/H demarcates transition between pure sliding and a combination of sliding and rocking mode of motion. However in Fig.4-23, this line has shifted downwards from 0.25g to 0.15g. That means that sliding motion is restricted only for low values of coefficient of friction ($\mu$<0.15).

8. A flexible body has an anomalous tendency of uplift at lower amplitudes if frequency of base excitation excites its free rocking phenomenon. Free vibrations caused by base excitation frequencies causes uplift and lead to low amplitude rocking motion both in the rest state or sliding state of motion.

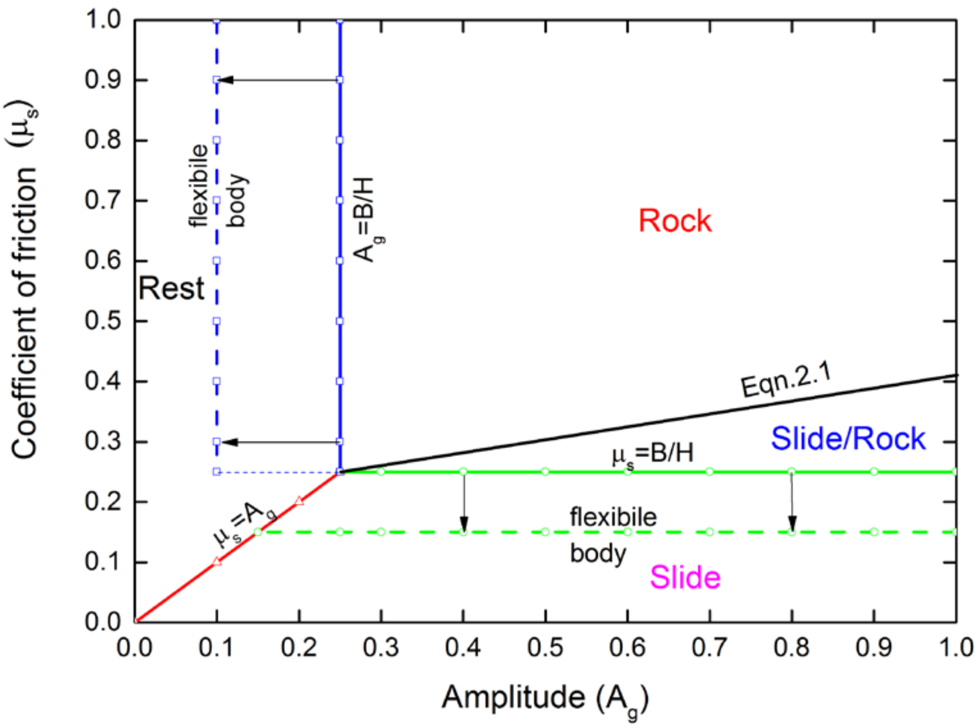


**Figure 4-23 Motion initiation diagram for a flexible test specimen TS4 (AR=4, p=2.9, α=0.24), showing different phases of motion**

## 4.4 Finite Element Modelling and Analysis

Three-dimensional finite element models of the test specimens were used for obtaining numerical solution. Three-dimensional finite element models of all the three test specimens viz. TS4, TS5 and TS6 were prepared in FE software. Part modelling and analysis technique is discussed in the next section.

### 4.4.2 Part modelling

All the three test specimens were fabricated out of mild steel material. Details of geometric and physical properties are already given in Table.4-1. As the thickness is less in comparison with longitudinal and lateral dimensions, shell elements were used for modelling top and bottom plates while three-dimensional beam elements were used for modelling four angles joining top and bottom plates.

A four node general-purpose shell element (S4R) with reduced integration and hourglass control was chosen. A three-dimensional beam element B31 was used for modelling four angles of L shaped section connecting top and bottom plates. Timoshenko beam (B31) allows for transverse shear deformation. This can be used for thick as well as slender beams. B31 beam is linearly interpolated and well suited for cases involving contact, such as the laying of a pipeline in a trench or on the seabed or the contact between a drill string and a well hole, and for dynamic versions of similar problems (impact).

In the present case, floor was very stiff in comparison with the test specimens and hence was modelled with rigid element R3D4, which is a three-dimensional, 4-noded bilinear quadrilateral element was selected for analysis.

All the three test specimens were assembled on top of the shake table as shown in Fig.4-24. Contact constrains were applied at the contacting surfaces between floor and specimens. Next section describes more about the interactions and boundary conditions applied. Material properties of test specimens were similar to that given earlier in Table.3-7.

### 4.4.3 Contact interactions and boundary conditions

While creating assembly of three test specimens and rigid floor, contact constraint was defined. In present case, surface based contact formulation was used for defining the contact. Rigid floor was selected as a master surface and contacting surfaces on the specimens were selected as slave surfaces. In addition to the contacting surfaces between floor and the test specimens, four connecting beams perpendicular to the direction of base excitation (i.e. X-axis), lying in the YZ plane, were also selected as slave surfaces. They were selected because of the possibility of contact with the master surface in case of overturning of the specimens. Contacting surfaces are shown with dots in the Fig.4-25. Contact properties were defined in the normal and tangential directions. In tangential directions, Coulomb friction model was used to relate the maximum allowable frictional (shear) stress across an interface to contact pressure between contacting bodies. Similarly, in normal direction, hard contact was selected to account for normal pressure/over closure relationship. For numerical enforcement of contact constraints in tangential and normal direction, Penalty algorithm was used. Two configurations (path) based contact tracking scheme was used in a finite sliding formulation with surface to surface discretization. However node to surface discretization was used for generating contact between beam element and the rigid surface. All the rigid bodies motion of floor were constrained and actual recorded time histories of base excitations were applied at reference node of the floor. Gravitational force was applied as a body force to the entire model.

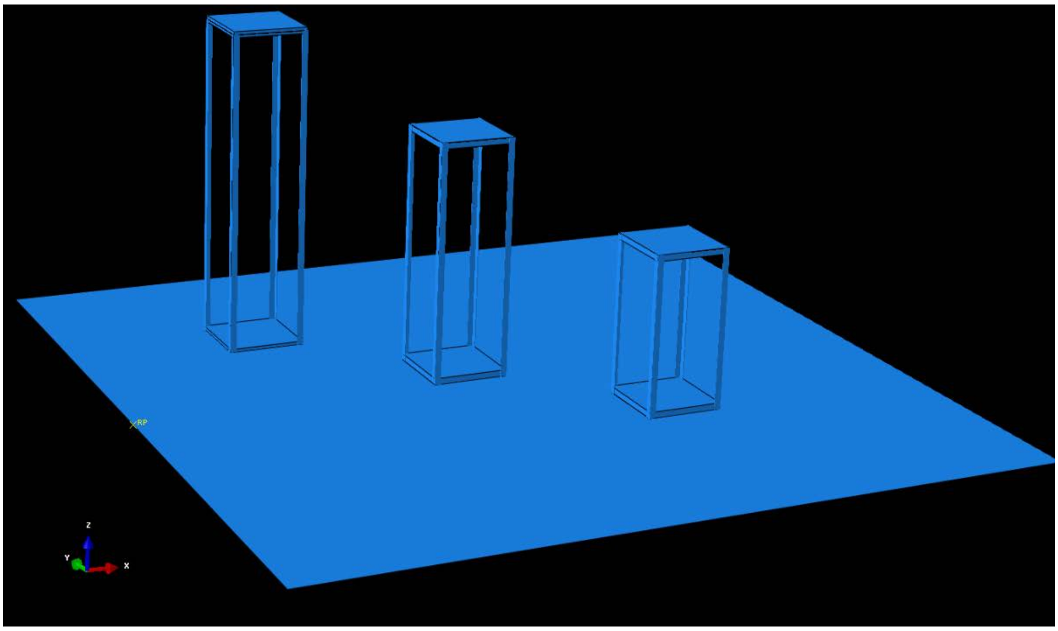

**Figure 4-24 Finite element model of test specimens TS4, TS5 and TS6**

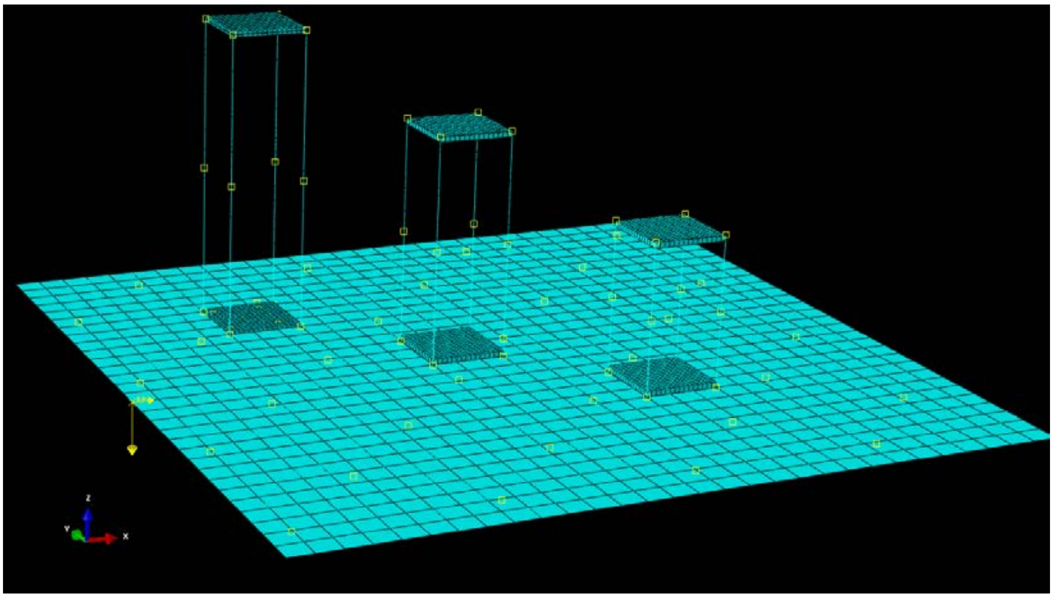

**Figure 4-25 FE Model of test specimens standing freely on the rigid floor. Contact interactions and boundary conditions are indicated.**

### 4.4.4 Modal Frequency Analysis

To evaluate fundamental dynamic property of test specimens, it is important to know fundamental frequencies of the test specimens. Natural frequencies of the test specimens in the fixed based boundary condition were evaluated using FE software. Lanczos solver was used for eigenvalue extraction. The fundamental frequencies of TS4, TS5 and TS6 are tabulated in Table.4-4. First three fundamental mode shapes of specimens TS4, TS5 and TS6 are shown in Figs.4-26, 4-27 & 4-28 respectively. Displacement gradients are shown by color scheme, whereas blue color indicates lowest displacement value and red color indicates the highest.

**Table 4-4 Modal frequencies of test specimens TS4, TS5 and TS6**

| Mode | Modal Frequencies(Hz) | | |
|---|---|---|---|
| | TS4 | TS5 | TS6 |
| 1 | 7.8 | 11.8 | 21.4 |
| 2 | 7.8 | 11.8 | 21.4 |
| 3 | 15.7 | 24.3 | 44.5 |

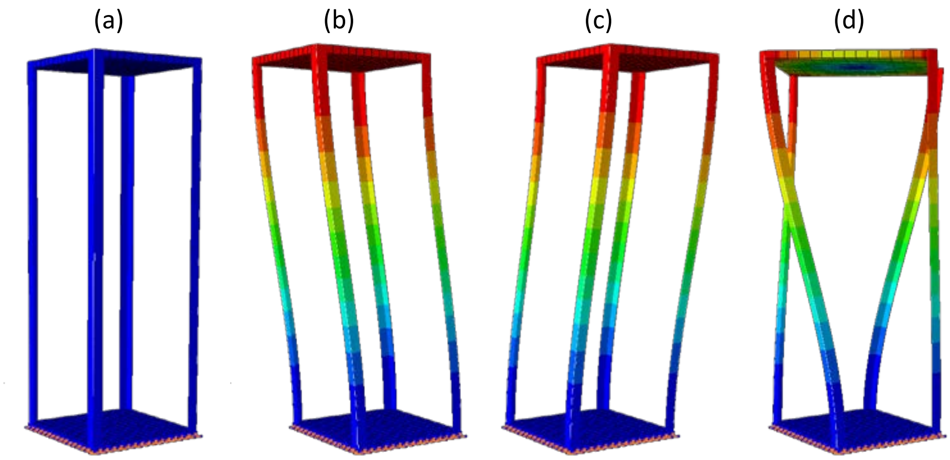


**Figure 4-26 Fundamental mode shapes of TS4. (a) un-deformed shape, (b) first mode shape, (c) second mode shape, (d) third mode shape**

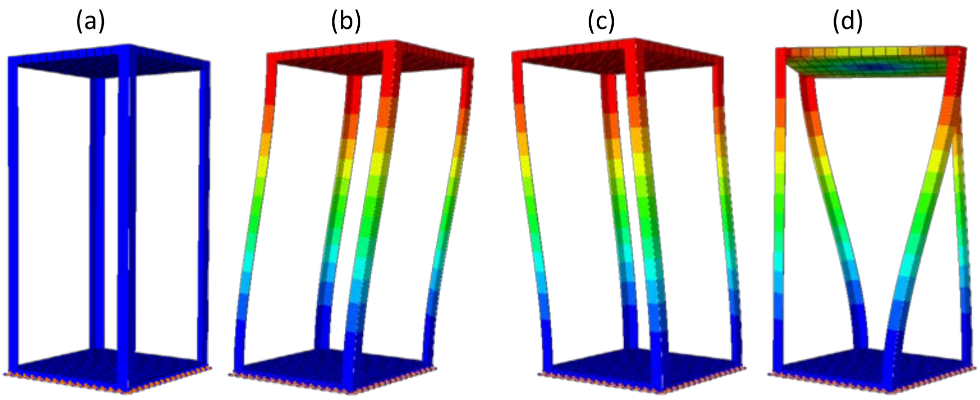


**Figure 4-27 Fundamental mode shapes of TS5. (a) un-deformed shape, (b) first mode shape, (c) second mode shape, (d) third mode shape**

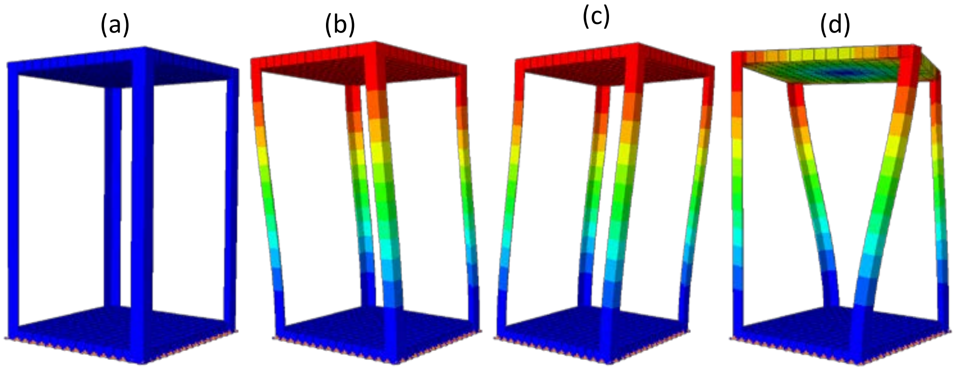


**Figure 4-28 Fundamental mode shapes of TS5. (a) un-deformed shape, (b) first mode shape, (c) second mode shape, (d) third mode shape**

### 4.4.5 FE Model Validation

Three-dimensional finite element model was utilized to perform numerical calculations on test specimens TS4, TS5 and TS6. Implicit solver was used to carry out numerical solution. Nodal accelerations and displacements at locations where actually sensors were installed during shake table experiments were obtained.

In order to validate numerical model, test specimen TS4 was selected.

Experimental results obtained for sliding mode of motion of TS4 are compared with the FE analysis results. Experimental results for the test run-1 of Table.4-3 are used for benchmarking analysis results. Peak slip displacements, peak rocking angles and acceleration amplification factors for the test run-1 are compared in the Figs.4-29, 4-30 and 4-31 respectively. Following are the observations:

1. In general finite element analysis results closely matched experimental values. Maximum deviation from the experimental results for peak slip displacements was 7.6 percent for 3Hz frequency as shown in Fig.4-29. For all other frequencies deviation was lesser than this.
2. For peak rocking angle, maximum deviation of 8.3 percent was observed at 6Hz base excitation frequency. Deviations at all other values was observed to be lesser than that.
3. Similarly for acceleration amplification factors, maximum deviation of 10 percent was observed at 2Hz frequency. Rest all points were well within this range.

Comparison of analysis results with the available experimental data indicated a good coherence. Hence the developed FE model is suitable for performing numerical calculations for test specimens TS4, TS5 and TS6. Moreover, model validation results of TS4 are valid for TS5 and TS6 also, because of similarity in used modelling and analysis methodology.

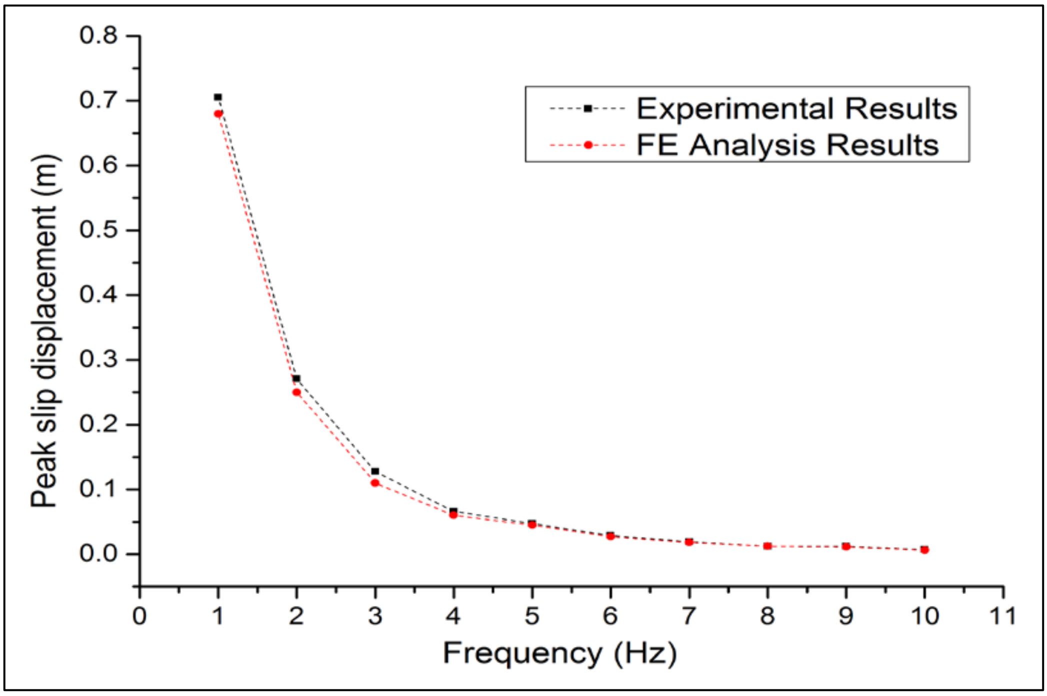


**Figure 4-29 Comparison of maximum slip displacements obtained from FEA and experimental results**

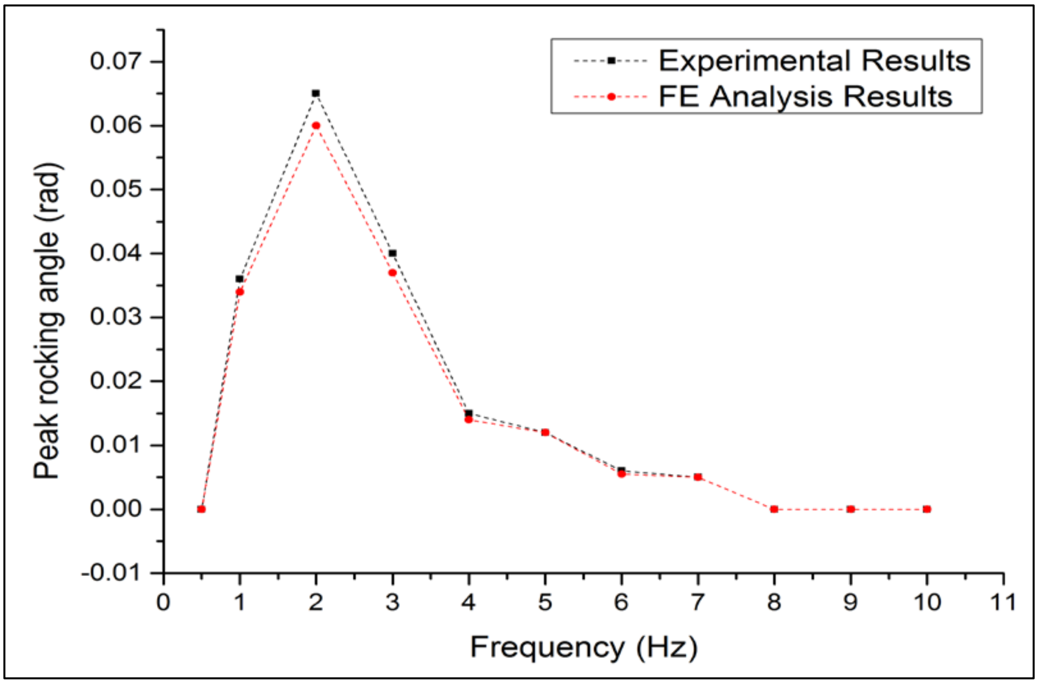


**Figure 4-30 Comparison of maximum rocking angles obtained from FEA and experimental results**

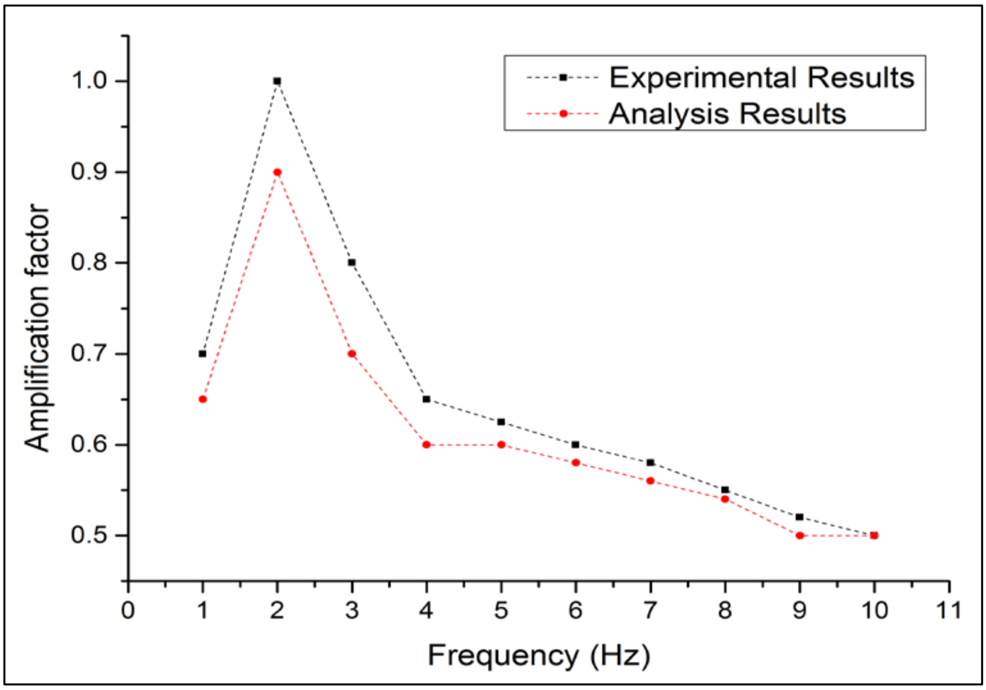


**Figure 4-31 Comparison of acceleration amplification factors obtained from FEA and experimental results**

## 4.5 Comparison of Dynamics of Rigid and Flexible bodies

In this section, comparison is drawn for geometrically similar pair of test specimens viz. TS1 and TS4, TS2 and TS5, TS3 and TS6. Dynamic behavior of these specimens under sliding and rocking mode of motion is compared. Different parameters important for stability and integrity are compared and presented.

### 4.5.2 Sliding Mode of Motion

For a free-standing nonstructural component (rigid or flexible), comparison is drawn for important parameters of sliding mode of motion.

#### *4.5.2.1 Peak Response*

Peak slip displacement is compared for geometrically similar test specimens. For the harmonic testing at $X_g$=0.8g (peak base acceleration) and $\omega$ = 0.5Hz to 10Hz, comparison is carried out between rigid and flexible test specimens. Fig.4-32 and Fig.4-33 presents variation of peak slip displacements and peak rocking angles respectively for all the six test specimens.

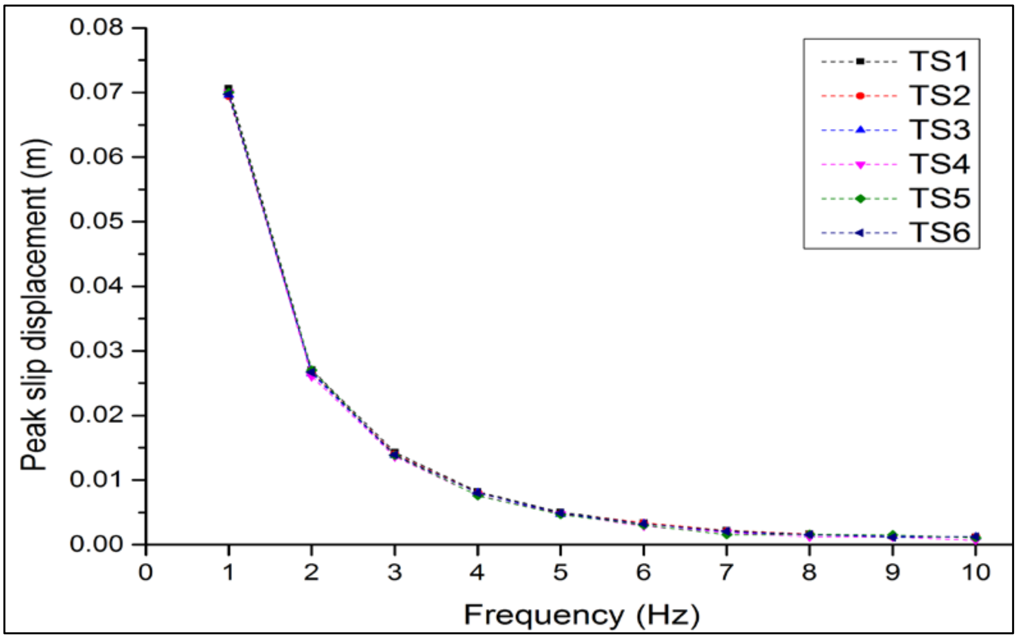


**Figure 4-32Variation of peak slip displacement of test specimens with frequency of excitation**

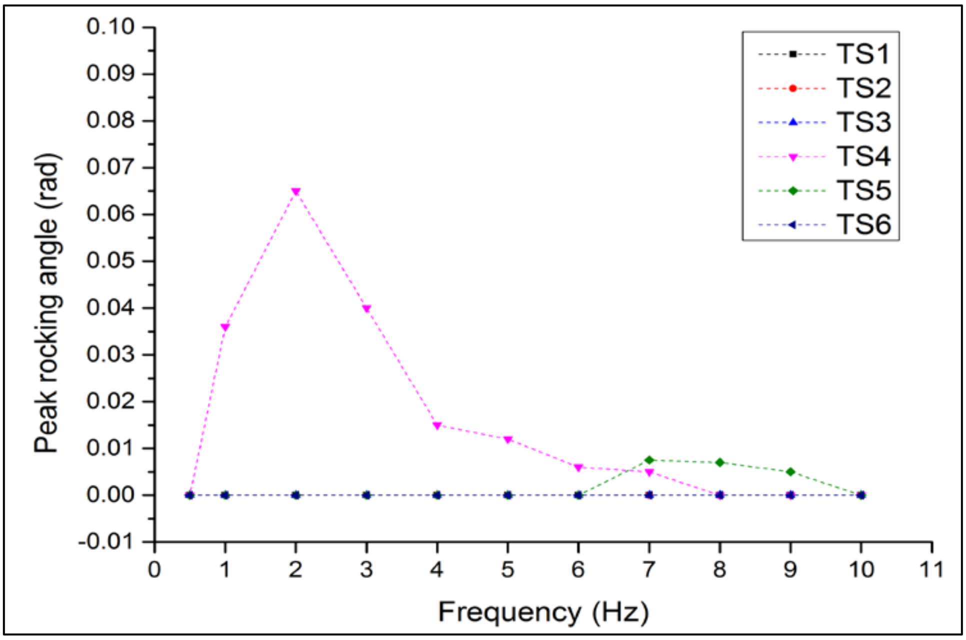


**Figure 4-33 Variation of peak rocking angle of test specimens with frequency of excitation**

Following are the important observations:

1. In general, there was a small difference observed between sliding behavior of geometrically similar rigid and flexible specimen. For geometrical pair of TS1 and TS4, maximum variation in peak slip was 0.006m, 0.010m and 0.007m at 1Hz, 2Hz and 3Hz frequency respectively. For all other frequencies difference was less than 0.005m as shown in Fig.5-1. This indicates that flexibility of a specimen effects its sliding dynamics. Rigid specimen TS1 consistently slipped higher displacements than the geometrically similar flexible TS4 for the frequencies ranging from 1Hz to 7Hz. For frequencies higher than 8Hz, slip difference was minimal (<1mm).It is interesting to note that for frequencies ranging from 1Hz to 7Hz, specimen TS4 was undergoing sliding cum rocking motion which can be seen by comparing Fig.4-32 and Fig.4-33. Moreover, these frequencies lie in the range of specimen's free rocking frequencies and hence frequency induced rocking motion was present as discussed in Section 4.2.5.1. Physical explanation of higher slip displacement of a rigid specimen TS1 compared to a flexible specimen TS4 for a particular range of frequencies corresponding to free rocking frequencies can be provided by energy balance approach. Energy input to the shake table in form of base excitations was used in generating sliding or rocking motion and a part of it is dissipated via frictional resistance or impact during rocking. In case of a rigid specimen only frictional sliding was the mechanism available for energy dissipation. On the other hand, in case of flexible specimen, due to presence of rocking motion for certain frequencies, additional impact mechanism was available for energy dissipation. Moreover, there was a presence of structural damping which also acts as an energy dissipating mechanism, although much smaller than impact. Hence, due to presence of frequency induced rocking motion, effective slip displacement of flexible specimen reduced.

2. Slip displacements of TS2 and TS5 were observed to be identical and difference was less than 0.002m for all the frequencies except 7Hz, 8Hz and 9Hz. At 7Hz, 8Hz and 9Hz, difference in slip displacement was 0.0065, 0.005 and 0.0072m respectively. It can be observed that these frequencies lie in the range of free rocking frequencies of TS5, and hence frequency induced rocking motion was present as shown in Fig.4-33. Using the energy balance approach discussed in the first point, this difference of slip behavior can be justified.
3. Test specimens TS3 and TS6 displayed identical slip behavior. Difference of slip displacement for entire range of frequencies was less than 0.001m. It is worth noting that flexible specimen TS6 did not initiate rocking motion in the range of test frequencies as shown in Fig.4-33. Hence, no difference in sliding behavior of specimens was observed.
4. Test response of geometrically similar flexible and rigid test specimens highlighted an important property. Sliding behavior of a rigid body is exactly identical to geometrically similar flexible body provided that frequency induced rocking behavior is not present. In case of presence of frequency induced rocking motion, significant dissimilarities are possible.
5. Effect of slenderness of rigid specimens for the same base dimensions was limited. Maximum variation in slip displacement observed was 0.005m for TS1 and TS3 at 1Hz frequency. For all other frequencies difference was less than this value. Similarly, for flexible test specimens maximum difference in peak slip displacement between TS3 and TS6 was 0.007m at 2Hz frequency.
6. An important difference between sliding behavior of rigid and flexible bodies is presence of rocking motion with sliding. As shown in Fig.4-33, flexible specimen TS4 was rocking for a wide range of frequencies (1Hz-7Hz), while geometrically similar

rigid specimen TS1 was not rocking at all. It can also be observed that none of the rigid specimens TS1, TS2 and TS3 initiated rocking motion while slender flexible specimens TS4 and TS5 initiated rocking motion. Moreover, it can also be observed that less slender flexible specimen TS6 behaved like rigid body and did not initiate uplift.

#### *4.5.2.2 Acceleration Amplification*

After observing differences in peak response quantities for sliding motion, now acceleration amplification factors of all the six specimens are compared. Fig.4-34 displays variation of amplification factors with frequency of base excitations. Following important points are observed.

1. A large variation in amplification factor was observed for geometrically similar TS1 and TS4 specimens. AF value for TS1 was 0.19 irrespective of frequency of excitation. On the other side AF value for TS4 varied from as high as 1 for 2Hz to 0.62 for 10Hz frequency as shown in Fig4-34. It means AF value of flexible specimen was dependent on frequency of base excitation, however same was independent of base excitation for a rigid specimen. The main reason behind high values of AF for TS4 was presence of frequency induced rocking motion.
2. AF value for TS5 was also observed to be dependent of frequency of base excitations. However variation in value was not much as was in case of TS4. On the other hand, AF value for geometrically similar TS2 remained at 0.19 irrespective of frequencies. It can be generalized that amplification factor of a rigid body for given contact conditions, is independent of slenderness and frequency of base excitations. On the other side, amplification factor of flexible body for same set of contact conditions is dependent of slenderness and frequency of base excitations. Moreover, in spite of presence of rocking motion or not, flexible specimens had higher AF values than geometrically similar rigid

specimens. The physical explanation for such a behavior is presence of free vibrations in a flexible specimen, even in case of pure sliding motion. These free vibrations are not sufficient to cause uplift but they can increase acceleration values transmitted to the top of a flexible specimen.

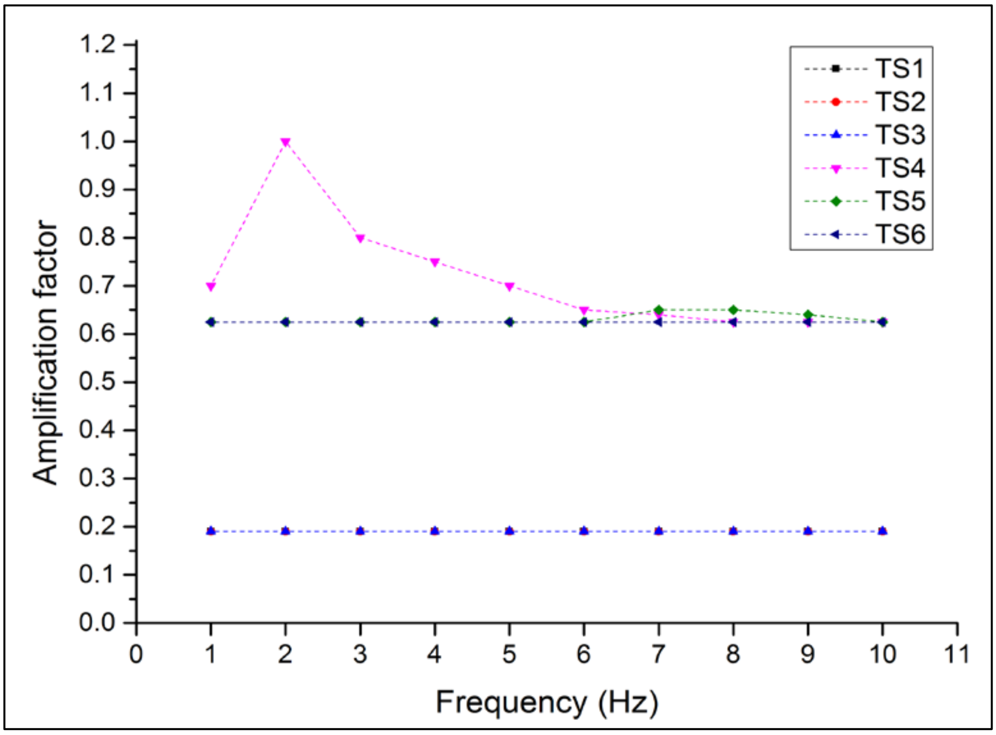


**Figure 4-34 Variation of amplification factor of test specimens with frequency of base excitation**

### 4.5.3 Rocking Mode of Motion

After comparing dynamic response of geometrically similar rigid and flexible test specimens in a sliding mode of motion, now differences in rocking mode of motion are discussed. Four main parameters are compared viz. initiation of motion, peak response, acceleration amplification and overturning instability. Next sections gives detail for the same.

#### *4.5.3.1 Motion initiation*

Initiation of rocking mode of motion for geometrically similar pairs of test specimens under similar boundary conditions are compared. Rocking initiation diagrams for geometrically similar pairs of TS1 and TS4, TS2 and TS5, TS3 and TS6 are plotted in Fig.4-35, Fig.4-36 and Fig.4-37 respectively as given below.

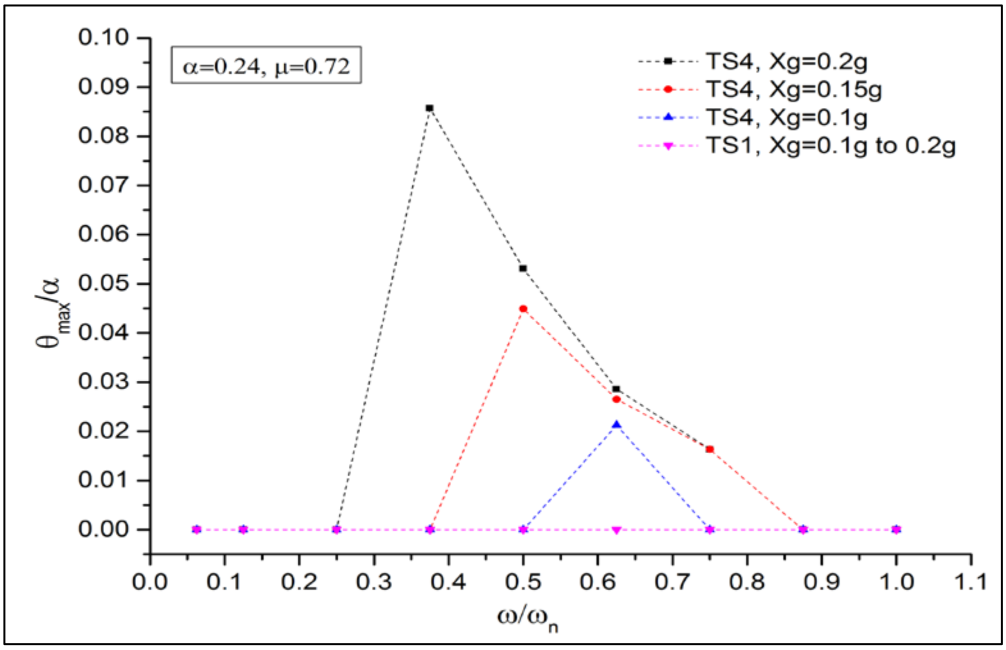


**Figure 4-35 Non dimensional graph showing variation of peak rocking angle with frequency ratio for TS1 and TS4**

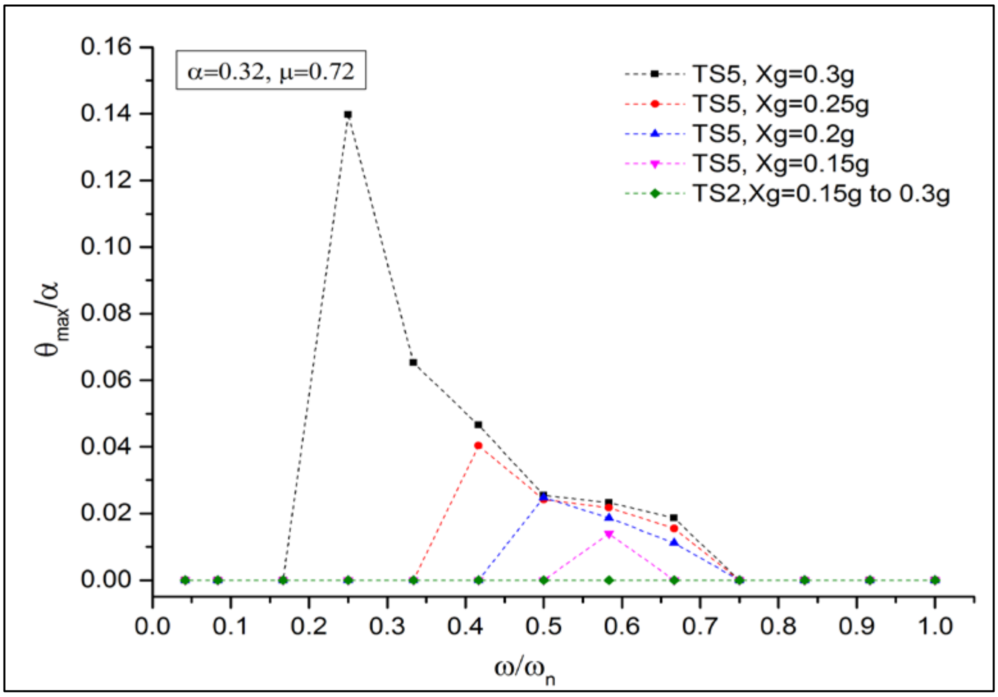


**Figure 4-36 Non dimensional graph showing variation of peak rocking angle with frequency ratio for TS2 and TS5**

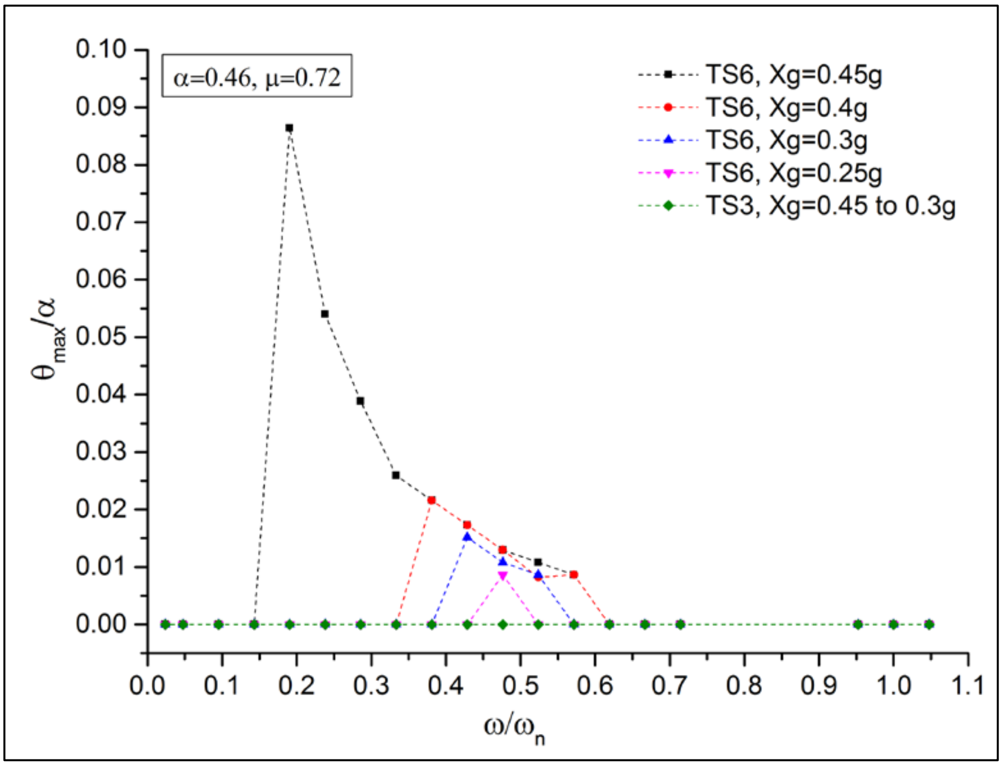


**Figure 4-37 Non dimensional graph showing variation of peak rocking angle with frequency ratio for TS3 and TS6**

With respect to Figs. 4-35 to 4-37, following are the conclusions:

1. Flexible specimen (TS4) initiated rocking motion at an amplitude of base excitation as low as 0.1g. However, it is interesting to note that geometrically similar rigid specimen TS1, could not initiate rocking motion up to 0.25g amplitude of base excitation. This observation highlights importance of free rocking frequencies which were responsible for this uplift initiation.
2. Similarly, flexible specimen (TS5) initiated rocking motion at an amplitude of base excitation as low as 0.15g. On the other side, geometrically similar rigid specimen TS2, could not initiate rocking motion up to 0.33g amplitude of base excitation. Once again this was due to frequency induced rocking motion.
3. Similar to other two cases, flexible specimen (TS6) initiated rocking motion at an amplitude of base excitation as low as 0.25g but geometrically similar rigid specimen TS1, could not initiate rocking motion up to 0.5g amplitude of base excitation. These observations indicate importance of frequency induced rocking phenomenon in flexible bodies. It is further highlighted that slenderness of the body has no direct effect on initiation of rocking motion. Free rocking frequencies of rigid specimens could not induce uplift, although there values were comparable to those for flexible specimens.

#### *4.5.3.2 Peak Response*

After observing differences in uplift behavior of test specimens, now peak rocking angles of geometrically similar specimens for different frequencies of base excitations are compared. All the specimens were subjected to harmonic excitation of $X_g$=0.8g and $\omega_r$= 0.5Hz to 10Hz. Results of geometrically similar TS1 and TS4, TS2 and TS5, TS3 and TS6 specimens are plotted in Fig.4-38, Fig.4-39 and Fig.4-40 respectively as shown below.

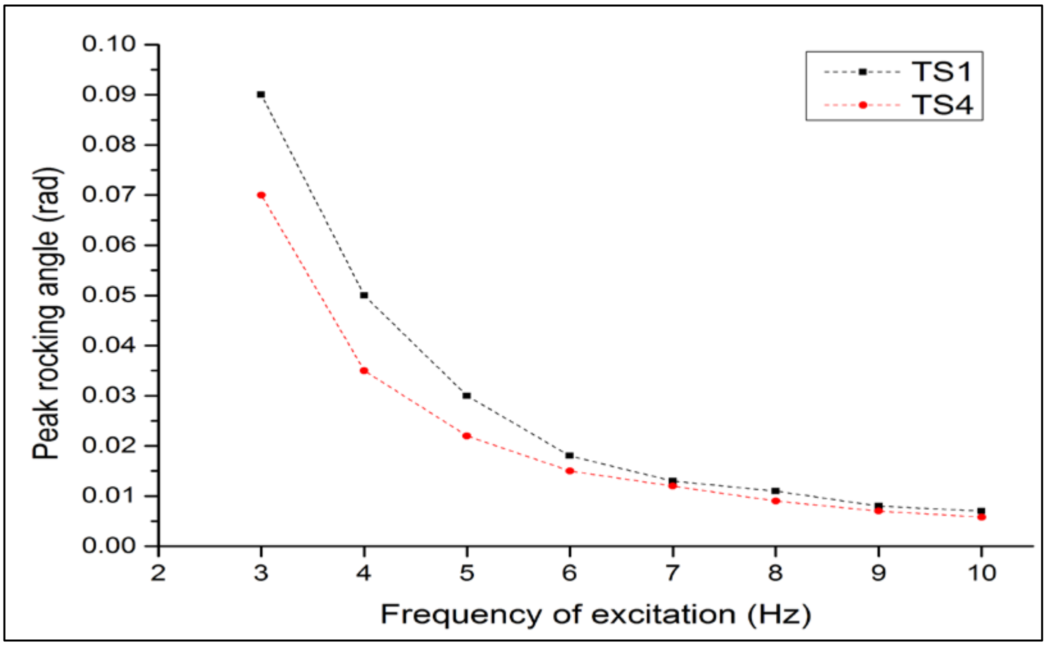


**Figure 4-38 Comparison of peak rocking angles of specimens TS1 and TS4**

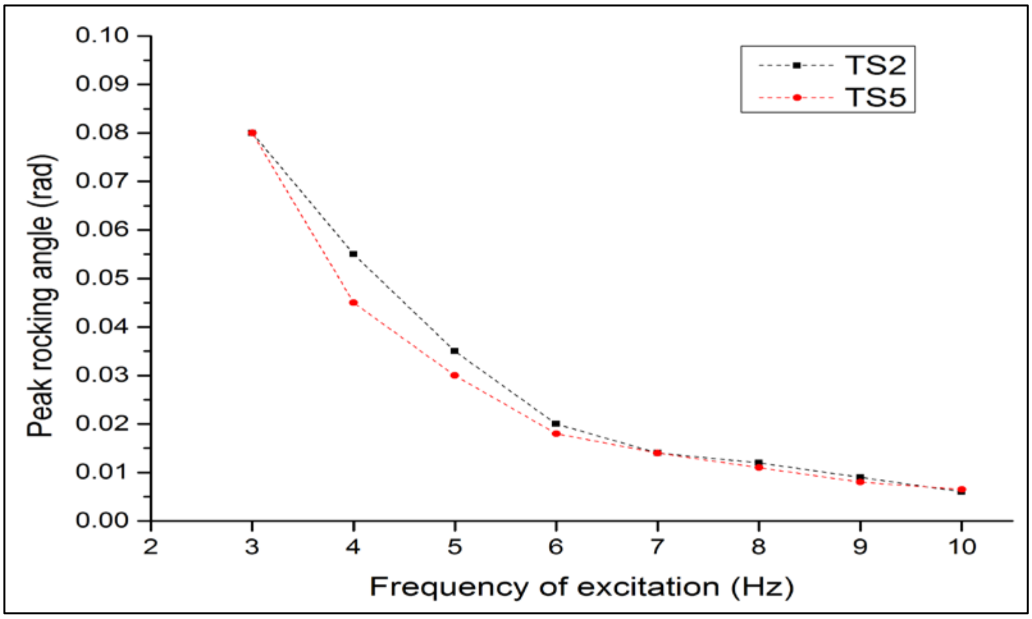


**Figure 4-39 Comparison of peak rocking angles of specimens TS2 and TS5**

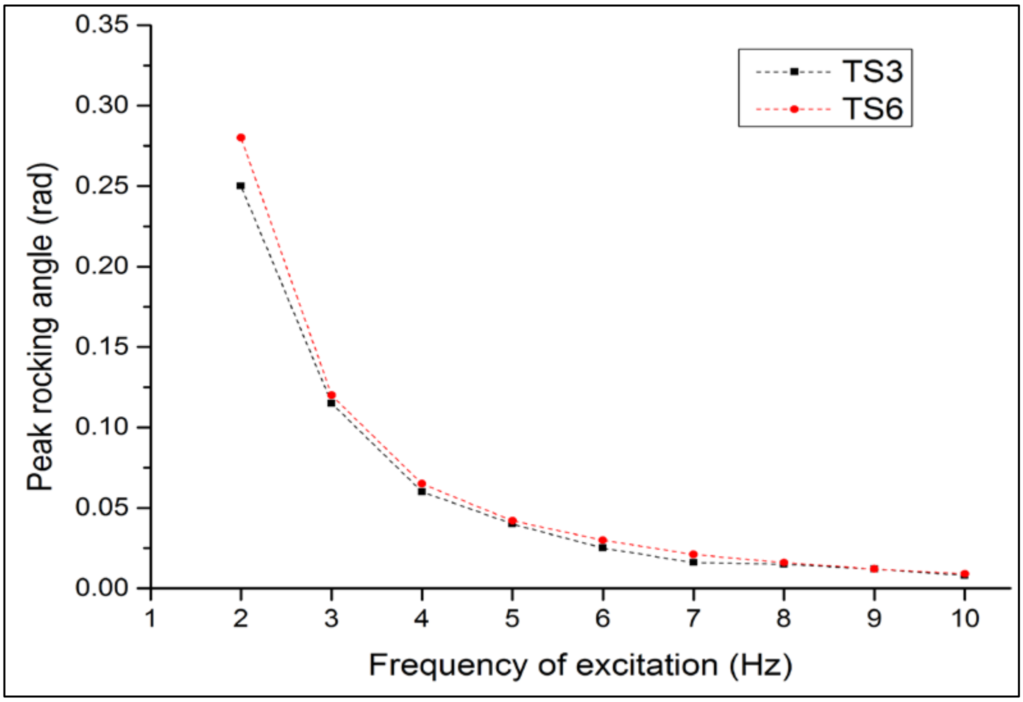


**Figure 4-40 Comparison of peak rocking angles of specimens TS3 and TS6**

Following important points can be noted:

1. Specimens TS1 and TS4 showed similar rocking behavior and overturned for frequencies of base excitations from 0.5Hz to 2Hz as shown in Fig.4-38. For frequencies higher than 2Hz, there was a marginal difference in peak rocking angles of both the specimens. Maximum difference observed was 0.02 radians (around 1 degree) at 3Hz frequency. With the increase of frequencies this difference reduces to a meagre value of 0.001radian.For a particular frequency, flexible specimen rocked slightly more than the geometrically similar rigid specimen. Frequency of base excitation had a reducing effect on peak rocking angles. With an increase of frequency from 3Hz to 10Hz angle reduced by tenfold. This is consistent with the earlier observations made in Chapters-3 and 4 and indicates presence of cutoff frequencies above which no rocking motion can exist. Here it is important to highlight that flexibility of the specimen has

very limited effect on rocking behavior, for the entire range of frequencies for a given amplitude and base conditions.

2. Specimens TS2 and TS5 showed similar rocking behavior up to 2Hz frequency and both overturned. For frequencies higher than 2Hz, both the specimens had similar rocking behavior as shown in Fig.4-39. Maximum difference of 0.02 radians was observed at 4Hz, while it was much lesser at other frequencies. Frequency of excitation again had a reducing effect on rocking angles.
3. Specimens TS3 and TS6 (refer Fig.4-40) also showed similar rocking behavior up to 1Hz frequency and both overturned. For rest of the frequencies differences was meagre, maximum being 0.03 radian at 2Hz.

Hence it can be interpreted from these results that rigid and flexible specimens rocking behaviors are identical except for the differences in overturning (Refer Subsection 4.5.2.4) and rocking initiation behavior ((Refer Subsection 4.5.3).

#### *4.5.3.3 Acceleration Amplification*

After discussing differences in peak response quantities for rocking motion, now acceleration amplification factors of all the six specimens are compared. Fig.4-41 displays variation of amplification factors with frequency of base excitations. AF corresponding to overturning are not plotted, since they have very high values. Rest of the points in rocking regions are plotted in the graph. Following important points can be observed.

1. At a fixed base amplitude, acceleration amplification factor for a rigid specimen TS1 is higher than its flexible counterpart TS4, for all frequencies of base excitation. This difference has a value of 0.3 at 2Hz which decreases to zero at 10Hz. At 10Hz, amplification factor graph of both the specimens reach a value of unity asymptotically. Rigid specimen amplified base acceleration higher than the flexible one. This behavior

can be explained by the presence of energy dissipating damping mechanism in a flexible body. Moreover, a flexible body can absorb a significant amount of energy by local elastic/plastic deformations during impact and hence generate a milder acceleration spike. This results in lower acceleration amplification and transmission to top of the body.

2. Similarly, AF for TS2 was much higher than the flexible counterpart TS5. The difference observed was as high as 4 at 2Hz frequency which reduced to 0.3 at 10Hz as shown in Fig.4-40. Higher rigidity and smaller dimension of TS2 led to higher acceleration amplification compared to TS1.
3. AF for TS3 was the highest and reached a value of 11 at 2Hz frequency. On the other side, flexible counterpart TS6 had a value of 4. That means the difference in AF was as high as 7. In this case also AF value decreased with increasing frequency, however even at 10Hz frequency AF for TS3 was 2. This highlights an important property of rigid bodies. In case of rocking rigid bodies applied base acceleration can be amplified manifold at the top. This observation has a significant effect on integrity and functionality of any component mounted/located at the top location.

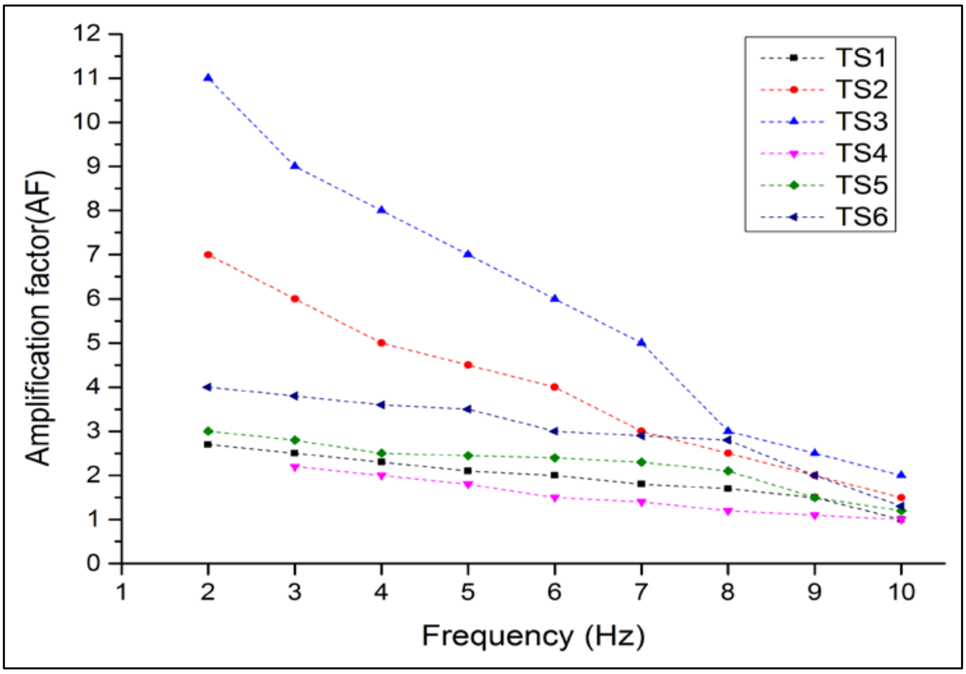


**Figure 4-41 Acceleration amplification factors for all the specimens TS1 to TS6**

#### *4.5.3.4 Overturning Instability*

It shall be interesting to compare overturning behavior of geometrically similar rigid and flexible bodies. For this comparison, TS1 and TS4 were selected. Both are geometrically similar with equal value of slenderness ($\alpha$=0.24). Overturning curves of both the specimens are plotted in a single graph as shown in Fig.4-42. Following are the observations with respect to graph.

1. For low frequency region ($\omega/p$ <0.3), rigid specimen TS1 fails in Mode-2, if amplitude of base excitation is increased. Flexible specimen TS4 also exhibits similar behavior and fails in Mode-2 with the increase of amplitude of base excitations. However, in case of TS4 the low frequency range is higher ($\omega/p$ <0.35). In this region slope of curve for TS4 is lesser than TS1. This means that for a given frequency, it requires higher amplitude to overturn a rigid specimen (TS1) than the flexible one (TS4).
2. In mid frequency range both the specimens first undergo Mode1 failure and then Mode 2 failure with the increase of amplitude. This frequency range differs for both the

specimens. For TS1, it's between 0.3 and 3.3, while it's 0.35 to 4.1 for TS4. In this frequency range, higher amplitudes are required to cause Mode2 failures then the low frequency range. However, presence of Mode1 failure reduces stability. It was observed during experiments, that Mode1 failure takes larger time than the Mode2 failure, which means if base excitation is present continuously for a required minimum time than only the Mode1 failure takes place. Moreover, Mode1 failure was observed to be accompanied by multiple rocking cycles and subsequent impacts with the base. In case of a flexible specimen, area corresponding to Mode1 failure is higher than geometrically similar rigid specimen. This means that in a mid-frequency range, flexible specimens has a higher tendency for Mode1 failure than the rigid specimen.

3. At higher frequencies, $\omega/p>3.3$ for TS1 and $\omega/p>3.3$ for TS4, both the specimens overturn with Mode2 failure with increase of acceleration value. Generally, it requires very large accelerations ($A/g\tan\alpha > 48$ for TS1 and $A/g\tan\alpha > 56$ for TS4) to overturn the specimens at higher frequencies. Usually such high amplitudes are not encountered in a seismic excitation.

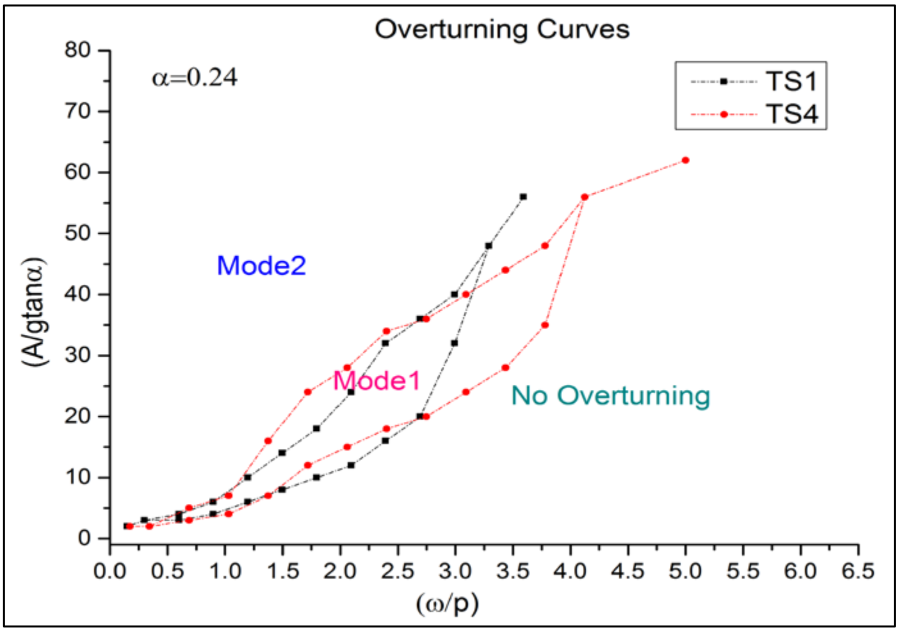


**Figure 4-42 Overturning curves of geometrically similar test specimens TS1 and TS4**

### 4.5.4 Motion Initiation Criteria

As discussed in Chapters 3 and 4, significant differences were observed in motion initiation criteria's of rigid and flexible specimens. 2D and 3D plots of motion initiation criteria diagrams for TS1 were already shown in Figs.2-3 and 3-33 respectively. Similarly, 2D plot for TS4 was shown in Fig.4-21. Now, differences between these plots will be discussed in the following:

1. In two dimensions, a rigid block TS1 can undergo three possible modes of motion from rest viz. sliding, rocking and a combination of sliding and rocking. Boundaries corresponding to various modes of motion are indicated in Fig.2-2 and Fig.3-33. In case of a rigid block, frequency of base excitation was also found to play an important role in determining initiation of a particular mode of motion and hence a 3D plot (Fig.3-33) was prepared to include effect of frequency as a third axis. It was observed that above a critical value of frequency (cut off frequency) a state of no motion exists. However, existing boundaries as shown in Fig.2-2 were observed to be valid below a plane defined by cutoff frequencies (Refer Fig.3-34). On the other side, in case of a flexible body TS4, existing boundaries in the two-dimensional map (Fig.2-2) were found to be dependent on frequency of base excitation, even at a values well below cutoff frequencies. Hence a new two-dimensional plot was prepared as shown in Fig.4-21. Interestingly, there were few major differences between Fig.2-2 for TS1 and Fig.4-21 for TS4. The foremost important difference was leftward shifting of boundary demarcating rest and rocking mode of motion. For a rigid block TS1, this boundary was defined by a vertical line $X_g = g \tan\alpha$. This boundary was found to be incorrect for a flexible body TS4. Experimental findings in Chapter-4, highlighted the presence of rocking motion and its effect on initiation of rocking motion from rest state. Flexible specimen started rocking at an amplitude of base excitation lesser than that given by

the vertical line $X_g$= g tanα. Hence, for TS4 this line has shifted to 0.1g. That means a negative shift of 0.15g from the existing value of 0.25g. This observation has a significant effect on stability of a flexible body in comparison to a rigid one. Due to this negative leftward shifting of the boundary, rest region for TS4 has considerably reduced. In other words, it can be interpreted that a flexible body is more prone to rocking initiation compared to a geometrically similar rigid body.

2. For a flexible specimen TS4, presence of rocking motion was observed in the region pertaining to sliding mode of motion. This means, when a rigid specimen TS1 was sliding its counterpart TS4 was undergoing a combination of sliding and rocking motion. The horizontal line given by $\mu_s$= B/H which demarcates transition between pure sliding and a combination of sliding and rocking mode of motion for a rigid body TS1 was shifted vertically downwards for TS4. Now after this shift, transition from slide/rock mode to sliding occurred at $\mu_s$=0.15, instead of the earlier value of 0.25. This indicates an increase in combination of sliding and rocking motion for the body. As discussed earlier, presence of rocking motion in the sliding mode increases acceleration amplifications. This observation is also significant from the stability point of view, since presence of rocking motion in sliding mode of motion adds concern for overturning check.
3. Motion initiation diagram for a flexible body has significantly lesser available rest area than its rigid counterpart. It has the highest rocking area and then slide/rock area. This indicates potentially unstable nature of a flexible body in terms of motion initiation.

## 4.6 Outcomes and Discussions

In this chapter, results of systematic experimental work performed on flexible test specimens of different aspect ratios was presented. Research carried out highlighted following specifics of dynamic behavior of flexible test specimens subjected to base excitations:

Dynamics of free-standing flexible bodies/NSC was studied using simple test models. Experimental and numerical studies highlighted novel findings. It was observed that initiation of rocking motion from rest state is a strong function of free rocking frequencies of a flexible body. For a specific set of base excitation frequencies corresponding to free rocking frequencies of a body, initiation of rocking motion is possible for an amplitude of base excitation, lower than statically required for uplift initiation. This observation can have significant repercussions of the stability of a flexible free-standing bodies. Initial uplift may be further amplified by any subsequent base excitation and thus may lead to even overturning of the body.

In addition to that, presence of rocking motion was observed in otherwise sliding mode of motion. This phenomenon was again dependent of frequencies of base excitations and was present only for frequencies in the range of free rocking frequencies. This observation has a direct effect on acceleration amplification factors and moreover, on energy dissipation due to impacts in addition to frictional dissipation.

Motion initiation criteria diagram for a flexible test specimen of four aspect ratio was developed. Effect of flexibility of the body on existing boundary conditions was demonstrated. Shifting of boundaries corresponding to transition from rest to rocking and Slide/rock to sliding mode of motion was observed. Reduction in area corresponding to rest state was observed. This can have an adverse effect on seismic stability of the body.

Various stability parameters like motion initiation, overturning instability, amplification factors, sliding and rocking dynamics were investigated and compared for geometrically similar rigid and flexible test specimens. Next chapter shall highlight seismic stability of an actual safety related component known as a glove box.

# CHAPTER 5 SEISMIC STABILITY OF A MECHANICAL CONTAINMENT SYSTEM: A GLOVE BOX

## 5.1 Introduction and Outline

Earlier chapters (Chapters3 and 4) brought out vital information about the dynamics of free-standing rigid and flexible bodies subjected to base excitations. Simple test specimens were analyzed to understand basic dynamic behavior of these bodies. Effects of variation of different system parameters on stability and integrity of such bodies was contemplated. Outcomes signified fundamental differences in response of a rigid and flexible body. By now, it is clear that both the cases shall be treated separately and appropriate solution technique is required to solve contact-impact dynamics problem arising due to base excitation. Now, in light of these findings, dynamics of a complex mechanical structure known as a glove box, shall be excogitated.

Nuclear facilities across the world use glove boxes as a primary containment structure for handling radiotoxic materials. In a fuel fabrication facility, three levels of confinements are provided for the safe handling of radiotoxic materials viz. tertiary, secondary and primary confinement. Tertiary confinement is provided by the outer civil structure of the facility. Secondary confinement is provided by the inner civil structure and ventilation system whereas primary confinement is provided by the glove box. Glove boxes (GB) are designed as Class I component as per the ASME Section III NB guidelines [72]. It is a safety related mechanical structure provided with ventilation and pressure regulatory system to maintain internal negative working pressure. Generally, it acts as a leak tight system with very low permissible leak rates of the order of 0.05% of its volume per hour as given by the relevant standards [60] [61] [2]. It is fabricated out of heat treated and annealed stainless steel sheets. Present research focuses on glove boxes used in fuel fabrication facilities in India. Generally, they are not anchored to the ground due to various operational and maintenance reasons and hence stands freely on floor as shown in Fig.5-1. A negative pressure of 250 $N/m^2$ is maintained with the help of a ventilation system. Glove ports and gauntlets are provided through which process and maintenance operations are performed. These boxes are anchored to a mild steel framework (stand) through bolts and the framework is placed freely on the floor. Generally they are arranged in series, wherein, a material transfer tunnel interconnects them to each other (see Fig.5-1). Dimensional details of a typical glove box is given in Table.5-1. Glove box is a classic example of a freestanding structure used in a nuclear industry.

As a part of research work carried out for this doctoral program, it is required to assess seismic stability and integrity of glove boxes. As mentioned earlier, glove box is a complex mechanical system which has various other auxiliary systems attached to it. Although it is standing freely on the floor, it has various piping like exhaust piping, service piping etc., which connects various service headers supported on the roof with the glove boxes. Consequently, as such it cannot be considered as a free-standing structure. However on the premise of a pragmatic assumption, it can be assumed as a freestanding structure. The underlying assumption here is that a flexible long piping connect boxes with the main header. Hence, in lieu of available flexibility in the piping system, restraining of free rigid body motions is limited, and thus can be safely ignored. Further, it is important to note that glove boxes are also used in different configurations. One of the configuration or layout is shown in Fig.5-1, whereas many boxes are interconnected to each other via material transfer tunnel. In another configuration, glove boxes are used as a standalone boxes with no interconnection. Hence formulation and solution of this problem requires deep excogitation. In this chapter, we will deliberate numerical formulation and solution for the case of a single standalone glove box system. However, case of multiple interconnected glove boxes will be discussed in the next two chapters (Chapter-6 and Chapter-7). Finally, as an outcome, a generalized formulation and solution methodology will be proposed to help designers in deciding on anchoring of glove boxes.

Section 5.2 of this chapter gives detail of various fundamental dynamic properties of a glove box structure. Then, Section 5.3 presents numerical formulation and solution technique for the case of a single standalone glove box using finite element software.

Section 5.4 presents results and findings on seismic stability assessment of a glove box structure. A parallel is drawn between the cases of a flexible body mentioned in Chapter-4 with that of a glove box. Then, Section 5.5 presents a novel methodology for evaluation of slip distance of a freestanding body. Developed method is valid only for a rigid body under sliding mode of motion. However it gives good conservative results of final slip displacement.

Section 5.6 presents result on validation of numerical methods used in this chapter.

In Section 5.7, motion initiation criteria diagram for a glove box structure is developed. This can be used as an effective tool for decision making on anchoring of the glove boxes with the floor. Finally, Section 5.8 brings out important observations and conclusions made from the systematic study carried out in this chapter.

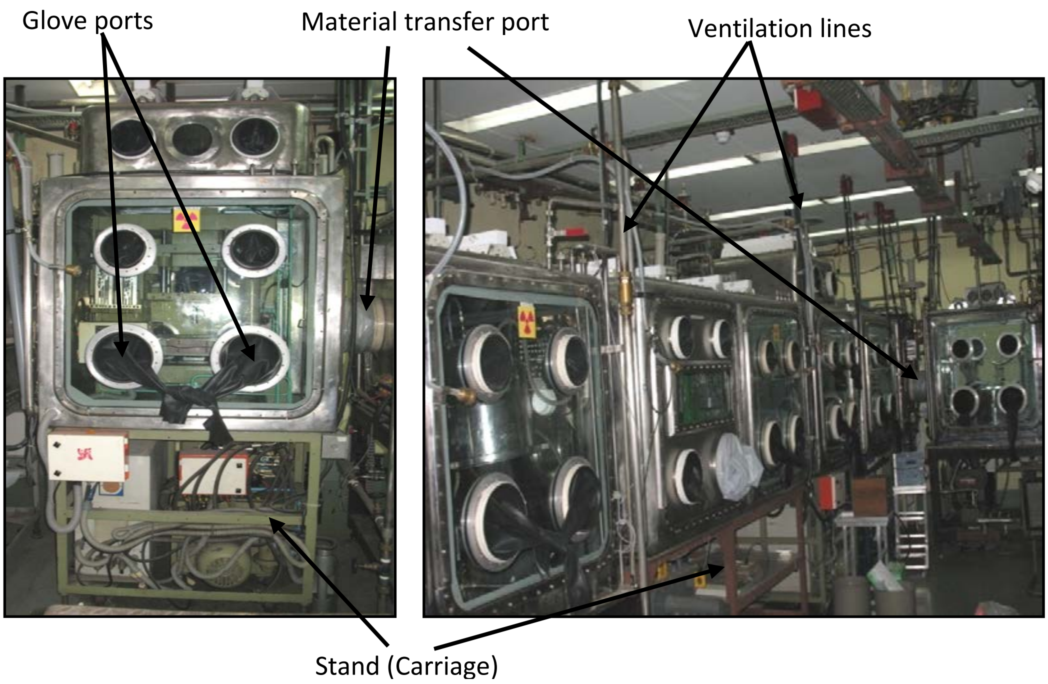


**Figure 5-1 A fuel fabrication laboratory showing various glove boxes freely standing on the floor**

**Table 5-1 Dimensional details of a glove box structure**

| **Glove box shell(top structure)** | | | | |
|---|---|---|---|---|
| Length(m) | Width(m) | Height (m) | Thickness(m) | Material of construction |
| 1 | 1 | 1 | 0.003 | Stainless steel (304) |
| **Bottom supporting plate** | | | | |
| Length(m) | Width(m) | Thickness(m) | | Material of construction |
| 0.960 | 0.960 | 0.009 | | Mild steel |
| **Carriage (stand)** | | | | |
| Length(m) | Width(m) | Height (m) | Thickness(m) | Material of construction |
| 1 | 1 | 1 | 0.006 | Mild steel |

## 5.2Dynamic Properties Evaluation

Before assessing seismic stability of a glove box system, it is required to find out its fundamental physical and dynamic properties. Free rocking frequencies ($\omega_r$) and fundamental modal frequencies ($\omega_n$) of a glove box were evaluated. Moreover, motion initiation criteria diagram for the case of a glove box was prepared.

### 5.2.1 Free Rocking and Natural Frequencies

Novel findings in Chapter-4 highlighted significance of free rocking frequency in initiating rocking instability in a freestanding flexible body. Hence it is imperative to first study free rocking characteristics of a glove box. Various important properties of a freestanding body like critical angle ($\alpha$), frequency parameter (p), Moment of inertia (I) and diagonal length (R) were evaluated. Equivalent two-dimensional model is shown in Fig.5-2, which gives various important properties of a GB.

To evaluate free rocking frequencies, initial angular rotation about an edge was given to initiate uplift. Once desired uplift was achieved, angular rotation was stopped and then the glove box was allowed to rock freely till rocking ends. Acceleration time histories at the top of the glove box were extracted and then Fast Fourier Transform (FFT) was done to determine free rocking frequencies about both horizontal axis (X and Z axis). Free rocking angles time history for few different cases of uplift are given in Figs.5-3 and 5-4. Fig.5-3 represents variation of rocking angle with time for different values of uplift of glove box about X-axis in ZY plane. Similarly, Fig.5-4 represents variation of rocking angle with time for different values of uplift of glove box about Z-axis in XY plane. After performing FFT on these values, free rocking frequencies for different uplifts starting from 0.001m up to 0.020m, about both X and Z axis are given in Fig.5-5. Coordinate system used in this chapter can be seen in Fig.5-6.

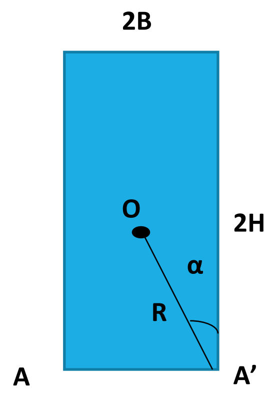


**Figure 5-2 Equivalent rigid block diagram of glove box showing various parameters**

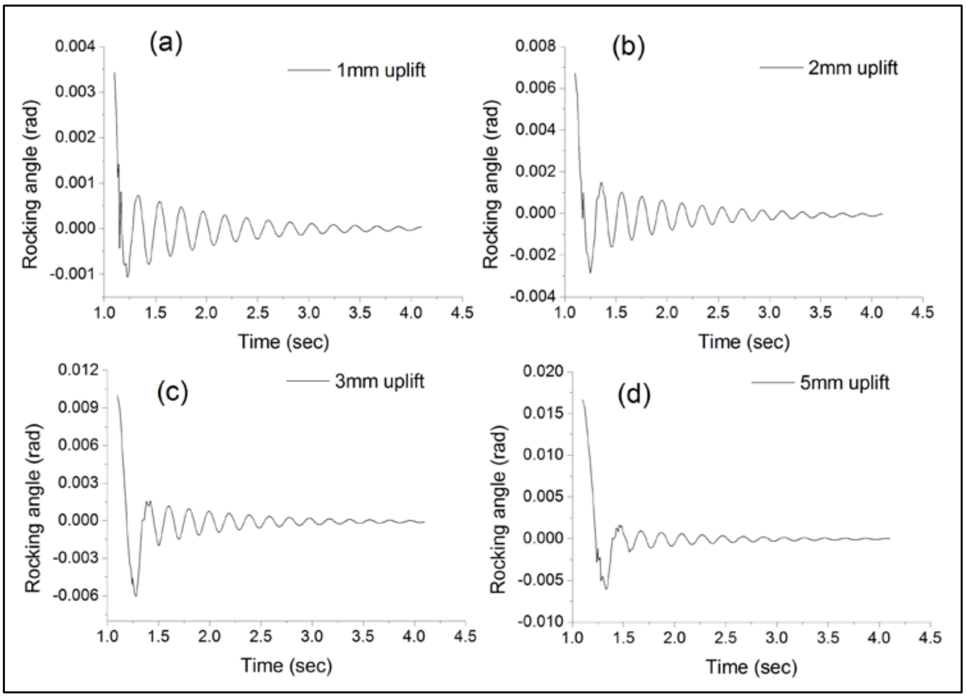


**Figure 5-3 Free rocking of glove box about X-Axis in ZY plane for different values of uplift**

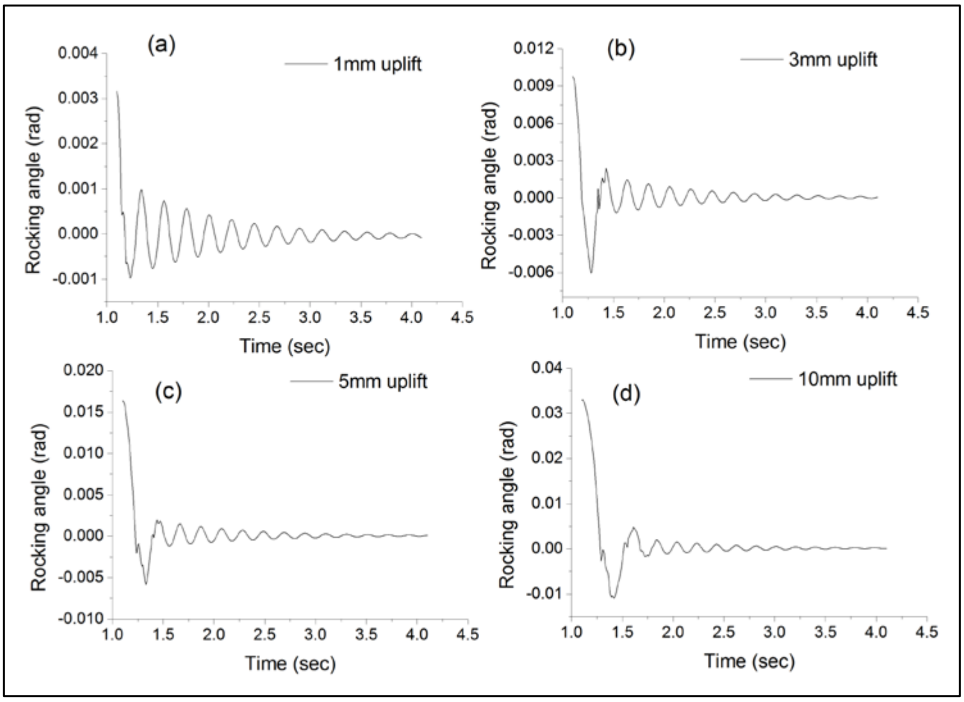


**Figure 5-4 Free rocking of glove box about Z-Axis in XY plane for different values of uplift**

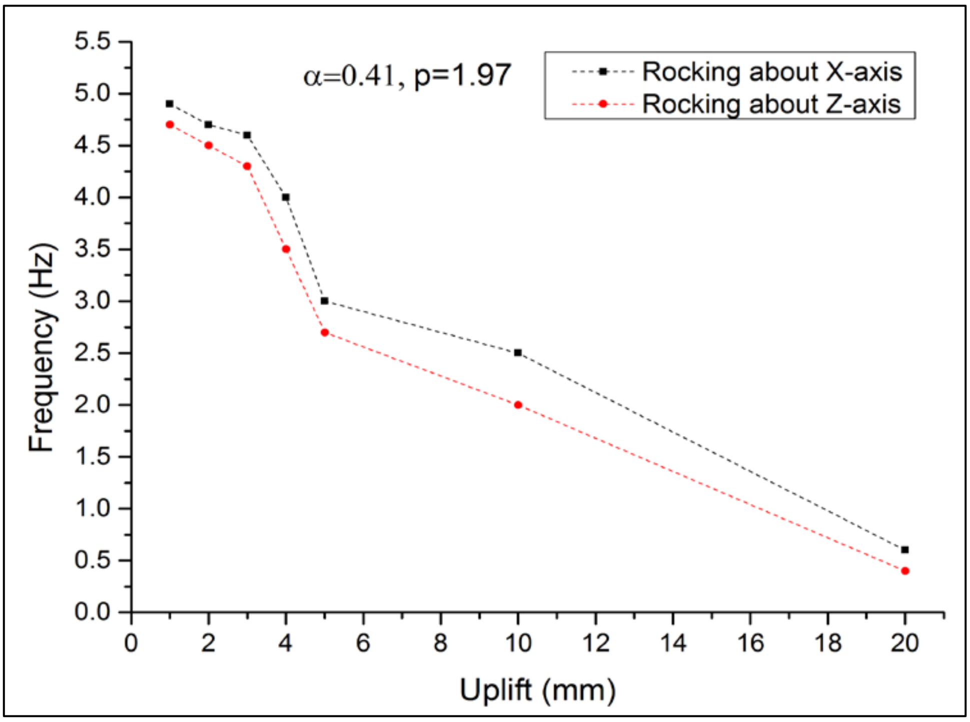


**Figure 5-5 Free rocking frequencies of a glove box about X and Z axis with different values of uplift**

These figures indicated similar trends as observed earlier for the cases of test specimens TS1-TS6. There was progressive reduction in free rocking frequency with the increase of uplift. Further, to find out fundamental mode shapes and Eigen frequencies of a glove box in fixed base conditions, Sine sweep test was carried out with a sweep rate of 0.5 octave per minute. All evaluated parameters are consolidated in Table.5-2.

**Table 5-2 Important characteristics of a glove box**

| AR | $p_{zz}$ (Hz) | $p_{xx}$ (Hz) | α (Rad) | R (m) | M (Kg) | $\omega_r$ (Hz) | C.G (x,y) (m) | $\omega_n$ (Hz) |
|---|---|---|---|---|---|---|---|---|
| 2.5 | 1.97 | 1.85 | 0.41 | 1.33 | 382 | 1.7-4.9 (along Z-axis) 2-4.7 (along X-axis) | 0.526,1.22 | 7.5,7.5,15.2 |

AR-aspect ratio, $p_{xx}$-frequency parameter about XX direction, $p_{yy}$- frequency parameter about YY direction, α-critical angle, R-diagonal length, M-mass, $\omega_r$-free rocking frequency, C.G.- location of centre of gravity from an edge, $\omega_n$- fundamental frequencies in modes 1,2 and 3,

## 5.3 Finite Element Analysis and Solution

Outcomes and results of extensive shake table testing carried out on six test specimens in Chapter3 and Chapter4 indicated need of an accurate three-dimensional finite element model for numerical calculations. Taking cue from these findings, it was decided to analyze glove box system using refined three-dimensional model. Nonlinear dynamic analysis had been carried out for determining the response of GB structure to three directional seismic loading. Following were the main objectives of the testing.

### 5.3.1 Objectives and Assumptions

Objective of analysis was twofold. Firstly, to develop a precise analysis model for carrying out numerical studies with the help of available experimental data; secondly, to utilize the developed and benchmarked finite element model for carrying out studies beyond design basis events. The main objective of FE analysis was, not only to check rigid body displacements and rotations but also to analyze the effect of elastic motions on overall seismic response. ABAQUS software was used to analyze glove box structure for seismic loading.

Finite element analysis was carried out with certain valid assumptions in line with the subject of research pursued for this doctoral program. Important assumptions are listed below:

1. In numerical analysis, glove box system was assumed to be a freestanding body. Which means that pressure regulating valve and connected piping were assumed to be flexible enough, not to constrain rigid body motions of the glove box. Thus main concern was to evaluate stability and integrity of the system.
2. Scope of analysis was, not to evaluate leak tightness of the structure which was already tested during shake table experiments. Hence, various connections, between glass panels and stainless steel frame, between aluminum panel and stainless steel frame were modelled as integral one (monolithic). However, material properties were suitably selected for all the panels as given in Table.5-3.
3. Actual test conditions of PVC sheet glued to concrete floor was not simulated in finite element analysis. Frictional properties evaluated during shake table testing were used an input to the FE model. Floor was modeled as a rigid body. This is a realistic assumption because objective of analysis was to assess seismic stability of the glove boxes and not to study floor material behavior which was sufficiently rigid because of underlying concrete slab.

With the above mentioned objectives and assumptions, extensive finite element analysis was carried out. Next section provide details of finite element modelling and analysis methodology.

### 5.3.2 Part Modelling

As mentioned earlier, glove box frame is made up of 3 mm thick stainless steel sheets. As the thickness was very less in comparison with longitudinal and lateral dimensions, shell elements were used for modelling. Here, a four node general-purpose shell element (S4R) with reduced integration and hourglass control was selected. GB top frame has an exhaust filter casing which has a HEPA filter inside it. HEPA filter box casing was also modeled with the shell element S4R. GB carriage structure (stand) was modelled by three nodes linear beam elements (B31) with 6 degrees of freedom at each node.

Different masses were lumped at appropriate places in the finite element model. For example, mass of gauntlets was lumped at respective glove ports, mass of HEPA filter was lumped at filter casing, piping and pressure regulatory valve mass was lumped at filter casing. Masses were lumped as a dead weight only and no rotary inertia was assigned. Similarly for the test cases of glove box with a central mass of machinery and eccentric mass of lead shield, masses were lumped at appropriate places in the FE model.

Ventilation pipe connected at the top of glove box was assumed long and flexible enough to allow free movement of GB on the floor. Other case where ventilation pipe was rigidly connected to structure was not considered for analysis. In the present case, floor was very stiff in comparison with the test specimens. Moreover, stresses and strains in the floor were of no research interest to us, hence it was modelled as a rigid body. Rigid element R3D4, which is a three-dimensional, 4-noded bilinear quadrilateral element was selected for.Various material properties used for glove box structure are given in Table.5-3. Glove box assembly consisting of glove box and floor is shown in Fig.5-6.

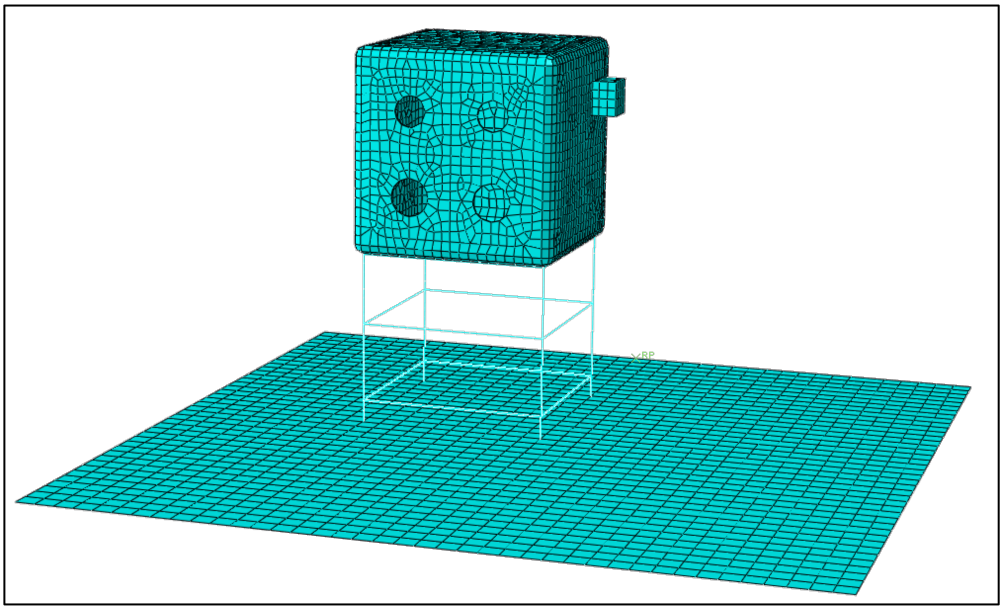

**Figure 5-6 Glove box finite element model**

**Table 5-3 Material and physical properties of glove box structure**

| S.No | Material Description | Mechanical Properties | | | |
|---|---|---|---|---|---|
| | | Young's Modulus(GPa) | Density (KN/m$^3$) | Poisons ratio | Thickness (m) |
| 1 | Stainless steel glove box frame | 210 | 8 | 0.3 | 0.003 |
| 2 | Mild steel bottom supporting plate, carriage(stand) | 210 | 8 | 0.3 | 0.009, 0.006 |
| 3 | Aluminum side panels | 70 | 2.7 | 0.35 | 0.01 |
| 4 | Front/back glass panels | 74 | 2.53 | 0.2 | 0.01 |

Mesh verification report for the glove box model was generated. It was observed that there was no analysis error, but there were certain analysis warnings arising out of poor aspect ratios of few quad elements. This was as expected because of complex geometry of the glove box structure

### 5.3.3 Contact Interactions and Constraints

As indicated in assembly drawing shown in Fig.5-6, glove box structure was contacting floor at four different points. Actually there was contact between four levelling screws supporting carriage and the bottom floor. The bottom surface of levelling screw was modelled with shell elements. Reason for selecting shell elements instead of using beam element to represent levelling screw was better performance and accuracy of shell to shell surface contact interaction. Abaqus uses surface to surface contact discretization when shell elements on the slave side (levelling screw) are in contact with shell elements of rigid floor on the master side. However if levelling screw is modelled as a beam element, then Abaqus uses node to surface discretization which is less accurate in terms of contact pressure and accuracy. Contact was created between four contacting surfaces corresponding to levelling screw and rigid floor. Contacting surfaces are shown with dots in the Fig.5-7. Contact properties were defined in the normal and tangential directions. Experimentally evaluated value of coefficient of friction was used for analysis. During shake table testing, glove box started sliding when the base acceleration changed from 0.1g to 0.2g. Hence, the coefficient of friction between the floor and legs of the glove box was taken as 0.15. The stick/slip formulation define a surface in the contact pressure–shear stress space along which a point transitions from sticking to slipping. In present analysis default model was used which assumes that the friction coefficient does not depend on field variables like slip rate, contact pressure and average temperature at contact point. For enforcement of friction constraint default Penalty method was used. This method permits some relative motion between surfaces in contact when they should be sticking. This value is known as elastic slip. The value of allowable elastic slip was chosen by the software to provide a conservative balance between efficiency and accuracy. Hence, default value was chosen to avoid any numerical convergence difficulties. Similarly, contact formulation in normal direction depends on two main factors: i) -Pressure-Overclosure relationship and ii) -Contact Constraint Enforcement Method.

i. Pressure-Overclosure Relationship- There are mainly two types of pressue-overclosure relationships available in Abaqus namely soft and hard. In this case, hard pressure – over closure relationship was chosen which minimizes the penetration of the slave surface into the master surface at the constraint locations and does not allow the transfer of tensile stress across the interface. With this relationship, software applies impact algorithm and destroys kinetic energy of the nodes on the surface when impact occurs.

ii. Contact Constraint Enforcement Methods- they determine how contact constraints imposed by a physical pressure -over closure relationship are resolved numerically in an analysis. There are three contact constraint enforcement methods available in Abaqus, namely direct method, Penalty method and Augmented Lagrange method. In the present analysis, Penalty method was used. It is a stiff approximation of hard contact. With this method, the contact force is proportional to the penetration distance, so some degree of penetration will occur. Advantages of the penalty method are that numerical softening associated with the penalty method can mitigate over constraint issues and reduce the number of iterations required in an analysis. The penalty method can be implemented such that no Lagrange multipliers are used, which allows for improved solver efficiency

Interested readers can refer to these references [66] [67] [68] [69] [70]. Two configurations (path) based contact tracking scheme was used in a finite sliding formulation with surface to surface discretization. Surface to surface discretization was used for generating contact between levelling screw (slave surface) and the floor (master surface).

### 5.3.4 Loads and Boundary Conditions

A glove box structure is subjected to various kinds of loading during normal operation. These include dynamic pressure loading, static equipment load, body forces (due to gravity), and eccentric loads arising due to lead shields. Apart from these operational loads there shall be service loads arising due to base excitations including seismic. For the present study, all the loads are considered to act simultaneously on a glove box structure. Details of applicable loadings and boundary conditions are given below:

1. Dynamic pressure load

   Internal faces of glove box is subjected to dynamic pressure loading. In actual operation negative pressure of 250Pa is maintained using pressure regulatory valve. However, this pressure is not static and slightly varies with time. In practical terms, these variations can be assumed negligible and hence a constant pressure of -250Pa can be applied on all the internal faces of the glove box.

2. Static equipment load

   There is a constant static loading at the bottom supporting face of the glove box arising due to the equipment or storage container. In the present case it is lumped uniformly at the bottom surface of the glove box.

3. Eccentric load

   Glove boxes are commonly provided with lead shielding on the operating face. Thickness of this shielding depends on type and amount of radiological material being handled. Generally this shielding is mounted on the operating face of the glove box where operator stands for performing various operations. Hence this acts as an eccentric load for the glove box. In present analysis calculated mass of the lead shield is assumed to be distributed uniformly across the operating face.

4. Body force

There is uniform body force arising due to gravity. This is constant in magnitude and acts vertically downward across the glove box model

5. Seismic base excitation

In case of an earthquake loading, it is important to assess stability and integrity of the glove box system. In present model, real earthquake time histories were applied as a boundary conditions at the reference point of the floor.

Top frame of the glove box was welded to the bottom carriage through a bottom supporting plate. To include this behavior in the glove box model, multi-point constraint was applied at the interface of top frame and bottom carriage. This constraint merges degrees of freedom of connecting nodes by using a beam element. All these loading and boundary conditions are shown in Fig.5-7.

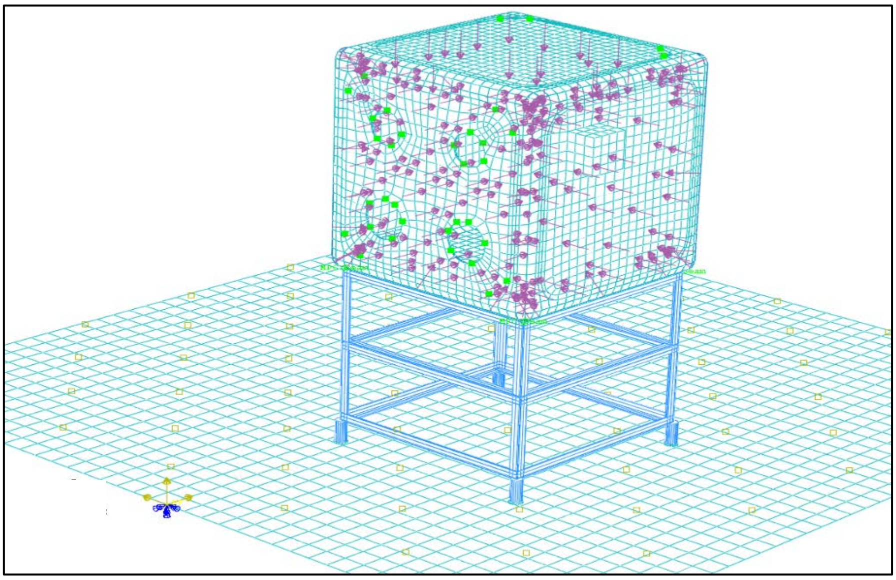

**Figure 5-7 Glove box model showing various loadings, contact and boundary conditions**

### 5.3.5 Modal Frequencies

A flexible structure undergoes various possible modes of deformation when rigid body degrees of freedom are constrained. These modes of deformations know as Eigenvectors have different frequencies which are known as Eigen frequencies. These frequencies plays a significant role in determining overall response of a structure to dynamic loading. These Eigen vectors and frequencies can only be determined after fixing rigid body modes of motions. In case of a freestanding structure, effect of these frequencies is not clear. There are many research papers which consider structures' natural frequencies to control dynamic response due to base excitations [51] [73] [65]. However, research presented here contradicts those findings. As observed in Chapter.4, that free rocking frequencies of the flexible test specimens dominated the dynamic response, with a meagre contribution from fundamental modal frequencies. This phenomenon will be further tested and elaborated for the case of a glove box. Fundamental frequencies of the glove box were evaluated earlier during shake table testing as given in Section 5.2. Now, they will be evaluated using FE model. Bottom surface of the carriage i.e. levelling screws were fixed and then Lanczos solver was used to extract Eigen values and Eigen modes up to a frequency value of 30Hz. Three eigenvalues were extracted corresponding to 90% mass participation. Eigen frequencies corresponding to these eigenvalues were 7.4Hz, 7.5Hz and 15Hz. Mode shapes corresponding to these frequencies are shown in Fig.5-8. In this figure color scheme is displaying displacement gradient over the glove box model. Red color indicates highest displacement while blue color indicates lowest.

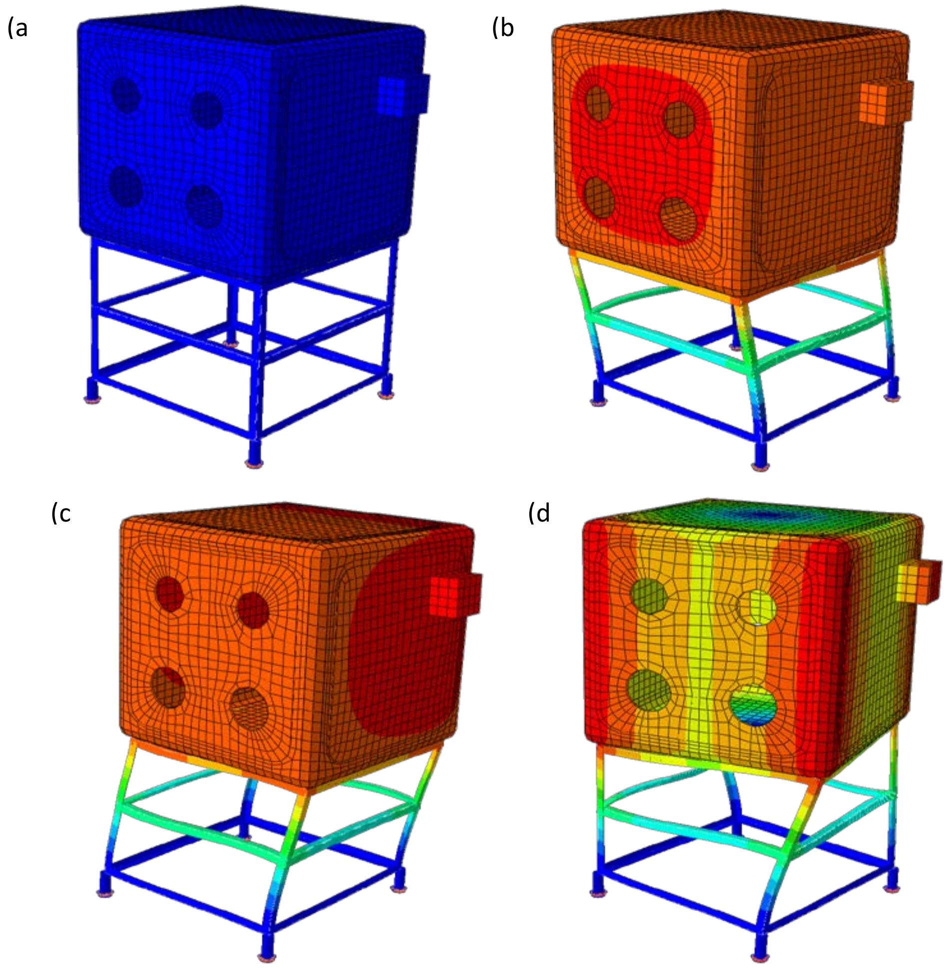


**Figure 5-8 Fundamental mode shapes of a glove box in fixed base boundary condition. (a) Un-deformed shape, (b) first mode shape, (c) second mode shape and (d) third mode shape**

### 5.3.6 Numerical Solution

Implicit solver was used to perform dynamic analysis to obtain response of structure to three-dimensional base excitation. Abaqus uses the Hilber-Hughes-Taylor time integration scheme [71] for numerical integration. For a moderate dissipation contact-impact problem, default values of parameters for the Hilber-Hughes-Taylor integrator used are given below [74]:

$$\alpha = -0.41421,\ \beta = 0.5,\ \Upsilon = 0.91421$$

These parameters can be adjusted, to vary the amount of artificial numerical damping. The numerical damping grows with the ratio of the time increment to the period of vibration of a mode. Negative values of α provide damping; whereas α = 0, results in no damping (energy preserving) and is exactly the trapezoidal rule (called as Newmark beta-method, with β = 0.25 and ϒ = 0.5). The setting α = –1/3, provides the maximum numerical damping. It gives a damping ratio of about 6% when the time increment is 40% of the period of oscillation of the mode being studied. Allowable values of α, β and ϒ are: $-\frac{1}{2} \leq \alpha \leq 0$ , $\beta > 0$, $\gamma \geq \frac{1}{2}$ . Moreover, two percent of critical damping was used as material damping for analysis. This value is in agreement with the damping value for welded steel structure given in relevant codes [75].

## 5.4Seismic Stability Assessment

In a bid to develop a generic glove box model, suitable to handle any variation in system input parameters, three-dimensional finite element model of the glove box system using FEM was developed.  Model benchmarking results shall be presented later in Section 5.7.

Now, results of analysis carried out to study effects of variation of different system parameters on the stability and integrity of the glove box system are presented. Similar to the shake table tests carried out earlier and described in Section 2.4.1, glove box was analyzed for three-dimensional, simultaneous seismic base excitations for different peak ground accelerations varying from 0.1g to 0.3g. Synthetic time histories used in analysis for peak base accelerations varying from 0.1g up to 0.3g are shown in Fig.5-9. Simulations were carried out for the three cases described earlier in Section 2.4.1 and repeated here for clarity.

- Case 1- Single glove box structure.
- Case 2- Single glove box structure with dead load of 2.5 KN.
- Case 3- Single glove box structure with eccentric load of 0.96 KN.

Nodal output response at various locations corresponding to accelerometers A1, A5 and A9 (Refer Fig.2-9 shown earlier) were obtained. Final glove box displacement values after the end of seismic excitations were obtained.

Variation of peak nodal acceleration values for Case1 and Case2 of glove box is plotted in Fig.5-10 and Fig.5-11 respectively. It shall be noted that peak base acceleration was varied from 0.1g to 0.3g. Similarly, Fig.5-12 shows peak nodal acceleration values obtained for Case3 of GB. Fig.5-13 shows glove box final horizontal displacements (X and Z direction) for all the three analysis cases.

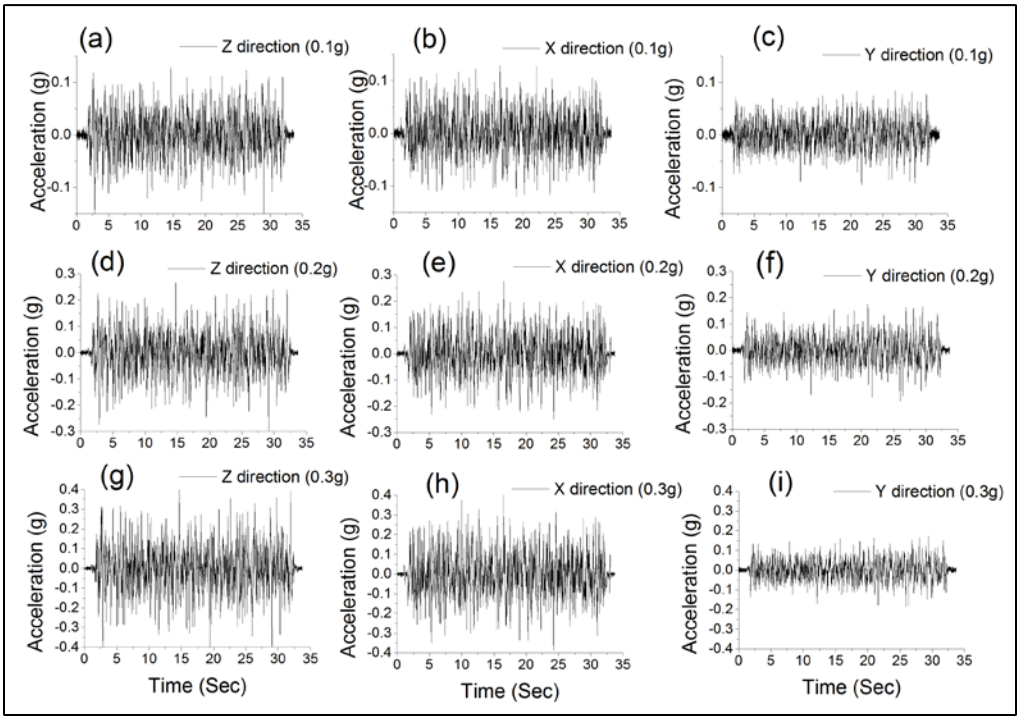


**Figure 5-9 Input base acceleration time histories. (a) 0.1g PGA in Z-direction, (b) 0.1g PGA in X-direction, (c) 0.1g PGA in Y-direction(vertical), (d) 0.2g PGA in Z-direction, (e) 0.2g PGA in X-direction, (f) 0.2g PGA in Y-direction(vertical), (g) 0.3g PGA in Z-direction, (h) 0.3g PGA in X-direction, (i) 0.3g PGA in Y-direction(vertical)**

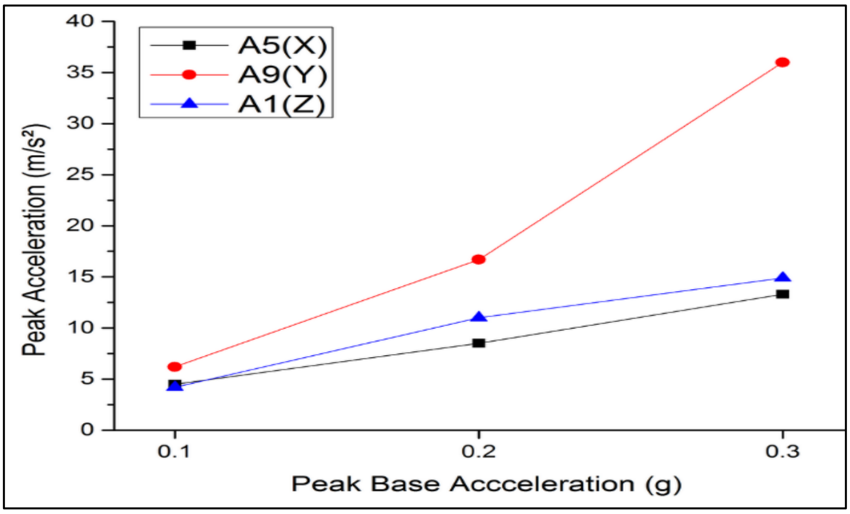


**Figure 5-10 Peak response acceleration of glove box at accelerometer locations of A5, A9 and A1 for Case-1.**

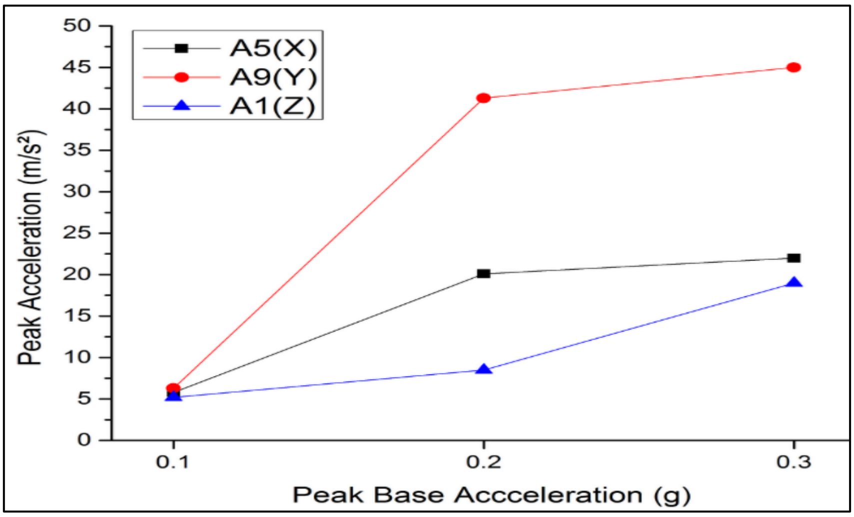


**Figure 5-11 Peak response acceleration of glove box for Case-2**

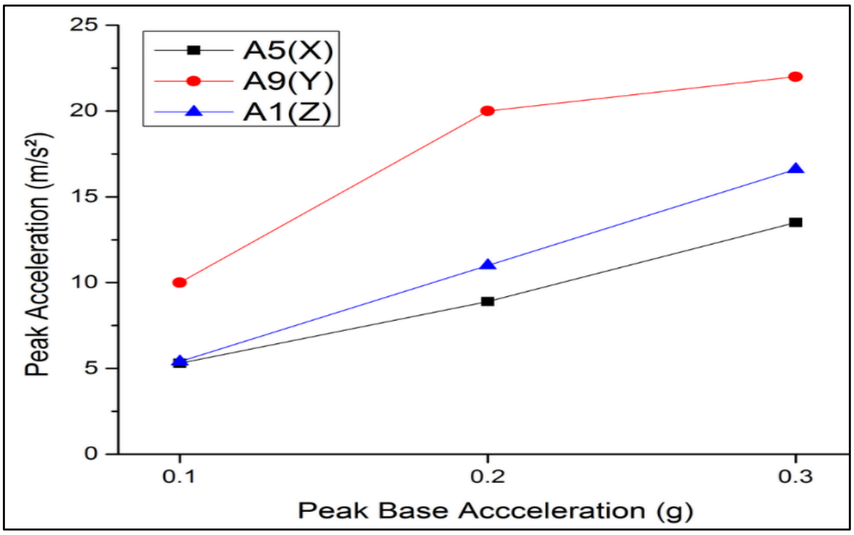


**Figure 5-12 Peak response acceleration of glove box for Case-3**

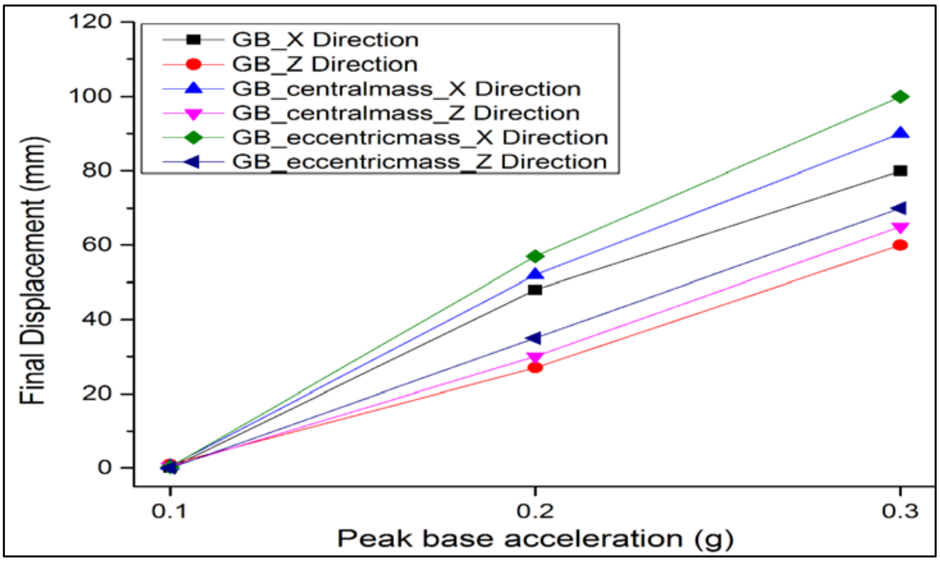


**Figure 5-13 Final horizontal (X&Z) displacements of glove box for different test cases**

To understand frequency distribution of response signals, Fast Fourier Transform (FFT) of nodal acceleration time histories is obtained. FFT graphs for only Case-1 of single glove box are plotted for brevity. Fig.5-14(a,b,c) shows FFT of input base excitations given to the shake table in Z , X and Y direction for 0.1g peak base accelerations respectively. Fig.5-15 (a,b,c) shows FFT of acceleration time histories at locations corresponding to A1(Z), A5(X) and A9(Y) accelerometers respectively at 0.1g peak base acceleration. Similarly, Fig.5-15(d,e,f) and Fig.5-15(g,h,i) shows FFT of acceleration time histories at locations of A1(Z), A5(X) and A9(Y) accelerometers for 0.2g and 0.3g PGA respectively. Following observations can be drawn from the analysis results:

a) It was observed for all the three cases that peak accelerations achieved at the top of GB and final GB displacements were nonlinear functions of peak base accelerations. Both accelerations and displacements increased nonlinearly with peak base excitations as seen from Fig.5-10 to Fig.5-13.

b) It was observed that in general, addition of central load (Case-2) and eccentric load (Case3) to the glove box increased peak accelerations as shown in Fig.5.11 and Fig.5.12. However due to eccentric loading, rotational instability was also observed.

c) Acceleration response was unequal in both the horizontal directions as seen in Figs 5-10 to 5-12. This was due to uneven distribution of mass and unequal stiffness of the structure.

d) As observed for the Case-1 as shown in Fig.5-15 (a,b,d,e,g,h), FFT of acceleration response of glove box in horizontal directions showed low frequency contents. The reason for the same was occurrence of rigid body motions (sliding and rocking). It is important to observe that at 0.1g PGA value, glove box was in rest state because that value of amplitude was not sufficient to initiate sliding or rocking motion. Hence it was expected that like the case of a fixed structure frequency response obtained from FFT should peak at first fundamental modal frequency of 7.5Hz. Contrary to the expectation, frequency response peaked at a much lower frequency of around 5Hz as shown in Fig.5-15(a,b). This behaviour can be well explained from earlier test results of flexible test specimens carried out in Chapter-4. As observed earlier for test specimens TS4, TS5 and TS6, in absence of amplitude induced sliding or rocking motion, it was possible to have frequency induced rocking motion. Hence, presence of frequency induced rocking led to peaking of response at 5Hz, which corresponds to free rocking frequency of the glove box as seen earlier in Fig.5-5.

e) Negative (downward) shift of frequency, corresponding to peak amplitude in FFT for horizontal directions(X and Z) with increase of peak base acceleration can be observed by comparing Fig.5-15(a),(d) and (g). This decrease in frequency with increase of peak base acceleration can be attributed to increase of rigid body motions (sliding, rotation and rocking) with increase of base excitations.

f) It is interesting to observe that as peak base acceleration was increased, amplitude of rocking of glove box increased thereby reducing frequency contents of output signal. This fact can be explained by the earlier observations on free rocking frequencies of a specimen. As amplitude of rocking increases, frequency decreases and vice versa.

Now after analysing response of glove box for seismic excitations, it is clear that predominant behaviour is rigid body motions (mainly sliding). Hence, a simplified numerical method is developed which can evaluate sliding displacements of a free-standing component. Next section discusses the details of proposed method.

**Figure 5-14 FTT of input acceleration time history for 0.1g PGA value. (a) Z-direction, (b) X-direction and (c) Y-direction**

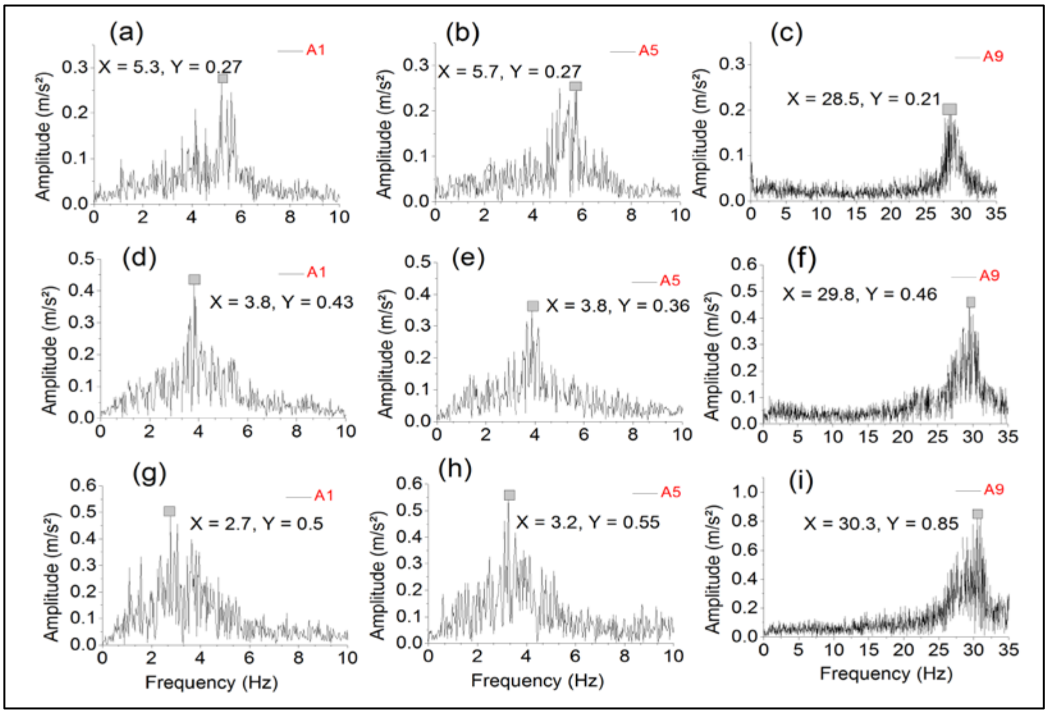


**Figure 5-15 FFT of response acceleration time histories of glove box for Case-1 (a,b,c)- Z, X and Y direction for 0.1g PGA, (d,e,f)- Z, X and Y direction for 0.2g PGA, (g,h,i)- Z, X and Y direction for 0.3g PGA**

## 5.5 Numerical method to estimate sliding displacement

The American Society of Civil Engineers (ASCE) have devised a simplified methodology to ascertain the sliding distance of a free-standing body [75]. The theory behind the method is reproduced here from the code for better understanding and clarity.

Firstly, define an effective coefficient of friction, $\mu_e$, by

$$\mu_e = \mu \, [1\text{-}0.4 \, A_v/g] \qquad 5.1$$

Whereas $\mu$ is static coefficient of friction, $A_v$ is peak vertical acceleration and g is acceleration due to gravity. Fig.5-16 shows the resisting force, $F_{RS}$ versus displacement diagram for a rigid body of mass M, with sliding resisted by an effective friction coefficient $\mu_e$ as given by Eqn.5.1. From the figure a relation between $F_{RS}$ and $\mu_e$ can be established as given below:

$$F_{RS} = \mu_e M g \quad 5.2$$

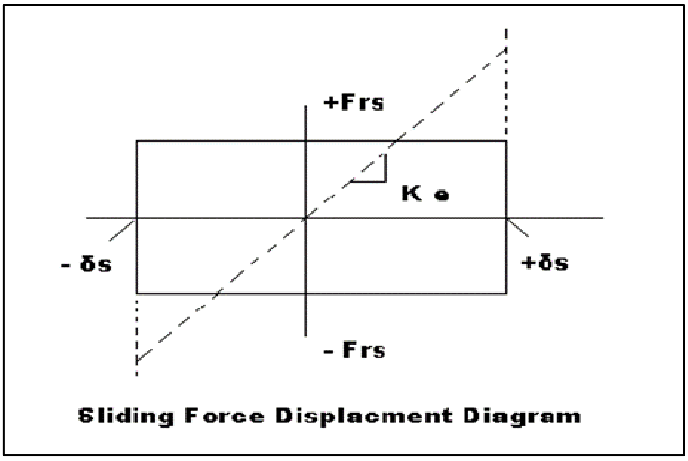


**Figure 5-16 Sliding force displacement diagram extracted from ASCE code**

Also shown in Fig.5-16 is an equivalent linear force deflection stiffness $K_e$ , which absorbs the same work done when displaced by δs (sliding displacement), where

$$K_e = 2 F_{RS} / \delta s = 2 \mu_e M g / \delta s = Cs M / \delta s \quad 5.3$$

Where Cs is a sliding coefficient defined as;

$$Cs = 2 \mu_e g$$

5.4

The effective frequency of this equivalent linear system is

$$fe_s = 1/ 2 \Pi [K_e / M]^{1/2} = 1/ 2 \Pi [Cs / \delta s]^{1/2}$$

5.5

Now, vector horizontal spectral acceleration, $SA_{VH,}$ which would displace this equivalent linear system by a distance δs, is given by:

$$SA_{VH=} K_e \delta s / M \quad 5.6$$

Thus for this equivalent linear system,

$$\delta s = Cs / (2\,\Pi\, fe_s)^2 \qquad 5.7$$

where $fe_s$ is the lowest natural frequency at which the horizontal 10% damped vector spectral acceleration $SA_{VH}$ equals Cs, where

$$SA_{VH} = [SA_{H1}^2 + 0.16\, SA_{H2}^2]^{1/2} \qquad 5.8$$

In which $SA_{H1}$ and $SA_{H2}$ are the 10% damped spectral accelerations for each of the two orthogonal horizontal components, where $SA_{H1}$ is the larger of the two spectral accelerations. Hence equivalent sliding displacement can be evaluated by using Eqn.5.7

Now utilising values of $\mu_e$, Cs and $fe_s$ obtained from the ASCE code given above, we apply energy conservation methodology to find out equivalent sliding displacement. In present case of glove box structure, it was observed that strains obtained from shake table testing were of very low magnitude. Hence, it can be assumed that contribution from strain energy and material damping term is not significant. The main source of energy dissipation is via rigid body sliding (frictional dissipation). Hence writing equation for energy balance for a particular cycle, we get:

Energy input to the table (E) = Energy dissipated in friction ($F_d$) + kinetic energy of the system (KE)

$$E = F_d + KE \qquad 5.9$$

Now, $E = W.\ \Delta D.\ g$ 5.10

where W- weight of glove box in Kgs,

$\Delta D$- Maximum displacement of the table,

g- acceleration due to gravity.

Also $F_d = 4.\ \mu_e\ .\ N.\ \Delta d$ 5.11

Where $\mu_e$ - equivalent coefficient of friction,

N- Normal reaction,

$\Delta$d- sliding displacement of glove box

Similarly, KE- $1/2.\ m.\ v^2$ 5.12

Where, m- mass of the glove box

$v^2 = (\Delta d.\ w)^2 = \Delta d^2\ (2\pi\ fe_s)^2$ 5.13

Eqn.5.9 is valid for that case when sliding starts. Hence, it would be used to evaluate sliding displacements for 0.2g and 0.3g peak base accelerations. For the case of 0.1g, peak base excitation negligible sliding displacement was observed in test results. Hence, Eqn.5.9 cannot be applied to this case. Now we calculate values of $fe_s$, μe and $C_s$ for all the cases and substitute them in Eqn.5.9to get the results. For better understanding sample calculation for one case of 0.2g peak base acceleration is shown here:

First find out equivalent coefficient of friction ($\mu_e$) from Eqn.5.1 as:

$$\mu_e = 0.15(1-0.4*2.2/9.81) = 0.136$$

It is to be noted that value of $A_v$ is obtained from 10% damped response spectrum for the site. Now determining $C_s$ from Eqn.5.4

$$C_s = 2*0.136*9.81= 2.679\ m/sec^2$$

Now for this Cs we have to find out corresponding minimum frequency ($fe_s$) from 10% damped spectral horizontal response spectra for acceleration $SA_{vh}$ value calculated from Eqn.5.8. We get $fe_s$ = 1.2Hz corresponding to Cs value from 10% damped response spectra. Now from test data, we know that the maximum table displacement ($\Delta D$) was 40mm. Hence, by using Eqn.5.9, we get a quadratic equation in $\Delta d$, given as below:

$$10517\ \Delta d^2 + 1975\ \Delta d - 145 = 0 \qquad 5.14$$

On solving Eqn.5.14, we get positive root as $\Delta d$= 56mm. similarly $\Delta d$ can be evaluated for case of 0.3g peak base excitation. Final values of sliding displacements, obtained from energy conservation method are given below:

a) for 0.2g peak base acceleration

**$\Delta$d= 56mm**

b) for 0.3g peak base acceleration

**$\Delta$d= 102mm**

Similarly sliding displacement can also be evaluated by using ASCE code. Eqn.5.7 gives sliding displacement values as given below:

a) for 0.1g peak base acceleration

**$\Delta$d= 4mm**

b) for 0.2g peak base acceleration

**$\Delta$d= 47mm**

c) for 0.3g peak base acceleration

**$\Delta$d= 124mm**

Comparison of final sliding displacements observed from test results, evaluated by FE analysis, ASCE code and energy conservation methodology is done in the next section.

## 5.6 Validation of Finite Element and Numerical Method Results

Developed finite element model was benchmarked using available shake table test data. Important recorded parameters like accelerations and displacements were compared. It was decided to compare peak acceleration response and final glove box displacements obtained from test and FE analysis for three different test cases 1-3 as given below.

*Case 1:* Single glove box structure.

*Case 2:* Single glove box structure with dead load of 2.5 KN

*Case 3:* Single glove box structure with eccentric load of 0.96 KN

Comparison is plotted in Figs.5-17 to 5-20. In addition to that, Fig.6-21 displays frequency contents of output response recorded by accelerometers A1 (Z), A5(X) and A9(Y) during shake table testing for Case-1 at 0.1g peak ground acceleration. This graph is compared with FFT of analysis response, as given earlier in Fig.5-15. Considering the data presented in Fig.5-17 to Fig.5-21, it can be observed that test and analysis results are in good agreement to each other. Maximum deviation observed is below 10 percentage. Hence, it can be concluded that developed finite element analysis model accurately predicted the response of glove box system and this model can be utilized to assess seismic stability and integrity of the glove box system subjected to different loading conditions.

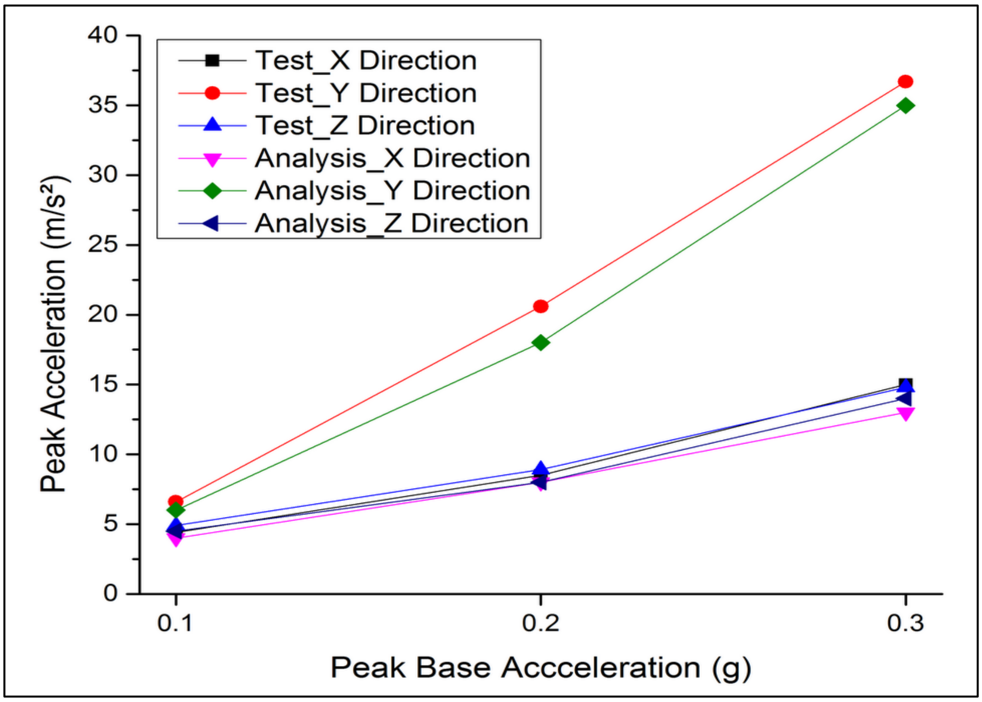


**Figure 5-17 Comparison of peak accelerations obtained from test and analysis for case1 of single glove box**

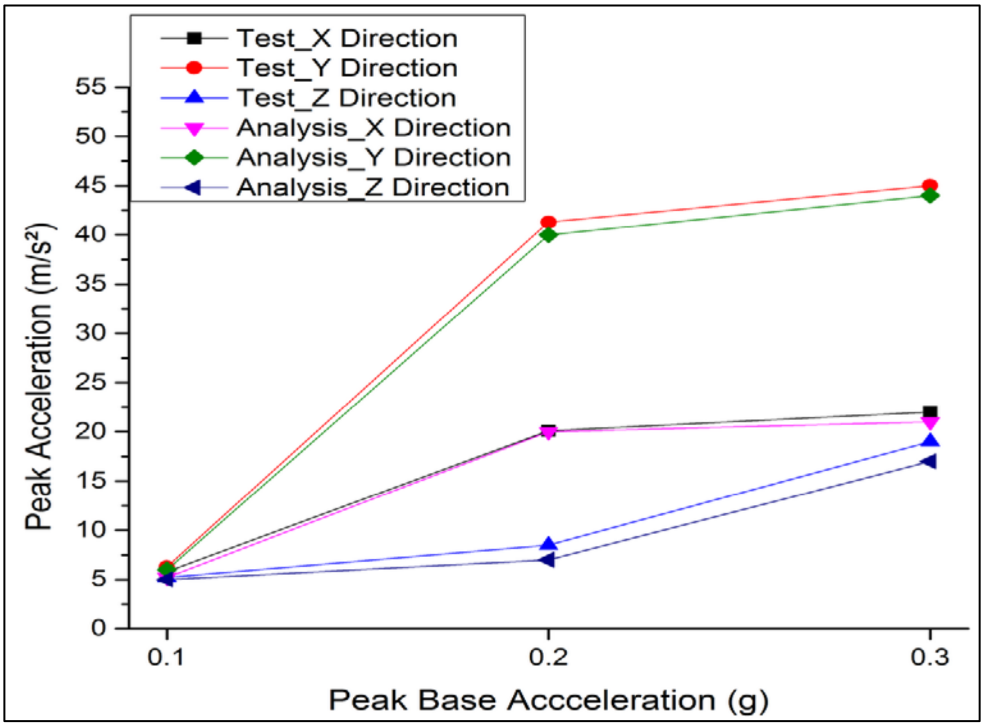


**Figure 5-18 Comparison of peak acceleration obtained from test and analysis for case2 of glove box with central load**

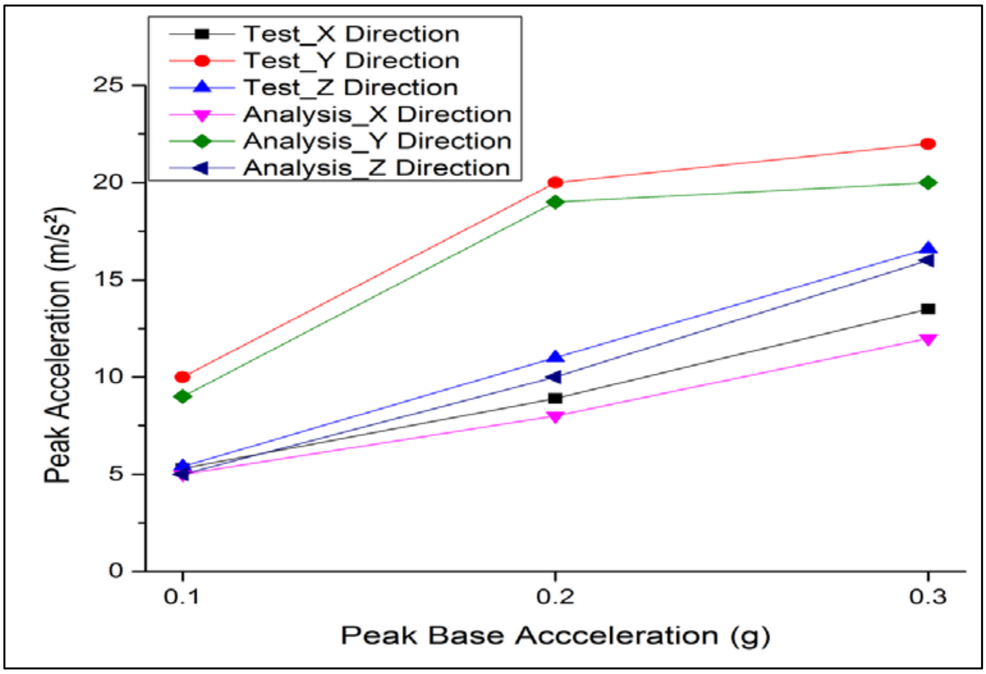


**Figure 5-19Comparison of peak acceleration obtained from test and analysis for case3 of glove box with eccentric load**

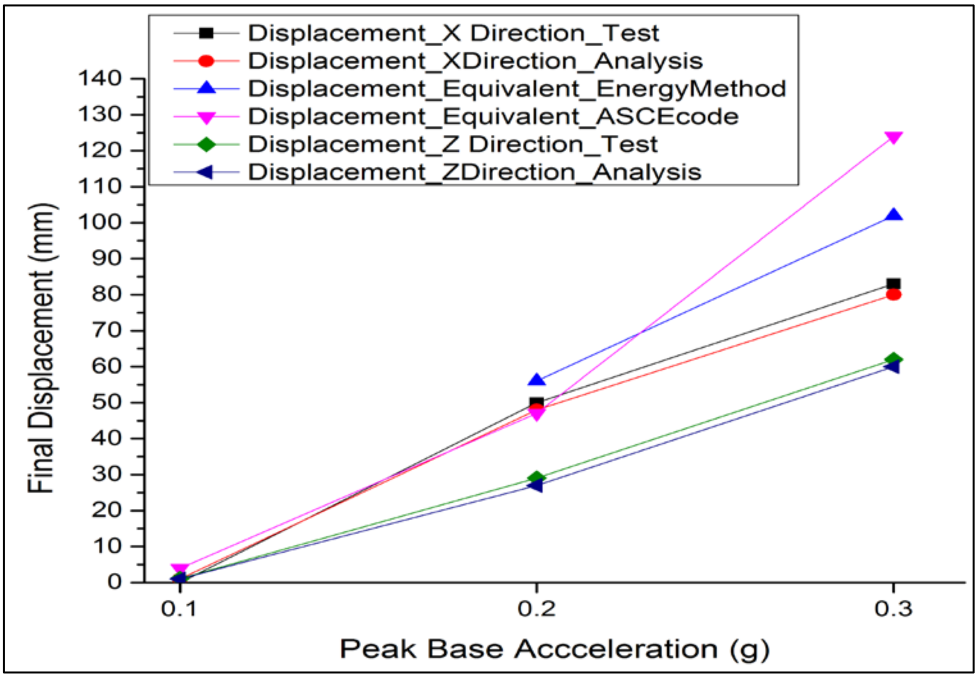


**Figure 5-20 Comparison of final displacements obtained from test, FE analysis and numerical method for case1 of single glove box**

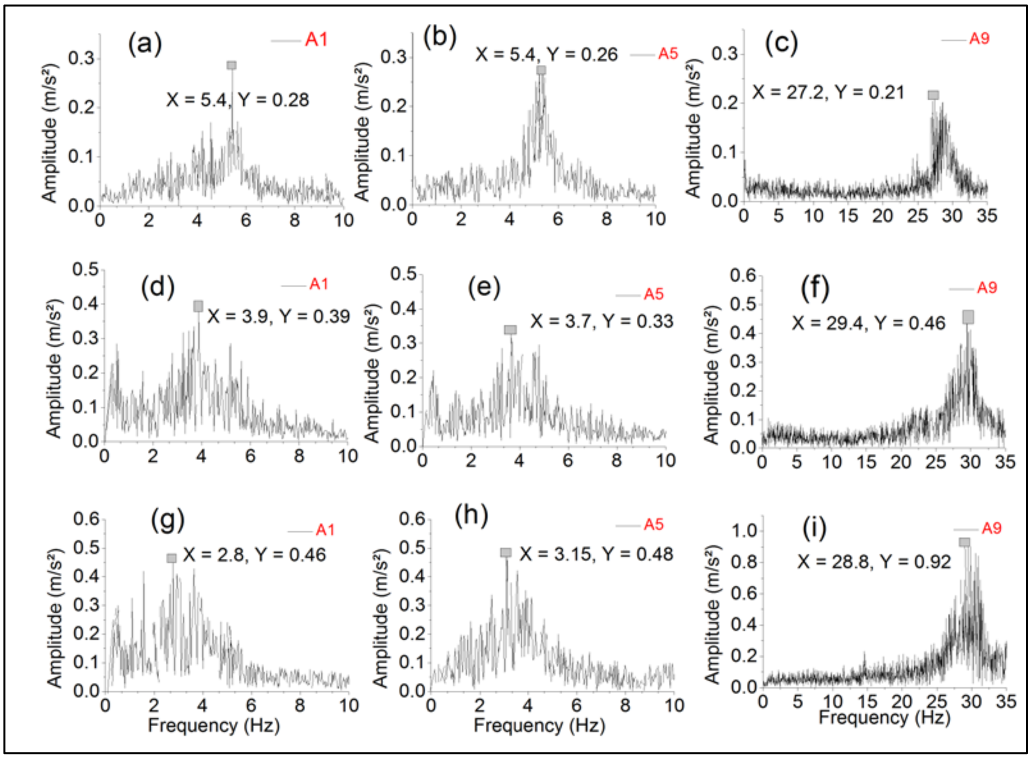


**Figure 5-21 FFT of acceleration signal recorded during shake table testing for case1 of glove box ,(a,b,c)- Z, X and Y direction for 0.1g PGA, ),(d,e,f)- Z, X and Y direction for 0.2g PGA, (g,h,i)- Z, X and Y direction for 0.3g PGA**

## 5.7 Motion Initiation Criteria Diagram

After understanding dynamics of a glove box structure, it is important to find out answer to a persisting question by the facility designers- “Whether a glove box requires to be anchored to the base?” To provide an appropriate answer, it’s important to understand initiation of motion of a glove box, when subjected to base excitations. Glove box is a flexible structure with finite stiffness in bending. Hence its behavior is similar to the test specimens (TS4-6) tested in Chapter-4. In Chapter-4, motion initiation criteria diagram for a flexible test specimen TS4 was developed as given in Fig.4-21. Similar diagram is required to be developed for a glove box which can assist designers in determining possible mode of motion a glove box can undergo when subjected to base excitations. As highlighted earlier in Chapter-4 and again in this chapter, presence of frequency induced rocking motion is important when frequencies of excitations coincide with range of free rocking frequencies of a body. Hence, motion initiation diagram for a glove box is developed for range of frequencies corresponding to free rocking frequencies of the glove box.

FE analysis was carried out to determine regions corresponding to frequency induced rocking motions. Finally, a motion initiation criteria map for a glove box is developed as shown in Fig.5-22. Now this diagram can act as a guideline for deciding anchoring of the glove box. If the parameter values like $\mu_s$ and $A_g$ are selected in such a way that glove box is lying in the region corresponding to rest state of the map, then it will be in stable state. In other words, a glove box will not initiate any mode of motion when subjected to base excitations.

At present, PVC sheets being used in laboratories have a lower value of $\mu_s$=0.15, due to which Sliding cum rocking motion initiates when amplitude of base excitation crosses 0.15g value. To avoid occurrence of this motion, it is suggested to fix steel plates locally on the areas of contact of carriage legs with the floor. That means four legs will be in contact with the steel plates which gives higher value of coefficient of friction. Coefficient of friction value between steel and steel was experimentally determined earlier and found to be 0.72.

Now corresponding to $\mu_s$=0.72, glove box shall remain in rest state till amplitude of base excitation is below 0.3g as can be easily seen from Fig.5-27. That means for any type of base excitation (random, harmonic etc.) with a maximum value of base excitation up to 0.3g, glove box structure will not initiate any mode of motion and hence remains in rest state. For, peak base excitation values between 0.3g -0.4g, glove box will initiate frequency induced rocking motion. Although, even in this state there are no chances of overturning instability, but higher acceleration amplification will take place. Hence, it can be conclude that glove box structure can remain free-standing without any risk of sliding or rocking instability up to 0.3g peak base acceleration value.

As a guideline to designers of future fuel fabrication facility, it is suggested to locally increase coefficient of friction value by providing steel sheets of minimum dimensions (0.1m length , 0.1m width, 0.006m thickness) at four contact points between stand(levelling screws) and floor. This will help in making glove box system seismically safe up to 0.3g pba value. For higher base accelerations a case study can be done by performing FE analysis and finding optimal solution.

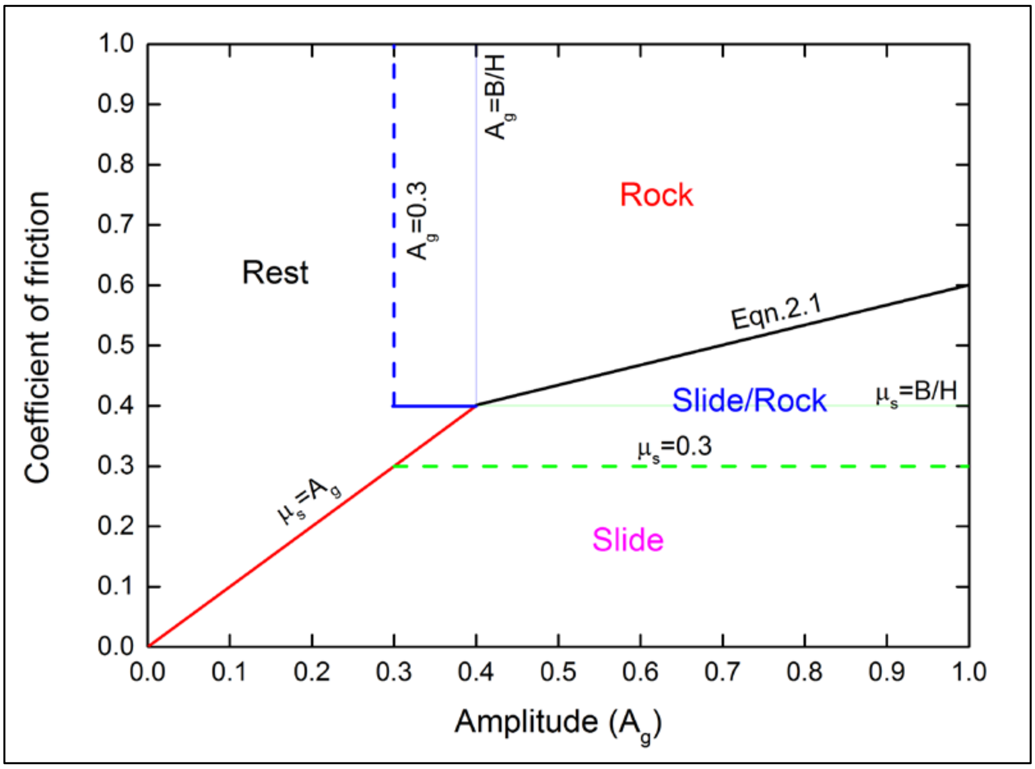


**Figure 5-22 Motion initiation diagram for a flexible body showing different regions for a glove box in a free rocking frequency sensitive zone**

## 5.8 Outcomes and Discussions

The seismic stability of the glove box structure was evaluated for the design and beyond design level of accelerations under various configurations. It was observed that the predominant mode of motion was sliding however very low amplitude rocking was also observed. The single glove box with various configurations with and without internal and eccentric mass, maintained integrity. Hence, the single glove box structure is safe for the designed seismic loads and anchoring of the structure with floor is not required.

Many important observations were made for seismic behaviour of freestanding structure, which were peculiar and different from seismic response of a fixed base structure. Important of them was peaking of horizontal acceleration response at frequencies different and lower than fundamental frequencies obtained for GB structure in fixed base conditions. Hence, even when structure was not sliding at 0.1g peak base acceleration, there was no peaking of response at GBs fundamental frequencies and in fact peaking was observed at much lower frequency of 5Hz corresponding to free rocking frequency of a glove box. This can be explained by the presence of frequency induced rocking behaviour discussed earlier in Chapter-4 for a flexible specimen.

Frequency response of a freestanding glove box in horizontal direction for 0.2g and 0.3g PGA values also peak at a lower frequencies. This peaking can be explained from earlier observations drawn in Chapter-4 for flexible test specimens (TS4, TS5 and TS6). As observed earlier for a flexible body, frequency induced rocking motion was accompanied with sliding motion. Since sliding motion is random in nature and does not have any signature frequency; hence, FFT of output response of a glove box has lower frequency contents pertaining to free rocking frequencies of the glove box. Moreover, negative shifting of peaks of FFT with increase of base excitations can be explained by reduction of free rocking frequencies with increasing amplitude of motion associated with higher peak base accelerations.

Nonlinear dynamic analysis results were coherent with the test results. Finite element software (ABAQUS) can be successfully utilised to predict the seismic response of free-standing structures. Estimation of sliding distance using energy conservation method and ASCE code, gives good conservative results. This method can also be utilized for obtaining quick estimates of sliding displacements of glove box. However, it gives only single maximum (equivalent) value. It can also be observed that as the excitation peak base acceleration value increases, corresponding displacement values also increases. While the peak acceleration value increases with base excitation, average acceleration obtained at higher excitations are less than the corresponding values at lower excitation due to onset of slipping.

# CHAPTER 6 SEISMIC STABILITY OF FLEXIBLY INTERCONNECTED GLOVE BOXES

## 6.1 Introduction and Outline

In the last chapter we have examined seismic stability of a single glove box structure for various possible load combinations and configurations. It was observed that the stability of the glove box system depends on various parameters like base excitation characteristics, contact surface behaviour and glove box mass distribution.

Now, in this chapter we deliberate on a more complex and generalised problem. Here we shall focus on the case of multiple freestanding glove boxes connected to each other. Two different types of connection will be studied. First type of connection can be with a flexible link which allows limited relative motion between the two interconnected glove boxes. This will be discussed in the present chapter. However, second type of connection considered is by a rigid link which doesn't allow any relative motion between the two and is the subject for Chapter-7. These two cases are of prime importance because of their wide applicability in working laboratories. Generally, glove boxes are used in series with interconnection between them to carry out material exchange. Hence these two cases has wide applications and thus are required to be evaluated. A series of shake table testing was carried out by a team of engineers at BARC to evaluate seismic performance of two interconnected glove boxes using synthetic earthquake time history. These results are used for this research program. We had evaluated these available test results and further used them in developing and benchmarking finite element model. This chapter shall focus on assessment of seismic stability of multiple connected free-standing glove boxes.

The glove boxes are generally used in series, where a material transfer tunnel interconnects them to each other as shown in Fig.6-1. A material transfer tunnel is simply supported on circular ports using O-rings. It is made up of stainless steel. In the event of an earthquake, freestanding interconnected glove boxes may freely slide or rotate on the floor, causing a breach of integrity and leak tightness. Material transfer tunnel is not welded to glove boxes to facilitate easy removal of boxes for decontamination and maintenance operations. Tunnel acts as a weak link between the two glove boxes and thus restrains relative movement between them.

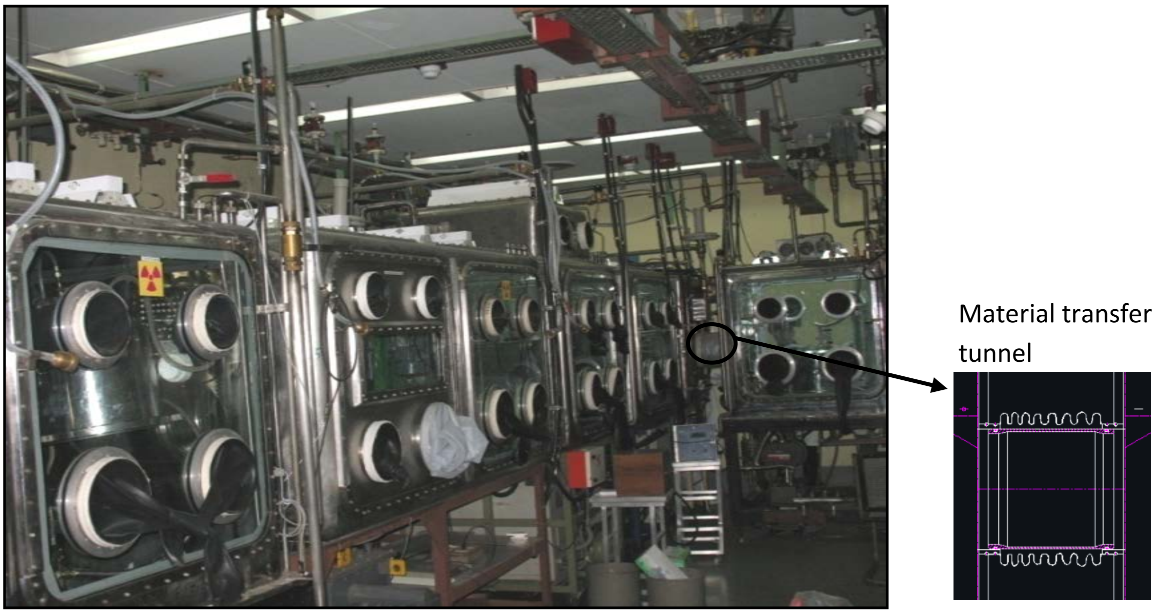


**Figure 6-1 Multiple glove boxes interconnected by material transfer tunnels**

Hence, it is necessary to check that the relative displacement between glove boxes is not excessive to cause breach of integrity for earthquake loading. Relative displacement of the tunnel beyond the allowed limit may lead to the slipping of the tunnel from O-rings and subsequent breach of integrity.

Section 6.2 presents finite element formulation and solution for the case of interconnected glove boxes. In this section both the boxes were assumed to be connected by a flexible tunnel. Finite element analysis results and important observations are presented for seismic stability and integrity of the glove box system in Section 6.3.

Section 6.4 extends the numerical method developed earlier using energy conservation method to the present case of flexibly interconnected glove boxes. Then, Section 6.5 present validation results for used numerical methods. Finally, chapter is concluded in Section 6.6, with the discussion on outcomes and results.

## 6.2 Finite element analysis and solution

### 6.2.1 Objectives and Assumptions

To establish the adequacy and appropriateness of analysis methods, finite element analysis (FEA) had been carried out on a full-scale three-dimensional model of interconnected glove boxes. The main objective of FE analysis was to check seismic stability of the glove boxes and thus evaluate displacements and rotations. FE analysis was carried out with the following assumptions:

1. In numerical analysis, interconnected glove boxes were assumed as freestanding structures. Which means that pressure regulating valve and connected piping was assumed to be flexible enough, not to constrain rigid body motions of the glove box. Thus main concern was to evaluate stability and integrity of the system.
2. Scope of analysis was, not to evaluate leak tightness of the structure which was already tested during shake table experiments. Hence, various connections, between glass panels and stainless steel frame, between aluminum panel and stainless steel frame were modelled as integral one (monolithic). However, material properties was suitably selected for all the panels as given in Table.
3. Actual test conditions of PVC sheet glued to concrete floor was not simulated in finite element analysis. Frictional properties evaluated during shake table testing were used an input to the FE model. Floor was modeled as a rigid body. This is a realistic assumption because objective of analysis was to assess seismic stability of the glove

boxes and not to study floor material behavior which was sufficiently rigid because of underlying concrete slab.

4. Gaskets (O-rings) used to fit material transfer tunnel with the transfer ports located on both the connecting glove boxes was not modeled. In F.E.A, contact interaction behavior arising due to gaskets was simulated by using test evaluated coefficient of friction value. This was a realistic assumption, since scope of this analysis was not to find out the deformations and related stresses in the gaskets.

### 6.2.2 Part Modelling

Interconnected glove boxes and floor were modelled using finite elements with contact between legs and floor as shown in Fig.6-2. Glove boxes frame and interconnected material transfer tunnel were modelled as four nodes shell elements (S4R) with 6 degrees of freedom at each node. Supporting structure (stand) was modelled as three nodes linear beam elements (B31) with 6 degrees of freedom at each node. The connection between tunnel and port was considered as a frictional joint. This was a realistic assumption, since tunnel was simply supported on the ports by using O-rings. We evaluated value of coefficient of friction by pull tests and found it to be 0.4, which was used for analysis. Ventilation pipes connected to glove boxes were assumed to be flexible enough to allow the free movement of GBs on the floor. Various material properties used in FE analysis are given in Table.6-1. Finite element model of two free-standing glove boxes interconnected by a material transfer tunnel is shown in Fig.6-2. In this case, critical point was to model contact interaction between the tunnel and both the glove boxes at each ends. Mesh verification report was generated and no analysis errors were observed.

### 6.2.3 Contact Interactions and Constraints

Contact properties in tangential direction were defined by taking coefficient of friction (μ) value as 0.15. Coulomb friction model was used to relate the maximum allowable frictional (shear) stress across an interface to contact pressure between contacting bodies. Contact properties for contact between material transfer tunnel and material transfer ports of two glove boxes were defined using surface to surface contact discretization. Penalty method was used to enforce contact constraint between mating surfaces. Tunnel was selected as a master surface and two other surfaces (material transfer ports) were selected as slave surfaces. Finite deformation formulation was used for numerical analysis.

**Table 6-1 Material properties of interconnected glove boxes**

| S.No | Material Description | Mechanical Properties | | | |
|---|---|---|---|---|---|
| | | Young's Modulus ($10^9$ N/m$^2$) | Density (Kg/m$^3$) | Poisons ratio | Thickness (m) |
| 1 | Stainless steel glove box frame and material transfer tunnel | 210 | 8000 | 0.3 | 0.003 |
| 2 | Mild steel bottom supporting plate and carriage(stand) | 210 | 8000 | 0.3 | 0.009, 0.006 |
| 3 | Aluminum side panels | 70 | 2700 | 0.35 | 0.01 |
| 4 | Front/back glass panels | 74 | 2530 | 0.2 | 0.01 |

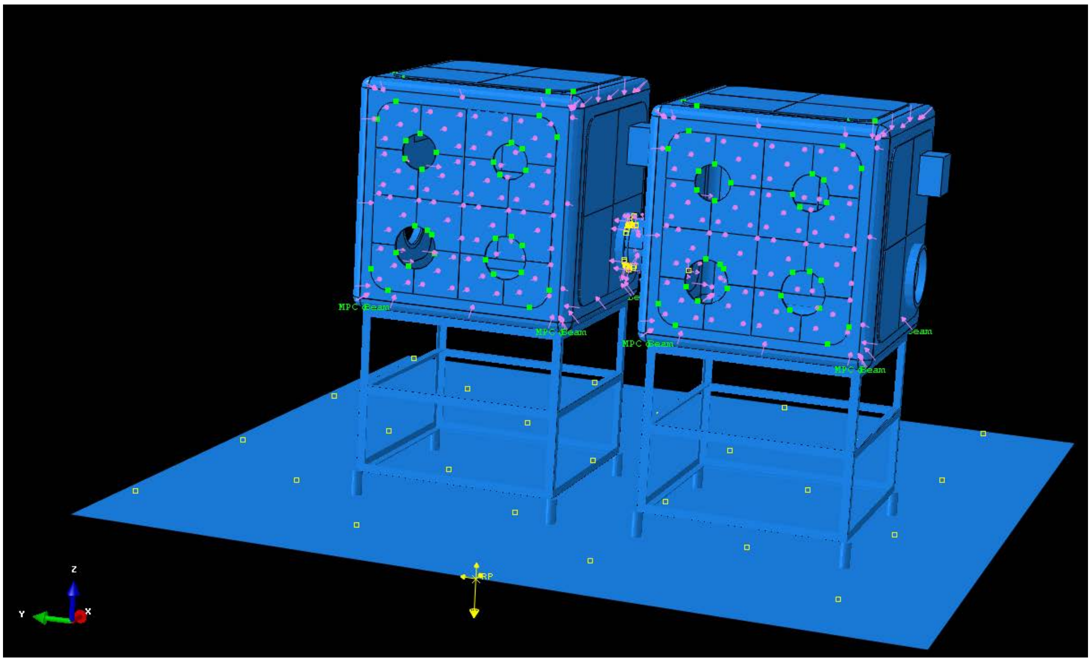

**Figure 6-2 Finite element model of two interconnected glove boxes**

### 6.2.4 Loads and Boundary Conditions

Two interconnected glove boxes were subjected to various kinds of loading during analysis. These include dynamic pressure loading, static equipment load, body forces (due to gravity), and eccentric loads arising due to lead shields and seismic load. For the present study, all the loads are considered to act simultaneously on a glove box structure. Details of applicable loadings and boundary conditions are given below:

1. Dynamic pressure load

   A constant pressure of -250Pa was applied all across the internal surfaces of both the boxes. In addition to that same amount of pressure was also applied on the internal surface of material transfer tunnel.

2. Static equipment load

One of the glove box was applied with a constant static loading at the bottom supporting face to simulate load arising due to the equipment or storage container. Mass was lumped uniformly at the bottom surface of the glove box.

3. Eccentric load

   In the present analysis, one of the glove box was modeled with eccentric lead shield. Effective weight of the shield was distributed all across front side panel of the box.

4. Body force

   This was uniformly applied to all the parts of the assembly. This was constant in magnitude and acts vertically downward.

5. Seismic base excitation

   Synthetic earthquake time histories were applied as a boundary conditions at the reference point of the floor to simulate earthquake loading.

Top frame of the glove box was welded to the bottom carriage through a bottom supporting plate. To include this behavior in the glove box model, multi-point constraint was applied at the interface of top frame and bottom carriage. This constraint merges degrees of freedom of connecting nodes by using a beam element. All these loading and boundary conditions are shown in Fig.6-3.

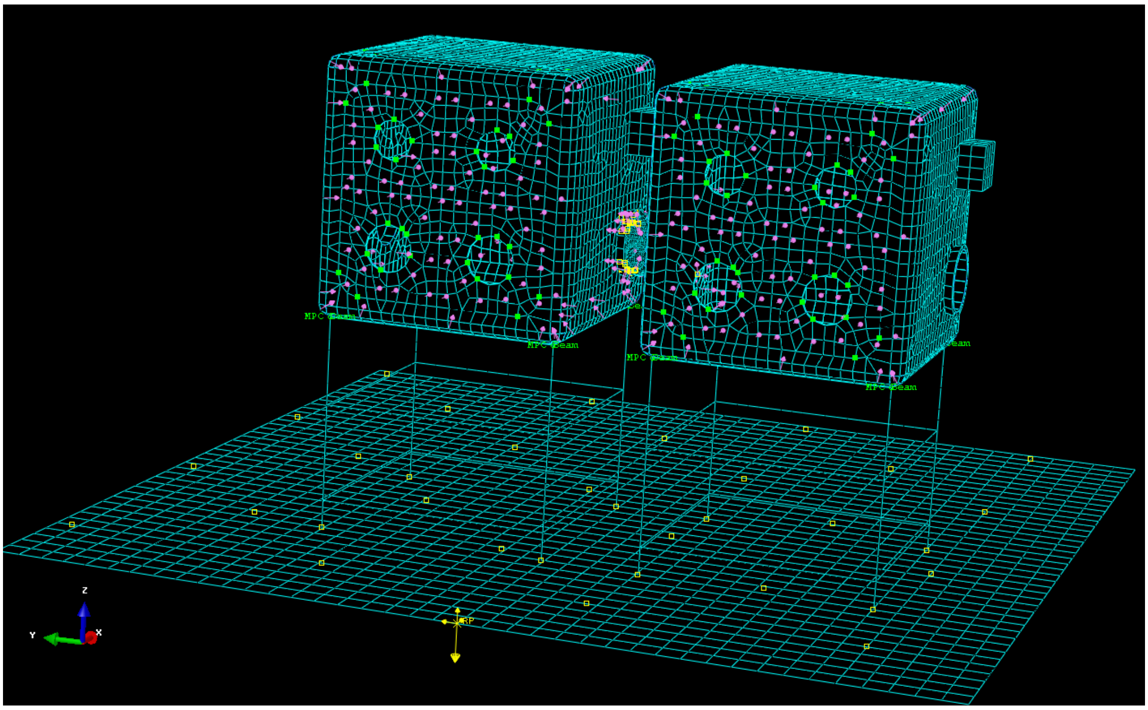

**Figure 6-3 FE model of interconnected glove boxes showing various loads and boundary conditions**

### 6.2.5 Modal Frequencies

Modal analysis was carried out to determine natural frequencies of interconnected GBs. Bottom surface of the carriage i.e. levelling screws were fixed and then Lanczos solver was used to extract Eigen values and Eigen modes up to a frequency value of 30Hz. Three eigenvalues were extracted corresponding to 90% mass participation. First two eigenvalues in flexure mode were determined as7.8Hz and third value in rotation about vertical axis was 8.7Hz as shown in Fig.6-4 (b, c and d) respectively. Displacement gradients were represented by colour scheme where red colour represents highest displacement and blue colour indicates lowest displacement value.

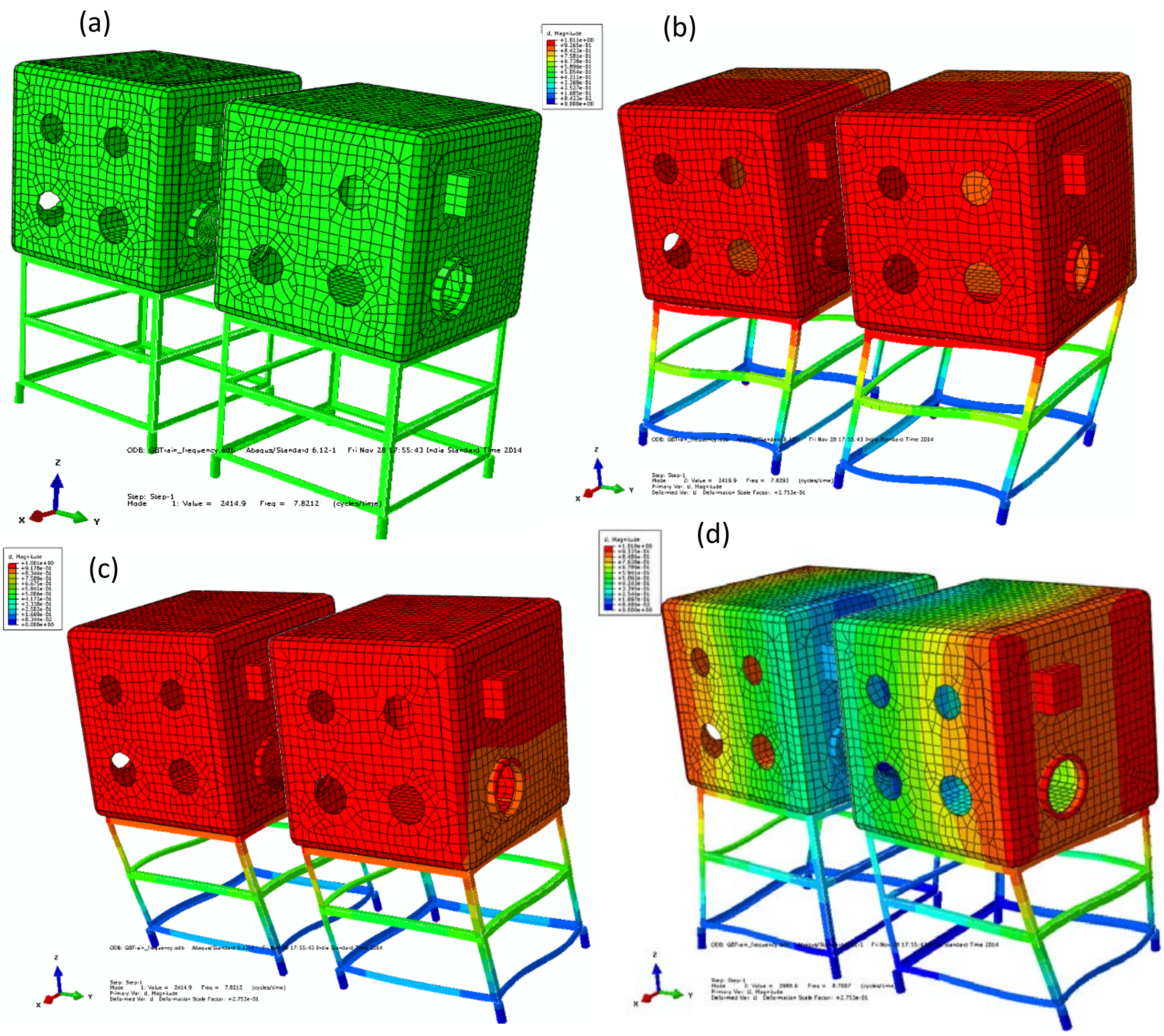


**Figure 6-4 Different mode shapes of interconnected glove boxes in fixed base conditions. (a) un-deformed shape, (b) first mode shape, (c) second mode shape, (d) third mode shape**

## 6.3 Seismic Stability Assessment

Seismic stability and integrity of interconnected glove boxes was evaluated. After carrying out modal analysis, nonlinear seismic analysis had been carried out using time integration method. Implicit solver was used to perform dynamic analysis. Moreover, two percent of critical damping was used as material damping for analysis. This value is in agreement with the damping value for welded steel structure given in relevant codes (ASCE, 2005). For calculating mass and stiffness related constants for Rayleigh damping, frequency range from 7.8Hz to 50Hz was considered.

The floor had been given base excitation simultaneously in three directions starting from 0.1g peak value up to 0.2g peak value. For 0.3g and 0.4g pba values, only two-dimensional (one horizontal and one vertical) excitation was given, in line with the conducted test procedure. Input time history used in analysis was same as recorded at shake table during testing as described earlier in the last chapter. In FE analysis, accelerations and displacements time histories were obtained at locations where sensors were installed during shake table testing.

Fast Fourier Transform (FFT) of acceleration time history results obtained from analysis was then carried out. Total six number of accelerometer (three on each GB in X, Y and Z direction) locations were taken for FFT analysis. Location of these accelerometers were already given in Fig.2-9. Details are as given below:

A1, A4 and A6 --- Accelerometers located on GB2 to record the response of structure in X, Y and Z direction (vertical) respectively.

A11, A13 and A16 -- Accelerometers located on GB1 to record the response of structure in X, Y and Z direction (vertical) respectively.

Objective of analysis was to study rigid body motions (sliding, rocking) and flexural deformations of the structure during seismic event. Input time histories were similar to those used for the case of a single glove box discussed in last chapter and shown in Fig.5-9. Peak values of accelerations obtained for different peak base excitations from 0.1g up to 0.4g pba value is given in Fig.6-5. Fast Fourier transforms of acceleration time histories are presented in Figs.6-6 to 6-9. Following observations and conclusions can be drawn:

1. Peak value of accelerations recorded by various accelerometers exhibited nonlinear relationship with peak base excitation. Magnitude of peak accelerations increased disproportionately with the magnitude of base excitation as shown in Fig.6-5.

2. Response in X (A1 & A11) and Y (A4 & A13) direction was dominated by rigid body motions (sliding and low amplitude rocking). For 0.1g pba value, no sliding motion was observed. In FFT for 0.1g pba value as shown in Fig.6-6, peaks at low frequencies of around 3Hz can be observed. Similar to the case of a single standalone glove box, here also this low frequency corresponds to free rocking frequency of the glove box structure. Negative shift in frequency, corresponding to peak amplitude of FFT, with increase of base excitation from 0.1g to 0.4g was observed as can be seen from Fig.6-3 to Fig.6-9. This was due to increase of rigid body motions with peak base excitations and reduction of free rocking frequencies with increase of amplitude of rocking motions.

3. FFT spectra for Y (A4 & A13) direction for 0.3g and 0.4g peak base accelerations, did not indicate negative frequency shift. This was as expected, due to absence of input base excitation given in Y direction.

4. For base excitation values up to 0.2g, relative sliding between two glove boxes was limited to 0.007m. Hence, material transfer tunnel maintained its position. However, at 0.3g pba value, material transfer tunnel tilted from its position. At 0.4g pba, relative displacement increased to 0.025m causing material transfer tunnel to slip off from the O-rings and breach of integrity was observed

5. Strains obtained in analysis were of very low magnitude. Maximum strain value was 240μm per meter. This indicated that there was insignificant deformations in the glove

boxes, as depicted during shake table testing also. Hence, contribution of flexural mode in overall response was limited.

Next section discusses a simple numerical methodology to quickly estimate sliding displacements of interconnected glove boxes.

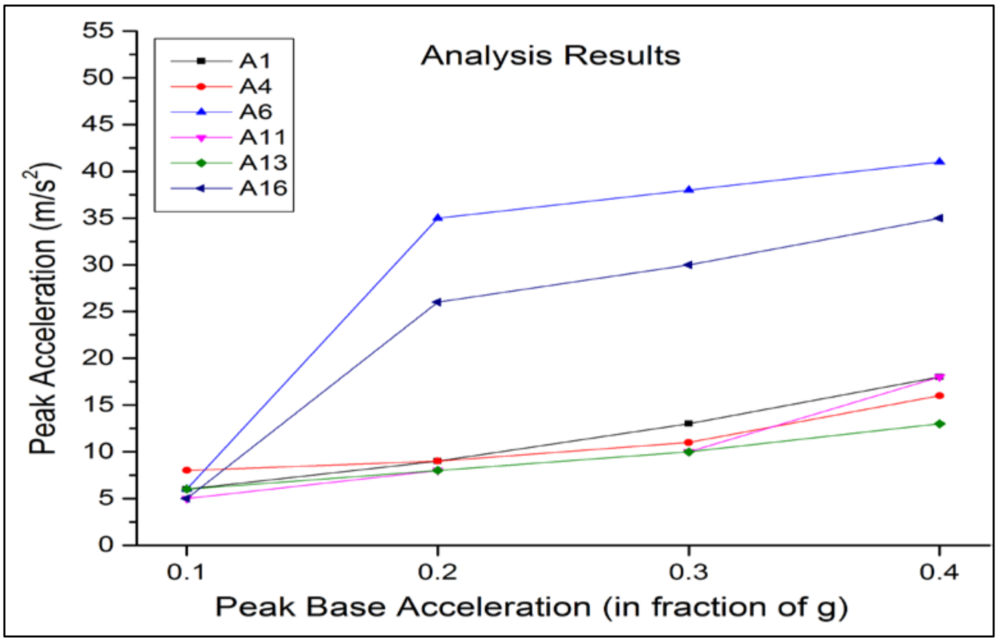


**Figure 6-5 Maximum acceleration values obtained by analysis, at various sensors locations for 0.1-0.4g peak base acceleration**

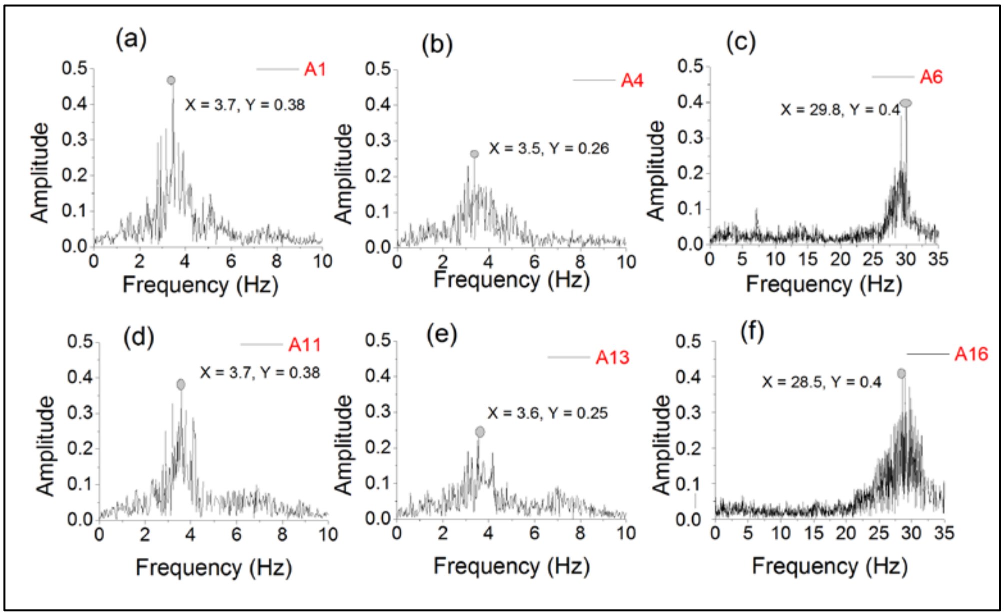


**Figure 6-6 FFT of response time history at 0.1g peak base acceleration (FE Analysis)**

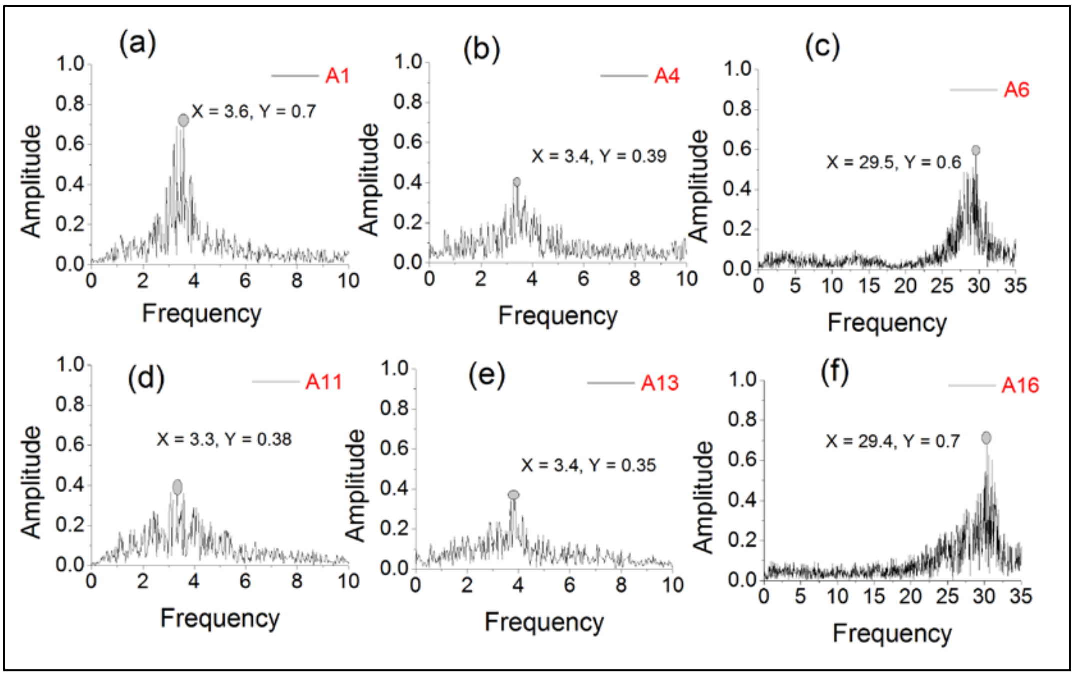


**Figure 6-7 FFT of response time history at 0.2g peak base acceleration (FE Analysis)**

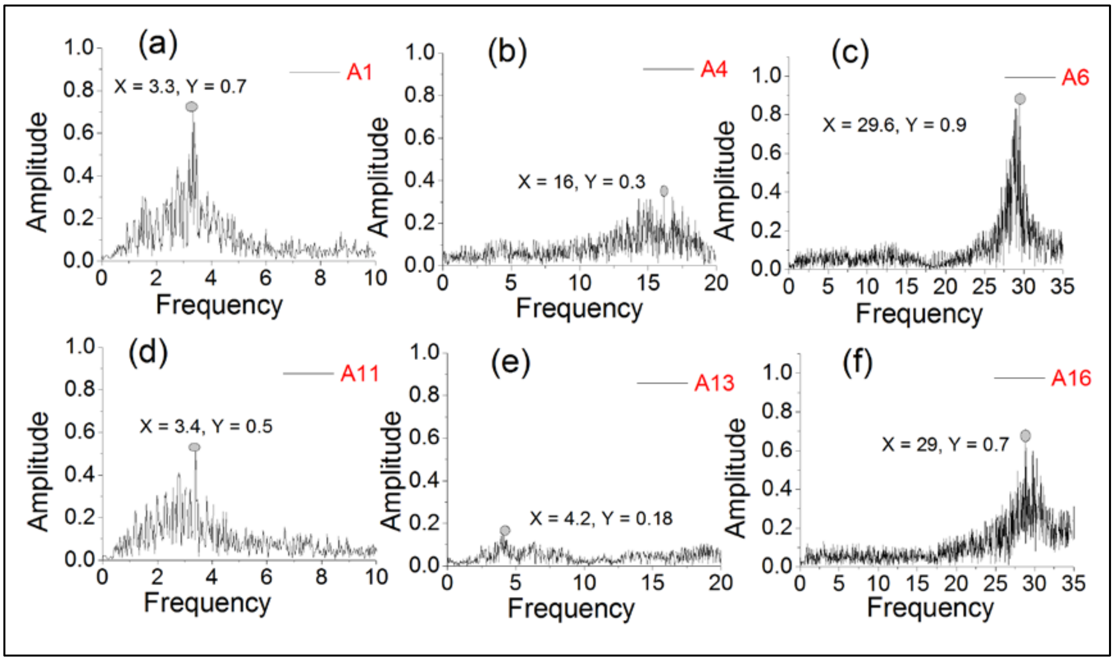


**Figure 6-8 FFT of response time history at 0.3g peak base acceleration (FE Analysis)**

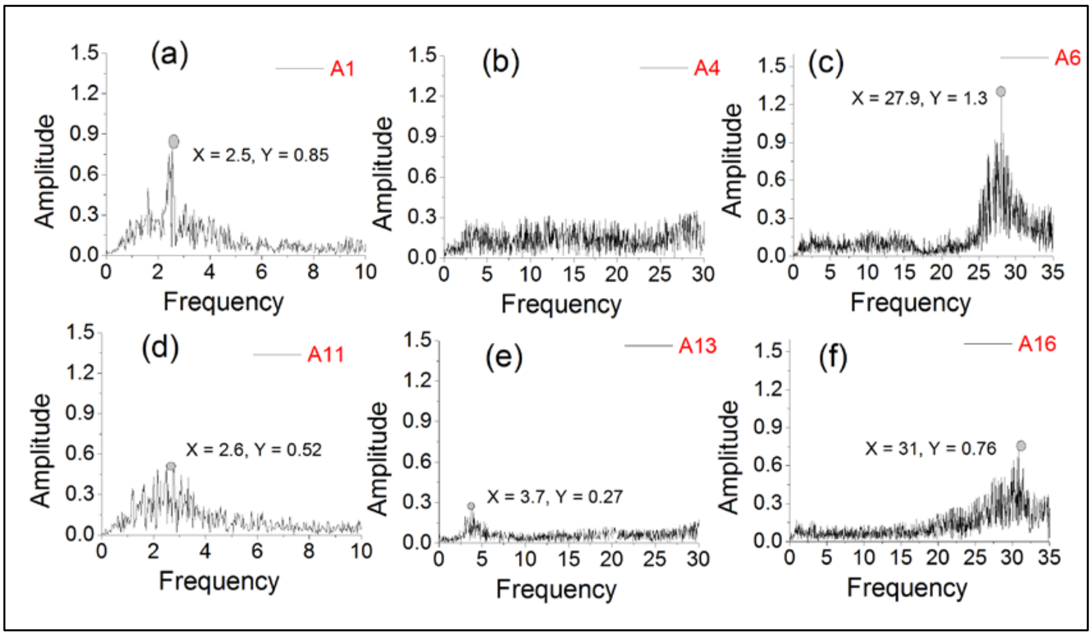


**Figure 6-9 FFT of response time history at 0.4g peak base acceleration (FE Analysis)**

## 6.4 Numerical Method to Estimate Sliding Displacement

A simplified numerical method as developed in last chapter was extended to this case also to estimate maximum sliding displacement of a free-standing structure. Details of this method were already presented in Section 5.5. Here, for clarity sample calculations for few cases are shown.

Energy conservation principle was applied for a full sliding cycle to determine equivalent sliding displacement. In the present case of interconnected glove boxes, it was observed that strains obtained in the structure due to shake table testing were of very low magnitude. Hence, it can be assumed that contributions from strain energy and material damping terms were not significant. We also observed that magnitude of rocking was very less during testing. Hence, energy loss due to impacts between base and legs would be of small magnitude and hence can be ignored. However, for higher base excitations when rocking phenomenon would be considerable, these losses should be considered for the energy balance. In the present case, main source of energy dissipation is via rigid body sliding (frictional dissipation). Hence, we can write an equation of energy balance for a particular cycle of maximum sliding as:

Using Eqn.5.14 derived earlier, for all the cases from 0.2g pba to 0.4g pba equivalent sliding displacement could be evaluated. This method gives a single equivalent value for the sliding displacement of a freestanding structure.

For 0.1g pba, Eqn.5.14 was not valid, since sliding had not started for that pba value. For better understanding of readers, a sample calculation for the case of 0.2g pba is presented.

Initially, calculate equivalent coefficient of friction ($\mu_e$);

$$\mu_e = 0.15(1-0.4*2.1/9.81) = 0.137$$

Here the value of Av is obtained from 10% damped response spectrum for 0.2g pba as shown in Fig.6-10 Now sliding coefficient (Cs) can be calculated as given below:

$$C_s = 2 \text{ X } 0.137 \text{ X } 9.81 = 2.69$$

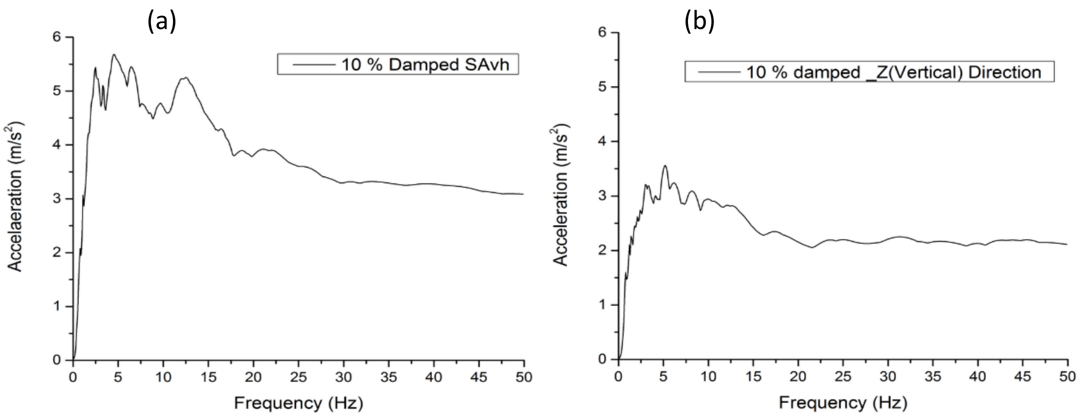


**Figure 6-10 Response Spectrum for 10% damping in (a) horizontal and (b)vertical direction**

Now corresponding to $C_s$ value evaluated above, equivalent sliding frequency ($f_{es}$) was determined from 10% damped response spectrum ($SA_{VH}$) (see Fig.6-10). In the present case, it was 1.1Hz. From the available test data, we get maximum table displacement value for 0.2g pba value as 40mm. In addition, mass of interconnected GBs was 1093Kg.

Now, we get a quadratic equation in terms of sliding displacement (δs) as a variable.

$$26105\,\delta s^2 + 5876\,\delta s - 429 = 0 \qquad 6.1$$

On solving for δs, we finally get δs= 0.058m (considering positive value).

Similarly, the above-mentioned steps can be repeated for 0.3g and 0.4g pba values. After solving for all the cases, we get the following results:

1. for 0.2g peak base acceleration

   $\delta s = 0.058$m

2. for 0.3g peak base acceleration

   $\delta s = 0.091$m

3. for 0.4g peak base acceleration

$\delta s = 0.134m$

We can also evaluate the conservative sliding displacement by using the ASCE code method, given by Eqn. 5.7. On solving Eqn.5.7, we get the following results:

4. for 0.1g peak base acceleration

   $\delta s = 0.004m$

5. for 0.2g peak base acceleration

   $\delta s = 0.056m$

6. for 0.3g peak base acceleration

   $\delta s = 0.105m$

7. for 0.4g peak base acceleration

   $\delta s = 0.165m$

Values of final sliding displacements obtained from the test, FE analysis, energy method and ASCE code are compared in next section for better understanding (see Fig.6-12).

## 6.5 Validation of Finite Element and Numerical Method Results

Developed finite element model was benchmarked using available shake table test data. Important recorded parameters like accelerations and displacements are compared. To check the validity and accuracy of analysis results, peak acceleration and final displacement values obtained from FE analysis are compared with the corresponding test values and shown in Figs.6-11 and Fig.6-12 respectively. Fig.6-12 also compares displacement values obtained from developed numerical method and ASCE code method. Furthermore, frequency contents of acceleration time histories are checked by comparing F.F.T. of acceleration time history obtained by FE analysis as shown in Figs.6-6 to 6-9, with that of corresponding test results as shown in Figs.6-13 to 6-16. Comparison of test results with analysis results indicates following important points:

1. Peak accelerations recorded during tests were found to be coherent with the corresponding analysis values. Maximum deviation observed was 14 percent of test value for A1 accelerometer in case of 0.4g pba (Refer Fig.6-11). Deviations for all other accelerometers readings were also more than 10 percent of test values for the case of 0.4g pba. However, for cases from 0.1g to 0.3g pba values, deviations were below 10 percent of test values.
2. Analysis values for final sliding displacements were in good agreement with the corresponding test values. Maximum deviation observed was 8 percent of the test value in the X direction for 0.4g pba (Refer Fig.6-12). All other variations were well below 8 percent.
3. For the case of 0.1g peak base acceleration, maximum deviation observed in peak value of amplitude of F.F.T. data is 5 percent of test value (Refer Fig.6-6 and Fig.6-13). However, it was 10, 12 and 13 percent for the cases of 0.2g, 0.3g and 0.4g peak base acceleration respectively (Refer Figs.6-7, 6-8, 6-9 and Figs.6-14, 6-15, 6-16).
4. Peaking of amplitude at lower frequency (around 3Hz) for horizontal directions F.F.T. was observed in analysis results, in line with the test results. Further, negative sift of frequency with increasing peak base acceleration value was also observed.

Hence, it can be inferred that analysis methods are adequate to predict non-linear behaviour of interconnected freestanding glove boxes.

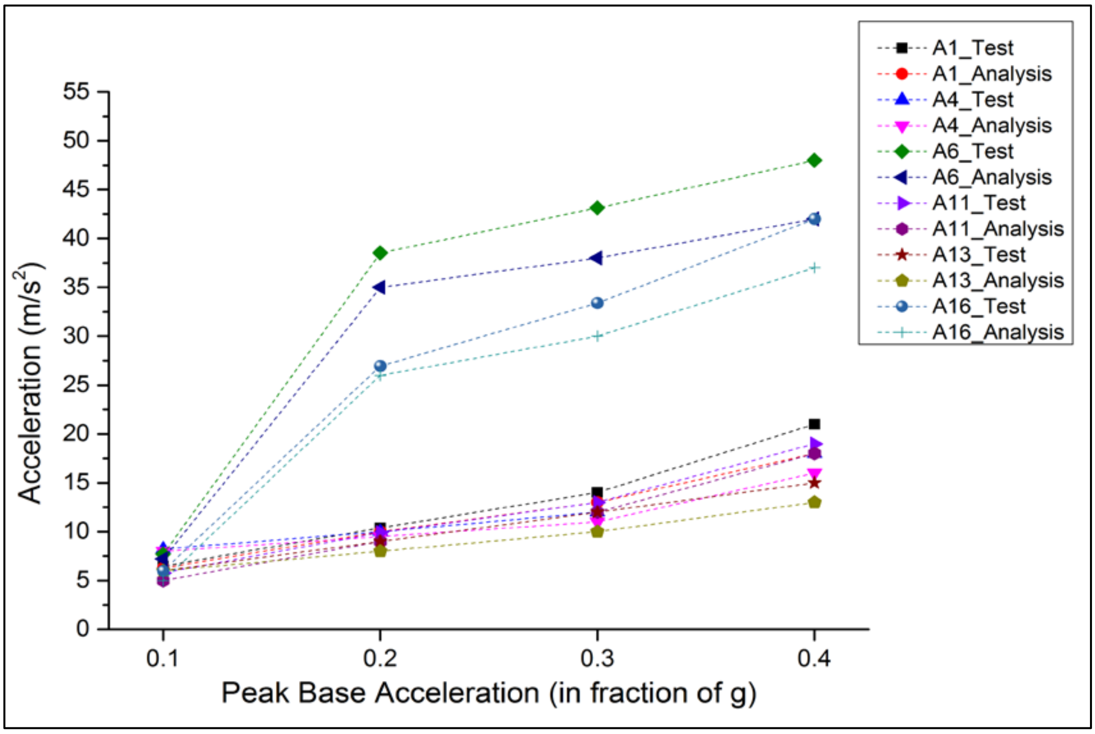


**Figure 6-11 Comparison of peak accelerations obtained by testing and analysis for various accelerometers**

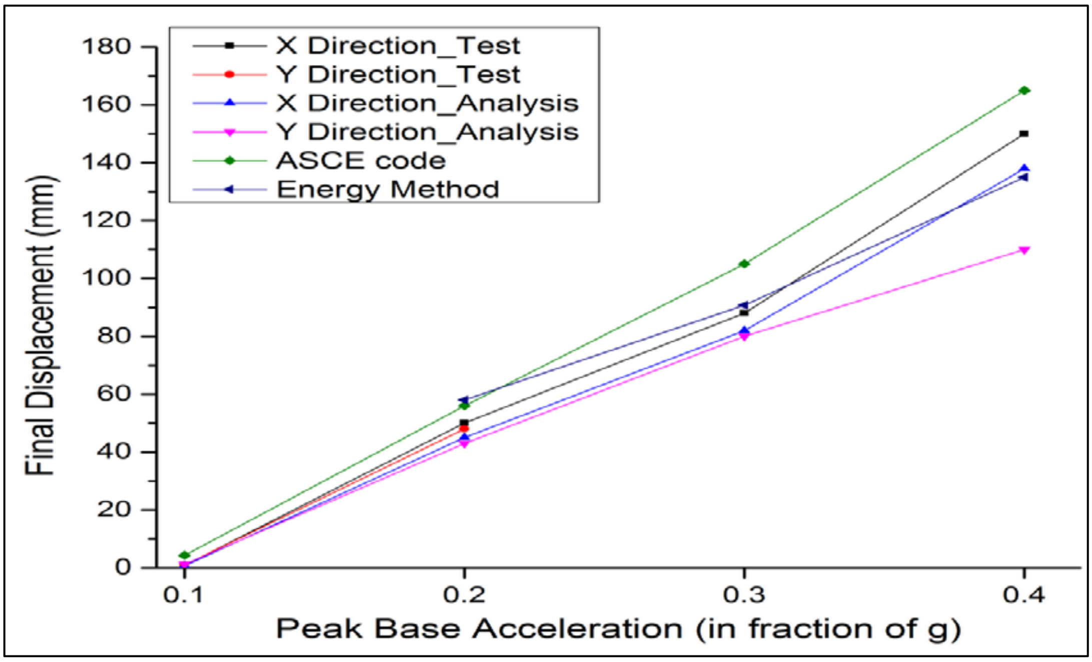


**Figure 6-12 Comparison of final displacements of interconnected glove boxes obtained by test and numerical methods**

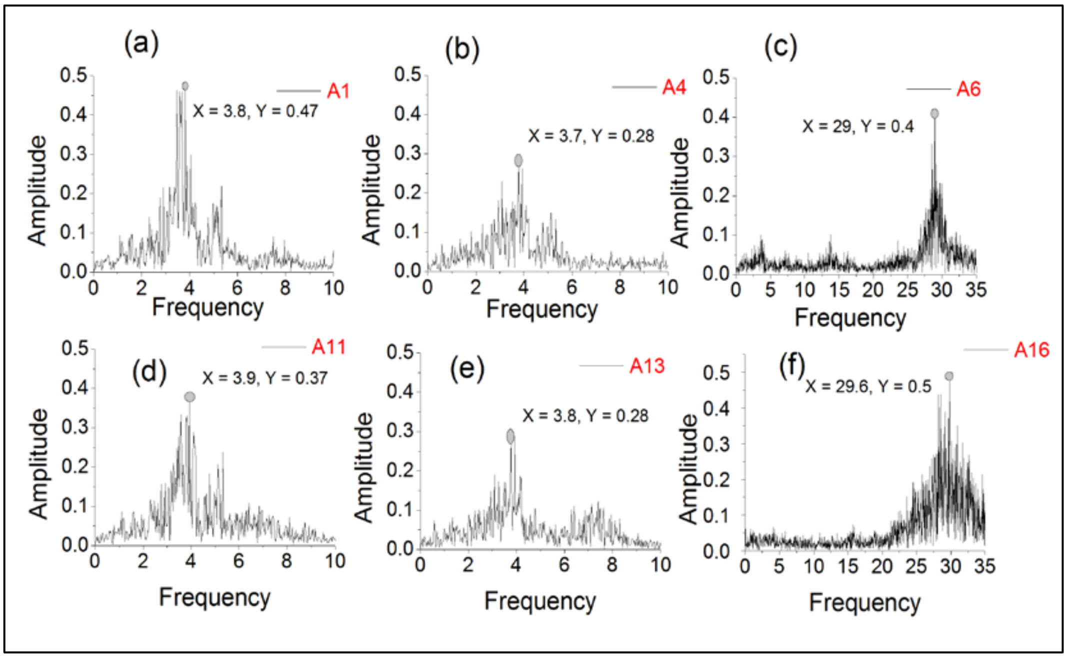


**Figure 6-13 FFT of acceleration signal recorded by accelerometers (a) A1, (b)A4, (c) A6, (d) A11, (e)A13 and (f) A16 for 0.1g pba value during shake table testing**

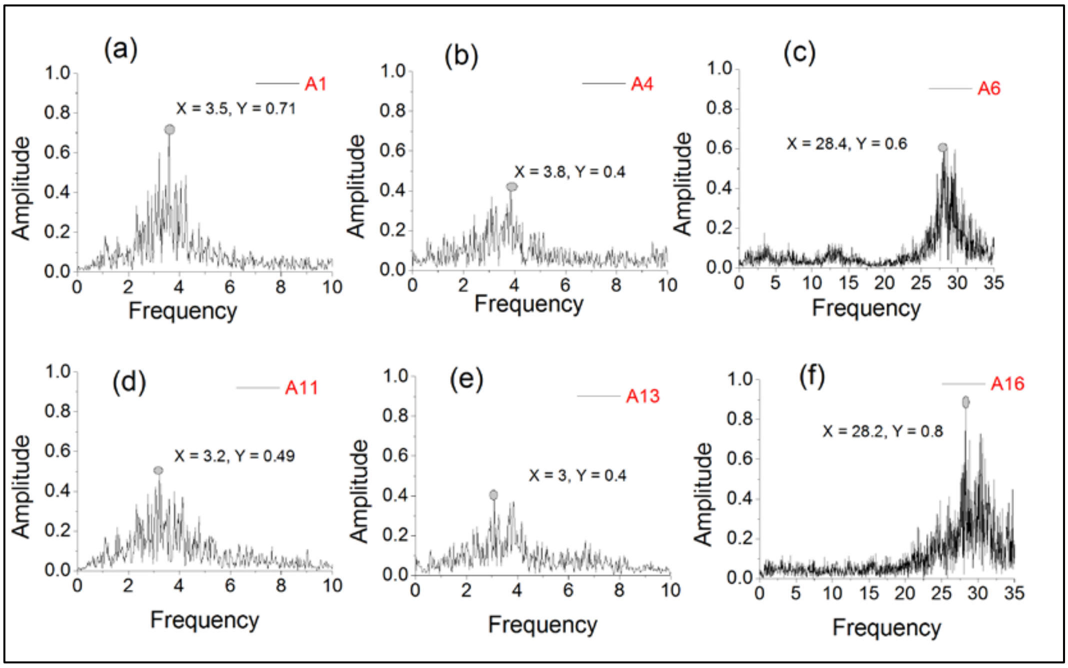


**Figure 6-14 FFT of acceleration signal recorded by accelerometers (a) A1, (b)A4, (c) A6, (d) A11, (e)A13 and (f) A16 for 0.2g pba value during shake table testing**

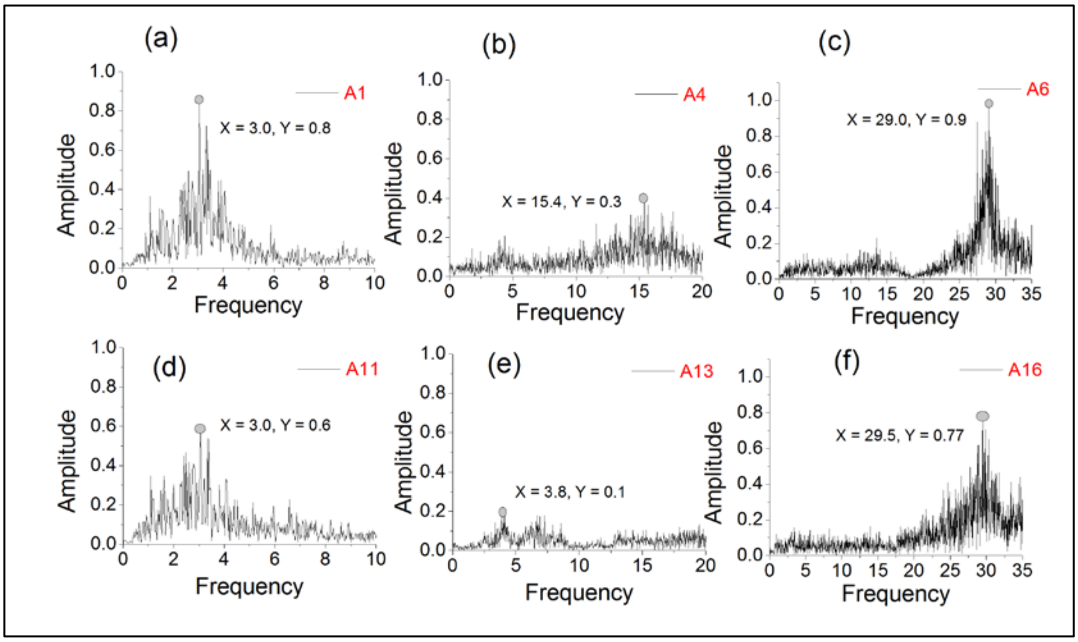


**Figure 6-15 FFT of acceleration signal recorded by accelerometers (a) A1, (b)A4, (c) A6, (d) A11, (e)A13 and (f) A16 for 0.3g pba value during shake table testing**

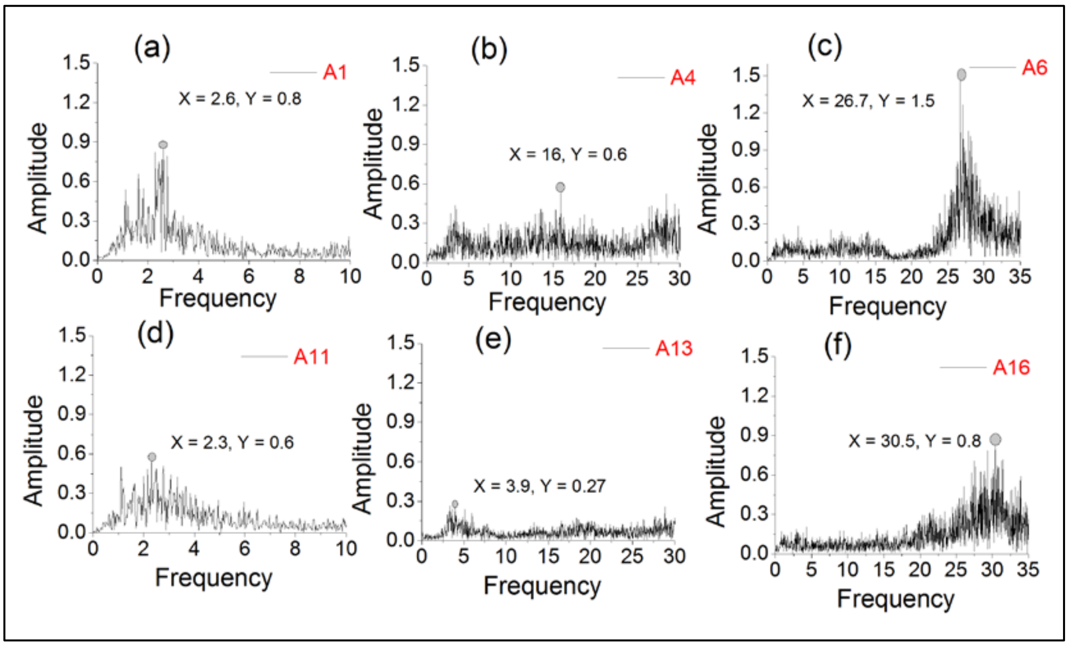


**Figure 6-16 FFT of acceleration signal recorded by accelerometers (a) A1, (b)A4, (c) A6, (d) A11, (e)A13 and (f) A16 for 0.4g pba value during shake table testing**

## 6.6 Outcomes and Discussions

It was clear from the results presented above, that the response of the system was highly nonlinear due to the presence of friction and vertical impact with floor. Low frequency rigid body motions (sliding and rocking) dominated test response in horizontal directions. A negative frequency shift with increasing peak base acceleration was observed in horizontal direction motion, indicating a predominance of rigid body motions at higher base excitations. Further, high frequency (around 30Hz) impacts were noted in vertical direction response due to the presence of low amplitude rocking motion. Frictional sliding dissipated major portion of energy input to the system. For correct prediction of the response of a freestanding system subjected to base excitations, it is very important to accurately model and represent contact dynamics.

Interconnected GBs maintained leak tightness and integrity up to design basis acceleration of 0.2g. Both GBs moved as a single structure and no relative movement was observed. Tests were also performed to check their stability for higher base accelerations which normally occur when they are located on higher floors for operations. It was observed that at 0.3g peak base acceleration value, relative motion was there and material transfer port connecting two glove boxes was tilted. At 0.4g peak base acceleration, substantial relative motion between two interconnected GB's was observed and breach of integrity was observed at 0.4g peak base acceleration.

Owing to the highly nonlinear behavior of the system due to presence of friction and impact at contact points, contact parameters were required to be meticulously selected in FE analysis. Implicit solver was used to analyze the system. Analysis results were found to be in good agreement with the corresponding test values. Simplified numerical method developed using an energy conservation technique provided a good quick estimate of maximum sliding displacement. This could be useful for determining upper bounds on displacements and hence, helpful in designing glove boxes layout.

To improve seismic stability for higher base acceleration values, modifications in glove box design is required. The other alternative could be to anchor glove boxes with the floor. Although, anchoring can enhance seismic stability of the system by arresting rigid body motions, it increases elastic motions like bending and related structural deformation. Relative deformations in the structural members, especially at the joint between glass and metal panel may compromise leak tightness of the system. Hence, keeping in mind above-mentioned constraints, designers have to maintain a fine balance between rigid body motions and elastic deformations. In present case, two glove boxes were interconnected by a flexible connection. Hence, it is important to constrain motion between the boxes before anchoring the boxes with the floor. Next chapter discusses a case where both of these boxes are rigidly connected to each other, in addition to a flexible connection via transfer port.

# CHAPTER 7 SEISMIC STABILITY OF RIGIDLY INTER-CONNECTED GLOVE BOXES

## 7.1 Introduction and Outline

In last chapter, we deliberated seismic stability of two glove boxes interconnected by a material transfer tunnel. We elaborated that the connection between material transfer tunnel and glove boxes was through deformable gaskets. This linkage can constrain sliding and rocking motion, till the frictional resistance at the contacting interface is overcome by external disturbing forces. Hence, for higher amplitudes of peak base excitations, relative sliding and rocking/rotational motion was observed. Integrity of the glove box system was breached at 0.4g peak ground acceleration seismic excitation.

To improve the seismic performance of interconnected glove boxes, it was proposed to rigidly connect both the boxes with each other. A cross bracing using mild steel angles was bolted between carriages (stands) of both the boxes. The objective of this cross bracing was to constrain relative displacements and rotations between the boxes. After this design modification, glove boxes were analyzed again using FE software. Research performed as a part of this chapter has been published in a peer reviewed journal.

Section 7.2 discusses finite element modeling and analysis methodology and gives detail of modal frequencies of interconnected glove boxes.

Section 7.3 reports numerical simulations carried out using FE methods to assess seismic stability of a glove boxes. After this Section 7.4 gives detail of numerical method for quick estimation of slip distance for free-standing body. Then, Section 7.5 presents validation results for numerical models viz. finite element model and energy conservation based numerical method. Finally, conclusions are drawn in Section 8.6.

## 7.2 Finite Element Analysis and Solution

Finite element analysis (FEA) has been carried out on full scale three-dimensional modified design model of interconnected GBs. The main objective of FE analysis was to check displacements and rotations of the interconnected gloveboxes. However, objective of analysis was not to evaluate leak tightness of structure during seismic excitations. Hence, various connections, between glass panels and stainless steel frame, between aluminum panel and stainless steel frame were modelled as the integral one (monolithic). Various material properties were provided as an input for analysis as given in Table.7-1. Interconnected glove boxes and floor was modelled using finite elements with contact generated between legs and floor as shown in Fig.7-1. Glove boxes frame and interconnected material transfer tunnel were modelled as four nodes shell elements (S4R) with 6 degrees of freedom at each node. Supporting structure (stand) and structural cross bracing was modelled as three nodes linear beam elements (B31) with 6 degrees of freedom at each node. The connection between tunnel and port was considered as a frictional joint. Contact properties in tangential direction were defined by taking coefficient of friction (μ) value as 0.15. For numerical enforcement of contact constraints in tangential and normal direction, Penalty algorithm was used. The mass of the filter box, eccentric shield, central load, regulating valve, clamping strips, glove ports, gauntlet etc. were lumped at appropriate places and was effective in three translational degrees of freedom.

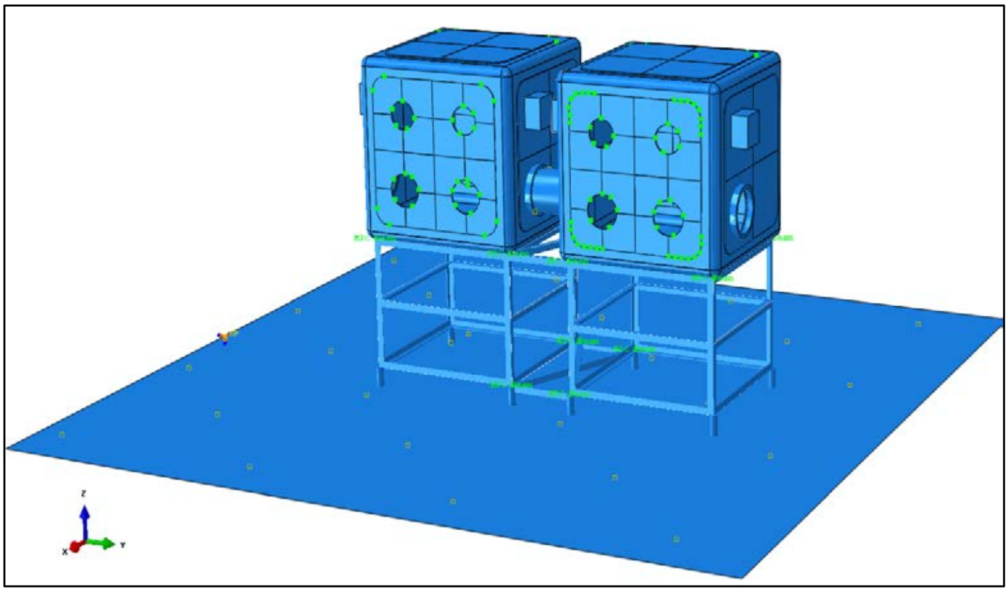

**Figure 7-1 Finite element model of two interconnected glove boxes showing various constraints and contact interactions**

**Table 7-1 Mechanical properties of modified glove box structure**

| S.no | Material Description | Mechanical Properties | | | |
|---|---|---|---|---|---|
| | | Young's Modulus (GPa) | Density ($Kg/m^3$) | Poisons ratio | Thickness (mm) |
| 1 | Stainless steel glove box frame and material transfer tunnel | 210 | 8000 | 0.3 | 3 |
| 2 | Mild steel bottom supporting plate and carriage(stand) | 210 | 8000 | 0.3 | 9,6 |
| 3 | Aluminium side panels | 70 | 2700 | 0.35 | 10 |
| 4 | Front/back glass panels | 74 | 2530 | 0.2 | 10 |
| 5 | Structural members (L shaped angles) | 210 | 8000 | 0.3 | 5 |

### 7.2.1 Modal Frequencies

Modal analysis was first carried out to determine natural frequency of interconnected GB’s. Lanczos method was used to calculate eigenvalues. First two eigenvalues in flexure mode were determined to be 8.1Hz and 8.2 Hz and third value in rotation about vertical axis was 10Hz as shown in Fig.7-2. In the figure, displacement gradients are represented by color scheme, where red and blue colors indicate highest and lowest value of displacement. After carrying out modal analysis, nonlinear seismic analysis had been carried out using time integration method. Next section presents finite element analysis results to determine seismic stability of modified interconnected glove boxes structure.

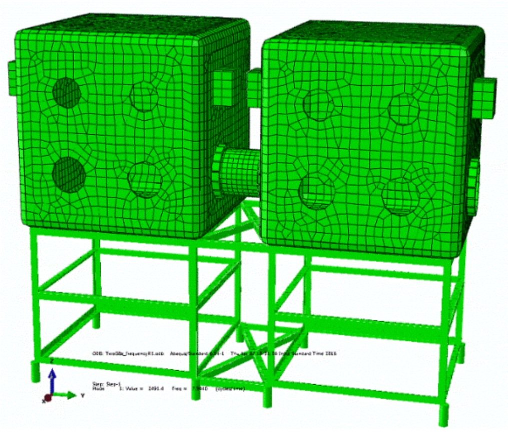

(a) Un-deformed

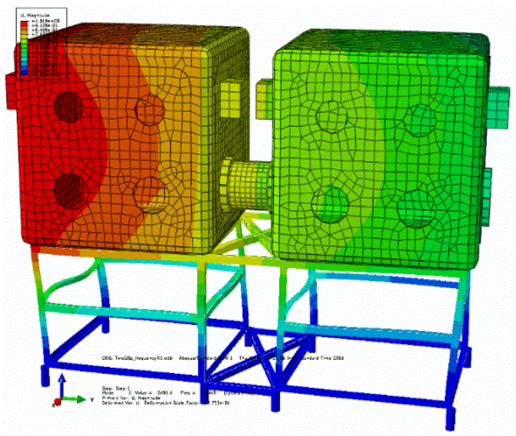

(b) First mode shape

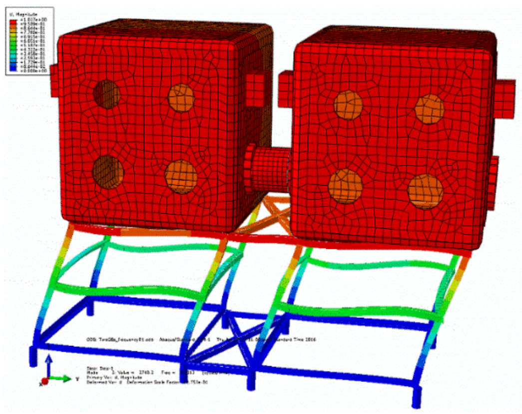

(c) Second mode shape

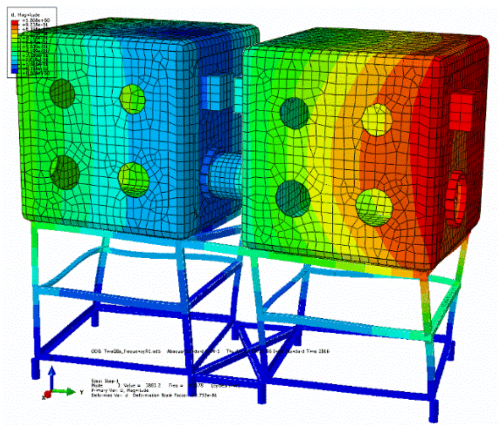

(d) Third mode shape

**Figure 7-2 fundamental mode shapes of Interconnected glove boxes**

## 7.3 Seismic Stability Assessment

The FE model had been given base excitation simultaneously in three directions starting from 0.1g peak value up to 0.4g peak value. Input time histories used in analysis were same as recorded at shake table during testing. In FE analysis, accelerations and displacements time histories, obtained at locations where sensors were installed during shake table testing are plotted. Peak acceleration values obtained from the finite element analysis at locations of various sensors is plotted in Fig.7-3.

Fast Fourier Transform (FFT) of acceleration time histories obtained at locations corresponding to various accelerometers was obtained. Total six number of accelerometers (three on each GB in X, Y and Z direction) were taken for FFT analysis. Location of these accelerometers was already shown in Fig.2-12. Details are as given below:

A1, A4 and A6 --- Accelerometers located on GB2 to record the response of structure in X, Y and Z direction (vertical) respectively.

A11, A13 and A16 -- Accelerometers located on GB1 to record the response of structure in X, Y and Z direction (vertical) respectively.

FFT of response accelerations is plotted in Figs.7-4 to 7-7. Following observations can be drawn from the analysis results:

1. Acceleration response increased nonlinearly with peak base excitation as shown in Fig.7-3.
2. Response in X (A1 & A11) and Y(A4 & A13) direction was dominated by rigid body motions (sliding and low amplitude rocking).Negative shift in frequency corresponding to peak amplitude of FFT, with increase of base excitation was observed. This was due to increase of rigid body motions, with peak base excitations. In FFT, observed peaks

at low frequencies of around 3Hz was predominantly due to rigid body motions like sliding and frequency induced rocking. (Refer Fig.7-4)

3. FFT spectra for Y (A4 & A13) direction for 0.3g and 0.4g peak base accelerations, doesn't indicate negative frequency shift. This was as expected, from the absence of input base excitation given in Y direction.
4. Interconnected GBs maintained integrity up to 0.4g PGA value. This shows that rigidly connected glove boxes have performed seismically better than corresponding boxes without rigid links.

After carrying out finite element analysis of modified configuration of glove boxes, numerical method results for estimation of slip displacements are discussed in next chapter.

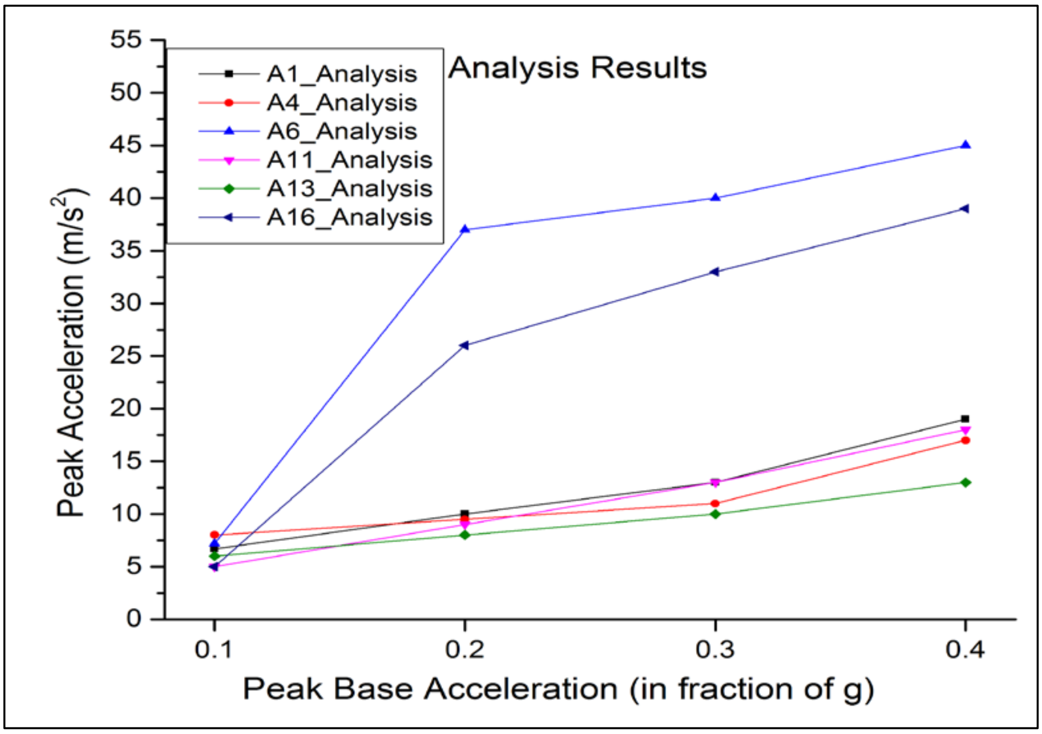


**Figure 7-3 Maximum acceleration values obtained by FE analysis at accelerometer locations for 0.1-0.4g peak base acceleration**

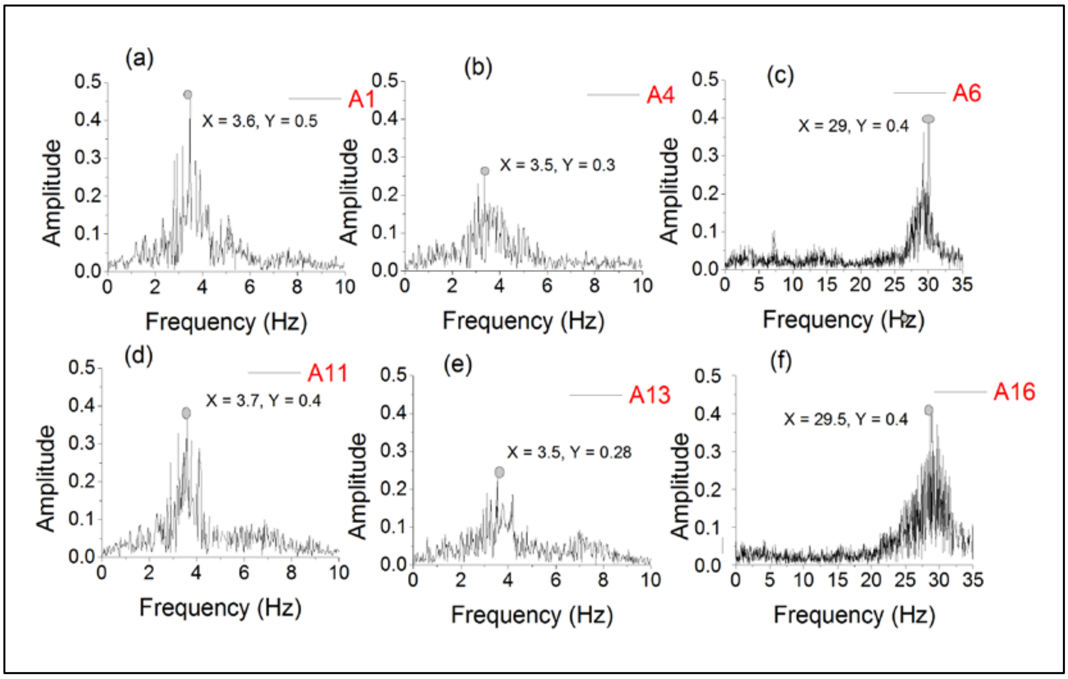


**Figure 7-4 FFT of response time history at 0.1g peak base acceleration (FE Analysis)**

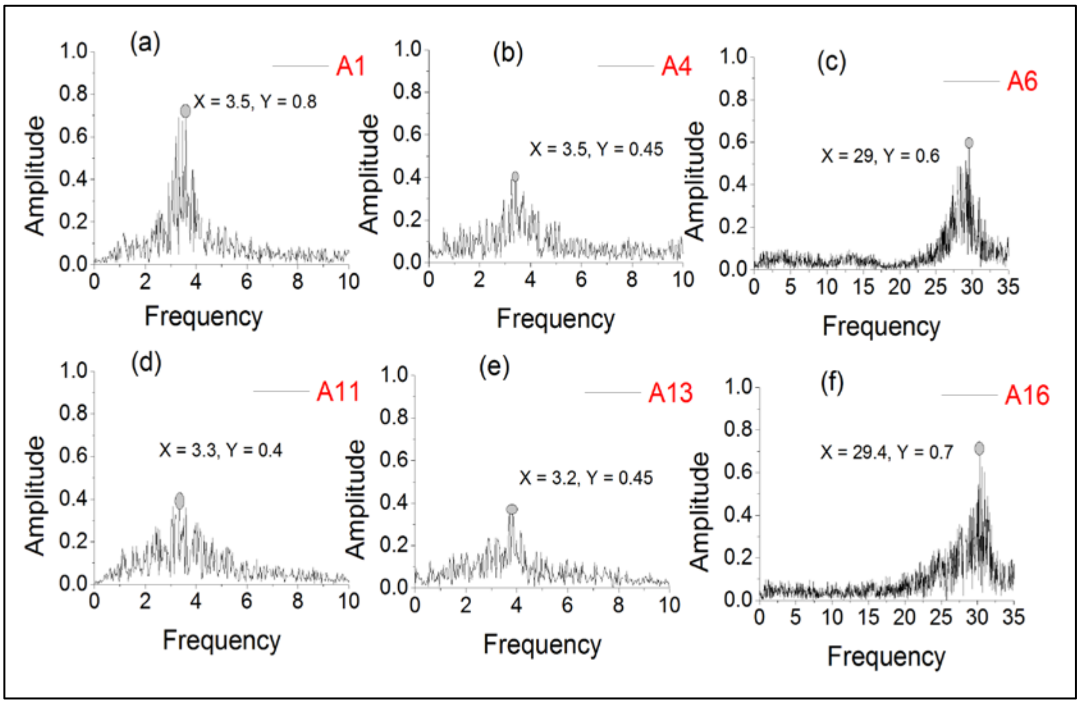


**Figure 7-5 FFT of response time history at 0.2g peak base acceleration (FE Analysis)**

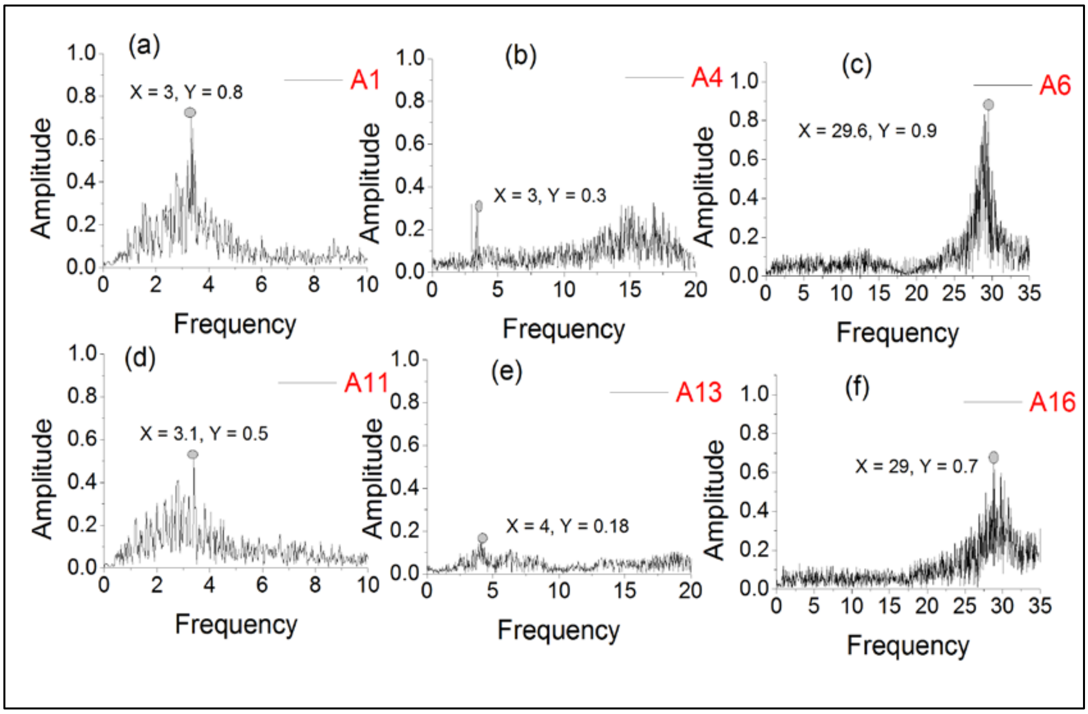


**Figure 7-6 FFT of response time history at 0.3g peak base acceleration (FE Analysis)**

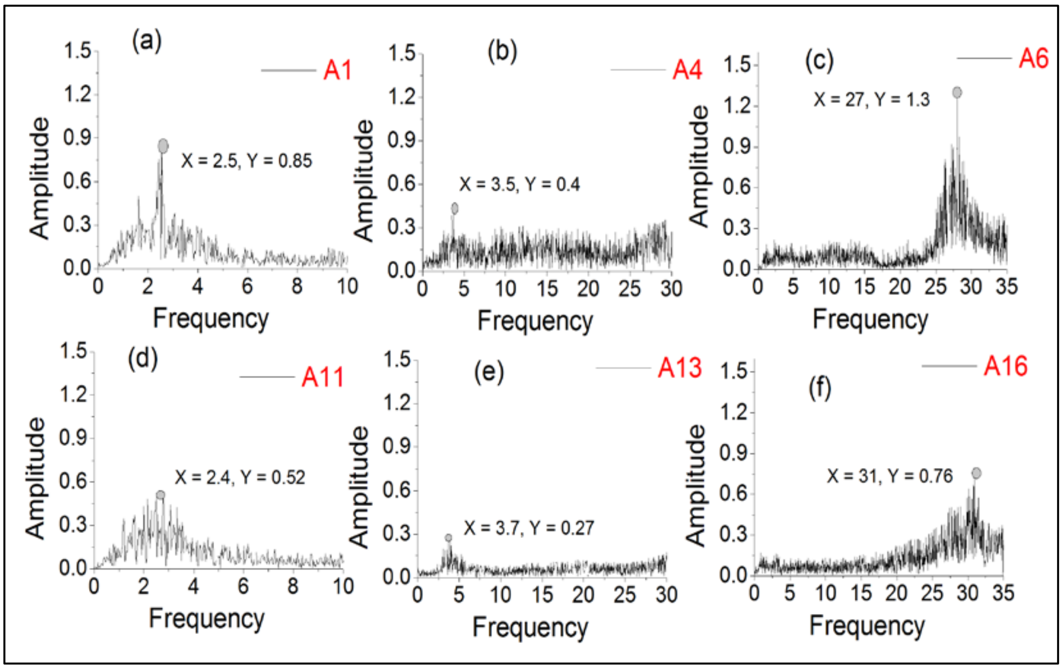


**Figure 7-7 FFT of response time history at 0.4g peak base acceleration (FE Analysis)**

## 7.4 Numerical Method to Estimate Sliding Displacement

The simplified numerical method is further extended to estimate maximum sliding displacement of modified configuration of glove boxes with rigid links. Methodology for obtaining equivalent sliding displacement is same as described earlier in Chapter-5. Hence, not repeated again here.

On solving for $\delta s$ by using quadratic equations developed earlier, we finally get these results:

1. for 0.2g peak base acceleration

   $\delta s = 57mm$

2. for 0.3g peak base acceleration

   $\delta s = 91mm$

3. for 0.4g peak base acceleration

   $\delta s = 134mm$

We can also evaluate the conservative sliding displacement by using the ASCE code method and results are as below:

1. for 0.1g peak base acceleration

   $\delta s = 4mm$

2. for 0.2g peak base acceleration

   $\delta s = 56mm$

3. for 0.3g peak base acceleration

   $\delta s = 105mm$

4. for 0.4g peak base acceleration

   $\delta s = 165mm$

Comparison of final sliding displacements obtained from the test, FE analysis, energy method and ASCE code is shown in Fig.7-9.

## 7.5 Validation of Finite Element and Numerical Method Results

Developed finite element model was benchmarked using available shake table test data. Important recorded parameters like accelerations and displacements were compared. To check the validity and accuracy of analysis results, peak acceleration and final displacement values obtained from FE analysis were compared with the corresponding test values and shown in Figs.7-8 and Fig.7-9 respectively. Fig.7-9 also compares displacement values obtained from developed numerical method and ASCE code method. Furthermore, frequency contents of acceleration time histories are checked by comparing F.F.T. of acceleration time history obtained by FE analysis as shown in Figs.7-4 to 7-7, with that of corresponding test results as shown in Figs.7-10 to 7-13. Comparison of test results with analysis results indicates following important points:

1. Peak accelerations recorded during tests were found to be coherent with the corresponding analysis values. Maximum deviation in analysis value observed was 12 percent of test value for A1 accelerometer in case of 0.4g pba (Refer Fig.7-8). Deviations for all other accelerometers readings were below 10 percent of test values.
2. Analysis values for final sliding displacements were in good agreement with the corresponding test values. Maximum deviation observed was 12 percent of the test value in the X direction for 0.4g pba (Refer Fig.7-9). All other variations were well below 12 percent.
3. For the case of 0.1g peak base acceleration, maximum deviation observed in peak value of amplitude of F.F.T. data is 8 percent of test value (Refer Fig.7-4 and Fig.7-10). However, it was 19, 11 and 14 percent for the cases of 0.2g, 0.3g and 0.4g peak base acceleration respectively (Refer Figs.7-5, 7-6, 7-7 and Figs.7-11, 7-12, 7-13).

4. Peaking of amplitude at lower frequency (around 3Hz) for horizontal directions F.F.T. was observed in analysis results, in line with the test results. Further, negative sift of frequency with increasing peak base acceleration value was also observed.

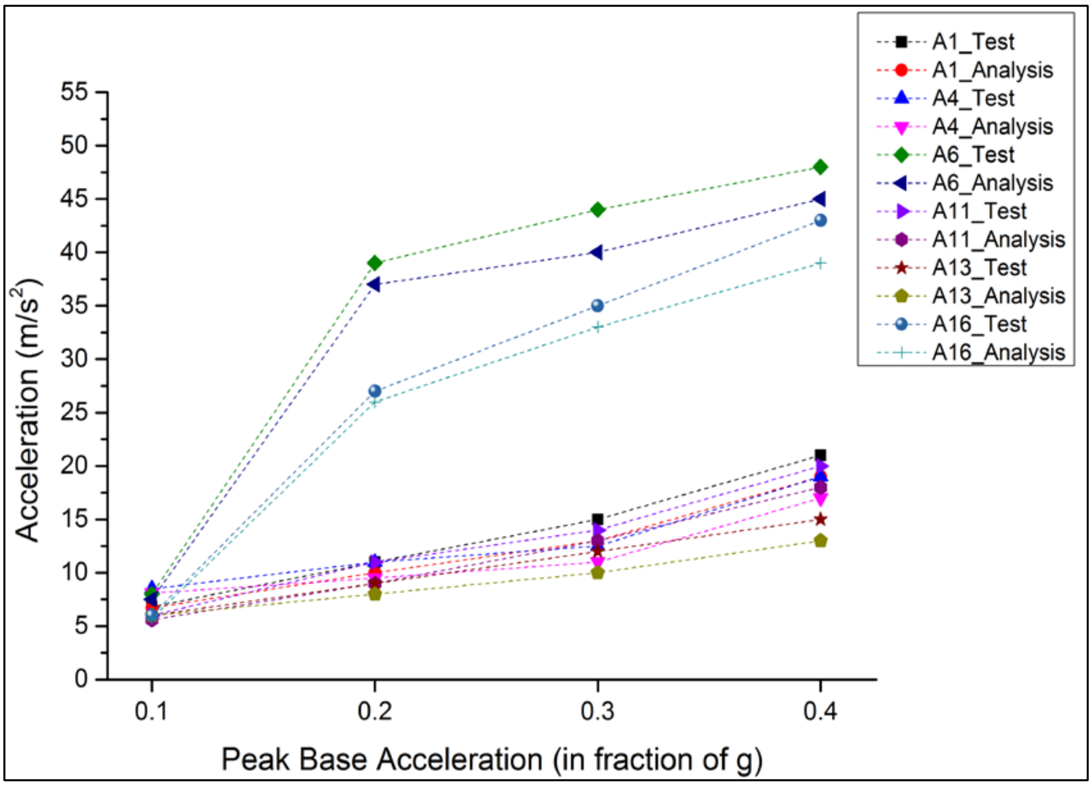


**Figure 7-8 Comparison of peak base accelerations obtained by Test and FE analysis**

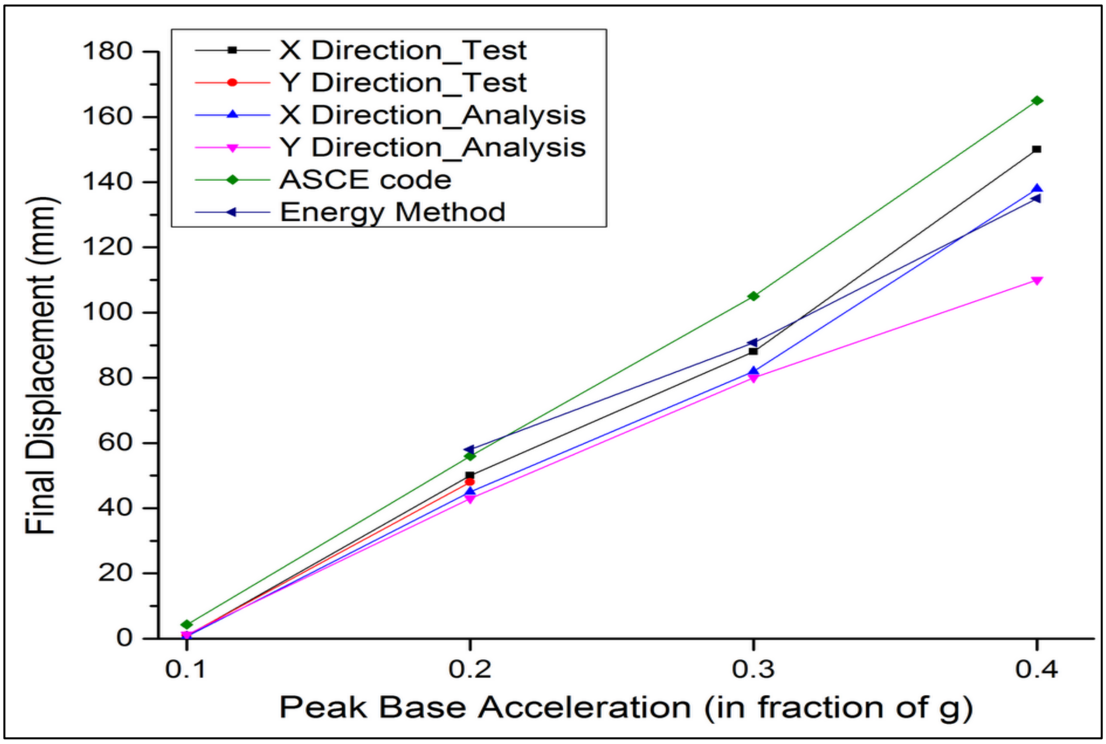


**Figure 7-9 Comparison of final displacement of interconnected glove boxes obtained by different methods**

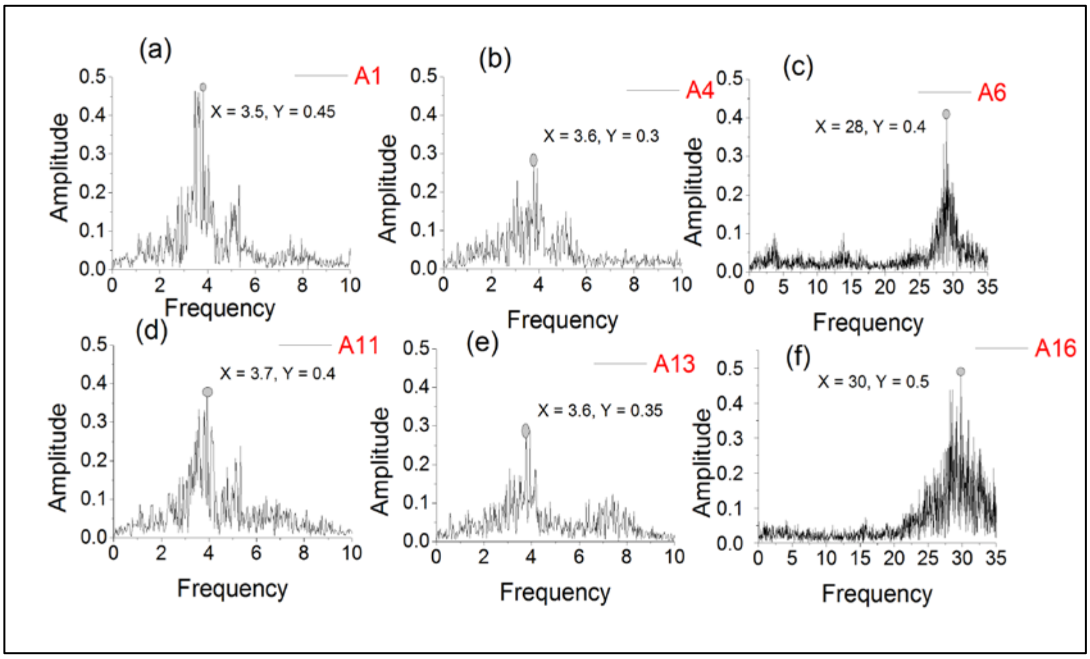


**Figure 7-10 FFT of acceleration signal recorded by accelerometers (a) A1, (b)A4, (c) A6, (d) A11, (e)A13 and (f) A16 for 0.1g pba value during shake table testing**

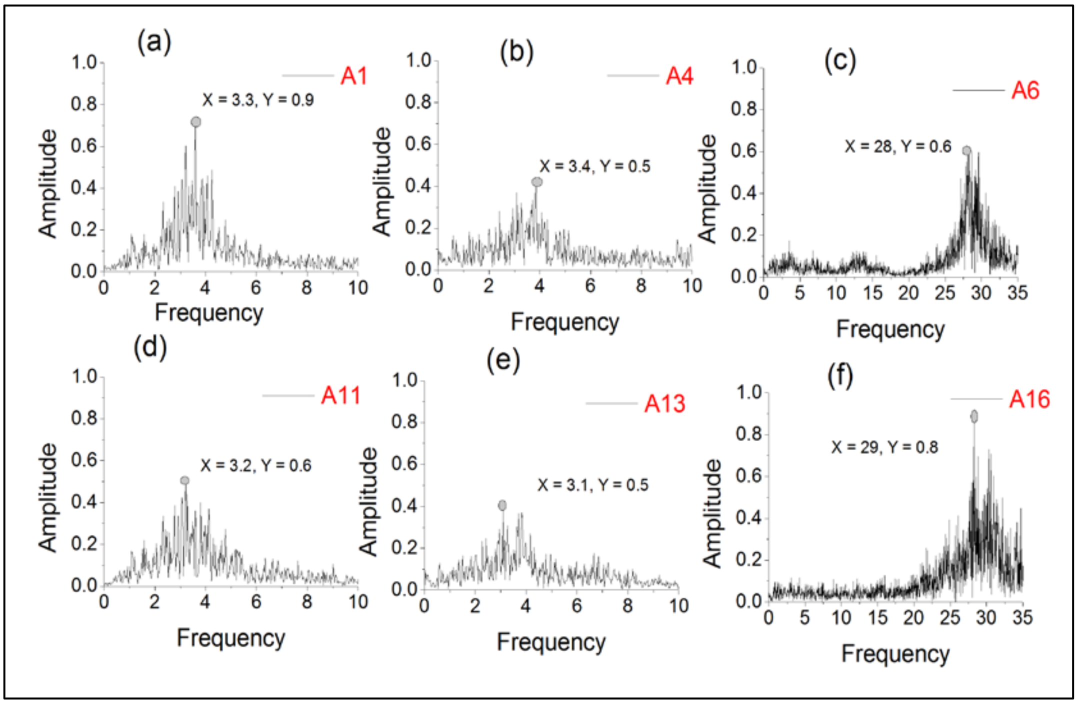


**Figure 7-11 FFT of acceleration signal recorded by accelerometers (a) A1, (b)A4, (c) A6, (d) A11, (e)A13 and (f) A16 for 0.2g pba value during shake table testing**

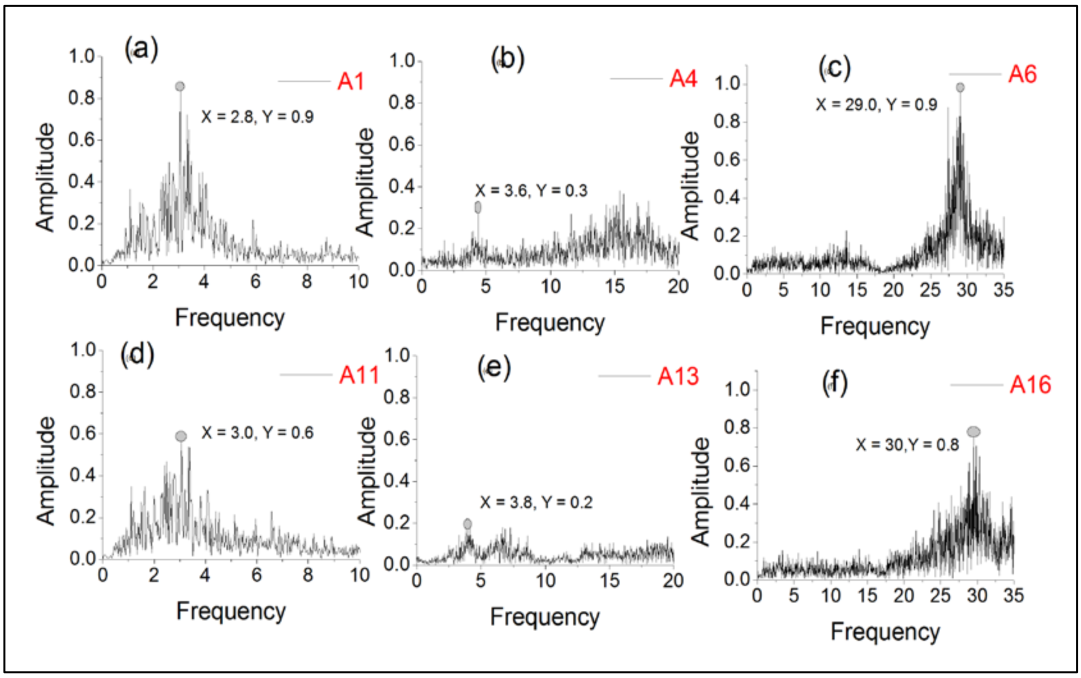


**Figure 7-12 FFT of acceleration signal recorded by accelerometers (a) A1, (b)A4, (c) A6, (d) A11, (e)A13 and (f) A16 for 0.3g pba value during shake table testing**

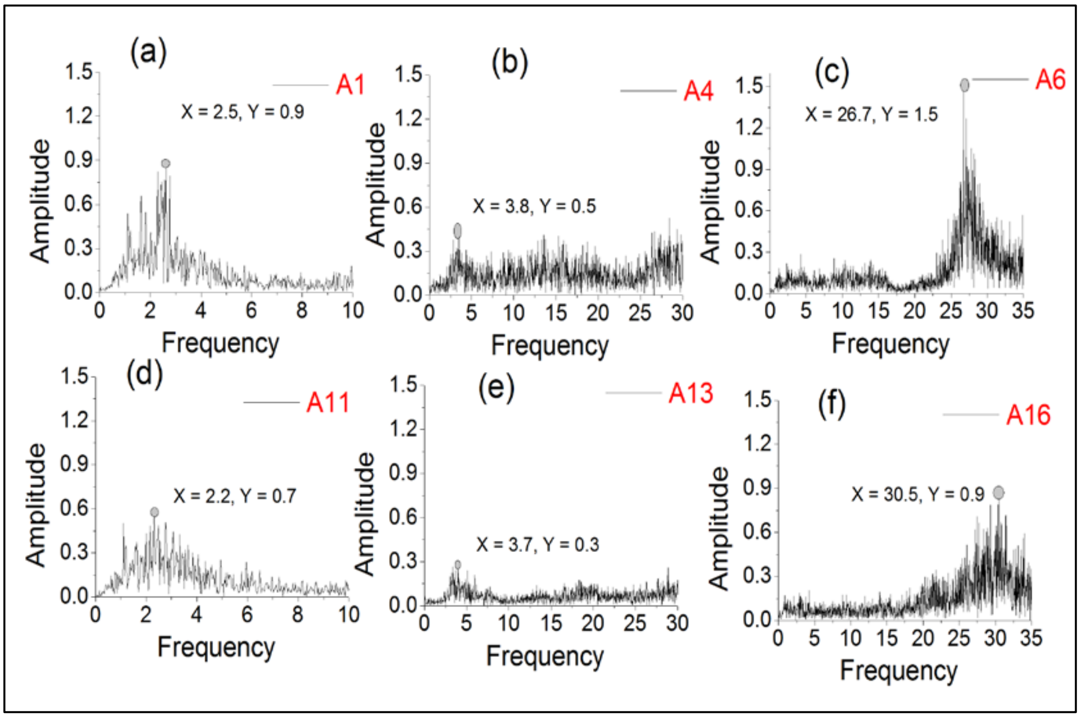


**Figure 7-13 FFT of acceleration signal recorded by accelerometers (a) A1, (b)A4, (c) A6, (d) A11, (e)A13 and (f) A16 for 0.4g pba value during shake table testing**

## 7.6 Observations and Discussion

Modified configuration of Interconnected GBs (with structural cross bracing) maintained integrity up to 0.4g peak ground acceleration value. As mentioned earlier, design modification were carried out to improve seismic stability of the interconnected glove box system. Hence, here we would briefly present comparison of both the cases and examine effect of introducing cross bracing on seismic stability of the system. Relative sliding displacements in both the horizontal directions of the glove boxes is compared. Fig.7-14 shows the comparison of relative sliding motion between the two boxes. It can be observed that in case of glove boxes interconnected only with a material transfer tunnel, relative displacement at 0.4g PGA value was of the order of 25mm, which led to the fall of the tunnel and hence breach of integrity. However, on the other hand, it was observed in case of modified design (glove boxes connected with structural cross members in addition to transfer tunnel), relative sliding motion between the boxes was reduced to less than 0.1mm. This also had repercussions on the leak tightness of the system as shown earlier in Table.2-2. Modified design successfully withstood seismic excitations up to 0.4g PGA value, without any leakages.

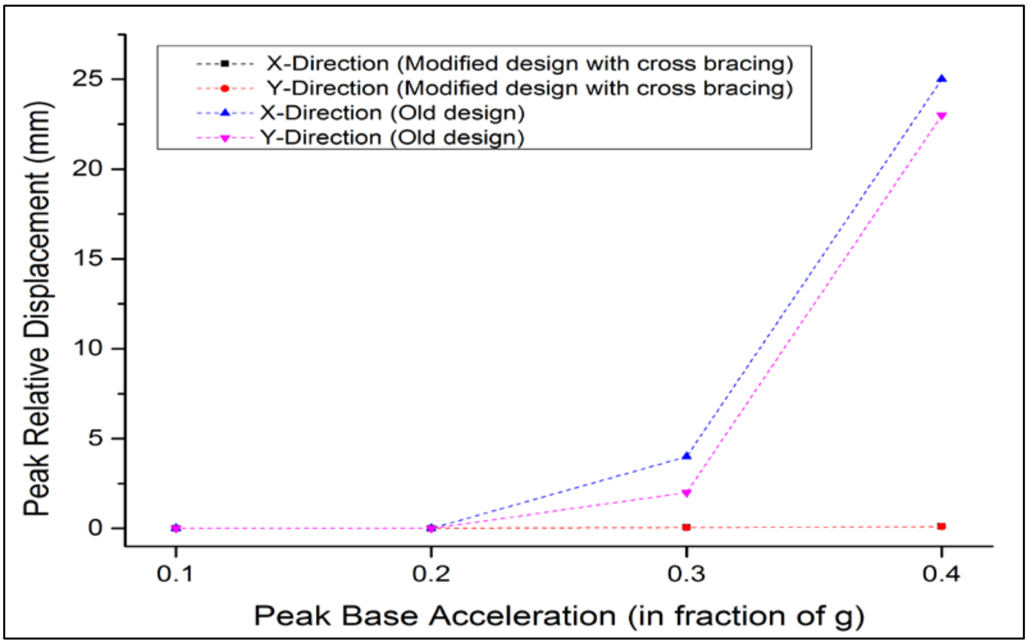


**Figure 7-14 Comparison of peak relative displacements between two glove boxes in the earlier and modified design**

In addition to that, FE analysis results were throughout coherent with the test results. Simplified numerical method predicted conservative displacement values as shown in Fig.7-9. Hence, this can be effectively utilized for estimating upper bounds on displacements.

Behavior of free-standing interconnected glove boxes on floor subjected to base excitation was nonlinear. Modified design of interconnected glove boxes sustained earthquake motion up to 0.4g peak base acceleration value without breach of integrity and leak tightness. Numerical calculations performed can give the facility designers a confidence that the free-standing glove boxes are also seismically safer. Hence this study would enable, the designers of a new facility, to take a judicious decision about anchoring of glove boxes with the floor.

Owing to the highly nonlinear behavior of the system due to presence of friction and impact at contact interfaces, FE analysis contact parameters were required to be meticulously selected to accurately represent the contact behavior. Analysis results were found to be in good agreement with test values. Hence, FE methods can be utilized for analyzing the system. Simplified numerical method developed using an energy conservation technique provided a good quick estimate of maximum sliding displacement.

# CHAPTER 8 CONCLUSIONS, CONTRIBUTIONS AND DIRECTIONS FOR FUTURE RESEARCH

The research carried out as a part of this doctoral program produced certain important outcomes. A generic investigation of the stability of a free-standing body subjected to base excitation was presented. An investigation on fundamental dynamics of flexible and rigid free-standing bodies was carried out. A clear distinction in dynamic behavior of a rigid and flexible body, when excited by a base excitations, was highlighted. Seismic stability of geometrically similar rigid and flexible test models of varying frequency parameters had been investigated. Supported by experimental and numerical investigations, effect of system parameters like base motion characteristics and aspect ratio on stability of a free-standing body was explored. Conclusions are given in the next section.

## 8.1 Conclusions

1. Base excitation frequency influences initiation of any mode of motion from rest state. With the increase of excitation frequency, motion of a body diminishes to a very low value corresponding to no motion state.
2. Experimental and numerical investigation revealed differences in dynamic response of geometrically similar rigid and flexible bodies. ***Free rocking frequencies*** were found to govern stability of a flexible free-standing structure.
3. It was shown that a flexible body can initiate rocking motion below the statically required minimum value of $g.\tan\alpha$, if it is excited by frequencies corresponding to its free rocking frequencies. On the other hand, a rigid body could not initiate rocking motion below a value of $g.\tan\alpha$. This indicated seismic vulnerability of a flexible body compared to geometrically similar rigid body to a particular range of frequencies pertaining to free rocking frequencies of the body.

4. Amplification factor for rocking motion of a rigid body was dependent on amplitude, frequency and aspect ratio of the body. However for sliding motion it was independent of all three parameters. Similarly for a flexible body AF for rocking was dependent on amplitude, frequency and aspect ratio of the body. On the other hand for sliding motion, AF was independent of aspect ratio but not of amplitude and frequencies of base excitation.
5. Values of parameters like rocking angles and sliding displacement were found to be strongly dependent on frequencies of base excitations in addition to the amplitude value. Both of them were observed to be inversely proportional to the frequencies of excitations as discussed in Sections 3.3.4 and 3.3.5.
6. Motion initiation criteria diagrams were developed for flexible bodies. This is the first time such a diagram is presented for a flexible body. Main feature of this diagram was increase of rocking and slide/rock region with the increase in flexibility. This resulted in lesser available rest region which in turns adversely affects seismic stability.
7. Overturning potential of rigid and flexible bodies was evaluated. Developed overturning curves highlighted presence of two distinct modes of failure. Higher probability of Mode-1 failure was observed in a flexible test specimen than the rigid one of same aspect ratio.
8. Rigid body motions dominated seismic response of a glove box. On a low grip base ($\mu_s$=0.15), despite of predominance of sliding motion, presence of low amplitude rocking motion was observed. A generalized and simple methodology was proposed in Section 5.7 to help the facility designers in taking a judicious decision about anchoring of the glove boxes.

## 8.2 Contributions

The following are specific innovative and novel contributions from the research work carried out as a part of this PhD.

1. ***Base excitation frequency*** was determined as a parameter governing motion initiation of a body from rest state. Three-dimensional motion initiation criteria diagrams were developed, using frequency as an independent axis.
2. Dynamics of a free standing flexible body was observed to be influenced by a new parameter known as ***free rocking frequencies***. This research highlighted a phenomenon of frequency induced uplift/rocking in a flexible body.
3. A relationship between amplitude of base motion required to uplift and free rocking frequencies of a flexible body was experimentally established and discussed in Section 4.2.4.
4. A methodology was proposed to determine requirement of anchoring (fixing to the base) of a free standing glove box. By using developed motion initiation criteria diagrams (Refer Fig.5.22), user can take a judicious decision about fixing/not fixing of the body. Discussion for enhancing stability of a glove box without anchoring was done.

## 8.3 Directions for Future Research

Present research focussed on evaluating dynamic behaviour of rigid and flexible free-standing bodies when subjected to base excitations. Extensive experimental and numerical results were presented and logical conclusions were drawn. However, it is felt that there are some areas which require further studies and if thoroughly investigated can lead to more scientific breakthroughs as given below.

1. For a rigid body of square base, planar excitations can lead to a response in the third direction. Same was observed during shake table testing of rigid test specimens. Hence it can be a subject of future study to investigate effects of motions in third dimension and its repercussions on stability of a body. Moreover, as noted response of specimens with the same aspect ratios ($\alpha$ value) will be different for different sizes (R value). Hence, blocks with the same aspect ratio but different sizes can be tested in rocking mode of motion. [63]
2. Frequency induced rocking phenomenon can be further investigated for flexible bodies of different stiffness. Effects of stiffness of a body in frequency induced rocking and its effect on overturning instability can be a future course of work.
3. Mode1 overturning failure was observed to be a complex behavior, in which for a certain combination of frequency and amplitude the specimen had multiple impacts with the base before overturning. This also affected total time required for overturning. Mode2 failures were prompt taking less than a second, while on the other side Mode1 failures were slow and even for some cases it took the specimen around 7 seconds to overturn. More investigation is required on this subject, which shall be taken up as future course of activities
4. Three-dimensional motion initiation criteria diagram for a flexible free-standing body can be developed. This requires evaluation of cut off frequencies corresponding to all possible states of a flexible body and then map them to form a three-dimensional diagram. This can be a significant contribution to the scientific community, since by looking at a simple diagram it would become possible to predict probable motion of a flexible body. Different diagrams can be built for different aspect ratios.

5. Effect of frequency induced vibrations on overturning instability of a flexible body can be taken for future studies. This can also include an interesting investigation of possibility of rocking resonance in a flexible body.

# REFERENCES

[1] FEMA, E-74, "Reducing the Risks of Nonstructural Earthquake Damage," Federal Emergency Management Agency, U.S.A, 2012.

[2] C852, "Standard Guide for Design Criteria for Plutonium Glove boxes," American Society for Testing Materials, 2009.

[3] J. Milne, "Experiments in observational seismology," *Trans. seism. soc. Japan,* vol. 3, pp. 12-64, 1881.

[4] J. Milne and F. Omori, "On the overturning and fracturing of brick columns by horizontal applied motion,," *Seismology journal,* vol. 17, pp. 59-86, 1893.

[5] F. Omori, "On the overturning and sliding of columns," *Publ. Earthquake Invest. Committee,* vol. 32, pp. 19-33, 1900.

[6] J. Perry, "Note on the rocking of a column," *Trans. seism. soc. Japan,* pp. 103-106, 1881.

[7] G. Housner, "The behavior of inverted pendulum structures during earthquakes," *Bull. seism. Soc. America,* 1963.

[8] M. Aslam, D. Scalise and W. Godden, "Earthquake Rocking Response of Rigid Bodies," *Journal of the Structural Division,* vol. 106, no. 2, pp. 377-392, 1980.

[9] C. Yim, A. K. Chopra and J. Penzien, "Rocking response of rigid blocks to earthquakes," *Earthquake Engineering and Structural Dyanamics,* vol. 8, pp. 565-587, 1980.

[10] Y. Ishiyama, "Motion of rigid bodies and critirea for overturning by earthquake excitations," *Earthquake Engineering and Structural Dyanmics,* vol. 10, pp. 635-650, 1980.

[11] P. R. Lipscombe and S. Pellegrino, "Free rocking of prismatic blocks," *Journal of Engineering Mechanics,* vol. 119, no. 7, pp. 1387–1410., 1993.

[12] N. Makris and Y. Roussos, "Rocking response of rigid blocks under near source ground motions," *Geotechnique,* vol. 50, no. 3, pp. 243-262, 2000.

[13] J. Zhang and N. Makris, "Rocking response of free-standing blocks under cycloidal pulses," *Journal of Engineering Mechanics,* vol. 27, pp. 473–483., 2001.

[14] N. Makris and D. Konstantinidis, "The Rocking Spectrum and the Limitations of Practical Design Methodologies," *Earthquake Engineering and Structural Dynamics,* vol. 32, no. 2, pp. 265-289, 2003.

[15] M. Priestley, R. Evison and A. Carr, "Seismic response of strcutures free to rock on their foundations," *Bullitien of the Newzealand national society for earthquake engineering,* vol. 11, no. 3, pp. 141-150, 1978.

[16] FEMA 356, "Prestandard and Commentary for the Seismic Rehabilitation of Buildings. Prepared by the: FEMA.," American Society of Civil Engineers for the Federal Emergency Management Agency. , Washington, DC, 2000.

[17] F. Prieto, P. Lourerno and C. Oliveira, "Impulsive Dirac-Delta Forces in the Rocking Motion," *Earthquake Engineering and Structural Dynamics,* vol. 33, no. 7, pp. 839-857., 2004.

[18] F. Prieto and P. B. Lourenco, "On the rocking behavior of rigid objects.," *Meccanica,* vol. 40, pp. 121-133, 2005.

[19] Y.-H. Chen, W.-H. Liao, C.-L. Lee and Y.-P. Wang, "Seismic isolation of viaduct piers by means of a rocking mechanism," *Earthquake Engineering & Structural Dynamics,* vol. 35, pp. 713–736, 2006.

[20] F. Pena, P. Lourenco and A. Campos-Costa, "Experimental dynamic behavior of free-standing multi-block structures under seismic loadings," *Journal of Earthquake Engineering,* vol. 12, pp. 953-979, 2008.

[21] H. Zhang, B. Brogliato and C. Liu, "Dynamics of planar rocking-blocks with Coulomb friction and unilateral constraints: comparisons between experimental and numerical data," *Multibody System Dynamics,* vol. 32, pp. 1-25, 2014.

[22] A. D. Egidio, R. Alaggio, A. Contento, M. Tursini and E. D. Loggia, "Experimental characterization of the overturning of three-dimensional square based rigid block," *International Journal of Non-Linear Mechanics,* vol. 69, pp. 137–145, 2015.

[23] D. Zulli, A. Contento and A. Egidio, "3D model of rigid block with a rectangular base subject to pulse-type excitation," *International Journal of Non-Linear Mechanics,* vol. 47, pp. 679-687, 2012.

[24] E. G. Dimitrakopoulos and T. S. Paraskeva, "Dimensionless fragility curves for rocking response to near-fault excitations," *Earthquake Engineering & Structural Dynamics,* vol. 44, no. 12, pp. 2015-2033, 2015.

[25] G. Amonton, "De la resistance cause'e dans les machines," *Mem l'Acedemie,* pp. 257-282, 1699.

[26] C. Coulomb, "Sur une application des regles de maximis & minimis a quelques problemes de statique, relatifs a I' architecture.," *Memoires de Mathematique & de Physique,* pp. 343-382, 1773.

[27] N. Newmark, "Effects of Earthquakes on Dams and Embankments."Fifth Rankine Lecture," *Geotechnique,* vol. 15, pp. 139-160, 1965.

[28] B. Choi and C. Tung, "Estimating Sliding Displacement of an Unanchored Body Subjected to Earthquake Excitation," *Earthquake Spectra,* vol. 18, no. 4, pp. 601-613, 2002.

[29] L. D. Garcia and T. Soong, "Sliding Fragility of Block-Type NonStructural Components. Part 1: Unrestrained Components," *Earthquake Engineering and Structural Dynamics,* vol. 32, pp. 111-129., 2003.

[30] L. D. Garcia and T. Soong, "Sliding Fragility of Block-Type NonStructural Components. Part 2: Restrained Components," *Earthquake Engineering and Structural Dynamics.,* vol. 32, pp. 131-149, 2003.

[31] T. Hutchinson and S. Chaudhuri, "Bench-Shelf System Dynamic Characteristics and Their Effects on Equipment and Contents," *Earthquake Engineering and Structural Dynamics,* vol. 35, no. 13, pp. 1631-1651, 2006.

[32] T. Taniguchi and T. Miwa, "A simple procedure to approximate slip displacement of freestanding rigid body subjected to earthquake motions," *Earthquake Engineering and Structural Dynamics,* vol. 36, pp. 481–501, 2007.

[33] H. Shenton III and N. Jones, "Base Excitation of Rigid Bodies. I: Formulation.," *Journal of Engineering Mechanics,* vol. 117, no. 10, pp. 2286-2306., 1991.

[34] H. Shenton, III and N. Jones, "Base Excitation of Rigid Bodies. II: Periodic Slide-Rock Response," *Journal of Engineering Mechanics,* vol. 117, no. 10, pp. 2307-2328, 1991.

[35] H. Shenton and N. Jones, "Critirea for initiation of slide, rock and slide-rock rigid body modes," *Journal of Engineering Mechanics,* vol. 122, no. 7, pp. 690-693, 1996.

[36] Y. Shao and C. Tung, "Seismic response of unanchored bodies," *Erathquake spectra,* vol. 15, no. 3, pp. 523-536, 1999.

[37] U. Andreaus and P. Casini, "On the rocking-uplifting motion of a rigid block in free and forced motion: influence of sldining and bouncing," *Acta Mechanica,* vol. 138, pp. 219-241, 1999.

[38] M.-Y. Jeong, H. K. Jeong and Y. Y. In, "Chaotic Rocking Vibration of a Rigid Block with Sliding Motion Under Two-Dimensional Harmonic Excitation," *KSME International Journal,* vol. 16, no. 9, pp. 1040--1053, 2002.

[39] T. Taniguchi, "Nonlinear response analysis of rectangular rigid bodies subjected to horizontal and vertical ground motion," *Earthquake Engginnering and Structural Dynamics,* vol. 31, pp. 1481–1500, 2002.

[40] A. D. Egidio and A. Contento, "Base isolation of slide-rocking non-symmetric rigid blocks under impulsive and seismic excitations," *Engineering structures,* vol. 31, no. 11, pp. 2723-2734, 2009.

[41] D. Konstantinidis and N. Makris, "Experimental and analytical studies on the response of freestanding laboratory equipment to earthquake shaking," *Earthquake Engineering and Structural Dynamics,* vol. 38, no. 6, pp. 827–848, 2009.

[42] D. Konstantinidis and N. Makris, "Experimental and analytical studies on the response of 1/4-scale models of freestanding laboratory equipment subjected to strong earthquake shaking," *Bull Earthquake Eng DOI,* vol. 8, pp. 1457–1477, 2010.

[43] C. E. Wittich and T. C. Hutchinson, "Shake table tests of stiff, unattached, asymmetric structures.," *Earthquake Engineering and Structural Dynamics,* vol. 44, pp. 2425–2443, 2015.

[44] K. Muto, H. Umemura and Y. Sonobe, "Study of the overturning vibrations of slender structures," in *Proceedings of the Second World Conference on Earthquake Engineering,*, Tokyo, 1960.

[45] J. W. Meek, "Effect of foundation tipping on dynamic response," *Journal of the Structural Division (ASCE),* vol. 101, pp. 1297 – 1311, 1975.

[46] C. Yim and A. Chopra, "Simplified earthquake analysis of structures with foundation uplift," *Journal of Structural Engineering (ASCE),* vol. 111, pp. 906 – 930, 1985.

[47] I. N. Psycharis and P. C. Jennings, "Rocking of slender rigid bodies allowed to uplift," *Earthquake Engineering and Structural Dynamics,* vol. 11, no. 11, pp. 57-76, 1983.

[48] I. N. Psycharis, "Dynamics of flexible systems with partial lift-off," *Earthquake Engineering and Structural Dynamics,* vol. 11, pp. 501 – 521, 1983.

[49] I. Psycharis, "Effect of base uplift on dynamic response of SDOF structures," *Journal of Structural Engineering (ASCE),* vol. 171, pp. 733 – 754., 1991.

[50] G. Oliveto, I. Calio and A. Greco, "Large displacement behaviour of a structural model with foundation uplift under impulsive and earthquake excitations," *Earthquake Engineering and Structural Dynamics,* vol. 32, pp. 369–393, 2003.

[51] S. Acikgoz and M. J. DeJong, "The interaction of elasticity and rocking in flexible structures allowed to uplift," *Earthquake Engineering and Structural Dynamics,* vol. 41, pp. 2177–2194, 2012.

[52] M. F. Vassiliou, R. Truniger and B. Stojadinović, "An analytical model of a deformable cantilever structure rocking on a rigid surface: development and verification.," *Earthquake Engineering and Structural Dynamics,* vol. 44, pp. 2775–2794, 2015.

[53] R. Truniger, M. F. Vassiliou and B. Stojadinović, "An analytical model of a deformable cantilever structure rocking on a rigid surface: experimental validation," *Earthquake Engineering and Structural Dynamics,* vol. 44, pp. 2795–2815., 2015.

[54] X.-F. Wang and P. Gould, "Dynamics of structures with uplift and sliding," *Earthquake Engineering and Structural Dynamics,* vol. 22, pp. 1085 – 1095, 1993.

[55] T. Fujita, K. Ohtani, M. Kozeki, T. Ide and K. Sakuno, "Earthquake Resistance Test of Full-Scale Glove Box," in *Trans. 10th SMiRT*, USA, 1989.

[56] S. Miura, S. Ousaka, Y. Kawada and H. Ito, "Earthquake resistance test of New type Glove box," in *Trans.17th SMiRT*, 2003.

[57] Bhabha Atomic Research Centre, "A report on Seismic Design Evaluation of Glove Boxes tested at CPRI," Bhabha Atomic Research Centre, Mumbai, 2010.

[58] Department of earthquake engineering (DEQ), IIT Roorkee, "Envelope spectra for 500 MWE plant on rock site, project number-P-483," Department of earthquake engineering, Roorkee.

[59] AERB/SG/S-11, "Seismic studies and design basis ground motion for nuclear power plant sites," The Atomic Energy Regulatory Board (AERB), 1990.

[60] I. 10648-1, "Containment enclosures -- Part 1: Design principles," International Organisation for Standardisation, 1997.

[61] I. 10648-2, "Containment enclosures -- Part 2: Classification according to leak tightness and associated checking methods," International Organization for Standardization, 1992.

[62] H. Shenton and N. Jones, "Critirea for initiation of slide, rock and slide-rock rigid body modes," *Journal of Engineering Mechanics,* vol. 122, no. 7, pp. 690-693, 1996.

[63] P. P. Labbe, "Report on thesis titled "Response Analysis of Freestanding Systems subjected to Seismic loading"," EDF, France, 2017.

[64] M. Apostolou, G. Gazetas and E. Garini, "Seismic response of slender rigid structures with foundation uplifting," *Soil Dynamics and Earthquake Engineering,* vol. 27, pp. 642–654, 2007.

[65] A. Egidio, R. Alaggio, A. Contento and M. Tursini, "Experimental characterization of the overturning of three-dimensional square based rigid block," *International Journal of Non-Linear Mechanics,* vol. 69, pp. 137-145, 2015.

[66] Abaqus, Abaqus 6.10, Analysis User’s Manual, Chapters 35-39, U.S.: Simulia, 2010.

[67] K. J. Bathe, Finite Element Procedures, Upper Saddle River, New Jersey: Prentice-Hall, Inc, 1996.

[68] J. C. Simo and T. Laursen, "An Augmented Lagrangian Treatment of Contact Problems Involving Friction," *Computers & Structures,* vol. 42, no. 1, pp. 97-116, 1992.

[69] K. Bathe and P. Bouzinov, "On the constraint function method for contact problems," *Computers and Structures,* vol. 64, no. 5-6, pp. 1069-1085, 1997.

[70] M. Anitescu, J. F. Cremer and F. A. Potra, "Formulating three dimensional contact dynamics problems," *Mechanics of structures and machines,* vol. 24, no. 4, pp. 405-437, 1996.

[71] H. M. Hilber, T. J. R. Hughes and R. L. Taylor, "Improved Numerical Dissipation for Time Integration Algorithms in Structural Dynamics," *Earthquake Engineering and Structural Dynamics,* vol. 5, pp. 283–292, 1977.

[72] American Society of Mechanical Engineers (ASME), "Boiler and Pressure Vessel Code, Section-III, Divison 1- Subsection NB," ASME, New York, 2010.

[73] S. Acikgoz and M. J. DeJong, "The rocking response of large flexible structures to earthquakes," *Bulletin of Earthquake Engineering,* vol. 12, no. 2, pp. 875–908, 2014.

[74] A. Czekanski, N. El-Abbasi and S. A. Meguid, "Optimal Time Integration Parameters for Elastodynamic Contact Problems," *Communications in Numerical Methods in Engineering,* vol. 17, pp. 379–384, 2001.

[75] "Seismic design criteria for structures, systems, and components in nuclear facilities," The American Society of Civil Engineers (ASCE) 43-05, 2005.